HAL
open science

Structural analysis and investigation of the Staphylococcus aureus ribosome and potential anticancer drugs

Daniya Kashinskaya

To cite this version:

Daniya Kashinskaya. Structural analysis and investigation of the Staphylococcus aureus ribosome and potential anticancer drugs. Structural Biology [q-bio.BM]. Université de Strasbourg, 2017. English. NNT : 2017STRAJ110 . tel-01987004

HAL Id: tel-01987004

https://theses.hal.science/tel-01987004v1

Submitted on 20 Jan 2019

HAL is a multi-disciplinary open access archive for the deposit and dissemination of scientific research documents, whether they are published or not. The documents may come from teaching and research institutions in France or abroad, or from public or private research centers.

L'archive ouverte pluridisciplinaire **HAL**, est destinée au dépôt et à la diffusion de documents scientifiques de niveau recherche, publiés ou non, émanant des établissements d'enseignement et de recherche français ou étrangers, des laboratoires publics ou privés.

UNIVERSITÉ DE STRASBOURG

ÉCOLE DOCTORALE des Sciences de la Vie et de la Santé

[IGBMC - CNRS UMR 7104 - Inserm U 964]

THÈSE présentée par :

[Daniya KASHINSKAYA]

soutenue le : **12 Décembre 2017**

pour obtenir le grade de : **Docteur de l'université de Strasbourg**

Discipline/ Spécialité : Biochimie, Biologie Moleculare et Structurale

TITRE de la thèse

[Structural analysis and investigation of the Staphylococcus aureus ribosome and potential anticancer drugs]

[Analyse structurale et étude du ribosome de Staphylococcus aureus et des médicaments antitumoraux potentiels]

THÈSE dirigée par :

[M. YUSUPOV Marat]	Directeur de Recherche, CNRS, IGBMC

RAPPORTEURS :

[Mme. SCHMITT Emmanuelle]	Directeur de Recherche, CNRS, l'Ecole polytechnique de Paris
[M. DIAZ Jean-Jacques]	Directeur de Recherche, Inserm, Centre de recherche en cancerologie de Lyon

---

AUTRES MEMBRES DU JURY :

[Mme. ROMBY Pascale]	Directeur de Recherche, CNRS, IBMC
[M. MASQUIDA Benoît]	Directeur de Recherche, CNRS, GMGM
[M. KOLB Vyacheslav]	Directeur de Recherche, Institut de recherche de protéines, Moscou

TABLE OF CONTENTS

LIST OF FIGURES 4

LIST OF TABLES 6

ACKNOWLEDGMENT 7

ABBREVIATIONS 8

RÉSUMÉ DE THÈSE 10

PREFACE 20

General Introduction 23

I RIBOSOME CHARACTERIZATION 24

1. RIBOSOME ORGANIZATION 24
2. SPECIFICATIONS OF BACTERIAL AND EUKARYOTIC RIBOSOME 25
3. PROTEIN SYNTHESIS AS A KEY PROCESS OF LIFE 28

3.1 INITIATION 29

3.2 ELONGATION 30

3.3 TERMINATION AND RECYCLING 31

4. HISTORICAL ASPECTS OF STRUCTURAL STUDIES OF THE RIBOSOME 32
5. X-RAY CRYSTALLOGRAPHY AND CRYO-ELECTRON MICROSCOPY OF THE RIBOSOME 33
6. RIBOSOME – POTENTIAL THERAPEUTIC TARGET 36

II MAIN CHARACTERISTICS OF *STAPHYLOCOCCUS AUREUS* 39

1. REGULATORY MECHANISMS OF VIRULENCE DETERMINANTS IN *S. AUREUS* 40
2. SUPER KILLER OF THE XXI CENTURY 43
3. ANTIBIOTIC RESISTANCE 45
4. MECHANISMS OF ANTIBIOTICS ACTION AND BACTERIAL RESISTANCE 46

4.1 MODIFICATIONS OF THE ANTIBIOTIC MOLECULE 47

4.2 DECREASED ANTIBIOTIC PENETRATION AND EFFLUX 48

4.3 CHANGES OF THE TARGET SITES 49

5. *S. AUREUS* RIBOSOME AS A TARGET FOR DEVELOPING NEW THERAPEUTIC DRUGS 50

III MAIN CHARACTERISTICS OF CANCER 53

1. CANCER CONTROL SYSTEM 53

2. MECHANISMS OF DRUG RESISTANCE 54
3. POTENTIAL ANTICANCER DRUGS AGAINST RIBOSOME ASSEMBLY 58

Part I - Structural analysis and investigation of the *Staphylococcus aureus* ribosome 65

IV RIBOSOME PURIFICATION 66

1. DESCRIPTION OF INITIAL RIBOSOME PURIFICATION PROTOCOL FROM *S. AUREUS*, DEVELOPED IN THE YUSUPOV LABORATORY 67

1.1 *S. AUREUS* CELL GROWTH 67

1.2 LYSIS 68

1.3 PEG PRECIPITATION AND SUCROSE CUSHION 68

1.4 SUCROSE DENSITY GRADIENT CENTRIFUGATION 68

1.5 RIBOSOME CONCENTRATION AND STORAGE 69

2. MODIFICATIONS OF RIBOSOME PURIFICATION PROTOCOL 70

2.1 CELL PREPARATION 70

2.2 LYSIS 70

2.3 SUCROSE DENSITY GRADIENT CENTRIFUGATION 72

2.4 RIBOSOME CONCENTRATION AND STORAGE 74

V RIBOSOME SAMPLE CHARACTERIZATION 74

VI COMPLEX FORMATION OF THE RIBOSOME FROM *S. AUREUS* WITH $tRNA^{fMet}$ AND mRNA 78

1. PURIFICATION OF THE INTACT $tRNA^{fMET}$ 80
2. $tRNA^{fMet}$ SAMPLE CHARACTERISZATION 83

VII CRYSTALLOGRAPHIC STUDIES OF *S.AUREUS* RIBOSOME 85

1. MACROMOLECULAR CRYSTALLIZATION IN THEORY 86

1.1 CRYSTALS GROWTH 87

1.2 MACROMOLECULAR CRYSTALLIZATION IN PRACTICE 87

2. CRYSTALLIZATION OF *S.AUREUS* RIBOSOME 91

2.1 CRYSTALLIZATION 92

3. POST – CRYSTALLIZATION TREATMENT 102

3.1 POST – CRYSTALLIZATION TREATMENT OF *S.AUREUS* RIBOSOME CRYSTALS 103

4. X-RAY DATA COLLECTION 105

PRESPECTIVES 108

Part II - Structural analysis and investigation of potential anticancer drugs 109

VIII BACKGROUND AND AIM OF THE PROJECTS 110

1. CRYSTAL STRUCTURE OF POTENTIAL ANTICANCER DRUG C45 BOUND TO THE 80S RIBOSOME 110

2. CRYSTAL STRUCTURE OF THE CHEMOTHERAPEUTIC DRUG CISPLATIN BOUND TO THE 80S RIBOSOME 112

IX RESULTS AND METHODS 113

1. PURIFICATION OF 80S RIBOSOME 113
2. CO-CRYSTALLIZATION 114
3. POST-CRYSTALLIZATION TREATMENT 115
4. X-RAY DATA COLLECTION AND STRUCTURE DETERMINATION 117

X STRUCTURAL INVESTIGATION OF POTENTIAL ANTI-CANCER DRUG C45 120

XI FLUORESCENCE RESONANCE ENERGY TRANSFER 123

DISCUSSION AND PERSPECTIVES 127

INVISIBLE CONNECTION BETWEEN PROJECTS 129

GENERAL CONCLUSION 130

LIST OF PUBLICATIONS AND COMMUNICATIONS 131

REFERENCES 132

LIST OF FIGURES

Figure 1: Structural organization and functional sites of the ribosome (adapted from Melnikov et al., 2012) 25

Figure 2: Composition of bacterial and eukaryotic ribosomes and the common core, based on X-Ray studies(Melnikov et al.,2012) 26

Figure 3: Bacteria- and eukaryote-specific proteins and RNA expansions of the small ribosomal subunit (Melnikov et al., 2012). 27

Figure 4: Bacteria- and eukaryote-specific proteins and RNA expansions of the large ribosomal subunit (Melnikov et al., 2012). 28

Figure 5: The translation cycle in bacteria and eukaryotes (Melnikov et al., 2012). 28

Figure 6: Structural evolution of Ribosome from 1983 to 2011. 35

Figure 7: Antibiotic binding sites on the 30S ribosomal subunits (Wilson, 2014)..... 37

Figure 8: Antibiotic binding sites on 50S ribosomal subunits (adapted from Wilson, 2014). 38

Figure 9: Schematic model of cell wall of gram-positive bacteria (http://rcvetsblog.blogspot.fr/2014/03/bacterial-cell-wall.html)..... 39

Figure 10: Regulation network of production of virulence factors in *S. aureus* (adapted from Chevalier, 2009)..... 41

Figure 11: Four waves of antibiotic resistance in *S. aureus* (Chambers and DeLeo, 2009)..... 44

Figure 12: Development of antibiotics and resistance (Clatworthy et al., 2007). 46

Figure 13: Antibacterial resistance mechanisms (adapted from Wilson, 2014). 47

Figure 14: Different types of efflux pumps in gram-positive and gram-negative bacteria (Piddock, 2006). 48

Figure 15: Schematic representation of the mechanism of action and resistance to linezolid (Munita and Arias, 2016). 49

Figure 16: Mechanisms of drug resistance (Molecular Genetics of Cancer, Figure 12). 55

Figure 17: Structure of the amicoumacin A complex with yeast ribosome (Prokhorova et al., 2016). 59

Figure 18: Crystal Structure of AglA-80S Ribosome (McClary et al., 2017). 60

Figure 19: The X-ray co-crystal structure of CL with the eukaryotic 80S ribosome (adapted from Könst *et al*., 2017). 61

Figure 20: Cisplatin-binding sites on the ribosome (Melnikov et al., 2016). 62

Figure 21: Cisplatin targets the mRNA channel in the ribosome (Melnikov et al., 2016)..... 63

Figure 22: Cisplatin modification site near the GTPase activating center of the ribosome (Melnikov et al., 2016). 64

Figure 23: Sucrose gradient profile. 69

Figure 24: Growth curves of Staph RN6390 (OD1 and 2) strain in the BHI medium. 70

Figure 25: Sucrose gradient profiles after experiment II. 72

Figure 26: Sucrose gradient profiles after experiment III. 73

Figure 27: Sucrose gradient profiles after experiment IV. 74

Figure 28: Polyacrylamide Gel Electrophoresis of *S. aureus* ribosome sample. 76

Figure 29: Electrophoresis of the *S. aureus* ribosome samples after two steps of sucrose cushion sedimentation purification protocol (experiment I). 77

Figure 30: Electrophoresis of the *S. aureus* ribosome samples with decreasing magnesium concentration after PEG precipitation and in the sucrose cushion step (experiment II). 78

Figure 31: Anion-exchange chromatography (Q-Sepharose 25 ml). 82

Figure 32: Denaturing 12% 8M urea PAGE of $tRNA^{fMet}$. 83

Figure 33: High-pressure liquid chromatography: C4-silica column. 84

Figure 34: Schematic representation of diffraction experiment. 85

Figure 35: Schematic phase diagram of protein crystallization (Krauss et al, 2013) 86

Figure 36: Idealized phase diagram of the trajectories of four different crystallization methods of reaching nucleation and metastable zones (adapted from Krauss et al, 2013). 90

Figure 37: Crystals of *S. aureus* 70S ribosome in the CrysChem plate. 96

Figure 38: Crystals of 70S ribosome with $tRNA^{fMet}$ with ratio 1:1. 100

Figure 39: Crystals of 70S ribosome with $tRNA^{fMet}$ and mRNA with ratio 1:1:1. 101

Figure 40: Scheme of post-crystallization treatment. 105

Figure 41: Diffraction patterns of different crystals. 107

Figure 42: Cytotoxicity and translation-inhibitory activities of lissoclimide analogues and CHX (adapted from Konst et al., 2017). 111

Figure 43: Computational modeling study of C45 compound. 112

Figure 44: Sucrose gradient profile. 114

Figure 45: Diffraction patterns of C45/80S complex crystals. 117

Figure 46: Unbiased difference density helped us to fit C45 unambiguously 117

Figure 47:. Diffraction patterns of ciplatin/80S complex crystals. 119

Figure 48: Chemical structure of C45 compound 120

Figure 49: C45, chlorolissoclimide and cycloheximide share the same binding pocket in the 60S E-site. 120

Figure 50: Comparison of binding sites between C45 and CL.....121

Figure 51: The X-ray crystal structure of C45 compound with the eukaryotic 80S ribosome reveals the molecular basis of translation inhibition. 122

Figure 52: Schematic representation of pre-translocation complex..... 124

Figure 53: Ligand-Induced changes of the Human 80S Pre-translocation Complex visualized by FRET..... 124

Figure 54: Quantification of the data for CHX, CL and C45. 125

Figure 55: Population histogram of a washout experiment with C45..... 126

LIST OF TABLES

Table 1: Published crystal conditions for 70S ribosomes (adapted from Pearson, 2011). **.....** 92

Table 2 Crystals of *S. aureus* 70S ribosome with presence PEG 8000 and NH_4SCN in the crystallization condition. **.....** 93

Table 3: Crystals of the *S. aureus* 70S ribosome after modification of purification protocol..... 99

Table 4: Data collection and refinement statistic of C45/80S complex. 118

ACKNOWLEDGMENT

First of all I would like to thank all jury members Dr. Emmanuelle Schmitt, Dr. Jean-Jacques Diaz, Dr. Vyacheslav Kolb, Dr. Pascale Romby and Dr. Benoît Masquida who kindly accepted my invitation and found the time to evaluate my PhD work.

I would like to wholeheartedly thank to my advisors Marat and Gula for the support, assistance and participation that they provided during all three years of my PhD education. My first meeting with them in the Kazan University, during my master education, fascinated me and their life's course and researches mainly motivated me to devote myself to science and in particular to the to the occupation of ribosome in the structural biology field. Thank you very much for the opportunity to realize my dream, I learned so much from you.

Thanks a lot to all current members of the ribosomal group Justine, Mumin, Alexey and former members Marie, David, Irina, Yuzuru for the support, advice and friendly atmosphere, you were not only my colleagues at the work, but became my good friends. I would like to express my special gratitude to Iskander, Simone and Melanie for their participation in my projects and assistance in their implementation.

I am thankful to the structural biology platform of IGBMC: Alistair and Pierre, they taught me various techniques in crystallization and helped me with advices on the cryo-protection of crystals.

Due to my first project, I had the opportunity to meet wonderful people at the IBMC. I express special gratitude to Pascale Romby and the members of her laboratory Stefano, Anne-Catherine, Isabelle, as well as to former members Pierre, Alessandra and Mélodie for their help, advices and support in my work.

During my PhD student time, I met and became friends with different people from different fields of science. I would like to thank all my friends Xieyang, Karima, Moamen, Firas, Anya, Damola, Vova, Grigory, Sasha and others for an unforgettably spent time together with you. I would like to say thank you to Alexey who helped me a lot at the beginning of my PhD in the Strasbourg and showed me this beautiful city. Thanks to Paul, the member of the SPB, with whom we together organized the career lunch during two years and had the opportunity to communicate with various people outside the academy. Thanks to my friends from Kazan: Katya, Nina and Lena for their support and love.

Most importantly, I would like to say thank you to my mother for the support of my aspiration in the scientific work. I am very grateful to my beloved husband for his understanding, care and constant support of me at any difficult moment.

Thanks to all of you that during important period of my life I always was together with such wonderful people like you.

"We can only be said to be alive in those moments when our hearts are conscious of our treasures." – Thornton Wilder

ABBREVIATIONS

Å	Angstrom unit (1Å =10^{-10} m)
aa-tRNA	aminoacyl-tRNA
ABC	ATP binding cassette
AglA	agelastatin A
agr	accessory gene regulator
AME	aminoglycoside modifying enzymes
anti-SD	anti-Shine Dalgarno sequence
DMF	dimethylformamide
A-site	aminoacyl site, (A-tRNA – A-site tRNA)
BHI	Brain Heart Infusion broth
BSI	blood stream infections
CAMP	cationic antimicrobial peptide
CA-MRSA	community-associated MRSA
CAT	chloramphenicol acetyltransferases
CHX	cycloheximide
CL	chlorolissoclimide
CML	chronic myelogenous leukemia
CNS	coagulase-negative staphylococci
Cryo-EM	cryo-electron microscopy
DAP	daptomycin
DMSO	dimethyl solfoxide
EDTA	ethylenediaminetetraacetic acid
EG	ethyloene glycol
E-site	exit site (E-tRNA – E-site tRNA)
GDP	guanosine diphosphate
GSH	conjugation of glutathione
GTP	guanosine triphosphate
HGT	horizontal gene transfer
HPF	hibernation-promoting factor
ICU	intensive care unit
LSU	Large Sub-Unit
MGE	mobile genetic element
MLST	multilocus sequence typing
MPD	3-methyl,1, 5-pentanediol
mRNA	messenger ribonucleic acid
MRP1	multidrug resistance-associated protein 1
MRSA	methicillin-susceptible *S. aureus*
MXR	mitoxantrone resistance protein
NHNS	National Healthcare Safety Network

NMR	nuclear magnetic resonance
PAGE	polyacrylamide gel electrophoresis
PEG	polyethylene glycol
P-site	peptidyl site, (P-tRNA – P-site tRNA)
PTC	peptidyl transferase centre
PVL	Panton–Valentine leukocidin
rRNA	ribosomal ribonucleic acid
sae	staphylococcal accessory element
sarA	staphylococcal accessory regulator A
SCCmec	staphylococcal chromosomal cassette mec
SD	Shine-Dalgarno
SDS	sodium dodecyl sulfate
smFRET	single-molecule fluorescence resonance energy transfer
SSSS	Staphylococcal Scalded Skin Syndrome
SSTI	soft tissue infections
SSU	Small Sub-Unit
tRNA	transfer ribonucleic acid
$tRNA^{fMet}$	N-Formylmethionine-tRNA
TSS	toxic shock syndrome
VAP	ventilator-associated pneumonia
VISA	vancomycin-intermediate *S. aureus*
VRSA	vancomycin-resistant S. aureus
YPD	Yeast extract Peptone Dextrose
σ^A	sigma factor A
σ^B	sigma factor B

RÉSUMÉ DE THÈSE

La biosynthèse protéique est un processus fondamental, retrouvé au sein de toutes les cellules, qui permet d'assurer le décodage de l'information génétique. Ce mécanisme de traduction implique de nombreux partenaires, protéines et acides nucléiques, et nécessite une parfaite coordination de leurs actions afin d'assurer la fidélité du transfert de l'information génétique. Le ribosome est l'acteur central de ce processus de traduction. Abondant dans les cellules et conservé au cours de l'évolution, celui-ci est composé de deux sous-unités, une petite et une grande, combinant des protéines et des acides nucléiques qui s'associent au cours de la traduction pour former un ribosome fonctionnel. Dans cet état, le ribosome est capable de catalyser l'addition séquentielle des acides aminés de la chaîne peptidique en cours de synthèse en utilisant l'ARN messager (ARNm) comme matrice et les ARN de transfert aminoacylés (aa-ARNt) comme substrats. Les deux sous-unités présentent des fonctions bien distinctes. Le décodage de l'information génétique contenu dans l'ARNm est assuré par la petite sous-unité tandis que la grande sous-unité catalyse la réaction de transpeptidation permettant la formation d'une liaison peptidique entre chaque acide aminé. Une dizaine de facteurs protéiques se lient successivement au ribosome afin de catalyser les différentes étapes de la traduction, à savoir: l'initiation, l'élongation, la terminaison et le recyclage. Bien que la synthèse des protéines conservée parmi tout les domaines du vivant, tous les organismes ont des spécificités. Soit, les bactéries Gram positives et Gram négatives ont leurs propres spécificités concernant la régulation et l'organisation de la machinerie traductionnelle.

Les structures à haute résolution des ribosomes et sous-unités ribosomales obtenues par cristallographie aux rayons X et microscopie électronique ont révolutionnées le domaine de la traduction des protéines. La connaissance des positions précises des résidus dans le ribosome dans divers états a conduit à une meilleure compréhension des mécanismes complexes de la synthèse des protéines. Les structures de complexes ribosomaux avec des antibiotiques et des composés antifongiques ont fourni un aperçu sans précédent de leurs mécanismes d'action et facilitent également la conception de médicaments plus efficaces (Garreau de Loubresse et al, 2014; revue Wilson, 2014). Il a été découvert que la plupart des inhibiteurs de la traduction se lient aux régions conservées des ribosomes (centre de peptidyltransférase, les sites de liaison d'ARNt, tunnel de sortie de la protéine, etc.). Cependant, les effets d'un même médicament sur des espèces différentes peuvent varier. Un excellent exemple est fourni par les bactéries résistantes à de nombreux antibiotiques couramment utilisés. Parmi celles-ci, *Staphylococcus aureus* (*S. aureus*), un agent pathogène qui provoque de graves et nombreuses infections chez l'homme. Cette bactérie est assez unique et donc, requiert une approche individuelle pour le traitement.

Les projets de la présente thèse ont progressé dans deux directions différentes et avec deux organismes différents: *Staphylococcus aureus* et *Saccharomyces cerevisiae*.

S. aureus est responsable des infections nosocomiales et infections sévères et peuvent causer une variété de maladies potentiellement mortelles chez l'homme. Ces infections comprennent l'endocardite, la péritonite, pneumonie nécrosante, la bactériémie, la méningite, l'ostéomyélite, l'arthrite septique, et les infections des os, des articulations et des organes (Fridkin et al, 2005).

S. aureus est un pathogène majeur d'une importance croissante en raison de sa haute résistance aux antibiotiques (Lowy, 1998). Un rapport par l'Organisation mondiale de la Santé (OMS) révèle que la résistance aux antimicrobiens, y compris la résistance aux antibiotiques n'est plus une prédiction pour l'avenir, elle se passe maintenant dans toutes les régions du monde et a le potentiel de toucher tout le monde, de tout âge, dans tous les pays. La résistance aux antibiotiques est maintenant une menace

majeure pour la santé publique. Selon ce rapport, pas moins de 60% des infections à S. aureus sont déterminées comme résistantes à la méthicilline (SARM) en Europe (World Health Organization, 2015).

Les gènes responsables de la résistance sont souvent transmis par des éléments génétiques mobiles tels que les plasmides et, par conséquent, populations bactériennes peuvent acquérir une résistance très rapidement. Divers mécanismes de résistance aux antibiotiques. Les bactéries peuvent empêcher la pénétration de l'antibiotique dans la cellule, le retirer de la cellule en utilisant une pompe d'efflux , de dégrader ou modifier l'antibiotique . Alternativement les bactéries peuvent muter , modifier ou protéger les cibles des antibiotiques. La conception de nouveaux agents antimicrobiens est fortement requise pour le traitement des maladies causées par *S. aureus*. Pour comprendre les aspects structurels de la résistance aux antibiotiques nous avons besoin de connaître la structure de leur cible. Par conséquent nous nous sommes concentrés sur la structure du ribosome, qui est la principale cible des antibiotiques les plus couramment utilisés. La résolution de la structure du ribosome de *S. aureus* sera la première étape vers la compréhension du mécanisme précis de sa résistance aux antibiotiques et facilitera la conception de nouveaux composés antistaphylococciques.

Les ribosomes bactéries et eucaryotes partagent une structure minimale conservée et présentent une série de protéines et d'éléments d'ARNr spécifiques à chaque domaine du vivant. Cette variation de structure se traduit par un changement de poids moléculaire. Avec une masse totale avoisinant 3.3 MDa, le ribosome eucaryote est 40% plus volumineux que son homologue bactérien. Bien que les étapes clés de la synthèse protéique soient conservées chez les bactéries et les eucaryotes, les fonctions endossées par le ribosome eucaryote présentent de nombreuses spécificités. Chez les bactéries, une dizaine de facteurs protéiques se lient successivement au ribosome afin de catalyser les différentes étapes de la traduction, à savoir : l'initiation, l'élongation, la terminaison et le recyclage. En revanche, les mécanismes de la synthèse des protéines chez les eucaryotes diffèrent à plusieurs niveaux. A titre d'exemple, jusqu'à treize facteurs distincts sont impliqués dans l'étape d'initiation de la traduction chez les eucaryotes. Par ailleurs, les étapes de terminaison et de recyclage s'opèrent de manière différente et requièrent la participation de facteurs non conservés chez les bactéries. L'assemblage du ribosome eucaryote est hautement contrôlé et implique une centaine de facteurs. Enfin, hormis son rôle prépondérant dans la synthèse protéique, le ribosome eucaryote et ses constituants participent activement à la régulation de l'expression des gènes.

Projet de recherche 1: Analyse structurale et étude du ribosome de Staphylococcus aureus.

Le projet dédié à de déterminer la structure cristallographique du ribosome de *S. aureus* a été initié en 2011 dans le laboratoire de Yusupov. Cependant, des difficultés spécifiques pour obtenir une diffraction à haute résolution des cristaux de ribosomes de *S. aureus* 70S n'ont pas permis de résoudre sa structure.

On sait que certains aspects de la synthèse des protéines diffèrent entre les bactéries Gram négatif et Gram positif. En outre, les bactéries pathogènes ont développé des mécanismes complexes de régulation de la traduction, qui fournissent une efficacité élevée de la pathogenèse et facilitent la survie dans des conditions stressantes. De plus, de nombreuses bactéries pathogènes (y compris *S. aureus*) montrent une résistance extrêmement élevée aux antibiotiques ciblant les ribosomes, qui est souvent médiée par des modifications du ribosome. La structure cristalline du ribosome des bactéries pathogènes multirésistantes Gram-positives *S. aureus* révélerait des caractéristiques structurelles particulières de la machinerie de traduction, ce qui nous amènera à mieux comprendre les spécifications de la régulation de sa synthèse protéique et de la survie des agents pathogènes. Plus important encore, il servira de modèle pour développer de nouveaux médicaments anti-staphylococciques et rendre le traitement médical plus efficace. De nombreux antibiotiques agissent en inhibant sélectivement la synthèse des protéines dans les

bactéries, sans perturber les ribosomes hôtes et, par conséquent, leurs cellules. Les structures cristallines d'antibiotiques produits naturellement et leurs dérivés semi-synthétiques liés aux particules ribosomiques ont fourni un aperçu de leurs mécanismes d'action, et ils facilitent également la conception d'antibiotiques plus efficaces pour cibler les bactéries multirésistantes.

Mon objectif principal de ce projet était d'élucider la structure du ribosome 70S complet de *S. aureus* en utilisant l'analyse des rayons X comme outil principal. Ainsi le projet consistait en des tâches suivantes:

- la préparation des cellules: culture, la récolte, lyse ;
- modification du protocole initial de purification du ribosome 70S de *S.aure*us (issu du laboratoire de Yusupov) qui fournira des ribosomes purs et stables, convenant à la cristallisation;
- stabilisation du ribosome 70S par deux voies de formation de complexe avec l'ARNt fMet, l'ARNm et avec le domaine N-terminal du facteur favorisant l'hibernation (HPF);
- traitement de cristallisation et de post-cristallisation: recherche de conditions de cristallisation, croissance de gros cristaux et préparation pour l'analyse par diffraction;
- développer la stratégie de collecte de données au synchrotron;
- résoudre la structure: traiter les données et construire le modèle.

Initialement, le protocole de purification des ribosomes de *S. aureus* a été créé et développé dans le laboratoire Yusupov (Khusainov et al., 2016) sur la base des protocoles utilisés pour les bactéries *Thermus thermophilus* (Gogia et al., 1986, Yusupov et al., 2001) et de levures *Saccharomyces cerevisiae* (Ben-Shem et al., 2011). Malheureusement, l'échantillon obtenu après ce protocole n'était pas assez homogène et les cristaux obtenus à partir de cet échantillon donnaient de mauvaises diffractions (19 Å), même après une optimisation des conditions de cryo-protection. Les derniers, selon l'analyse cryo -EM des ribosomes, nous avons obtenu un résultat dans lequel environ 10% de ribosomes ont une contamination par l'ARNt (A / P, P / p, P / E, E) et presque tous liés au site P du ribosome. Ainsi, l'ARNt peptydil qui a probablement un peptide à la surface du ribosome pourrait influencer la diffraction. Donc, ma tâche principale était de se débarrasser des impuretés de l'ARNt. Pour atteindre cet objectif, un certain nombre d'expériences ont été réalisées pour modifier le protocole de purification des ribosomes.

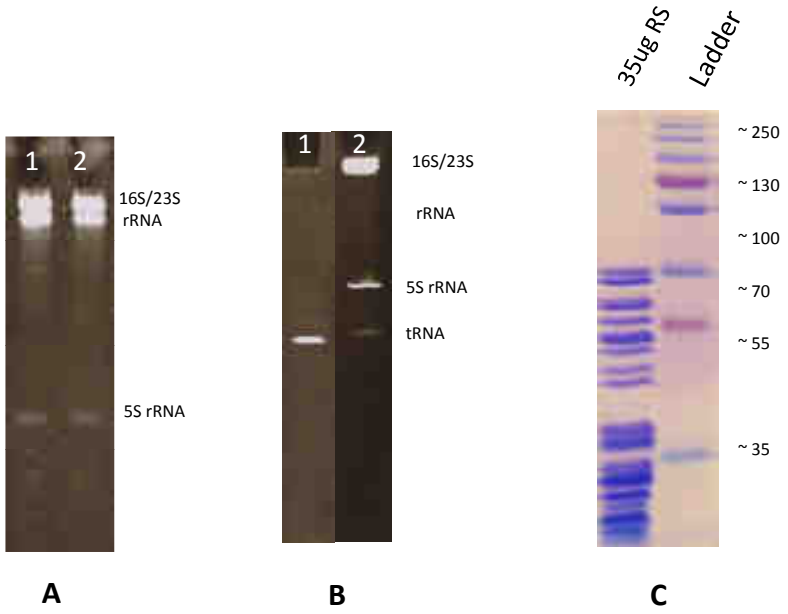

Fig I: Gel de polyacrylamide Electrophorèse de l'échantillon de S. aureus ribosome. A) Dénaturation de l'ARN PAGE 4%: 1 - après modification du protocole de purification (9µg), 2 - sans modification du protocole de purification (contrôle) (9µg). B) Dénaturation de l'ARN PAGE 12%: 1 - tRNAfMet (1µg), 2 - après modification du protocole de purification (9µg). C) SDS PAGE unidimensionnelle: après modification du protocole de purification.

Selon la Fig IA, nous avons observé trois bandes correspondant à l'ARNr 23S, 16S et à l'ARN 5S pour le contrôle et pour l'échantillon de ribosome après modification du protocole de purification. Cependant, en raison de la PAGE 4%, nous ne pouvons pas interpréter les résultats concernant la contamination par l'ARNt, car la taille du pore du gel était grande pour une petite taille d'ARNt. A cet effet, a été réalisée PAGE 12% (Fig IB) et nous avons pu observer une réduction de l'intensité dans les bandes de contaminations ARNt comparer avec témoin (pour plus de détails voir le chapitre avec la caractérisation de l'échantillon de ribosome). Nous avons analysé l'échantillon après modifications du protocole pour éliminer les protéines non ribosomiques et le gel SDS a démontré la pureté de l'échantillon ribosomique et n'a pas révélé de contamination par des protéines de haut poids moléculaire comme les composants du complexe pyruvate déshydrogénase, qui co-purifient parfois avec des bactéries ribosomes (Fig IC).

Particules cristallines initiales de ribosome 70S de *S. aureus* ont été obtenus en utilisant une recherche robotique. Après plusieurs étapes d'optimisation de cristallisation, de grands cristaux tridimensionnels ont été obtenus. Typiquement, les cristaux sont apparus de façon reproductible dans les 7 - 10 jours et ont atteint leur taille moyenne (100 × 50 × 20 µm) après deux semaines supplémentaires.

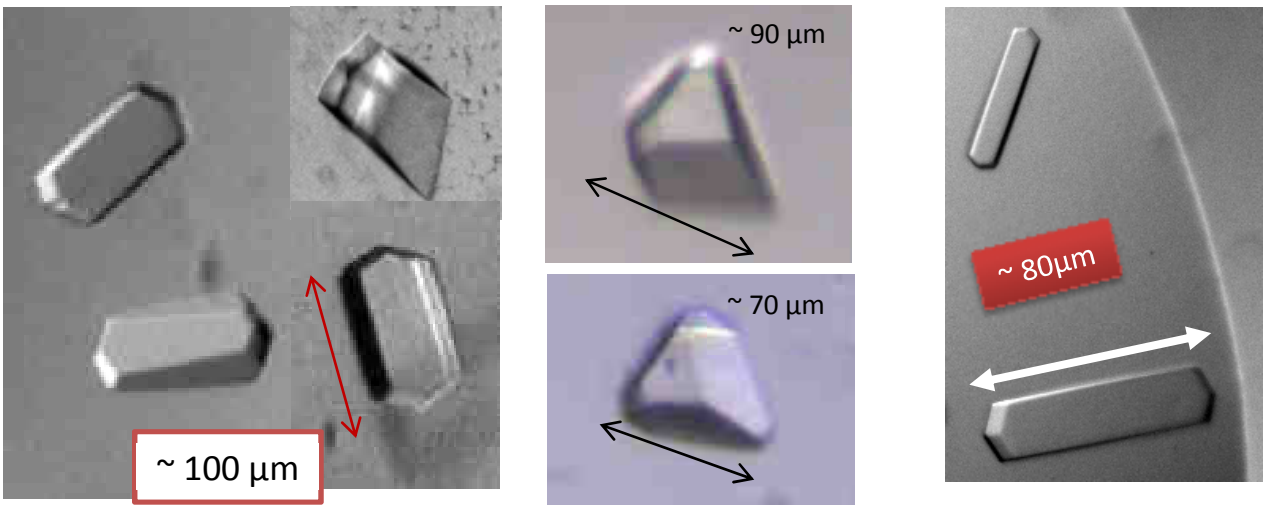

2µl + 2µl CrysChem plate
100 mM Tris-Acetate pH 7.0
400 mM KSCN
5.5 % PEG 8000
10% MPD
2.0 mM Spermedine
8 mg/ml Ribosomes

2µl+2µl CrysChem plate
100 mM Tris-Acetate pH 7.0
400 mM KSCN
5.2-6.0 % PEG 8000
10% MPD
10 mM $Mg(OAc)_2$
8 mg/ml Ribosomes

0.2µl+0.2µl MRC 2 drop plate
100 mM Tris-Acetate pH 7.0
9 mM Mg(OAc)2
500 mM NH4SCN
5 % PEG 8000
6% MPD
2% PEG400
10% Sucrose
8 mg/ml Ribosomes

Fig II: Les cristaux du ribosome 70S de *S. aureus*

La taille des cristaux de ribosome de *S. aureus* est suffisante pour l'analyse par diffraction aux rayons X. Les conditions de déshydratation et de cryo-refroidissement ont été optimisées pour les cristaux obtenus. Les premières données de diffraction de cristaux du ribosome 70S de *S. aureus* ont été recueillies. La diffraction de ces cristaux atteint au maximum 17.5 Å, le groupe de l'espace a été déterminée comme $P4_22_12$ et la taille de l'unité asymétrique était: 450 × 450 × 280 Å. Dans le but d'améliorer la diffraction des cristaux à partir du ribosome de *S.aureus*, nous avons essayé de stabiliser notre macromolécule en raison de la formation complexe avec l'ARNt fMet et l'ARNm et les cristaux obtenus apparaissaient de façon reproductible dans les 30-35 jours et atteignaient leur taille moyenne (200 × 80 × 20 µm) après deux semaines supplémentaires.

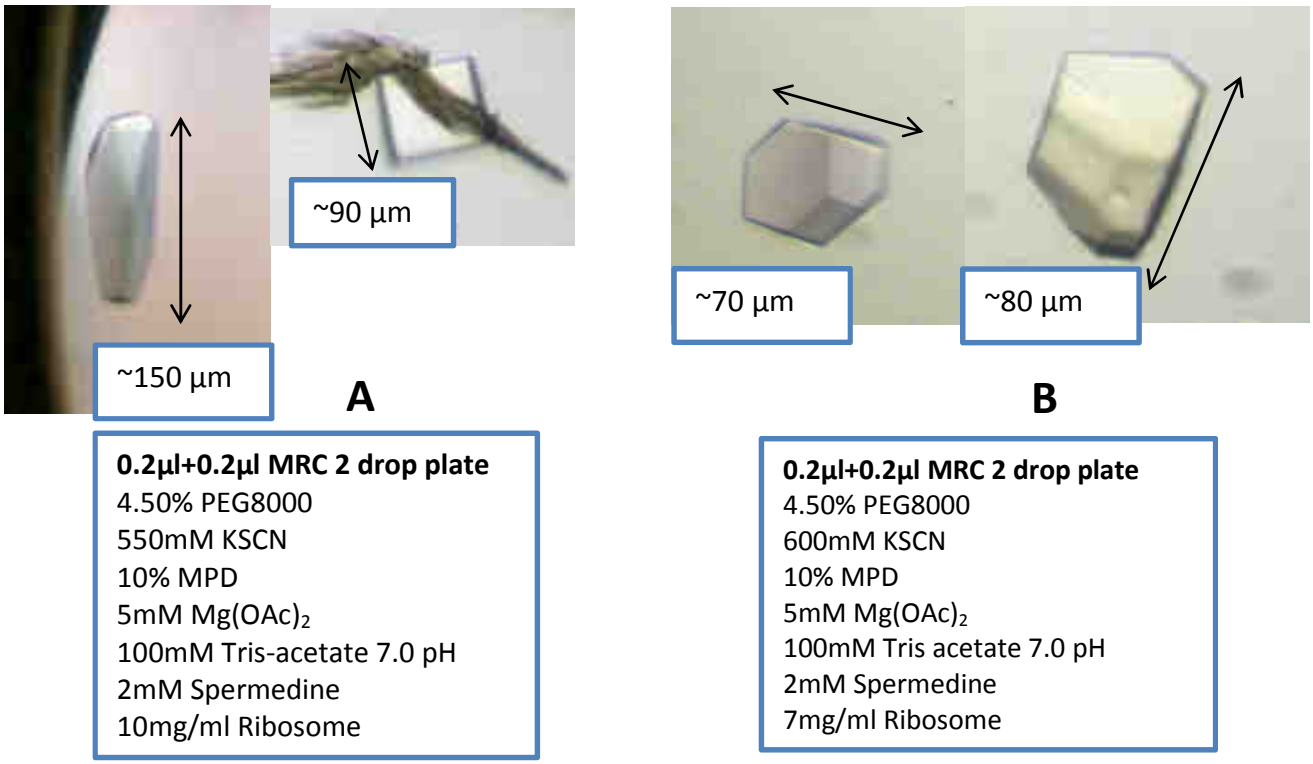

Fig III: Les cristaux du ribosome 70S avec ARNt fMet (A) et avec ARNt fMet et l'ARNm (B).

S. aureus facteur de promotion de l'hibernation (HPF) domaine N – terminal (SaHPF-NTD) se lie à la petite sous-unité est similaire à ses homologues de *E. coli* HPF, E. coli YfiA, et un YfiA spécifique de plaste (Khusainov et al, 2017). Et selon la suggestion (Polikanov et al., 2012) que YfiA empêche la tête (30S) de déplacer du ribosome et stabilise la macromolécule entière. Nous avons décidé de co-cristalliser le SaHPF-NTD avec le ribosome afin de stabiliser notre assemblage et potentiellement améliorer notre résolution des ribosomes de *S. aureus*.

Nous avons obtenu des cristaux qui apparaissent reproductiblement dans les 7 à 15 jours et ont atteint leur taille moyenne (100 × 50 × 20 µm) après deux semaines supplémentaires. Tous ces cristaux après formation complexe ont été diffractés à une résolution maximale de 17.5 Å.

Toutes les études obtenues dans ce travail faciliteront les recherches ultérieures dans la direction cristallographique du ribosome 70S de *S. aureus*, qui aidera à obtenir une structure à haute résolution dans un proche avenir. Les résultats obtenus serviront de base pour le développement de nouveaux composés contre la bactérie pathogène et extrêmement résistante qu'est *S. aureus*.

***Projet de recherche 2:* Analyse structurale et étude des médicaments antitumoraux potentiels**

Le ribosome est un propulseur central de tout procédé cellulaire. Il est donc considéré comme la cible privilégiée des petites molécules inhibitrices. Certains inhibiteurs spécifiques du ribosome eucaryote (naturels ou synthétisés chimiquement) sont maintenant considérés comme de potentiels médicaments anticancéreux.

Il est fermement établi que la quantité de ribosomes est fortement corrélée avec le taux de synthèse des protéines et la croissance et la prolifération des cellules. Il est important de prendre en compte dans le cas des cellules cancéreuses, ce qui montre une augmentation globale de la synthèse des protéines pour favoriser leur comportement hyperprolifératif. Le ribosome est donc devenu une importante cible

druggable. Les inhibiteurs de la synthèse des protéines eucaryotiques ont montré un potentiel thérapeutique important pour traiter une large gamme de cancers humains. En tant qu'exemple principal, en 2012, la FDA a approuvé le premier inhibiteur de la traduction, l'alcaloïde d'homoharringtonine naturel, tel que Synribo pour le traitement de la leucémie myéloïde chronique. Pour étudier le mécanisme d'action de ces inhibiteurs ciblant le ribosome eucaryote, dans le laboratoire Yusupov a résolu récemment la structure de 17 molécules petites différentes ciblant le ribosome 80S de *S. cerevisiae* (Garreau de Loubresse et al, 2014; Prokhorova et al.,2016; McClary et al.,2017).

Mon objectif principal était de déchiffrer le mécanisme moléculaire de liaison des inhibiteurs spécifiques antitumoraux, qui par la suite pourraient conduire à définir d'autres stratégies de conception de médicaments pour obtenir de nouveaux composés avec une puissance plus élevée tout en ayant une cytotoxicité inférieure. Je m'intéressais particulièrement à l'analyse de la structure du médicament chimiothérapeutique cisplatine et d'un analogue nouvellement synthétisé du chlorolissoclimide (nommé C45) avec les ribosomes eucaryotes.

Les médicaments chimio-thérapeutiques peuvent causer une neurotoxicité périphérique (neuropathie) et une neurotoxicité centrale (déficits cognitifs mineurs, encéphalopathie, démence, coma). Le cisplatine, utilisé contre diverses tumeurs malignes, induit une neurotoxicité périphérique, souvent accompagnée d'une aggravation hors thérapie, d'un signe de Lhermitte et de crampes musculaires. La neurotoxicité périphérique se développe chez environ 50% des patients traités au cisplatine. Une connaissance détaillée des sites de liaison du cisplatine au niveau de l'ARN ribosomique peut non seulement constituer un outil de prédiction des sites de modification d'autres ARN cellulaires essentiels, mais aiderait également à concevoir des études expérimentales sur la nature polyvalente de la cytotoxicité du cisplatine. Par conséquent, cela aiderait à résoudre les problèmes d'effets secondaires importants.

Notre groupe a récemment publié une étude multidisciplinaire dans laquelle nous démêlons le mécanisme d'action du chlorolissoclimide (CL), un composé qui partage la similarité chimique avec le cycloheximide (CHX), mais présentant une cytotoxicité inférieure prometteuse (Könst et al., 2017). CL se lie au site E de la sous-unité 60S et crée de nouvelles interactions par rapport à CHX. En détails, il crée une interaction inhabituelle d'empilement d'halogène-π avec le résidu G2794 à travers son atome de chlore. Nous nous sommes intéressés à ce nouveau type d'interaction avec le ribosome et nous avons donc décidé de résoudre la structure cristalline du S.cerevisiae 80S en complexe avec un autre composé de lissoclimide, porteur d'un atome de chlore supplémentaire. Le couplage de structures à haute résolution avec la conception de médicaments assistée par ordinateur et l'analyse de transfert d'énergie par résonance de fluorescence à une seule molécule (smFRET) guidera davantage la conception d'inhibiteurs plus sélectifs et moins cytotoxiques.

Le modèle eucaryote du ribosome que j'ai utilisé était celui de *S. cerevisiae* qui a été étudié pendant plusieurs années dans notre laboratoire, ce qui en fait un outil bien connu pour les études structurales. À ce jour, 70% des cristaux de ribosomes de S. cerevisiae diffractent à des résolutions proches de 3.0 Å. Le protocole pour obtenir la structure du médicament anticancéreux potentiel et du cisplatine avec le ribosome eucaryote se composait de 6 étapes principales:

1) la croissance des cellules de levure;

2) purification du ribosome 80S à partir de S. cerevisiae;

3) la co-cristallisation du ribosome avec des médicaments antitumoraux potentiels appropriés à l'analyse par diffraction des rayons X;

4) cryo-protection et déshydratation du cristal (pour remplacer les molécules d'eau dans les cristaux et les protéger pendant le processus de refroidissement, cette étape est également nécessaire pour augmenter le tassement des molécules dans les cristaux);

5) la collecte de données à haute résolution et la résolution du problème de phase;

6) le modèle de construction et de raffinement.

Dans le cas du projet C45, grâce à des connaissances issues de la synthèse semi-synthétique et de la synthèse analogique, nous avons approfondi notre compréhension de la relation structure-activité dans la famille des inhibiteurs cytostatiques inhibiteurs de la traduction.

La structure cristalline du ribosome 80S de S. cerevisiae dans le complexe avec un échantillon synthétique de l'inhibiteur C45 a été résolue à une résolution maximale de 3.1 Å. Nous avons découvert la base structurelle de l'inhibition de la protéine syntèse avec l'étude co-cristallographique de C45 synthétique lié au ribosome. Le mode de liaison intéressant comprend un nouveau deux face sur l'interaction de chlore-π du ligand avec deux résidus de guanine. Cette interaction favorable basée sur la dispersion semble permettre une stabilisation du composé C45 dans le site E du ribosome, et donc des effets apparentés pourraient être exploités dans la conception d'autres ligands d'acide nucléique.

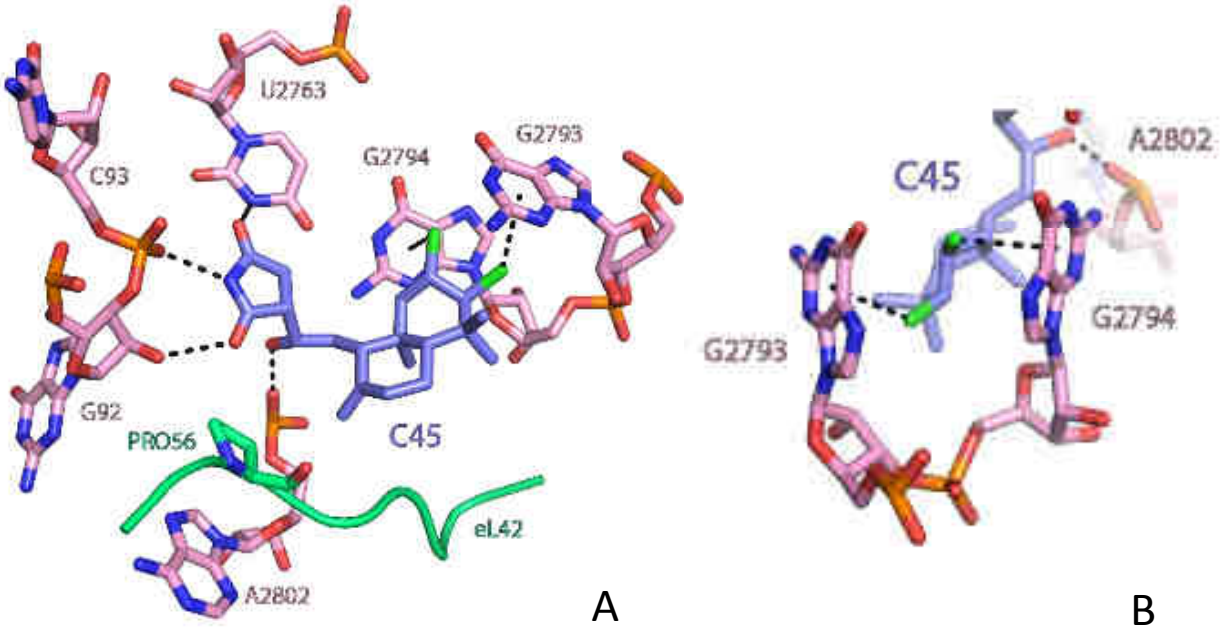

Fig IV: La structure cristalline aux rayons X du composé C45 avec le ribosome 80S eucaryote révèle la base moléculaire de l'inhibition de la traduction. A) Détails des interactions qui se produisent entre la molécule C45 (bleue, représentée par des bâtonnets) et les résidus voisins. Des contacts directs ont lieu avec les nucléotides G92, C93, U2763, A2802, G2794 et G2793 de l'ARNr 25S. B) Zoom de la poche de liaison de C45, avec le dichlorure diaxial dans le système d'anneau décalin créer une conformation en bateau torsadé dans laquelle les chlorures pseudoquatoriaux sont prêts pour deux interactions face-sur la géométrie halogène-π avec les guanines G2793 et G2794 de l'ARNr 25S.

Selon l'analyse de structure, le site de liaison C45 est situé à l'extrémité CCA de l'ARNt du site E sur les LSU, comme indiqué précédemment pour le chlorolossoclimide (CL) et les inhibiteurs de glutarimide

cycloheximide (CHX) et lactimidomycine (LTM) (Fig V). La comparaison de la liaison de C45 avec celle de CHX et CL montre un réseau similaire d'interactions de la fraction contenant de l'imide avec un certain nombre de nucléotides universellement conservés de l'ARNr 25S, à savoir G92, C93 et U2763

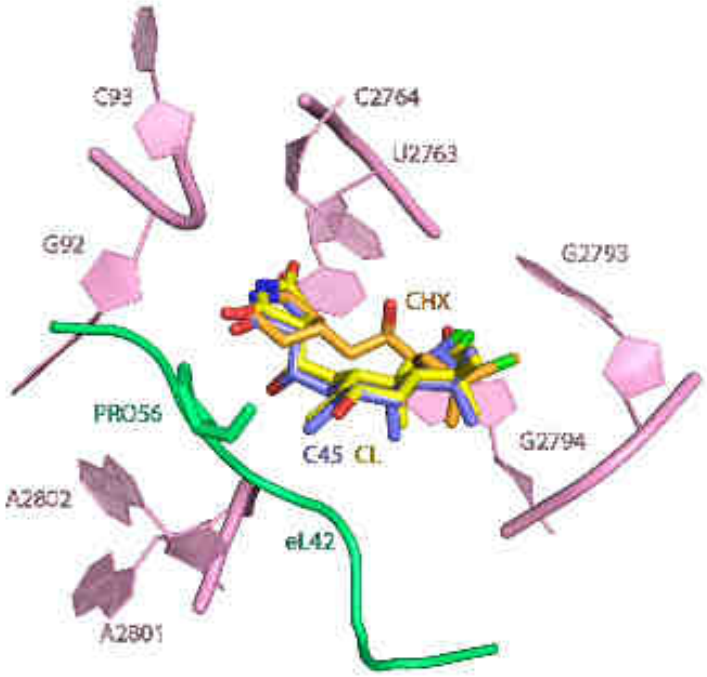

Fig V: C45, le chlorolissoclimide et la cycloheximide partagent la même poche de liaison dans le site E du 60S.

En outre, selon l'analyse FRET dans le complexe de pré-translocation ribosome humain, nous observons que C45 s'équilibre très lentement avec le ribosome sur une échelle de temps de dizaines de minutes, cependant, il a un très long temps de résidence une fois lié. De plus, nous avons calculé une constante de dissociation pour C45 et elle est en moyenne de 50 à 150 µM. En comparaison, CHX et CL sont respectivement d'environ 5.5 µM et 11.5 µM, montrant ainsi des affinités de liaison similaires. Le C45 est un liant plus faible que le CL, ce qui est bien corrélé avec les données publiées (Konst et al., 2017).

Concernant le projet complexe cisplatine / 80S, nous avons trouvé le rapport optimal du cisplatine (37.5 µM) pour le processus de co-cristallisation avec le ribosome eucaryote. Ceux-ci nous ont permis d'obtenir une bonne forme et une bonne taille de cristaux pour effectuer d'autres expériences de diffraction. En outre, nous avons déterminé l'influence du détergent (Deoxy-Big Chap) sur la formation du complexe cisplatine avec le ribosome. Très probablement dans ce cas, l'incubation du complexe avec le détergent, avant le processus de cristallisation, a réduit l'affinité de liaison du cisplatine au ribosome 80S. Nous avons également observé que le cisplatine lui-même influait sur la croissance cristalline et changeait de forme cristalline, passant du parallélépipède rectangulaire habituel au prisme hexagonal. Nous avons pu améliorer la diffraction des cristaux jusqu'à 4 Å. Ces données, nous avons obtenu uniquement dans les cristaux qui ont été trempés en présence de cisplatine (250 µM). Cependant, le rendement de la résolution moyenne était très faible, seulement 5%, ce qui rend difficile la construction de la structure. Dans le cas du ribosome de co-cristallisation avec le cisplatine, nous n'avions pas plus de 6-7 Å de résolution. Ainsi, le projet nécessiterait beaucoup de procédures d'optimisation et aussi, très probablement, l'évitement de l'osmium hexamine dans les cristaux, pour pouvoir utiliser le signal anormal provenant des quelques atomes de Pt

qui devraient se lier étroitement au ribosome. Cependant, jusqu'à présent, le traitement des S.cerevisiae 80S ribosome cristaux sans osmium hexamine donné que la diffraction pauvre.

En dépit du fait que l'osmium hexamine et le platine ont les mêmes sites de liaison dans le ribosome 80S de S.cerevisiae et appartiennent au groupe des métaux lourds, le remplacement de l'osmium hexamine dans la procédure de cryo-protection par le platine entraîne une réduction de la diffraction des cristaux.

La tentative d'exclure l'osmium des conditions normales de cryoprotection a échoué, et l'on peut donc conclure qu'il est nécessaire de changer le concept de processus de cryo-protection des cristaux de ribosomes 80S dans leur ensemble. A son tour, notre laboratoire est en train de développer cela de manière plus robuste.

PREFACE

The projects of the present PhD thesis have progressed in two different directions and with two diverse organisms: *Staphylococcus aureus* and *Saccharomyces cerevisiae.*

The first project is dedicated to determine the crystal structure of the 70S ribosome from *S. aureus* and was initiated in 2011 in the Yusupov's laboratory. However, specific difficulties to obtain high resolution diffraction of *S. aureus* 70S ribosome crystals did not give the opportunity to solve its structure.

It is known that some aspects of protein synthesis differ between Gram-negative and Gram-positive bacteria. Additionally, pathogenic bacteria have evolved complex mechanisms of translation regulation, that provides high efficiency of pathogenesis and facilitate survival under stressful conditions. Moreover, many pathogenic bacteria (including *S. aureus*) show extremely high resistance to ribosome-targeting antibiotics, which is often mediated by modifications of the ribosome. The crystal structure of the ribosome from Gram-positive multi-resistant pathogenic bacteria *S. aureus* would reveal peculiar structural features of translation machinery, thus will lead us to better understanding the specifications of regulation of its protein synthesis, and pathogen survival. Most importantly, it will serve as a model system for developing new anti-staphylococcal drugs and make medical treatment more efficient. Many antibiotics act by selectively inhibiting the protein synthesis in bacteria, without perturbing the host ribosomes and, therefore, their cells. Crystal structures of naturally produced antibiotics and their semi-synthetic derivatives bound to ribosomal particles have provided insight into their mechanisms of action, and they are also facilitating the design of more effective antibiotics for targeting multidrug-resistant bacteria.

My main goal of this project was to elucidate the structure of full 70S ribosome from *S. aureus* using X-ray analysis as a main tool. Thus the project consisted of next tasks:

- preparing the cells: growing, harvesting, breaking;
- modification of initial protocol of purification 70S ribosome from *S.aureus* (comes from Yusupov's laboratory) which will provide pure and stable ribosomes, suitable for crystallization;
- stabilization of 70S ribosome by two way of complex formation with tRNA ^{fMet}, mRNA and with N-terminal domain of hibernation promoting factor (HPF);
- crystallization and post-crystallization treatment: searching for crystallization conditions, growing big crystals and preparation for diffraction analysis;
- developing the strategy of data collection at the synchrotron;
- solving the structure: processing the data and building the model.

Results of my work on the determination of high resolution structure of the ribosome from *S. aureus* will be discussed in the following chapters.

In the second direction, the project aim is to determine the structure of potential anticancer drugs targeting the eukaryotic ribosome.

Ribosome is a central prop of all cellular process and it is thus considered as the favored target for small-molecules inhibitors. It is therefore intuitive that some eukaryotic specific inhibitors of the ribosome, natural product and chemical synthesized, are now considered as potential anticancer drug.

My main goal was to decipher the molecular mechanism of binding of specific antitumor inhibitors, which subsequently might lead to define further drug-design strategies to obtain new compounds with higher potency while having lower cytotoxicity.

I was particularly interested in the structure analysis of the chemotherapeutic drug cisplatin and a newly synthesized analogue of chlorolissoclimide (named C45) with the eukaryotic ribosomes.

Chemotherapeutic drugs may cause both peripheral neurotoxicity, consisting mainly of a peripheral neuropathy, and central neurotoxicity ranging from minor cognitive deficits to encephalopathy with dementia or even coma. Cisplatin – the platinum analogs, used for various malignancies, is the most important drug inducing peripheral neurotoxicity, with often off-therapy worsening, Lhermitte's sign, muscle cramps. Peripheral neurotoxicity develops in approximately 50% of patients receiving cisplatin. Platinum compounds are active in the treatment of solid tumors, but peripheral neuropathy is the major non-hematological dose-limiting adverse effect especially for cisplatin. For the moment, there is no effective strategy for the management of the neurotoxicity induced by platinum agents. Detailed knowledge of cisplatin binding sites in the ribosomal RNA may not only provide a tool for prediction of modification sites in other essential cellular RNAs, but will also help design experimental studies of the multifaceted nature of cisplatin cytotoxicity. Consequently, this structural knowledge might help to solve problems related to the strong side effects.

To study the mechanism of action of inhibitors targeting the eukaryotic ribosome, our group recently solved the structure of 17 different small molecules targeting the *S. cerevisiae* 80S ribosome (Garreau de Loubresse et al., 2014; Prokhorova et al., 2016). Additionally, our group recently published a multidisciplinary study in which we unravel the mechanism of action of chlorolissoclimide (CL), a compound sharing chemical similarity to cycloheximide (CHX), but showing promising lower cytotoxicity (Könst et al., 2017). CL binds to the E-site of the 60S subunit and creates novel interactions compared to CHX. In details, it creates an unusual halogen-π stacking interaction with residue G2794 through its chlorine atom. We were interested in this new type of interaction with the ribosome and therefore we decided to solve crystal structure of the *S.cerevisiae* 80S in complex with another lissoclimide compound, bearing an additional chlorine atom. The coupling of high-resolution structures with computationally-driven drug design and single-molecule fluorescence resonance energy transfer (smFRET) analysis will further guide the design of more selective and less cytotoxic inhibitors.

The eukaryotic model of the ribosome that I used was the one from *S. cerevisiae* that has been studied for several years in our laboratory, making it a well-understood tool for structural studies. To date, 70% of the *S. cerevisiae* ribosome crystals are diffracting at resolutions close to 3.0 Å. The protocol for getting the structure of the potential anticancer drug and cisplatin with the eukaryotic ribosome consisted of 6 main steps:

1) growing of yeast cells;
2) purification of 80S ribosome from *S. cerevisiae*;
3) co-crystallization of the ribosome with potential antitumor drugs suitable for X-ray diffraction analysis;
4) cryo-protection and dehydration of the crystal (to replace water molecules in the crystals and protect them during the cooling process. This step is also necessary to increase the packing of the molecules in the crystals);

5) data collection of high resolution data and, solving of the phase problem;
6) model building and refinement.

The results of my work on the determination of high resolution structures of potential antitumor drugs with the eukaryotic ribosome will be discussed in the in the following chapters.

General Introduction

I RIBOSOME CHARACTERIZATION

Ribosomes play a pivotal role in the molecular life of every cell. This assemble is fundamental macromolecular machines that function at the heart of the translation machinery, allowing the conversion of information encoded within messenger RNA (mRNA) into proteins. Ribosome itself becomes the link between the gene and the displayed protein. The genetic information encoded within DNA is transcribed into the form of mRNA within the cell nucleus, and this is then used as the template to produce the protein, using the ribosome as the translational machinery to assemble the full-length protein molecule. Normally, once the full-length protein has been produced, the ribosome dissociates from the mRNA, but if the signal instructing the ribosome to dissociate is missing, the ribosome stops at the end of the mRNA, providing a link between the mRNA and the newly produced protein.

1. RIBOSOME ORGANIZATION

All ribosomes are composed of two subunits, called small ribosomal subunit (SSU) and large ribosomal subunit (LSU). Ribosomes are composed of about equal amounts of rRNA (ribosomal ribonucleic acid), and proteins, with a little proportion of lipids and certain metallic ions such as Mg, Ca and Mn. Proteins and rRNA are the major constituents of ribosomes.

Subunits consist of rRNA(s) and proteins with average ratio of 2:1 RNA to protein (the exceptions are mitochondrial and chloroplast ribosomes which have ratios 1:2 and 3:2 respectively (see for review Sharma and Agrawal, 2012). rRNA(s) generally represents more than 80% of the total RNA present in cells (Warner, 1999). About 60% of total rRNA presents a helical configuration like DNA, but its base composition is not like that of Watson – Crick Model of DNA.

The rRNA contains specific number of methyl groups. At least a portion of RNA contains intramolecular hydrogen bonds. Regions of the molecule in the form of hairpin loops forming two stranded helices. Obviously, the configuration of rRNA in solution may not be the same as its configuration, where it is associated with ribosomal protein. About 2/3 of the mass of the ribosome consists of RNA and 1/3 of protein. Ribosomal proteins are among the most highly conserved proteins across all life forms. Many ribosomal proteins, particularly those of the large subunit, are composed of a globular, surfaced-exposed domain with long finger-like projections that extend into the rRNA core to stabilise its structure. Most of the proteins interact with multiple RNA elements, often from different domains. In the large subunit, about 1/3 of the rRNA nucleotides are at least in van der Waal's contact with protein.

The ribosome is an asymmetric macromolecular complex and each subunit has particular structural and functional organization, thus carries out different functions in translation (Figure 1).

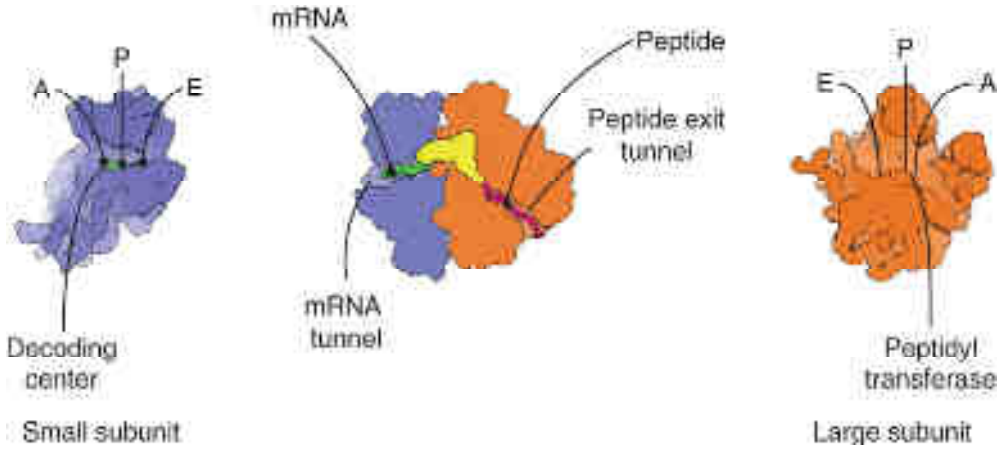

Figure 1: Structural organization and functional sites of the ribosome (adapted from Melnikov et al., 2012). The two ribosomal subunits (left and right) assemble together to form the full ribosome (center). Main functional sites and natural ligands (mRNA, tRNA) are annotated.

The small subunit is responsible for the decoding process where aminoacyl-tRNA (aa-tRNA) is selected according to the mRNA sequence. Its major functional sites are the mRNA path used to conduct mRNA during translation, the decoding center responsible for decoding, and the tRNA binding sites (A, P and E). The A-site serves to bind aminoacyl-tRNA as it enters into the ribosome during protein synthesis, the P-site holds tRNA carrying the nascent polypeptide chain (peptidyl- tRNA), and the E-site (exit) is where tRNA dissociates from the ribosome. During translation, tRNAs are translocated from the A to the P-site and from the P to the E-site. The large subunit catalyzes peptide bond formation. Its major functional sites are the tRNA binding sites (A, P and E), the peptide exit tunnel that extends through the body of the large subunit, and the peptidyl transferase centre (PTC). The PTC is responsible for peptide bond formation and is located at the entrance to the peptide tunnel in a conserved region on the interface that is mainly composed of rRNA. As a result of peptide bond formation in the PTC, the nascent polypeptide chain is transferred from the peptidyl-tRNA in the P- site to the aa-tRNA in the A-site, thus extending the nascent chain by one amino acid.

2. SPECIFICATIONS OF BACTERIAL AND EUKARYOTIC RIBOSOME

Despite the universal conservation of the core, ribosome composition varies between domains of life, taxonomic subgroups, organelles and even within a single individual, although to a smaller extent. Ribosomes may contain their own set of specific moieties: specific proteins, insertions and extensions of conserved proteins and expansion segments of rRNAs.

Ribosomes in the cytoplasm of eukaryotic cells have a sedimentation coefficient of about 80S (MW about 4.5 x 106) and are composed of 40S and 60S subunits. In prokaryotic cells, ribosomes are typically about 70S (MW about 2.7 x 106) and are formed from 30S and 50S subunits. Sedimentation coefficients are used to characterize and to name isolated or associated subunits.

Both the 70S and the 80S ribosomes are asymmetric assemblies of more than 50 different proteins and three or four RNA chains. Each ribosomal component is present in the ribosome as a single copy except for stalk proteins (L7 and L12 in bacteria, P proteins in eukaryotes) that are present in four or six copies. Early genetic data, corroborated by structural studies, revealed that bacterial and

eukaryotic ribosomes share a common structural core, comprising 34 conserved proteins and ~4,400 RNA bases, which harbors the major functional centers of the ribosomes, such as the decoding site, peptidyl transferase center and tRNA-binding sites (Figure 1).

Major differences in ribosome composition are observed between domains of life. Apart from the core, the bacterial ribosome (*E. coli* or *T. thermophilus*) contains 21 bacteria-specific proteins, a few extensions of the conserved proteins and of ribosomal RNA. The eukaryotic ribosome (*S. cerevisiae*) contains 46 eukaryote-specific proteins (800 kDa) and extensions and insertions in most of the proteins of the core (200 kDa), and the rRNA harbors several extensions in the conserved rRNA chains (about 800 nucleotides that account for 350 kDa) (Ben-Shem et al., 2011; Melnikov et al., 2012). Within each domain of life, the ribosomes usually contain the same set of rRNA and protein chains, and all divergence is achieved via variations of length and sequence of ribosomal components, mainly rRNA.

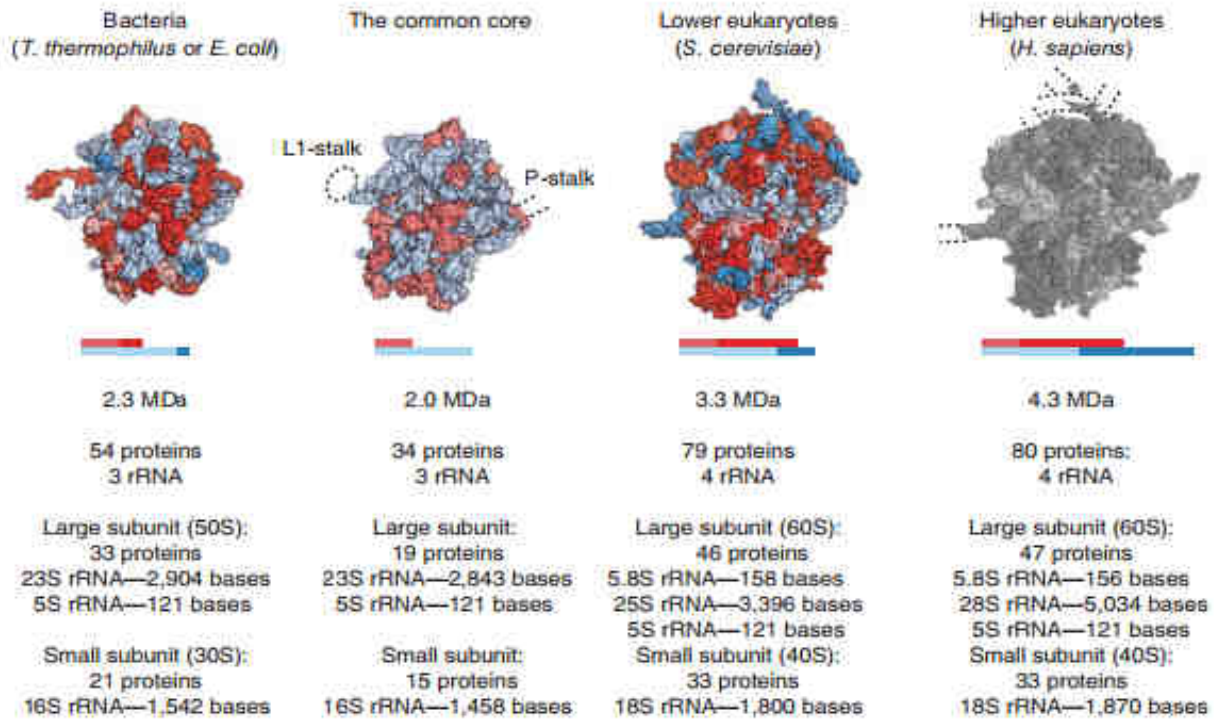

Figure 2: Composition of bacterial and eukaryotic ribosomes and the common core, based on X-Ray studies. The figure is based on X-ray and Cryo-EM structures from Armache et al., 2010, Ben-Shem et al., 2011, Jenner et al., 2010, Jarasch et al., 2012 (Melnikov et al., 2012).

Small subunits 30S and 40S have similar shapes, including the landmarks known as 'head', 'body', 'platform', 'beak' and 'shoulder' (Figure 3). The mRNA- and the three tRNA-binding sites are located on the subunit interface. The mRNA enters through a tunnel located between the head and the shoulder and wraps around the neck of the 30S subunit. The mRNA exit site is located between the head and the platform. The decoding center of the small subunit, where the codon and anticodon are paired is located on the interface surface and is made up of three domains from the head, shoulder and the penultimate stem. When comparing the overall structures, it is evident that there are extensive differences between eukaryotes and bacteria on the small ribosomal subunit solvent side (Figure 3C, D). These differences are directly correlated to the much more complex pathway of translation initiation known to exist in eukaryotic cells.

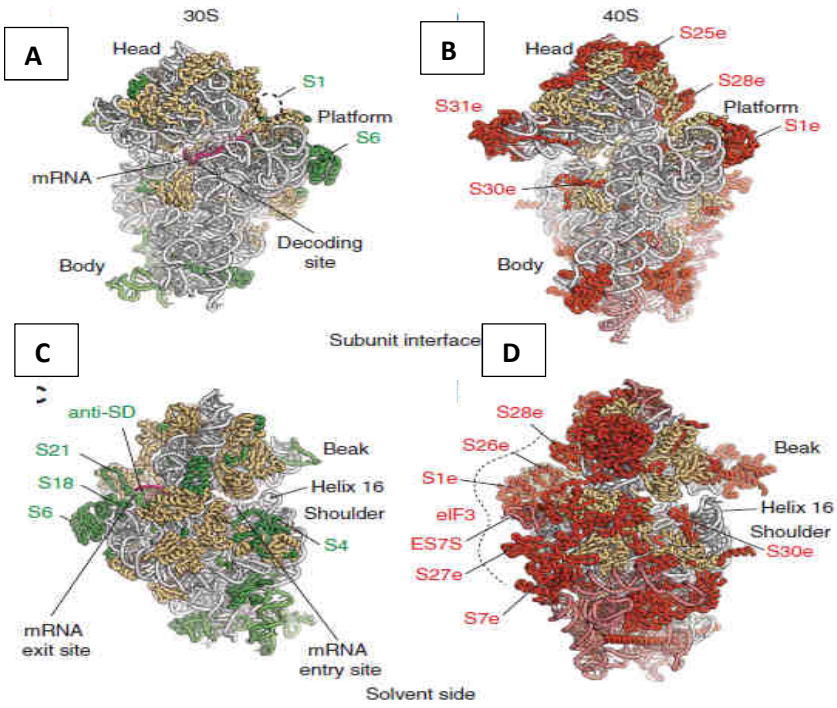

Figure 3: Bacteria- and eukaryote-specific proteins and RNA expansions of the small ribosomal subunit (Melnikov et al., 2012).

In case of the large subunits 50S and the 60S, they include the 'central protuberance', 'L1-stalk' and the 'L7/L12-stalk' ('P-stalk' in eukaryotes) (as we discussed before) (Figure 4). On the 60S ribosomal subunit, 27 eukaryote-specific proteins, multiple insertions and extensions of conserved proteins and several rRNA expansion segments are concentrated on the periphery of the subunit forming an almost continuous ring-shaped assembly enveloping the core (Figure 4B, D). This ring-shaped assembly comprises two clusters of eukaryote-specific moieties, for which little is known in terms of biological function.

Located on the interface side of the large ribosomal subunit are the three (A, P and E) tRNA-binding sites and the PTC where the peptide bond formation is catalyzed. This PTC is adjacent to the entrance of a tunnel along which nascent proteins progress before they emerge from the ribosome on the solvent side. The overall absence of bacteria- and eukaryote-specific moieties on the central regions of both the solvent and interface sides of the subunit is consistent with the universally conserved functions of these areas. This is seen at the PTC on the intersubunit surface that is relatively devoid of bacteria- and eukaryote-specific moieties as well as around the peptide tunnel on the solvent side, which is used for ribosome association with membranes during protein synthesis (Figure 4A–D). However, important structural differences between the 50S and the 60S subunits—are in the organization of the peptide tunnel and the surrounding area—which can be understood in terms of functional divergence (Melnikov et al., 2012).

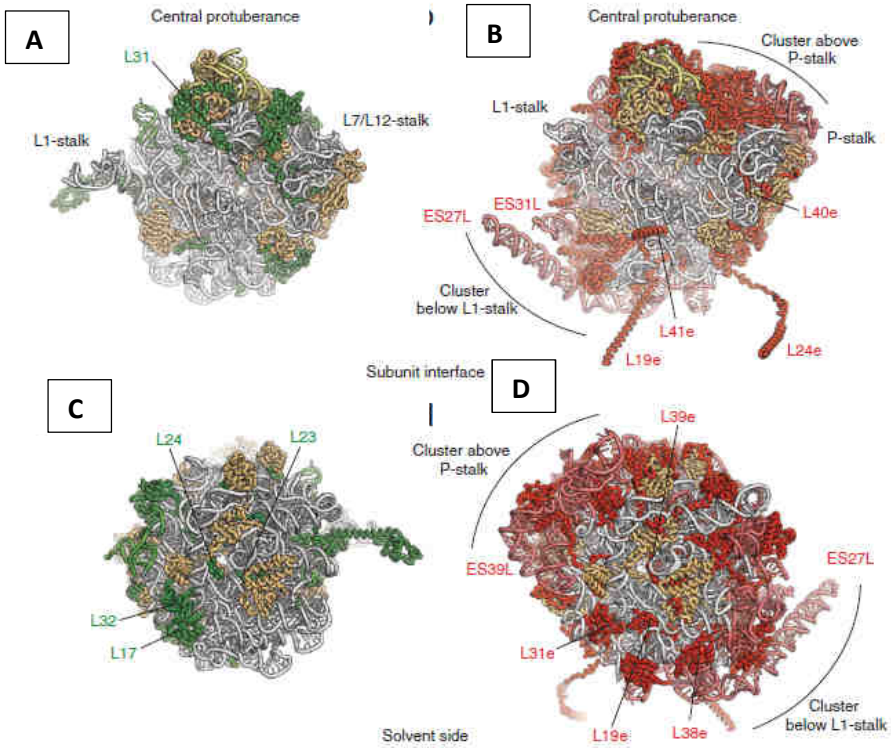

Figure 4: Bacteria- and eukaryote-specific proteins and RNA expansions of the large ribosomal subunit (Melnikov et al., 2012).

3. PROTEIN SYNTHESIS AS A KEY PROCESS OF LIFE

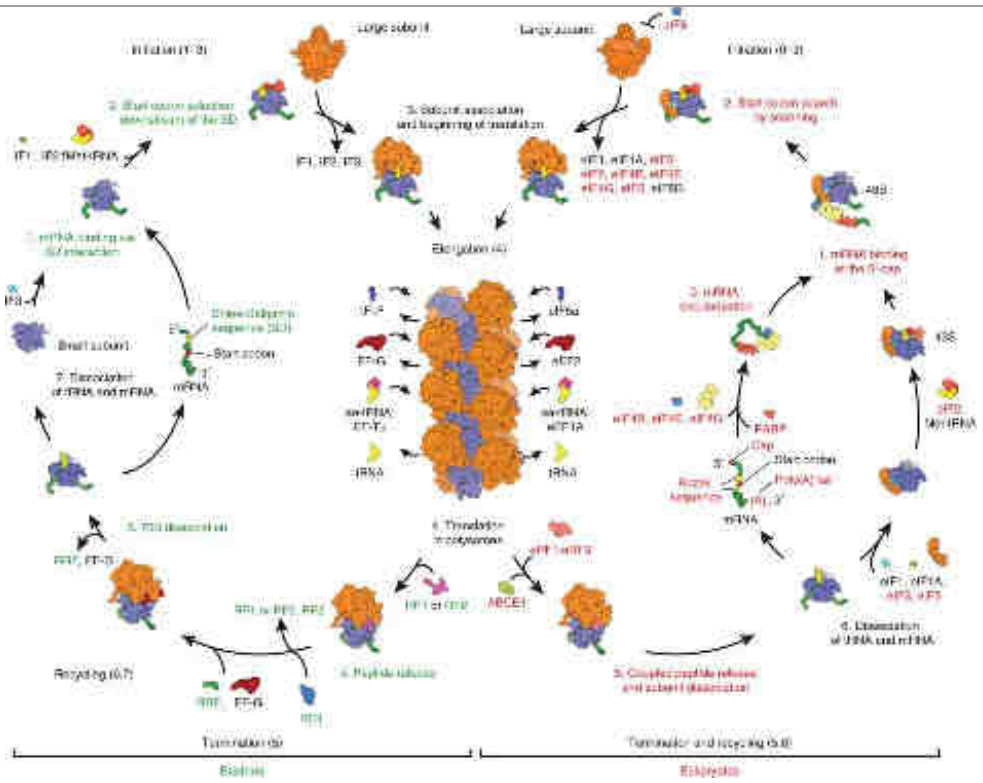

Figure 5: The translation cycle in bacteria and eukaryotes (Melnikov et al., 2012).

Translation is a four-stage process that includes the steps of initiation, elongation of the polypeptide chain, termination and recycling of the ribosomes. Each of these steps is assisted by protein factors termed initiation factors (IFs in bacteria or eIFs in eukaryotes), elongation factors (EFs or eEFs), release factors (RFs or eRFs) and recycling factors. The elongation step is the most conserved between bacteria and eukaryotes and is assisted by homologous elongation factors (Rodnina and Wintermeyer 2009).

3.1 INITIATION

Initiation of mRNA translation aims at assembling both ribosomal subunits and at positioning the mRNA start codon (AUG) together with initiator $tRNA^{Met}$ in the P site.

In bacteria, mRNA often exhibits a specific conserved sequence (Shine-Dalgarno sequence, SD) upstream to the AUG start codon that is complementary to the 3' end of the 16S rRNA in the small subunit (anti-SD). Formation of an SD/anti-SD duplex allows the 30S subunit to bind the mRNA and orient the AUG in the P-site. Initiator $tRNA^{fMet}$ is subsequently recruited and the large subunit joins the complex. Three initiation factors (IF1, IF2 and IF3) coordinate the process by binding to the 30S and leave the ribosome once initiation is complete (Figure 5.1-3). The mRNA and initiator N-formylmethionyl tRNA then join the complex, with IF-2 (which is bound to GTP) specifically recognizing the initiator tRNA. IF-3 is then released, allowing a 50S ribosomal subunit to associate with the complex. This association triggers the hydrolysis of GTP bound to IF-2, which leads to the release of IF-1 and IF-2 (bound to GDP). The result is the formation of a 70S initiation complex (with mRNA and initiator tRNA bound to the ribosome) that is ready to begin peptide bond formation during the elongation stage of translation.

Initiation in eukaryotes is more complicated and requires 13 canonical initiation factors composed of more than 30 polypeptides participate in the process and exhibit singularities at every stage, which are designated eIFs.

Before being enrolled in translation initiation, the 40S subunit associates with factors to form the 43S complex (Figure 5.0-3). This initiation-competent particle is composed of five distinct initiation factors: eIF1, eIF1A, eIF2/GTP/Met-$tRNA_i^{Met}$ ternary complex (TC), eIF3 and eIF5A (Jackson et al., 2010; Hinnebusch, 2011).

The assembly of initiation factors to the 40S subunit is sequential. When mRNA translation is completed, ribosomes are dissociated into subunits during the stage of recycling. However, deacetylated tRNA and mRNA remain attached to the small subunit. In this context, eIF3, 1 and 1A subsequently bind the 40S subunit and participate cooperatively in the removal of mRNA-tRNA ligands (Pisarev et al., 2007). Thus, initiation factors prepare the subunit for initiation and link the two opposite stages of translation. In addition, the binding of eIF1 and eIF1A respectively in P and A site induces an open conformation of the pre-initiation complex required to further accommodate mRNA. The 43S complex assembly is achieved when all three factors (1, 1A and 3) cooperate together to recruit and position eIF2 ternary complex and eIF5B on the solvent side. eIF2 is a heterotrimer GTPase protein which forms a stable complex with initiator Met-$tRNA_i^{Met}$ in the presence of GTP while eIF5B is a GTPase-activating protein (GAP) specific to eIF2 (Aitken and Lorsch, 2012).

The 43S complex is loaded at the 5' end of the mRNA. However, the distance between the 5' extremity and the AUG start codon can reach a thousand nucleotides. To meet its destination, the 43S complex slides on the mRNA 5'UTR, in a process called mRNA scanning, until it recognizes the start codon (Figure 5.2). Scanning requires both unwinding of mRNA structure and movement of the 43S complex

along the messenger. Evidences indicate that the ATP-dependent RNA helicase eIF4A, the most abundant initiation factor, participates in the process (von der Haar and McCarthy, 2002). The 43S complex is in a scanning-active conformation ready to encounter the AUG start codon. In fact, the mRNA latch is open and the initiator Met- $tRNA_i^{Met}$ is positioned in the P-site but not fully accommodated. When the AUG codon arrives in the P-site, the complete accommodation of Met-$tRNA_i^{Met}$ allows codon-anticodon base-pairing and triggers a cascade of reactions. As a consequence, eIF1 dissociates from the complex, its absence provokes the closing of the mRNA latch. The 43S complex switches to a scanning-inactive state. In parallel, eIF1 departure allows eIF5 to be repositioned in order to stimulate the eIF2 Pi release. Now in a GDP state, eIF2 leaves the initiation complex accompanied by eIF5. The departure of these factors promotes the binding of eIF5B-GTP, a GTPase initiation factor mediating subunit joining. Upon 60S subunit joining, eIF5B hydrolyzes its GTP that induces a conformational rearrangement of both subunits. After hydrolysis, eIF5B-GDP dissociates from the 80S ribosome as well as eIF1A. eIF3 however may remain associated with the ribosome during elongation, to some extent. At this step, initiation is over, leaving the ribosome associated with the mRNA and initiator Met-$tRNA_i^{Met}$ in P-site ready to engage the elongation stage (Aitken and Lorsch, 2012).

3.2 ELONGATION

After the initiation complex has formed, translation proceeds by elongation of the polypeptide chain. The mechanism of elongation in bacteria and eukaryotic cells is very similar (Figure 5.4). The initiator methionyl tRNA is bound at the P site. The first step in elongation is the binding of the next aminoacyl tRNA to the A site by pairing with the second codon of the mRNA. The aminoacyl tRNA is escorted to the ribosome by an elongation factor (EF-Tu in bacteria, eEF-1α in eukaryotes), which is complexed to GTP. The GTP is hydrolyzed to GDP as the correct aminoacyl tRNA is inserted into the A site of the ribosome and the elongation factor bound to GDP is released. The requirement for hydrolysis of GTP before EF-Tu or eEF-1α is released from the ribosome is the rate-limiting step in elongation and provides a time interval during which an incorrect aminoacyl tRNA, which would bind less strongly to the mRNA codon, can dissociate from the ribosome rather than being used for protein synthesis. Thus, the expenditure of a high-energy GTP at this step is an important contribution to accurate protein synthesis; it allows time for proofreading of the codon-anticodon pairing before the peptide bond forms.

Once EF-Tu (or eEF-1α) has left the ribosome, a peptide bond can be formed between the initiator methionyl tRNA at the P site and the second aminoacyl tRNA at the A site. This reaction is catalyzed by the large ribosomal subunit, with the rRNA playing a critical role (as already discussed). The result is the transfer of methionine to the aminoacyl tRNA at the A site of the ribosome, forming a peptidyl tRNA at this position and leaving the uncharged initiator tRNA at the P site. The next step in elongation is translocation, which requires another elongation factor (EF-G in bacteria, eEF-2 in eukaryotes) and is again coupled to GTP hydrolysis. During translocation, the ribosome moves three nucleotides along the mRNA, positioning the next codon in an empty A site. This step translocates the peptidyl tRNA from the A site to the P site, and the uncharged tRNA from the P site to the E site. The ribosome is then left with a peptidyl tRNA bound at the P site, and an empty A site. The binding of a new aminoacyl tRNA to the A site then induces the release of the uncharged tRNA from the E site, leaving the ribosome ready for insertion of the next amino acid in the growing polypeptide chain.

As elongation continues, the EF-Tu (or eEF-1α) that is released from the ribosome bound to GDP must be reconverted to its GTP form (Figure 5.4). This conversion requires a third elongation factor, EF-Ts (eEF-1βγ in eukaryotes), which binds to the EF-Tu/GDP complex and promotes the exchange of bound GDP for GTP. This exchange results in the regeneration of EF-Tu/GTP, which is now ready to escort a new aminoacyl tRNA to the A site of the ribosome, beginning a new cycle of elongation. The regulation of EF-Tu by GTP binding and hydrolysis illustrates a common means of the regulation of protein activities. Similar mechanisms control the activities of a wide variety of proteins involved in the regulation of cell growth and differentiation, as well as in protein transport and secretion (Cooper, 2000).

3.3 TERMINATION AND RECYCLING

Translation termination takes place when the end of the coding sequence is reached by the ribosome and a stop codon (UAA, UGA, or UAG) enters the A site. Termination **in eukaryotes** is catalyzed by two protein factors, eRF1 and eRF3, that appear to collaborate in the process (Stansfield et al. 1995; Zhouravleva et al. 1995; Alkalaeva et al. 2006). The class I factor, eRF1, is responsible for high-fidelity stop codon recognition and peptidyl-tRNA hydrolysis. The class II factor, eRF3 - a translational GTPase. Although bacteria also possess both class I (RF1 and RF2) and class II (RF3) release factors with similar nomenclature, there are striking structural and mechanistic differences between the classes in eukaryotes and bacteria. The release factors bind to a termination codon at the A site and stimulate hydrolysis of the bond between the tRNA and the polypeptide chain at the P site, resulting in release of the completed polypeptide from the ribosome.

After polypeptide release, both ribosomal subunits remain associated and contain a deacetylated tRNA in P-site, the mRNA and eRF1 (RF1 and RF2 in bacteria) in A-site. The post-termination complex has to be dissociated to promote the recycling of its components. Until recently, the mechanism responsible for ribosome recycling in eukaryotes, which is not conserved in bacteria, remains largely unclear. The first step consists of ribosome dissociation into subunits. The discovery of a new protein Rli1 in yeast (ABCE1 in human) resolves the situation (Khoshnevis et al., 2010; Pisarev et al., 2010). Rli1 is a multidomain protein composed of two nucleotide binding domains, a helix-turn-helix motif and an iron sulfer cluster (FeS) domain. Cryo-EM reconstructions of ribosomal complexes in the presence of termination factor homologs (Dom34/Hbs1) provide a structural understanding of the process (Becker et al., 2011; Becker et al., 2012; Franckenberg et al., 2012). When bound to the ribosome, the FeS domain of Rli1 makes contacts with eRF1. In fact, Rli1 appears to stimulate eRF1-mediated peptide release thus coupling termination to recycling (Shoemaker and Green, 2011).In addition, eRF1 is required for Rli1-mediated subunit dissociation. Rli1 binds to the ribosome in ADP-bound state. ATP binding and/or subsequent hydrolysis is suspected to provide the mechanic movement to split the ribosome in two subunits (Becker et al., 2012; Franckenberg et al., 2012).Interestingly, although not conserved, this scenario exhibits similarities with bacterial recycling. To complete recycling, the 40S-tRNA-mRNA complex has to be dissociated. A subset of initiation factors eIF1-eIF1A-eIF3 binds the 40S subunit and cooperatively promotes the release of tRNA and mRNA (Pisarev et al., 2007). Initiation factors remain on the small subunit, ready to engage initiation.

In bacteria, the class II release factor RF3, induces dissociation of the class I (RF1 and RF2) release factor, bringing the ribosome to the post-termination state containing an mRNA and a deacylated P-site tRNA (Freistroffer et al. 1997). To allow for a new round of initiation, the post-termination

ribosome is split into its large and small subunits (50S and 30S, respectively) in a GTP hydrolysis-dependent manner (Karimi et al. 1999; Hirokawa et al. 2005; Peske et al. 2005; Zavialov et al. 2005) by another GTPase, elongation factor G (EF-G), and ribosome recycling factor (RRF) (Hirashima and Kaji 1973; Janosi et al. 1996). After the split, binding of initiation factor 3 (IF3) to the 30S subunit prevents premature re-formation of a 70S ribosome (Hirokawa et al. 2005; Peske et al. 2005). Whether the deacylated tRNA and the mRNA dissociate from the 70S ribosome or from the 30S subunit after splitting and what role IF3 plays in the recycling process have been controversial. The latter model is based on experiments showing that: (1) RRF together with EF-G can induce splitting of the post-termination complex; (2) IF3 is required for recycling of the 30S subunit for formation of a new 70S initiation complex; (3) IF3 can induce dissociation of tRNA from the mRNA-bound 30S subunit (Karimi et al. 1999).

4. HISTORICAL ASPECTS OF STRUCTURAL STUDIES OF THE RIBOSOME

Ribosomes, which are “the heart of the protein biosynthesis” have been the focus of structural studies for more than 50 years. The reconstitution of some of the morphological features of the ribosome was performed many years ago. In the past ten years, high-resolution structures provided molecular details of different intermediates in ribosome-mediated translation. Together, these studies have revolutionized our understanding of the mechanism of protein biosynthesis. This success depended strictly on the advances in biochemical, biophysical and genetic studies and macromolecular crystallography that have been made during last decades.

At present the methods of structural biology are at the forefront in the understanding the molecular mechanisms of protein synthesis. Modern structural approaches are bringing fundamental biochemical knowledge about the ribosome accumulated during last century to an atomic level (when visualization of interactions between atoms is available). Pioneering works on structural investigation of biological material (mainly single proteins and nucleic acids) were made in the middle of 20th century using X-ray crystallography: structures of vitamin B12 (Hodgkin et al., 1956), insulin (Blundell et al., 1971), penicillin (Crowfoot et al., 1949) by D. Hodgkin and coworkers; helical structure of the DNA (Watson and Crick, 1953) by R. Franklin, J. Watson, F. Crick, M. Wilkins; structure of protein haemoglobin (Perutz et al., 1960); and many others. Later, in 1984 the laboratory of K. Wüthrich produced the first protein structure determined by NMR (nuclear magnetic resonance), a spectroscopy technique (Williamson et al., 1985). The same year can be considered as an origin of cryo-electron microscopy (cryo-EM) of biological materials, when the first images of adenovirus embedded in a vitrified layer of water were shown (Adrian et al., 1984). The importance of all this discoveries and their colossal impact in biology, chemistry and medicine cannot be overestimated.

Although solving structures of proteins and nucleic acids became possible, structures of big macromolecular complexes such as ribosome remained enigmatic. Massive, asymmetric, highly flexible macromolecular complex composed of two types of molecules (RNA and proteins), the ribosome was always extremely difficult object for structural analysis.

Use of NMR technique is commonly limited by the size of the molecule to analyse, typically 25 – 100 kDa, although sometimes NMR can be used to obtain structural information in large but symmetric systems as big as 900 kDa (Fiaux et al., 2002). At the same time, electron microscopy is limited for

working with small objects but suitable for resolving the big ones. Hence, the first 3D reconstructions of the ribosome were obtained using electron microscopy. In 1983 A. Spirin with colleagues modelled the 70S ribosome from *E. coli* showing the main structural features of both subunits (Vasiliev et al., 1983; see also Vasiliev, 1974; Lake 1976 and refs therein; Kastner et al., 1981). During next decades, J. Frank and colleagues worked on ribosome structure determination using cryo-electron microscopy technique. They have achieved significant progress in that area, by reaching 11.5 Å resolution of 70S ribosome in 2000 and contributed to the development of cryo-EM method in general (Wagenknecht et al, 1989; Stark et al., 1995; Gabashvili et al., 2000).

In the middle of 1980s two groups started to work in the direction of X-ray crystallography, the most developed, the most accurate and the most reliable method. However, this method is one of the most challenging one, because the researcher need to produce highly ordered radiation tolerant solid crystals, which requires a lot of stable homogeneous material and specific conditions. Obviously, this becomes excessively difficult task working with the ribosome which is large, asymmetric, flexible, and very dynamic RNA-protein complex. However, years of work and the sharing of experience have enabled researchers to achieve this aim.

5. X-RAY CRYSTALLOGRAPHY AND CRYO-ELECTRON MICROSCOPY OF THE RIBOSOME

X-ray crystallography is the presently the only one technique that conceivably provide the high-resolution structural information of the ribosome.

It has been clear for decades that X-ray crystallography can provide high-resolution structures for macromolecules, but its relevance to the ribosome was uncertain for a long time. The reason for this was that for many years there were no ribosome's crystals available, first because of its size, and second because the noncrystallographic symmetry (proven to be so important in determining the structures of comparably large assemblies like viruses) does not exits in the ribosome.

The first crystals of the large ribosomal subunit were obtained from the thermophilic bacterium *Bacillus stearothermophilus* and extreme halophilic archaeons *Haloarcula marismortui*. in the Max Plank Institute (Berlin) by H. Wittmann and A. Yonath in 1982. Their pioneering work provided the crystals of the large bacterial and archaeal 50S subunits diffracting to 18 Å resolution (Yonath et al., 1984; Yonath et al., 1986; Shoham et al., 1986).

Then, in 1983 new extreme thermophile *Thermus thermophilus* was introduced in the field of ribosome crystallography in the group of Dr. M. Yusupov from the Institute of Protein Research, Academy of Sciences of USSR (Puschino). In this group purification procedures of the ribosomes were developed and reported for the first time crystallization procedures of small ribosomal 30S subunit and full 70S ribosome (Trakhanov et al., 1987; Yusupov et al., 1987). From 1995 to 2000, V. Ramakrishnan from Cambridge University (UK) and A. Yonath groups published the *T. thermophilus* 30S structure at atomic resolution (Schluenzen et al. 2000, Wimberly et al. 2000). In 2000, T. Steitz (Yale University, USA) with colleagues produced a 2.4 Å electron density map of the *H. marismortui* 50S subunit (Ban et al., 2000).

The first crystal structure of full 70S ribosome from *T. thermophilus* containing bound functional ligands such as a messenger RNA and three transfer RNAs was solved at 7.8 Å resolution in 1999 in collaboration between M. Yusupov, G. Yusupova and H. Noller (University of California, Santa Cruz) (Cate et al., 1999). In 2001 the resolution of this crystal form was extended to 5.5 Å, providing for the first time detailed analysis of the interactions between the subunits and their interactions with messenger RNA and tRNAs in the A-, P- and E-sites (Yusupov et al., 2001, Yusupova et al, Cell, 2001). Within the next few years, a similar crystal form pushed their resolution to 3.7 Å (Korostelev et al., 2006). The group of J. Cate (University of California, Berkeley, USA) developed experimental protocol for *E. coli* 70S ribosome and reached 3.5 Å resolutions (Schuwirth et al., 2005; Zhang et al., 2009). The resolution limits were soon surpassed again with discovery of a new crystal form of *T. thermophilus* which diffracted to 2.8 Å (Selmer et al., 2006). Once the procedures of ribosome purification and crystallization became well established many of functional complexes have been determined and provided unprecedented insights into process of protein synthesis in bacteria. In 2009 V. Ramakrishnan, T. Steitz and A. Yonath received the Nobel Prize in chemistry for the studies of the structure and function of the ribosome.

However, many questions remained unanswered. Genome analysis, biochemical and biophysical characterization, electron microscopy studies of eukaryotic ribosomes have shown the differences in protein translation between eukaryotes and bacteria .In addition, in 2010, the first structure of the full eukaryotic ribosome from *Saccharomyces. cerevisiae* was solved at 4.2 Å (Ben-Shem et al., 2010) in the laboratory of M. Yusupov (IGBMC, Strasbourg, France). Only one year later the same group reported the crystal structure of the 80S ribosome from *S. cerevisiae*—including nearly all ribosomal RNA bases and protein side chains as well as an additional protein, Stm1—at a resolution of 3.0 angstroms (Ben-Shem et al., 2011). This allowed scientist to observe movement between subunits, and also permitted cryo-EM scientist to use it as a model to fit in their cryo-EM maps. Since then, considerable amounts of eukaryotic ribosome structure have been solved by this technique. Structures of the large 60S and small 40S ribosomal subunits of *Tetrahymena thermophila* at 3.5 Å and 3.9 Å respectively were obtained by N. Ban (ETH, Zurich, Switzerland) and his colleagues (Klinge et al., 2011; Rabl et al., 2011). The crystal structure of mammalian ribosome obtained so far is rabbit 43S initiation complex solved at 11 Å resolution in the laboratory of T. Steitz (Lomakin and Steitz, 2013).

Significant advances in deciphering detailed mechanisms, fidelity and stalling of protein synthesis using X-ray analysis were made by the laboratories of H. Noller, M. Yusupov, J. Cate, T. Steitz, V. Ramakrishnan, who carried out many unique studies on crystal structures of different intermediate states of translating or stalled ribosome (references marked by *).

The relatively "young" but extremely ambitious technique of cryo-electron microscopy (cryo-EM) is currently receiving a lot of attention from structural biologists. Some would even call it "the new era of cryo-EM" where structures at near-atomic resolution are no longer the prerogative of X-ray crystallography or NMR spectroscopy (W. Kühlbrandt, 2014a; W. Kühlbrandt, 2014b). Indeed, cryo-electron microscopy made a huge progress during last several years and due to technological and computational developments is able to reach near atomic resolution (Fischer et al., 2015; Khatter et al., 2015; Bartesaghi et al., 2015). Notably, the ribosome played an important role in this development.

Cryo-EM technique has been used to visualize different functional states of ribosome with tRNA, translation cofactors or other natural ligands (Spahn et al., 2004(a, b); Halic et al., 2006(a, b); Becker et al., 2009).

However, despite these studies, their research and cryo-EM technique improvement, the limited and the absence of molecular model of the ribosome hindered an expanded analysis, and so the translation mechanism remained a mystery for ten years.

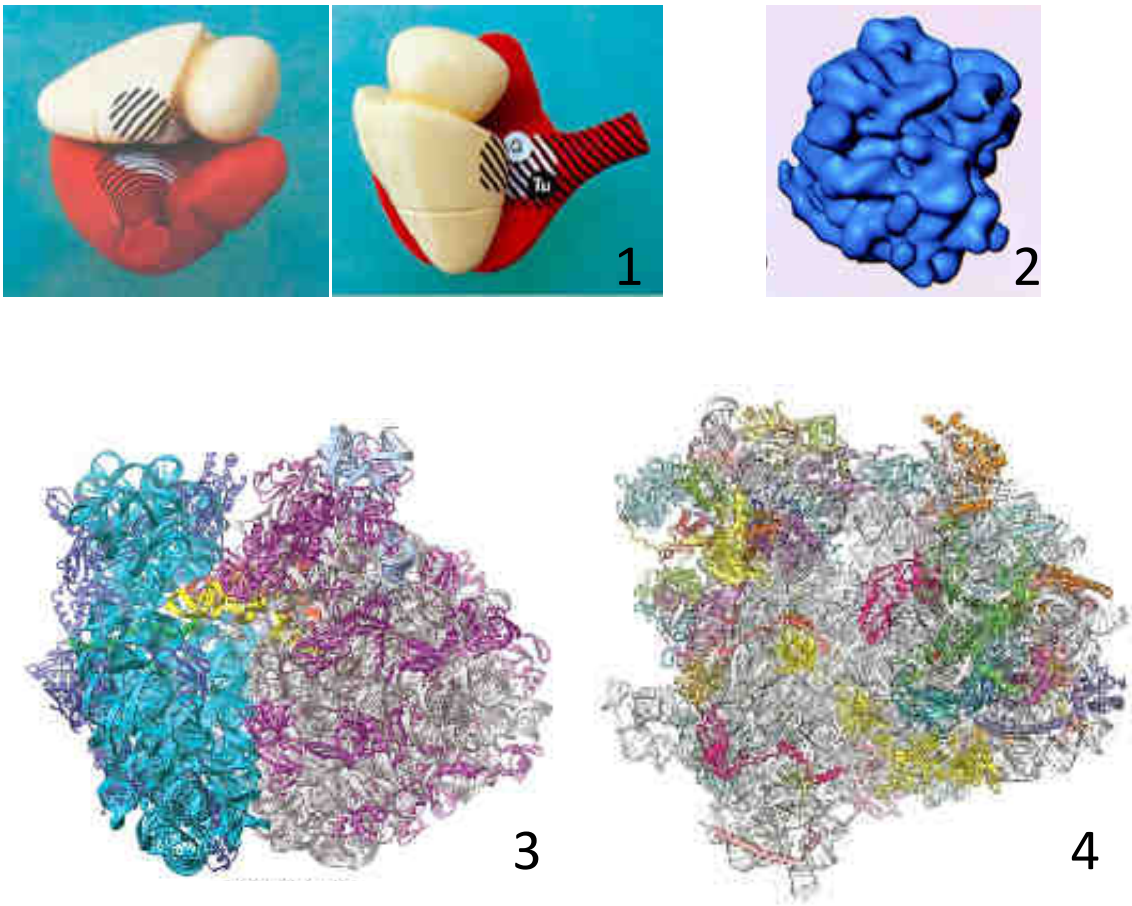

Figure 6: Structural evolution of Ribosome from 1983 to 2011. 1) *Escherichia coli*, electron microscopy (Vasiliev et al., 1983). 2) *Saccharomyces cerevisiae,* electron microscopy (Frank et al., 2000). 3): *Thermus thermophiles*, X-ray crystallography (Yusupov et al., 2001); 4): *Saccharomyces cerevisiae* (Ben-Shem et al*.,* 2011*)*

Due to last development in X-ray crystallography, cryo-electron microscopy have shed light on high resolution structures of the ribosomes from pathogenic organism *Trypanosoma brucei* (Hashem et al., 2013), *Plasmodium falciparum* (Wong et al., 2014), humans (Anger et al., 2013, Khatter et al., 2015). Also several full ribosomes from gram-positive bacteria has been solved by cryo-EM microscopy such as *Bacillus subtilis* at 3.5 Å (Sohmen et al., 2015) and, recent work, human pathogen bacteria *Mycobacterium smegmatis* by Ben's group at 3.3-Å resolution (Hentschel et al., 2017).

Furthermore, it revealed the structures of mitochondrial ribosomal subunits and the full mito-ribosome (Greber et al., 2014 and 2015; Kaushal et al., 2014; Brown et al., 2014; Amunts et al., 2014

and 2015), the chloroplast ribosome (Manuell et al., 2007), the membrane bound mammalian ribosomes (Voorhees et al., 2014) and many functional complexes that were difficult to get by X-ray crystallography (see references marked by **).

Also, by cryo-electron microscopy, recently in M.Yusupov laboratory has been solved full ribosome from *Staphylococcus aureus* (Khusainov et al., 2016). This prospective work gives us an opportunity to see the differences in the structure of the ribosome of pathogenic bacteria from the others and to understand their possible mechanisms of resistance. However, cryo–EM study couldn't give all necessary information to design of more effective drug for targeting multidrug resistant bacteria. In this case X-ray study will help to complete all those gaps.

Nowadays, the most used techniques aimed at solving structures of biological macromolecules are cryo-electron microscopy and X-ray crystallography. Method of cryo-electron microscopy very robust and straightforward, but it didn't reach atomic resolution yet. Whereas, even if it requires more material and longer investigation for screening of suitable conditions, X-ray crystallography is the only method able to provide the high resolution structure of ribosome. Thus, crystallography is the most suitable method to obtain high resolution at ~3 Å and even higher, especially for projects with antibiotic and small molecule drugs development and their investigation, where necessary to be very precise.

6. RIBOSOME – POTENTIAL THERAPEUTIC TARGET

rRNA is the most commonly exploited RNA target for small molecules. The bacterial ribosome comprises 30S and 50S ribonucleoprotein subunits, contains a number of binding sites for known antibiotics and is an attractive target for novel antibacterial agents. The large difference between bacteria and eukaryotic rRNA enables rRNA-targeting against a broad spectrum of pathogenic bacteria (Howard et al., 1996). Recently, the application of X-ray crystallography has elucidated many antibiotic-binding sites on the ribosomal subunit (Brodersen et al., 2000; Carter et al., 2000) facilitating the design of novel antibiotic.

The ribosome is one of the main antibiotic targets in the bacterial cell. After decades of biochemical studies, and more recent structural studies, have revealed the molecular basis by which a large and diverse array of antibacterial agents specifically inhibit protein synthesis.

The initial structural insights into the mechanism of antibiotic action on the ribosome were obtained from crystal structures of antibiotics in complex with the 30S subunit of *Thermus thermophilus*, the 50S subunit of *Deinococcus radiodurans* and the 50S subunit of the archaeon *Haloarcula marismortui (*Wilson, 2009). However, the ability to determine the structures of the 70S ribosome from *T. thermophilu*s (Selmer, 2006) and *Escherichia coli* (Schuwirth et al., 2005) at high resolution has led to a rapid increase in the number of structures of 70S–antibiotic complexes over the past 10 years. Crystal structures of almost all of the major ribosome-targeting antibiotic classes in complex with the ribosome have already obtained.

The majority of known compounds target the elongation cycle, including all of the clinically important antibiotic classes: the aminoglycosides, chloramphenicols, fusidic acids, lincosamides, macrolides, oxazolidinones, streptogramins and tetracyclines (Walsh, 2003). Although a number of compounds

specifically target the initiation phase, they are limited in terms of clinical application owing to problems with drug specificity (edeine and pactamycin), toxicity (evernimicin) and solubility (thiopeptides and thermorubin). Several antibiotics inhibit the termination and recycling phases of translation, but these compounds usually have a more pronounced effect during the elongation phase. However, fusidic acid and blasticidin S are exceptions because they inhibit recycling and termination, respectively, at substantially lower concentrations than the concentration needed to inhibit elongation (Savelsbergh et al, 2009; Svidritskiy et al., 2013).

Despite the large size of the ribosome, relatively few sites are targeted by our current arsenal of antibiotics. On the 30S subunit, the antibiotic binding sites are clustered along the path of the mRNA and tRNAs (Figure 7). Antibiotics that bind to the 30S subunit, such as edeine and kasugamycin, inhibit translation initiation by preventing a stable interaction between the initiator tRNA and the start codon at the P-site. The majority of other 30S-targeting antibiotics inhibit translation elongation by interfering with either the delivery of tRNAs to the A-site (for example, tetracyclines and streptomycins) or the subsequent translocation of the mRNA–tRNA complex through the ribosome (such as the aminoglycosides hygromycin B, neomycin, pactamycin and spectinomycin; and the tuberactinomycins viomycin and capreomycin).

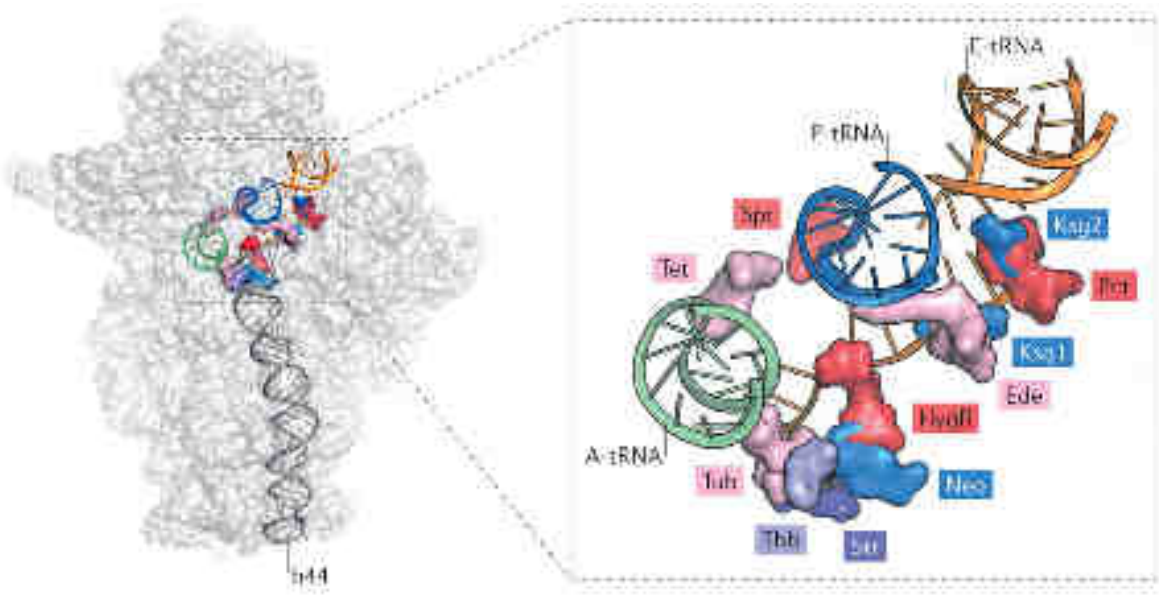

Figure 7: Antibiotic binding sites on the 30S ribosomal subunits (Wilson, 2014). Overview and enlargement of antibiotic binding sites along the mRNA binding channel of the 30S subunit, including tetracycline (Tet), spectinomycin (Spt), kasugamycin (Ksg1 and Ksg2), pactamycin (Pct), edeine (Ede), hygromycin B (HygB), neomycin (Neo), streptomycin (Str), thermorubin (Thb) and tuberactinomycins (Tub).

On the 50S subunit, most of the antibiotic binding sites cluster at or near the peptidyl-transferase centre (PTC), where peptide-bond formation occurs (Figure 8). Exceptions include the orthosomycins (evernimicin and avilamycin), which interact with 23S rRNA helices H89 and H91 and interfere with the binding of IF2 (Belova et al., 2001; Mikolajka et al., 2011); and the thiostrepton-like thiopeptides, which interact with H43 and H44 of the 23S rRNA and interfere with the binding of EF-G, EF-Tu and IF2 (Wilson, 2011) (Figure 8). PTC targeting antibiotics inhibit peptide-bond formation by perturbing or preventing the correct positioning of the aminoacylated ends of tRNAs in the PTC.

The binding sites of PTC-targeting antibiotics overlap with the A-site tRNA (for example, chloramphenicol, lincosamides (clindamycin), oxazolidinones (linezolid), puromycin and sparsomycin) or the P-site tRNA (blasticidin S), or span both the A- and P-sites (for example, the pleuromutilin and streptogramin A (SA) classes) (Figure 8.A). The binding sites of the macrolide and streptogramin B (SB) classes are located adjacent to the PTC within the ribosomal exit tunnel. Most macrolide and SB members do not inhibit peptide-bond formation per se but rather prevent elongation of most nascent chains, which leads to peptidyl-tRNA drop off and the abortion of translation. Below I discuss the structural basis for the inhibition of tRNA delivery, translocation and peptidyl transfer by ribosomal antibiotics.

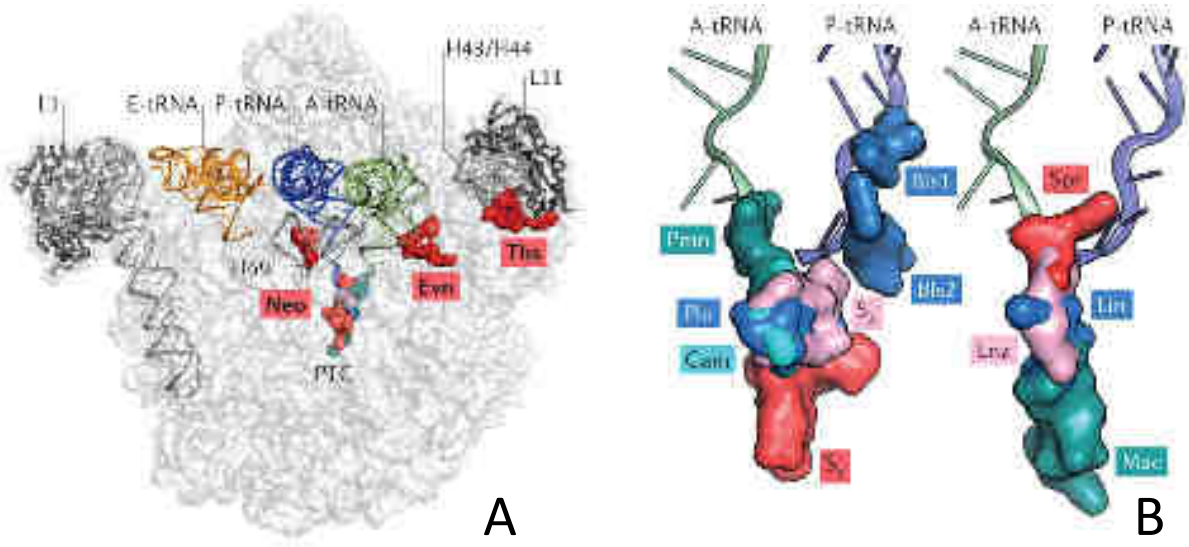

Figure 8: Antibiotic binding sites on 50S ribosomal subunits (adapted from Wilson, 2014). A) Overview of the binding sites of neomycin (Neo), evernimicin (Evn) and thiostrepton (Ths) on the 50S subunit. B) Antibiotics at the PTC. Enlargement of the binding sites of blasticidin S (Bls1 and Bls2), sparsomycin (Spr), lincomycin (Lin), linezolid (Lnz), macrolides (Mac), puromycin (Pmn), pleuromutilins (Plu), chloramphenicol (Cam) and streptogramins A and B (SA and SB) relative to the A-site and P-site tRNAs.

II MAIN CHARACTERISTICS OF *STAPHYLOCOCCUS AUREUS*

The genus Staphylococcus is composed of many species of Gram-positive cocci with diameters of 0.5 – 1.5 µm that are distinguished microscopically by their characteristic organization into clusters of organisms as compared to the chain-like arrangement of the genus Streptococcus. Biochemically, a principle difference between the two genera is the ability of staphylococci to produce the enzyme catalase, which breaks down hydrogen peroxide to water and oxygen. To date, there are at least 40 species and 11 sub-species in the genus Staphylococcus, many of which preferentially colonize the human body. Of significance to humans *Staphylococcus aureus* and *Staphylococcus epidermidis* are the two most characterized and studied strains due to their medical importance.

Staphylococci are non-motile, non-spore forming facultative anaerobes that grow by aerobic respiration or by fermentation. Pathogenic species are commonly identified by their ability to produce coagulase, and thus clot blood. Members of Staphylococcus genus are catalase-positive and oxidase-negative, distinguishing them from the genus streptococci, which are catalase-negative, and have a different cell wall composition to staphylococci. This Staphylococcus can nevertheless become pathogenic under certain circumstances, for example in immunodeficient patients (AIDS patients, those undergoing radiotherapy or chemotherapy, or newborn babies) or when foreign materials are inserted into the body (joint prostheses, prosthetic heart valves, probes, catheters, etc.). The implanted material can then become contaminated by strains from the mucocutaneous flora of the patient or hospital staff. This type of infection is mainly nosocomial (hospital-acquired) or iatrogenic (resulting from a medical procedure).

S. aureus is the one species that has the ability to produce the major virulence factor coagulase, an enzyme that causes plasma to clot and Coagulase-negative staphylococci (CNS) a group of many species that are usually not distinguished from one another by clinical laboratories.

S. aureus is a major pathogen of increasing importance due to high antibiotic resistance (Lowy, 1998). The species name aureus refers to the fact that colonies often have a golden colour when grown on solid media.

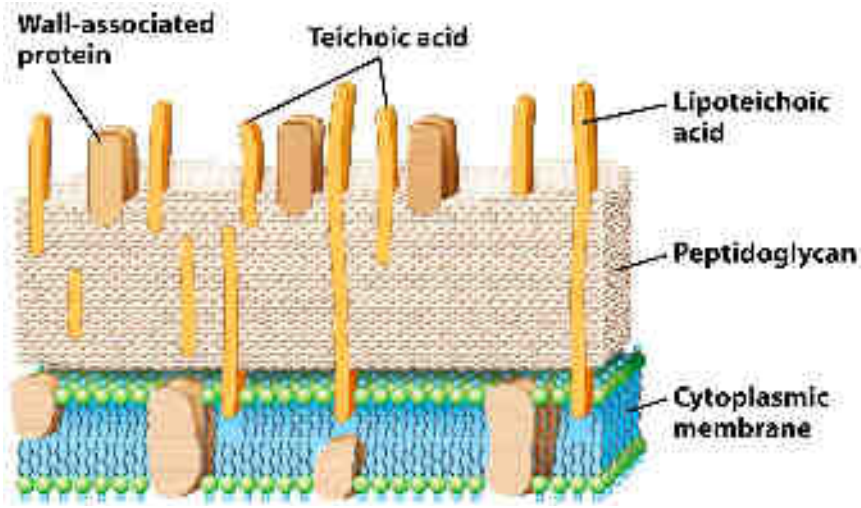

Figure 9: Schematic model of cell wall of gram-positive bacteria (http://rcvetsblog.blogspot.fr/2014/03/bacterial-cell-wall.html).

The cell wall of *S. aureus* is a tough protective coat, about 20 – 40 nm thick (Shockman and Barrett, 1983). About 50% of the cell wall mass is made of peptidoglycan (Waldvogel, 1990). Another cell wall constituent is a group of phosphate-containing polymers called teichoic acids, which contribute about 40% of cell wall mass (Knox and Wicken, 1973). Teichoic acids contribute a negative charge to the staphylococcal cell surface and play a role in the acquisition and localization of metal ions, particularly divalent cations, and the activities of autolytic enzymes (Wilkinson, 1997). Peptidoglycan and teichoic acid together only account for about 90% of the weight of the cell wall, the rest is composed of surface proteins, exoproteins and peptidoglycan hydrolases (autolysins). Some of these components are involved in attaching the bacteria to surfaces and are virulence determinants.

S. aureus is nearly everywhere in nature and 25 to 30% of the population has it on the skin, hair and/or in the upper respiratory tract. It is found in both animals and humans. This microorganism is responsible for severe nosocomial and community-acquired infections. It can cause a variety of self-limiting to life-threatening diseases in humans. Some skin conditions caused by Staphylococcal exfoliative toxins include blisters, skin loss, pimples, furuncles, impetigo, folliculitis, abscesses, poor temperature control, fluid loss, and secondary infection (Murray et al., 2002; Le Loir et al., 2003; Fridkin et al., 2005). Certain strains of *S. aureus* produce the superantigen TSST-1, which is responsible for toxic shock syndrome (TSS) (Murray et al., 2002), from which mortality is very high; death can occur within 2 hours (Chen et al., 2007). Deeply penetrating *S. aureus* infections can be severe. Such infections include endocarditis, peritonitis, necrotizing pneumonia, bacteremia, meningitis, osteomyelitis, septic arthritis, and infections of bones, joints and organs (Murray et al., 2002; Einstein, 2008; Fridkin et al., 2005).

This pathogen can also cause disease by means of elaborating exotoxins. Two rare but well characterized entities are TSS often, but not always, associated with tampon use and Staphylococcal Scalded Skin Syndrome (SSSS) a condition of babies in which toxin causes widespread sloughing of skin. A common, but infrequently definitively diagnosed, toxin mediated disease is “food poisoning” caused by ingestion of enterotoxin in food contaminated with *S. aureus*. This is manifest by vomiting occurring very shortly (1 – 6 hours) after ingestion and lasting less than 24 hours.

S. aureus is a successful pathogen due to a combination of nasal carriage and bacterial immune-evasive strategies (Kluytmans et al., 1997; Cole et al., 2001). It can grow in a pH range from 4.2 to 9.3 and in salt concentrations of up to 15% (Le Loir et al., 2003). The bacteria can survive for up to 42 days on carcasses and organs, for up to 7 days on floors, for up to 46 hours on glass, after exposure to 17 or 7 hours of sunlight or UV respectively, for 60 days on meat products, for up to 7 days on coins, or from 30 min to 38 days on skin (Cimolai, 2008). It has evolved a number of regulatory mechanisms to control the synthesis of its multiple virulence factors in response to the host, stresses and environmental changes (Lowy, 1998).

1. REGULATORY MECHANISMS OF VIRULENCE DETERMINANTS IN *S. AUREUS*

The diverse array of cell wall and extracellular components involved in *S. aureus* virulence implies that the pathogenicity of this bacterium is a complex process requiring the tightly coordinated expression of these factors during different stages of infection (colonization, avoidance of host defense, growth and cell division, and bacterial spread) (Novick and Jiang, 2003; Torres et al, 2010). Indeed, the

regulation of the virulence genes in S. aureus appears to follow a strategy that begins with the establishment of the bacterium in the host, followed by the attack of its defenses. For this, *S. aureus* begins by upregulating the expression of genes coding for surface proteins involved in adhesion and defense against the host immune system; and only late in infection it starts to up-regulate the production of toxins that facilitate tissue spread (Bien et al., 2011; Novick and Geisinger, 2008; Cheung et al., 2004). To control the production of the virulence determinants during infection, *S. aureus* has several regulatory systems that respond to bacterial cell density (quorum-sensing) and environmental cues (e.g. nutrient availability, temperature, pH, osmolarity, and oxygen tension) (Torres et al., 2010; Wu et al., 1996; Novick et al., 1993; Cheung et al., 1992). These systems can be divided into two broad categories: two component signal transduction systems and global transcriptional regulators (Cheung et al., 1992; Cheung et al., 2002)

The two-component regulatory systems in *S. aureus* include the accessory gene regulator (*agr*) (Peng et al., 1988) and the staphylococcal accessory element (*sae*) (Giraudo et al., 1994).

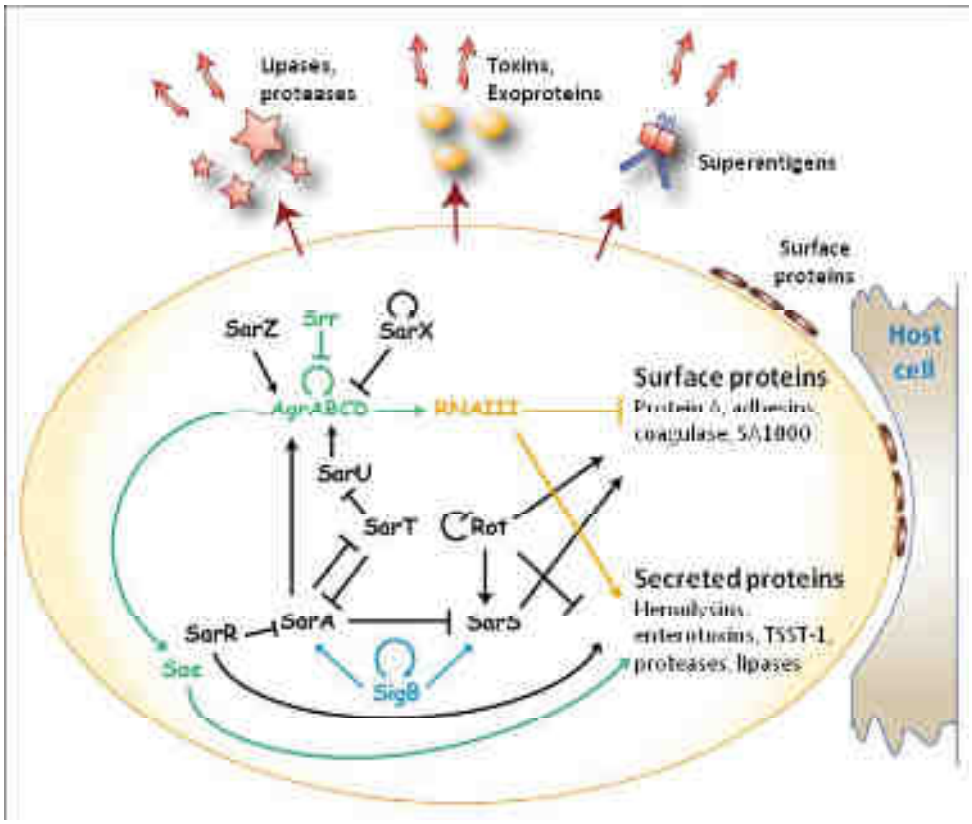

Figure 10: Regulation network of production of virulence factors in *S. aureus* (adapted from Chevalier, 2009).

The ***agr*** locus regulates more than 70 genes, of which 23 are related to virulence (Ziebandt et al., 2004). It is responsible for upregulating the expression of many exoproteins (e.g. α-hemolysin, serine proteinase, TSST-1, enterotoxins, and proteases), and down-regulating the synthesis of cell wall-associated proteins (e.g. FnbpA, FnbpB, and SpA) (Novick et al., 2008; Novick et al., 1993 Morfeldt et al., 1995; Oscarsson et al., 2006). The *agr* locus carrying two divergently transcribed transcripts, RNAII and RNAIII (Kornblum et al., 1990). The RNAII transcript encodes a two-component signal transduction system which responds to the extracellular concentration of a secreted octapeptide also encoded by RNAII (Ji et al., 1995; Novick., 1995). The RNAII locus contains four genes, agrB, agrD, agrC and agrA

(Kornblum et al., 1990). Induction of this quorum-sensing mechanism results in production of the 514-nucleotide RNAIII transcript that is the actual effector of virulence gene expression (Janzon et al., 1990; Novick et al.,1993). RNAIII acts primarily on target gene transcription; however, the molecular details of how RNAIII stimulates transcription of exoproteins such as α-toxin and represses transcription of surface proteins like Protein A remain obscure (Novick et al., 2003).

The ***sae*** locus codes for another two-component system that regulates the expression of many virulence factors involved in bacterial adhesion, toxicity and immune evasion (Rogasch et al, 2006). This includes the up-regulation of α-, β- and γ- hemolysins (Goerke et al., 2005; Liang et al., 2006) and the down-regulation of SpA (Giraudo et al., 1997).

Several global regulatory systems have been identified in *S. aureus*, including the staphylococcal accessory regulator A (***sarA***) (Cheung et al., 2001) and its several homologues (Cheung and Projan, 1994). The DNA binding protein S*arA*, is required for maximal expression of RNAIII. The s*arA* up-regulates the expression of some virulence factors (e.g. Fnbps, α- and β-hemolysins) and down-regulates others (e.g. SpA and proteases) (Chan and Foster, 1998). Furthermore, *sarA* independently of *agr* regulates transcription of selected target genes by a mechanism that apparently involves direct binding of *SarA* to the promoter region (Chien et al., 1999; Tegmark et al., 2000; Wolz et al., 2000). Genome sequencing has revealed that the *S. aureus* genome encodes at least 13 proteins that have homology to *SarA*, and presently a regulatory role in virulence gene expression has been verified for 7 of these (*SarS, SarT*, *SarU*, *SarV*, *Rot*, *MgrA*, and *TcaR*) (Cheung et al., 2002). As an example, *SarS* was identified as a direct activator of spa transcription, and it was verified that the strong induction of spa transcription, observed in the absence of the agr locus, was partly due to enhanced transcription of SarS (Cheung et al., 2001; Tegmark et al., 2000). The *agr*-mediated down-regulation of *sarS* transcription involves another Sar homologue, namely *SarT*. Apparently *SarT* functions as a positive activator of sarS transcription by directly binding to the *sarS* promoter, thereby stimulating transcription (Schmidt et al., 2003). Additionally, *Rot*, originally identified in a transposon mutagenesis search as a repressor of toxins, was shown to be a positive regulator of *spa* transcription (McNamara et al., 2000; Saïd-Salim et al, 2003). Preliminary data, moreover, showed that *Rot* was required for transcription of *sarS*, indicating that the positive effect of *Rot* on *spa* transcription is also mediated through *SarS* (Saïd-Salim et al, 2003). Finally, the complexity of the regulatory circuit controlling spa transcription was strengthened by the recent finding that *MgrA*, yet another *Sar* homologue, impacts negatively on spa transcription by independently of *SarT*, controlling *SarS* expression (Ingavale et al., 2005)

The regulation of virulence determinants may also involve ***sigma factors*** (σ), which are proteins that bind to the core RNA polymerase to form the holoenzyme that binds to specific promoters (Moran et al, 1993). *S. aureus* have two sigma factors: the primary *sigma factor*, ***σA***, which is responsible for the expression of housekeeping genes essential for growth (Deora et al, 1997); and the alternative *sigma factor* ***σB***, which regulates the expression of different genes involved in cellular functions (e.g. stress response) (Deora and Misra et al, 1996) and at least 30 virulence genes (Horsburgh et al, 2002; Bischoff et al, 2001). It up-regulates capsule, FnbpA and coagulase, and downregulates hemolysins and serine protease A (Ziebandt et al, 2004; Entenza et al, 2005; Bischoff et al, 2004). All the above mentioned regulators do not exert their influence singly; instead they form an interactive regulatory network to ensure that specific virulence genes are expressed only when required.

2. SUPER KILLER OF THE XXI CENTURY

A fundamental biological property of *S. aureus* is its ability to asymptomatically colonize healthy individuals. Approximately 30% of humans are nasal carriers (Kluytmans et al., 1997), such that, in these individuals, the microorganism is part of the normal flora. *S. aureus* carriers are at higher risk of infections and they are presumed to be an important source of the *S. aureus* strains that spread among individuals. Nasal colonization rates by *S. aureu*s among hospitalized patients are comparable to those of the general population. However, methicillin-resistant *S. aureus* (MRSA) carriage among the general population is less than 1%, (Graham et al., 2006) whereas S. aureus (MRSA) prevalence in nosocomial bacteremia is over 50% in certain countries (The European Antimicrobial Resistance Surveillance System, 2009). The primary mode of transmission of this organism is by direct contact, usually skin-toskin contact, and various host factors can predispose individuals to infection, including the loss of the normal skin barrier, the presence of underlying diseases such as diabetes or AIDS, and defects in neutrophil function. To these factors, antibiotic pressure, length of stay in an intensive care unit (ICU), colonization pressure, professional healthcare workload, hand hygiene levels, isolation treatment measures, and environmental contamination have been proposed as important factors in the acquisition and transmission of *S. aureus* in ICUs (Grundmann et al., 2002).

Infections caused by *S. aureus*, above all by antibiotic-resistant strains, have reached epidemic proportions globally (Grundmann et al., 2006). The capacity of this microorganism to cause a spectrum of human disease reflects an incredible ability to adapt to microenvironments in the human body and suggests that the pathogenesis of *S. aureus* is a complex, regulated process (Loughman et al., 2009). As described before, staphylococcal pathogenesis is multifactorial, involving three classes of factors accounting for approximately 100: secreted proteins, including superantigens, cytotoxin and tissue degrading enzymes; cell-surface bound proteins (MSCRAMMs, i.e., microbial surface components recognizing adhesive matrix molecules), including fibrinogen binding protein, other adhesins and anti-opsonins; and cell surface proteins, including the polysaccharide capsule and components of the cell wall peptidoglycan.

The classic staphylococcal infection is an abscess: organisms entering the tissue of a host produce a series of extracellular proteins and other factors, such as cell wall and capsular components, which enable them to coagulate fibrinogen, adhere to the intercellular matrix, degrade tissue components, and lyse local cellular elements. This evokes a potent innate immune response that includes interleukins, opsonins, complement, and phagocytes. Additionally, humans have circulating antibodies to most staphylococcal antigens, and these will obviously participate in the initial response. These antibodies, the innate immune response, and fibrin generated by the organism, wall off the lesion creating a pocket within which a battle between the organism and phagocytes is waged, generating pus. Although everyone gets superficial skin infections, staphylococcal infections can be initiated occasionally in deep tissue sites and these result in deep tissue infections that often require surgery. *S. aureus* can also alight on the heart valves, more often in intravenous drug abusers or the elderly. Heart valve lesions, known as vegetations, consist largely of platelets, fibrin organisms, and neutrophils and their structure is considered akin to biofilm formed on inanimate surfaces. A particularly troublesome, but non-fatal, condition is osteomyelitis, which again can occasionally occur spontaneously, but much

more often follows an open fracture. A special set of pathological conditions, toxinoses, are caused by single toxins. In many cases, the purified toxin can generate all the symptoms; in some cases, the living organism must be present, contributing, for example, to the ability to adhere to the extracellular matrix or to resist eradication by the host. Examples are TSS, scalded skin syndrome, and necrotizing pneumonia (Panton–Valentine leukocidin (PVL)) (Stefani and Goglio, 2010).

Such a complex and integrated set of weapons of virulence genes suggests that distinct networks of virulence genes are likely activated in response to host signals; in vitro results have demonstrated regulation in a population density manner under the control of global regulators such as the *agr* system (Cheung et al., 2004). The overall burden of staphylococcal disease caused by antibiotic-resistant S. aureus, above all by the methicillin-resistant strains, is increasing in many countries, in both healthcare and community settings (Campanile et al., 2009; Stefani et al., 2009). American update by the National Healthcare Safety Network (NHNS) (Hidron et al., 2008) performed on antimicrobial-resistant organisms responsible for healthcare-associated infections, *S. aureus* was the most prevalent isolate in skin and soft tissue infections (SSTIs), in blood stream infections (BSI), and in ventilator-associated pneumonia (VAP); in the case of surgical site infections its prevalence changed as follows: neurologic < orthopedic < cardiac < vascular < obstetric/ gynecological. The authors found an overall MRSA prevalence of 56.2% and their data were comparable to data from other surveillance systems in the USA and Europe (CDC National Nosocomial Infections Surveillance, 1999). It is clear that MRSA is still the number one cause of hospital associated infections. The mortality rate associated with invasive infections is approximately 20% (Klevens et al., 2007) and in the USA, but also in some countries in Europe, these infections are probably the leading cause of death by any single agent; fatalities resulting from these infections are estimated to surpass those caused by HIV/AIDS

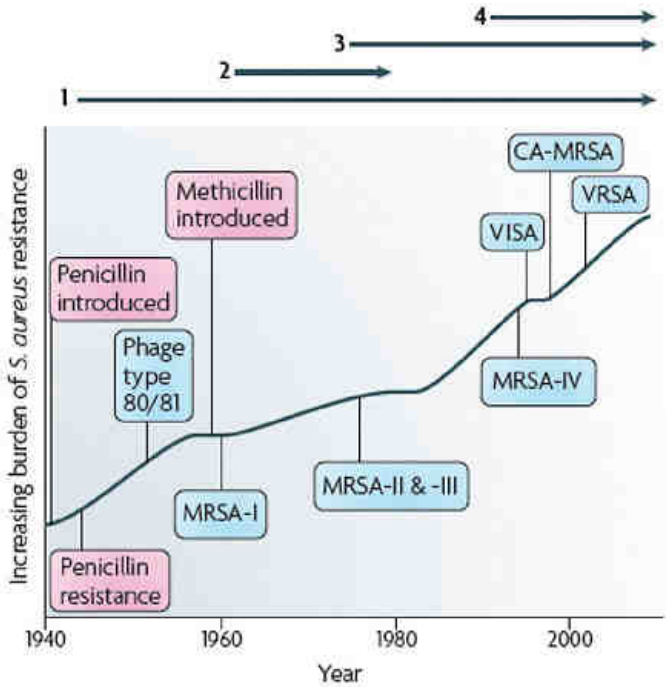

Figure 11: Four waves of antibiotic resistance in *S. aureus* (Chambers and DeLeo, 2009). **Wave 1** (indicated above the graph), which continues today, began shortly after the introduction of penicillin into clinical practice in the 1940s. The first pandemic antibiotic-resistant strains, from the lineage known as phage type 80/81, were penicillin-resistant and produced Panton-Valentine leukocidin (PVL). **Wave 2** began almost immediately following the introduction of methicillin into clinical practice with

the isolation of the first MRSA strain (an archaic clone), which contained staphylococcal chromosome cassette mecl (SCCmecl) (indicated on the graph as MRSA-I); this wave extended into the 1970s. **Wave 3** began in the mid to late 1970s with the new emergence of MRSA strains that contained the new SCCmec allotypes, SCCmecll and SCCmeclll (MRSA-II and MRSA-III), marking the ongoing worldwide pandemic of MRSA in hospitals and health care facilities. The increase in vancomycin use for the treatment of MRSA infections eventually led to the emergence of vancomycin-intermediate S. auereus (VISA) strains. **Wave 4**, which began in the mid to late 1990s, marks the emergence of MRSA strains in the community. Community-associated MRSA (CA-MRSA) strains were susceptible to most antibiotics other than β-lactams, were unrelated to hospital strains and contained a new, smaller, more mobile SCCmec allotype, SCCmecIV (MRSA-IV) and various virulence factors, including PVL. Vancomycin-resistant S. aureus (VRSA) strains, ten or so of which have been isolated exclusively in health care settings, were first identified in 2002.

Given the problems caused by the development of antibiotic-resistant *S. aureus*, vaccination may well have a significant role to play in controlling this organism in the future. A number of companies are developing products intended for active or passive immunization against *S. aureus* infections, including a capsular polysaccharide vaccine that has been subjected to a clinical trial with hemodialysis patients (Fattom et al., 2004), a monoclonal antibody (Hall et al., 2003), and human immunoglobulin that is enriched for antibodies that recognize clumping factor A (Vernachio et al., 2003).

An increased understanding of how *S. aureus* colonizes the nares could allow improved methods for controlling nasal and skin carriage. Recent studies of mutant strains defective in wall teichoic acid (WTA) in a rat model of nasal colonization implicated WTA in colonization (Weidenmaier et al., 2004). Also, several different surface proteins can promote adherence of *S. aureus* to squamous epithelial cells isolated from the nares (Roche et al, 2003) and could act as adhesins involved in nasal colonization. Another mystery that deserves greater attention is the question of why some members of the population never carry *S. aureus*, while others are persistent carriers.

The study by Melles et al., 2004, in combination with MLST analysis (Feil et al., 2003), provides a solid foundation for analysis of novel hypervirulent or epidemic drug-resistant S. aureus clones that might arise in the future. One thing seems certain: *S. aureus* will continue to respond to challenges imposed by humans' continued attempts to combat its carriage and development of related disease.

---

3. ANTIBIOTIC RESISTANCE

In the modern life, the problem of resistance to antibiotics, by the World Health Organization is singled out as one of the main threats for all mankind. Whereas erlier multidrug resistant bacteria were mainly found in hospitals that were the main source of infection, in the 21st century multidrug resistance is increasingly being recorded in various public places, from which it can be concluded that the reservoirs of antibiotic resistant bacteria are present outside the hospital. The genetic plasticity of bacterial pathogens, which causes specific reactions leading to mutational changes, is a vivid example of bacterial adaptation and the top of evolution, which as a consequence leads to the fact that the strongest survives. The acquisition of genetic material or alteration of gene expression causes

resistance to virtually all antibiotics currently available in clinical practice. Therefore, it is very important to have a full understanding of the causes and mechanisms of the emergence of resistance, and structural biology in solving these problems is the first and important step for revealing the general picture and constructing further ways to striving multidrug-resistant bacteria.

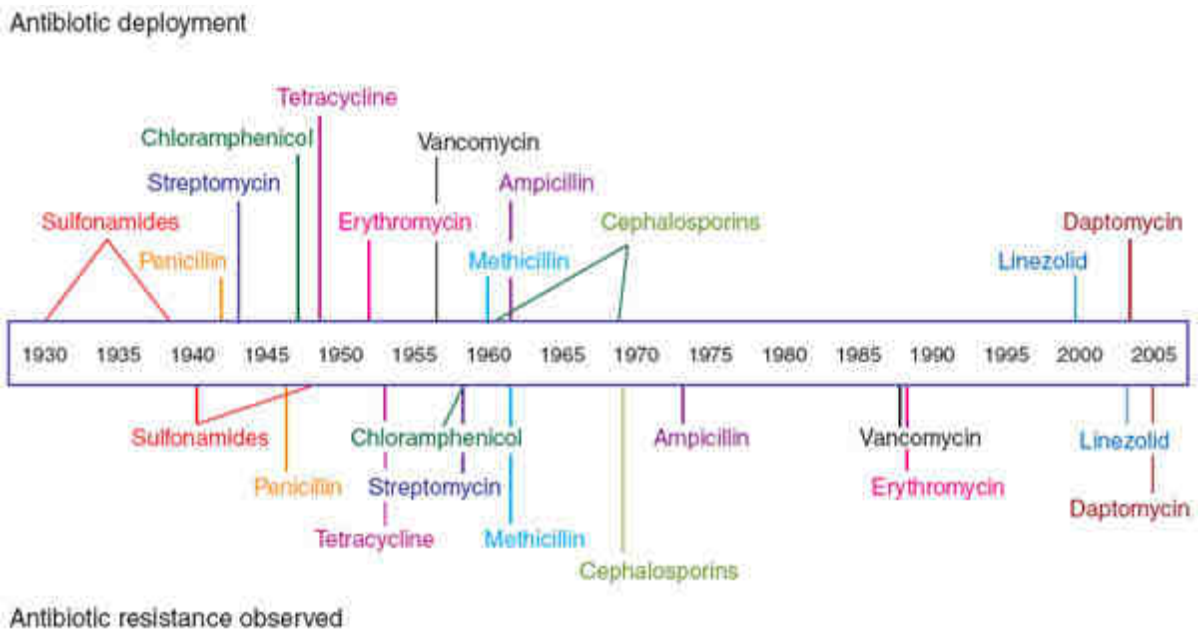

Figure 12: Development of antibiotics and resistance (Clatworthy et al., 2007).

4. MECHANISMS OF ANTIBIOTICS ACTION AND BACTERIAL RESISTANCE

Through years of evolution, pathogen bacteria have developed sophisticated mechanisms to resistance against antibiotics. This provided them survival in the most hostile environments and the most important in the human body. At the moment have been formulated three main classes of resistance mechanisms according to biochemical route such as modifications of the antimicrobial molecule, decreased antibiotic penetration and efflux, changes of the target sites.

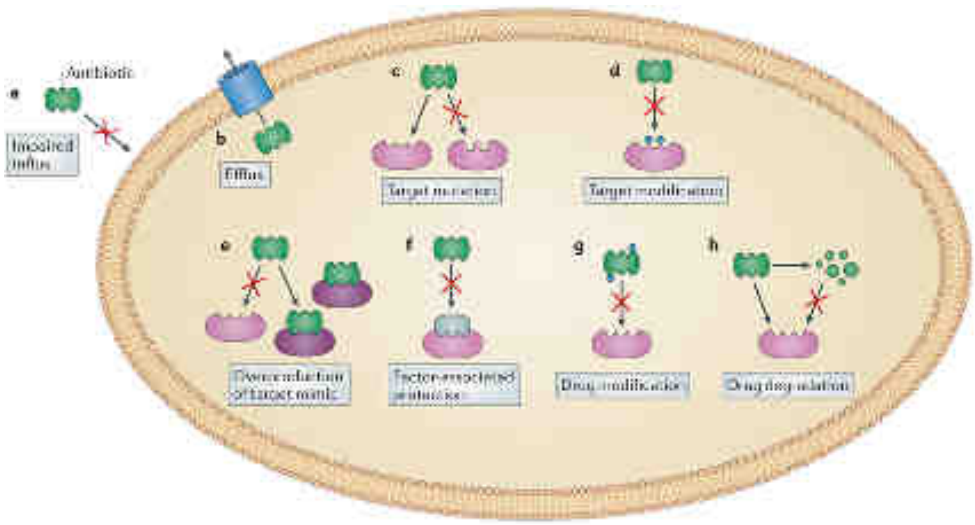

Figure 13: Antibacterial resistance mechanisms (adapted from Wilson, 2014). a) Impaired influx owing to low membrane permeability. b) Active efflux of the drug from the cell. c) Target modification. d) Target alteration, which lowers the affinity of the drug for the target. e) Overproduction of a molecule that mimics the target, which lowers the effective drug concentration so that the target remains unbound. f) The recruitment of a specialized protein factor to actively remove the drug from the target. g) Modification of the drug. h) Degradation of the drug.

4.1 MODIFICATIONS OF THE ANTIBIOTIC MOLECULE

Enzymatic alteration. The production of enzymes capable of introducing chemical changes to the antimicrobial molecule such as acetylation (aminoglycosides, chloramphenicol, streptogramins), phosphorylation (aminoglycosides, chloramphenicol), and adenylation (aminoglycosides, lincosamides) is a well-known mechanism of acquired antibiotic resistance in both gram-negative and gram-positive bacteria. Also, most of the antibiotics affected by these enzymatic modifications induce their mechanism of action by inhibiting protein synthesis at the ribosome level (Wilson, 2014). One of the classical examples involves the chemical modification of chloramphenicol (antibiotic that inhibits protein synthesis by interacting with the PTC of the 50S ribosomal subunit) by the expression of acetyltransferases known as CATs (chloramphenicol acetyltransferases) (Schwarz et al., 2004).

Degradation of the drug. Another traditional enzymatic alteration, which lead to destroying the amide bond of the β-lactam ring of the β-lactam antibiotic molecules by the action of β-lactamases, were first described in the early 1940s, one year before penicillin was introduced to the market, however, there is evidence of their existence for millions of years (Abraham and Chain, 1940; D'Costa et al, 2011). Infections caused by penicillin-resistant *S. aureus* became clinically relevant after penicillin became widely available and the mechanism of resistance was found to be a plasmid-encoded penicillinase that was readily transmitted between *S. aureus* strains, resulting in rapid spreading of the resistance trait (Bush, 2013). In order to overcome this problem, new β-lactam compounds with wider spectrum of activity and less susceptibility to penicillinases (such as ampicillin) were manufactured. However, during the 1960s a new plasmid-encoded β-lactamase capable of hydrolyzing ampicillin was found among gram negatives. From then on, the development of newer generations of β-lactams has systematically been followed by the rapid appearance of enzymes capable of destroying any novel compound that reach the market, in a process that is a prime example of antibiotic driven adaptive bacterial evolution (www.lahey.org/studies).

4.2 DECREASED ANTIBIOTIC PENETRATION AND EFFLUX

Many of the antibiotics used in clinical practice must penetrate the outer and/or cytoplasmic membrane in order to exert its antimicrobial effect. The outer membrane acts as the first-line of defense against the penetration of multiple toxic compounds, including several antimicrobial agents. For example porins, known as a water-filled diffusion channels, could help to lead antibiotic resistance in case of hydrophilic molecules such as β-lactams, tetracyclines and some fluoroquinolones which are particularly affected by changes in permeability of the outer membrane (Pagès et al., 2008). There are classical examples of porin-mediated antibiotic resistance such as three major proteins produced by *E. coli* (known as OmpF, OmpC and PhoE) and the *P. aeruginosa* OprD (also known as protein D2) (Munita and Arias, 2016).

Efflux pumps. The first described system able to pump tetracycline out of the cytoplasm of *E. coli* dates from the early 1980s and has been named efflux pumps system (McMurry et al., 1980), thus efflux pumps can also result in antimicrobial resistance. Since then, many classes of this have been characterized in both gram-negative and gram-positive pathogens. There are 5 major families of efflux pumps: the ATP-binding cassette family (ABC), the major facilitator superfamily (MFS), the multidrug and toxic compound extrusion family (MATE), the small multidrug resistance family (SMR), the resistance-nodulation-celldivision family (RND) (Figure 14) .The differences in the families could be found in terms of structural conformation, energy source, range of substrates they are able to extrude and in the type of bacterial organisms in which they are distributed. These systems may be substrate-specific (for a particular antibiotic such as tetracycline and macrolides in pneumococci) or with broad substrate specificity, which are usually found in multiple drug resistance bacteria (Poole, 2005). Also, this mechanism of resistance influences a wide range of antimicrobial classes including protein synthesis inhibitors, fluoroquinolones, β-lactams, carbapenems and polymyxins.

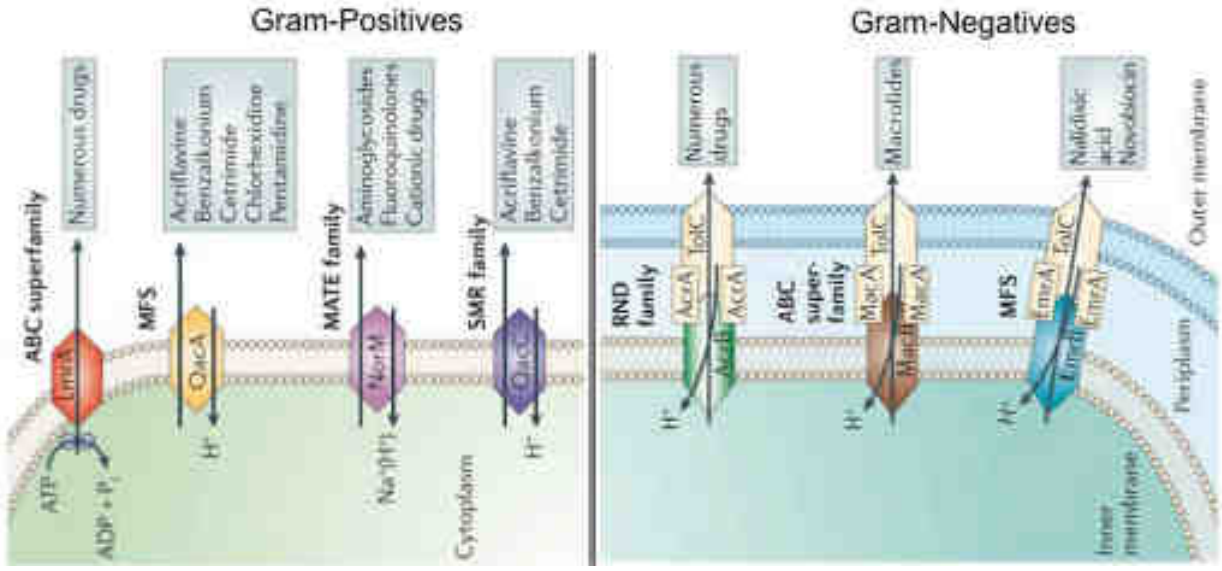

Figure 14: Different types of efflux pumps in gram-positive and gram-negative bacteria (Piddock, 2006).

4.3 CHANGES OF THE TARGET SITES

Bacteria developed different strategies of antimicrobial resistance in the directions of avoiding the action of the antibiotics by modifications (that result in decreased affinity for the antibiotic molecule) or protection (avoiding the antibiotic to reach its binding site) their target site. Almost all of the clinically relevant genes involved in this mechanism of resistance are carried by MGEs (mobile genetic elements).

Bacteria developed various ways of **target modifications** such as point mutations in the genes encoding the target site, enzymatic modification of the binding site, replacement or bypass of the original target.

Mutational changes. Antibiotic resistance due to mutational changes was described according to oxazolidinones actions (linezolid and tedizolid). These drugs inhibits protein synthesis by interfering with the positioning of the aminoacyl-tRNA at the A site. Linezolid is the most widely used antibiotic of this class, mechanisms of linezolid resistance include mutations in genes encoding the domain V of the 23S rRNA and/or the ribosomal proteins L3 and L4, and methylation of A2503 (*E. coli* numbering) in the 23S rRNA mediated by the Cfr enzyme (Figure 15) (Mendes et al., 2014). Regardless of the position and type of genetic change, these mutations result in decreased affinity of the drug for its ribosomal target (Munita and Arias, 2016).

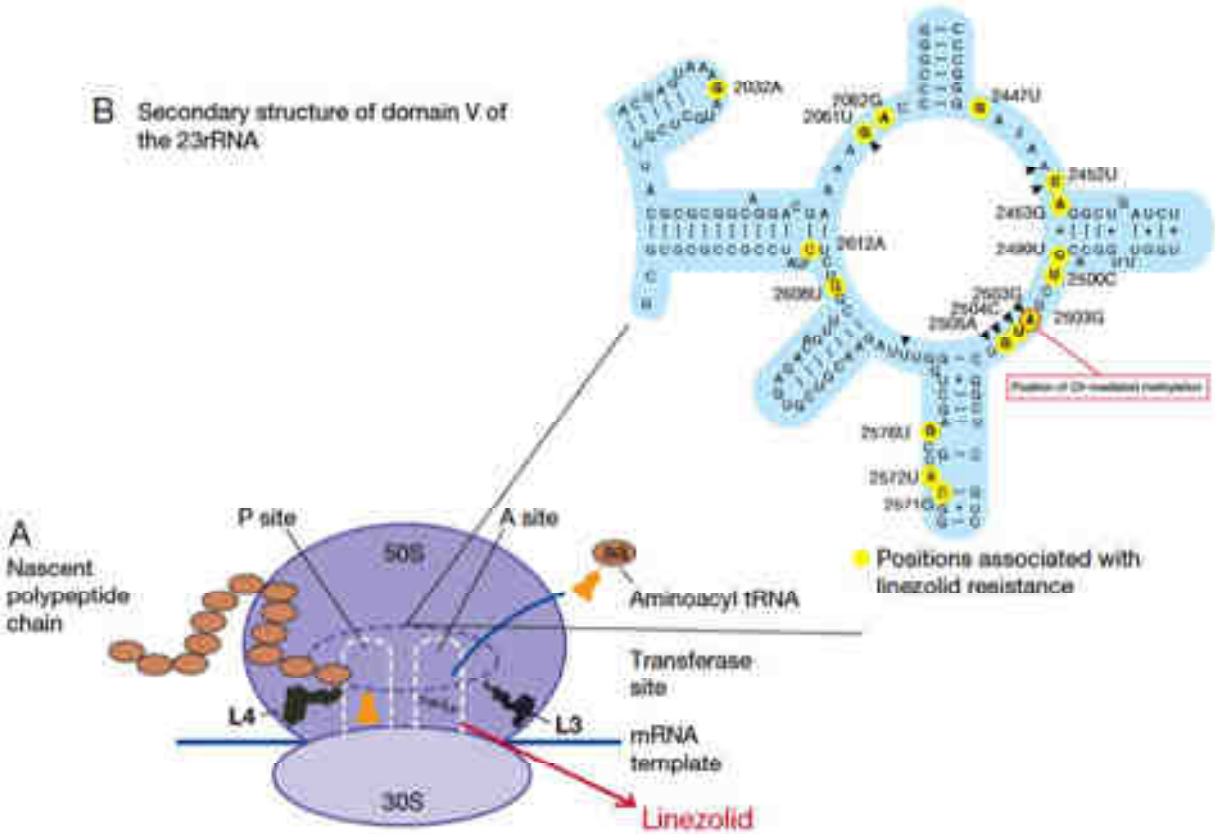

Figure 15: Schematic representation of the mechanism of action and resistance to linezolid (Munita and Arias, 2016).

Enzymatic modification. One of the best characterized examples of resistance through enzymatic modification of the target site is the methylation of the ribosome catalyzed by an enzyme encoded by the erm genes (erythromycin ribosomal methylation), which results in macrolide resistance. These

enzymes are capable of mono- or dimethylating an adenine residue in position A2058 of the domain V of the 23rRNA of the 50S ribosomal subunit. Due to the fact that macrolides, lincosamides, and streptogramin B antibiotics have overlapping binding sites in the 23S rRNA, expression of the *erm* genes confers cross-resistance to all of these antibiotics (Leclercq, 2002; Weisblum, 1995). More than 30 different *erm* genes have been described, for example in staphylococci, the most important erm genes are *ermA* (mostly distributed in a transposon in MRSA) and *erm(C)* (found in plasmids in methicillin-susceptible *S. aureus*).

Bacteria are capable of developing of new targets, by using complete replacement strategy that accomplishes similar biochemical functions of the original target however are not inhibited by the antimicrobial molecule. The methicillin resistance in *S. aureus* and vancomycin resistance in enterococci are the most relevant clinical examples of this strategy.

"Bypass". One of the route of avoiding the antimicrobial action is overproducing the antibiotic target, which named "bypass" of the metabolic pathway. One of the example that is associated with *S.aureus* resistance to β-lactams results from the acquisition of a foreign gene mecA often located in a large DNA fragment designated staphylococcal chromosomal cassette mec (SCCmec). The antibacterial activity of β-lactams relies on their ability to disrupt cell wall synthesis through inhibition of PBPs (enzymes responsible for the transpeptidation and transglycosylation of peptidoglycan units emerging from the cytoplasm). In its turn mecA gene encodes PBP2a, a PBP that has low affinity for all β-lactams (penicillins, cephalosporins and carbapenem) and thus acquisition of mecA renders most β-lactams useless against MRSA (Munita and Arias, 2016).

Another important example of the replacement and bypass strategy to achieve resistance is related to vancomycin resistance. Development of high-level vancomycin resistance in *S. aureus* (vancomycin-resistant *S. aureus*, VRSA) was first described in 2002 and was the result of acquisition by an MRSA strain of the vanA gene cluster from a VRE (*E. faecalis*) isolate (Sievert et al., 2008).

One of the best studied examples of **target protection** is tetracycline resistance determinants TetO and TetM proteins which interact with the ribosome and dislodge the tetracycline from its binding site in a GTP-dependent manner. Dönhöfer et al. showed that TetM directly dislodges and releases tetracycline from the ribosome by an interaction between the domain IV of the 16S rRNA and the tetracycline binding site. Furthermore, this interaction alters the ribosomal conformation, preventing rebinding of the antibiotic (Dönhöfer et al., 2012). TetO has also been shown to compete with tetracycline for the same ribosomal space and to alter the geometry of the binding site of the antibiotic, displacing the molecule from the ribosome and allowing protein synthesis to resume (Li et al., 2013).

5. *S. AUREUS* RIBOSOME AS A TARGET FOR DEVELOPING NEW THERAPEUTIC DRUGS

The implementation of antimicrobial therapy in clinical practice has been one of the most successful advances of modern medicine, paving the way for complex and highly sophisticated medical interventions that has allowed to significantly prolong the living span of the population around the globe. In order to survive, bacteria, in a process likely pressed by the increase use of antimicrobials in clinical practice, have developed complex and creative strategies to circumvent the antibiotic attack. Indeed, infections that are untreatable due to multidrug resistance of the infected organism have

become more common in clinical settings. This dire scenario has been worsened by a shortage of research and development on antibiotics. If we are to tackle this problem, efforts on research and development need to be heavily increased and supported. A complete understanding of the mechanisms by which bacteria become resistant to antibiotics is of paramount importance to design novel strategies to counter the resistance threat. We are in need of developing antibiotics with the understanding that the microorganism will respond to them and resistance will develop. Therefore, efforts to develop antibiotics and study mechanisms of resistance should be continuous, resilient and steady.

One of the main attractive target for development new therapeutic drugs is ribosome. A fortiori there are already some examples of successfully introduced synthetic antibiotics, linezolid and tedizolid that were developed for treatment of serious infections caused by Gram-positive bacteria that are resistant to several other antibiotics. As already mentioned, unrevealing the structure of ribosomes from Gram-negative bacteria has led to significant progress in understanding antibiotics action. However, this knowledge cannot be always expanded to Gram-positive bacteria that have differences in translation apparatus. Thus, solving the structure of *S. aureus* 70S ribosome will lead us to better understanding of the regulation of protein synthesis in Gram-positive bacteria, their mechanisms of antibiotics resistance. Structure of S. aureus ribosome will provide insights for design of new drugs against this pathogen.

The first work that shed light on the structure of the *S. aureus* ribosome was solved by A.Yonath's group. The crystal structure of large ribosomal subunit from *S. aureus* with complexes of known antibiotics (linezolid and telithromycin) and with new potential antibiotic (pleuromutilin derivative) (Eyal et al., 2015) showed specific structural motifs that may indicate possible features involved in species-specific responses to antibiotics. This work provided unique structural tools for discriminating between pathogenic bacteria and the microbiome, namely the useful bacterial species within the human body, mainly in the gut flora.

Later, thanks to two ribosome groups Yusupov's and Yonath's, structural information about *S.aureus* ribosome started to appear more often. Almost all the works were carried out by cryo-electron microscopy and NMR.

First full 70S ribosome structure from *S. aureus* has been solved by cryo-electron microscopy (as already discussed in X-ray and cryo-EM microscopy of the ribosome chapter) at 3.8 Å in 2016. Comparative analysis with other known bacterial ribosomes pinpointed several unique features specific to *S. aureus* around a conserved core, at both the protein and the RNA levels (Khusainov et al., 2016).

Recently several works has been published, deserving huge attention, in the study of the formation of 100S ribosome dimer in the *S. aureus*. Formation of 100S ribosome dimer is generally associated with translation suppression in bacteria. These works are represent one of the first milestones toward unraveling the mechanism for ribosome hibernation in *S. aureus*, which should help guide the development of more selective treatments against this pathogen.

First work under this direction was published by Yusupov's laboratory and they reported the structures of hibernating ribosomes from *S. aureus* containing a long variant of the hibernation-promoting factor (HPF) that was solved using cryo-electron microscopy. They showed that the N-terminal domain of S. aureus HPF binds to the 30S subunit, which is the same for shorter variants of HPF in other species. In case of C-terminal domain of *S. aureus* HPF, it protrudes out of each ribosome in order to mediate dimerization. Ribosome association into disomes is stabilized by helix 26 of the 16S ribosomal RNA.

Also was confirmed that ribosomes in the 100S particle adopt both rotated and unrotated conformations (Khusainov et al., 2017).

Another work which was continuing this story was done by Yonath's group and showed more detail information about interactions of 100S. This is first structure of the native 100S ribosome from *S. aureus* which has been solved by cryo-EM and revealed the molecular mechanism of its formation. They showed that 100S dimer is formed through interactions between rRNA h26, h40, and protein uS2, involving conformational changes of the head as well as surface regions that could potentially prevent RNA polymerase from docking to the ribosome (Matzov et al., 2017).

In addition, studies continued at full speed in the direction of binding *S.aureus* with already known and new antimicrobial agents. For example, novel pleuromutilin antibacterial compound (lefamulin), highly active against multi-resistant pathogens, has been co-crystalized with 50S ribosome from *S.aureus*. According the crystal structure, lefamulin is bound at the PTC. They also showed that all pleuromutilins bind to ribosomes at the same pocket and form three hydrogen bonds between the drug's acetyl carbonyl with the NH and NH2 of G2061 and between C11 hydroxyl group with the phosphate group of G2505 (Eyal et al., 2016). According to cryo-electron microscopy Yonath's group observed an unorthodox mechanism of resistance to the antibiotic linezolid in the 70S ribosomes from a clinical isolate of *S.aureus*. This structural information demonstrated that a single amino acid deletion in ribosomal protein uL3 confers linezolid resistance despite being located 24 Å away from the linezolid binding pocket in the peptidyl-transferase center. The mutation induces a cascade of allosteric structural rearrangements of the rRNA that ultimately results in the alteration of the antibiotic binding site (Belousoff et al., 2017).

Despite the fact that large-scale studies are going in the direction of the structural investigation of the *S.aureus* ribosome, the crystal structure of 70S ribosome has not yet been solved. In connection with the lack of information integrity the overall picture remains incomplete. As a result, there is a problem of a full understanding of the resistance mechanisms and the lack of essential structural model for testing potential antimicrobial compounds and, consequently, developing new antibiotics against multidrug-resistant bacteria.

III MAIN CHARACTERISTICS OF CANCER

Cancer is a major burden of disease worldwide. Each year, tens of millions of people are diagnosed with cancer around the world, and more than half of the patients eventually die from it. In many countries, cancer ranks the second most common cause of death following cardiovascular diseases. With significant improvement in treatment and prevention of cardiovascular diseases, cancer has or will soon become the main cause of death worldwide. As elderly people are most susceptible to cancer and population aging increases in many countries, cancer will remain a major health problem around the globe (Ma and Yu, 2006).

The word cancer came from the Greek word “karkinos” to describe carcinoma tumors by a physician, Hippocrates (460–370 B.C), but he was not the first to discover this disease. Some of the earliest evidence of human bone cancer were found in mummies in ancient Egypt and in ancient manuscripts dating in 1600 B.C (Brothwell, 1967). The world’s oldest recorded case of breast cancer hails from ancient Egypt in 1500 BC and it was recorded that, at the time, there was no treatment for the cancer, only palliative cures. According to inscriptions, surface tumors were surgically removed in a similar manner as they are removed today.

Cancer is a class of diseases characterized by out-of-control cell growth. There are over 100 different types of cancer, and each is classified by the type of cell that is initially affected. Some types of cancer cells often travel to other parts of the body through blood circulation or lymph vessels, where they begin to grow (metastasis). Generally cancer cells develop from normal cells due to damage of DNA. Most of the time DNA damages are repaired by complex mechanisms of DNA repair; however, when the body is not able to deal with them, the cells accumulate damages and, in turn, they can develop cancers.

A central feature of today's molecular view of cancer is that cancer does not develop all at once, but across time, as a long and complex succession of genetic changes. Each change enables precancerous cells to acquire some of the traits that, altogether, give rise to the malignant growth of cancer cells.

1. CANCER CONTROL SYSTEM

There are two types of genes proto-oncogenes and tumor suppressor genes regulate process of triggering cancer. In the normal cells, these genes control the cell cycle, the sequence of events by which cells enlarge and divide. However, when proto-oncogenes genes are mutated, they become oncogenes, which in turn stimulate an excessive division. Mutations in tumor suppressor genes lead to removing the critical inhibition step of cell division that normally prevents excessive growth. As the result both of these mutations collectively lead to uncontrolled cell division that occurs in human cancers.

Besides the proto-oncogenes and tumor suppressor genes which controls the proliferation cells, there are at least three other systems (DNA repair pathway, p53 protein, telomeres) that can help them to avoid runaway cell division. The DNA repair pathway operates in virtually every cell of the body, detecting and correcting errors in DNA. During all lifetime, a person's genes are under constant attack,

both by carcinogens imported from the environment and by chemicals produced by the cell itself. Also, errors may occur during DNA replication and in most cases, such errors are rapidly corrected by the cell's DNA repair system. However when the system stops working the mutation becomes a permanent feature in that cell and in all of its descendants. Despite the fact that DNA repair pathway system is highly effective and many years typically must pass before all the mutations required for cancer to develop occur together in one cell there is mutations in DNA repair genes can undermine this repair system and change the cells behavior dramatically.

A second system involves the p53 protein which in the normal cells, not only halts cell division, but induces apoptosis in abnormal cells. However p53 is mutated in many types of cancer cells and this contributes to the growth of tumors and it makes cancer cells resistant to chemical treatment.

The telomeres are the DNA segments at the ends of chromosomes and these segments shorten each time chromosome replicates. In the normal, healthy cells whenever the telomeres are shorter than some threshold length, they trigger an internal signal that causes the cell to stop dividing. However, if the cells continue dividing further shortening of the telomeres eventually causes the chromosomes to break apart or fuse with one another that are inevitably leads to death of the cell. In case of cancer cells have been discovered that telomerase (enzyme) systematically replaces telomeric segments that are trimmed away during each round of cell division. Telomerase is present in most cancer cells and enables the cells to proliferate endlessly.

2. MECHANISMS OF DRUG RESISTANCE

Cancer drug resistance constitutes a major impediment in medical oncology. Clinically, resistance can arise prior to or as a result of cancer therapy. There are different mechanisms adapted by cancerous cells to resist to the treatment: alteration in drug transport, metabolism, mutation, amplification of drug targets, epithelial-mesenchymal transition, epigenetic modifications, as well as genetic rewiring which can lead to impaired apoptosis (Housman et al., 2014). Tumor heterogeneity may also contribute to resistance, where small subpopulations of cells may acquire or stochastically already possess some of the features enabling them to emerge under selective drug pressure. Making the problem even more challenging, some of these resistance pathways lead to multidrug resistance, generating an even more difficult clinical problem to overcome.

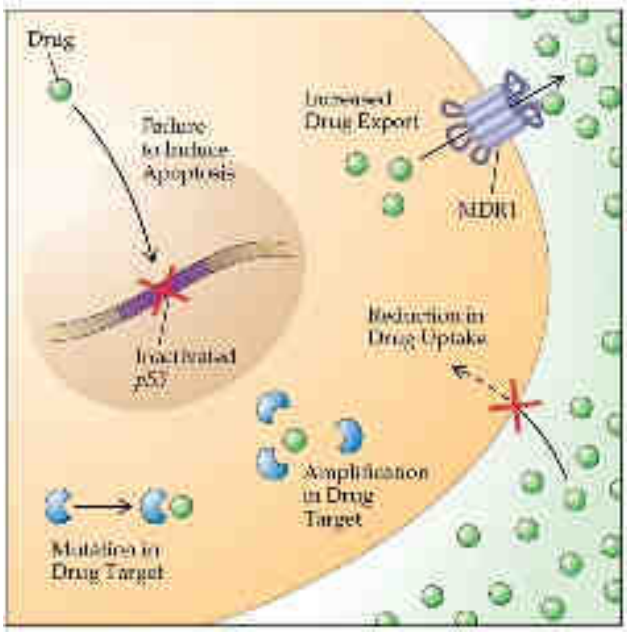

Figure 16: Mechanisms of drug resistance (Molecular Genetics of Cancer, Figure 12).

Both primary and acquired resistance can be caused by alterations to drug metabolism including its **uptake, efflux,** and **detoxification**. The means by which drugs enter cells depend on their chemical nature, and it mainly necessitates the use of receptors, which they bind to and transmit their effects without cellular entry, or transporters, which allow their cellular entry (Gottesman, 2002). At this level, resistance can result from mutations that modify activity or reduce the expression of surface receptors and transporters. On the other hand, enhanced drug efflux is frequently caused by increased expression of ATP binding cassette (ABC) membrane transporters (Gottesman et al., 2002). Among the 48 known ABC transporters in humans, the increase of three members, P-gp (MDR1 gene product), Multidrug resistance-associated protein 1 (MRP1) and mitoxantrone resistance protein (MXR), have been correlated with cancer resistance to various drugs (Gottesman, 2002; Gottesman et al., 2002). For instance, P-gp transports a wide variety of hydrophobic anti-cancer drugs such as vinblastine, doxorubicin, vincristine and taxol (Gottesman et al., 2002). MRP1 on the other hand, transports negatively charged natural-product drugs in addition to drugs that have been modified by the conjugation of glutathione (GSH), glucuronic acid or sulfate (Jedlitschky et al., 1996; Hipfner et al., 1999; Konig et al., 1999; Borst et al., 2000); finally, MXR overexpression has been correlated with resistance to topoisomerase I inhibitors, anthracyclines, and mitoxantrone (Gottesman, 2002).

To exert their cytotoxic effects, many anti-cancer drugs must undergo metabolic activation. To circumvent the effects of these drugs, cancer cells develop resistance through decreased **drug activation** (Kufe and Spriggs, 1985; Bardenheuer et al., 2005). This occurs via the downregulation or mutation of enzymes involved in this metabolic pathway, such as deoxycytidine kinase in the case of cytarabine (Sampath et al., 2006). Drug inactivation can also play a major role in the development of resistance. These mechanisms include, for example, conjugation of the drug to GSH, a powerful anti-oxidant that protects the cells against the damaging effects of reactive oxygen species (Wilson et al., 2006). GSH conjugation to platinum drugs, such as oxaliplatin and cisplatin used in the treatment of various types of cancers, renders them substrates for ABC transporters which enhances drug efflux (Meijer et al., 1992; Ishikawa and Ali-Osman, 1993). Furthermore, the topoisomerase I inhibitor, irinotecan, used for treating colon cancer, have been shown to become inactivated via phase I drug metabolizing enzymes, CYP450 (Xu and Villalona-Calero, 2002). Finally, binding of platinum drugs,

particularly cisplatin, to metallothionein (MT), a small cysteine-rich protein, is another means of drug inactivation (Kelley et al., 1988; Kasahara et al., 1991).

In case of **alteration of drug targets**, many cancer cells develop an overreliance or dependency on an oncogene. This is referred to as oncogene addiction (Arber et al., 1997; Weinstein, 2002; Weinstein and Joe, 2006; Sharma and Settleman, 2007). Targeting such oncogenes provided a basis for the development of targeted therapies. There are several examples of such targeted therapies: (a) imatinib targeting BCR/ABL tyrosine kinase in chronic myelogenous leukemia (CML) (Hughes et al., 2003), (b) gefitinib and erlotinib targeting the epidermal growth factor receptor (EGFR) tyrosine kinase domain in non-small cell lung carcinoma (Lynch et al., 2004; Shepherd et al., 2005; Taron et al., 2005), and (c) trastuzumab targeting human epidermal growth factor receptor-2 (HER-2) receptor in breast carcinomas (Slamon et al., 2001; Piccart-Gebhart et al., 2005). Unfortunately, the long term effectiveness of these drugs is hindered by the development of drug resistance due to mutation of the targeted protein (Gioeli, 2011; Wong and Lee, 2012). In the case of BCR/ABL and EGFR inhibitors, resistance emerges as a result of mutations occurring at the gatekeeper residues of the kinase domain which disables drug binding (Gorre et al., 2001; Blencke et al., 2003; Kobayashi et al., 2005; Pao et al., 2005; Soverini et al., 2005; Balak et al., 2006; Jabbour et al., 2006, 2008; Nicolini et al., 2006; Apperley, 2007; Costa et al., 2007; Bean et al., 2008; Gioeli, 2011). Furthermore, it has been demonstrated that mutations conferring resistance can be detected prior to treatment in small subpopulations of tumor cells suggesting that these mutant forms were selected via the targeted therapy used (Hofmann et al., 2003; Toyooka et al., 2005; Inukai et al., 2006). In conclusion, understanding how mutations in the target proteins confer resistance enables the development of new therapeutic approaches to overcome resistance. For instance, the second generation CML inhibitors have been developed based on mutational studies of patients who have become Gleevec resistant.

Other mechanisms by which cancerous cells circumvent the effects of targeted inhibitors have also been described, including amplification of alternative oncogenes or inactivation of alternative survival pathways (le Coutre et al., 2000; Engelman et al., 2007). In some cases, targeting of one protein alone (to which cells are showing dependency on) can become ineffective because another parallel pathway supports tumor survival. In this case, the two pathways develop a synthetic lethal relationship (Hartman et al., 2001; Tucker and Fields, 2003). This way, the loss/inactivation of one of these genes would be supported by the other pathway and for a more effective treatment, one would need to target both pathways (Luo et al., 2009; Nijman, 2011).

Additionally, resistance could result from **cell death inhibition** evasion of apoptotic pathways triggered by the acquisition of either inactivating mutations in genes coding for apoptotic proteins, such as p53, or activating mutations in genes coding for anti-apoptotic proteins, such as B cell lymphoma 2 (Teicher, 2006). Indeed p53 mutations have been correlated with *de novo* resistance to doxorubicin treatment in patients with advanced breast cancer, as well as resistance to anthracyclines in a mouse sarcoma tumor model (Aas et al., 1996; Levine, 1997).

The **repair of damaged DNA** has a clear role in anticancer drug resistance. In response to chemotherapy drugs that either directly or indirectly damage DNA damage response (DDR) mechanisms can reverse the drug-induced damage. For example, platinum-containing chemotherapy drugs such as cisplatin cause harmful DNA crosslinks, which can lead to apoptosis. However, resistance to platinum-based drugs often arises due to nucleotide excision repair and homologous

recombination, the primary DNA repair mechanisms involved in reversing platinum damage (Bonanno et al., 2014;Olaussen et al., 2006; Selvakumaran et al., 2003). Thus, the efficacy of DNA-damaging cytotoxic drugs depends on the failure of the cancer cell's DDR mechanisms. Inhibition of repair pathways used in conjunction with DNA damaging chemotherapy could sensitize cancer cells and therefore increase efficacy of the therapy.

Impaired gene regulation lies at the heart of many disorders, including developmental diseases and cancer. Although all somatic cells have the same genetic information contained within the sequence of their DNA, only a portion of this information is utilized in each cell, and a large fraction of cellular transactions is dedicated to regulating its expression at four main levels: transcriptional, co-/post-transcriptional, translational and post-translational. These regulatory processes rely heavily on the use of modifications that target the three biopolymer mediators of genetic information, DNA, RNA and proteins. Interestingly, all three of them can be chemically modified by methylation. This modification is usually catalyzed by methyltransferase enzymes that use S-adenosylmethionine (SAM) as a methyl group donor. In general, methylation does not change the sequence of these polymers, but modifies their biochemical properties and interaction partners. Consequently, methylation is often considered as an epigenetic modification which is an important set of mechanisms that cause resistance to cancer treatment and can also influence carcinogenesis. Although methylations of DNA and histones have been a major research focus since the 1980s and 1990s, respectively, the study of RNA methylations has lagged mainly due to technical challenges for its detection (Xhemalce, 2013). However, recent technical advances and the discovery of novel RNA methylases and demethylases have announced the birth of a new field, termed RNA epigenetics (He, 2010).

Methylation is involved in many steps of RNA biology, with it counting for more than two-thirds of the >100 chemically distinct known RNA modifications (Cantara et al., 2011). However, despite the abundance of RNA methylations, little is known about the function of most of these modifications. RNA methylations are generally catalyzed post-transcriptionally and can be divided into two major groups depending on their localization on the RNA polymer: they either decorate the RNA extremities: 5'- and 3'-ends or occur on specific residues on the bases or 2'-hydroxyls of the RNA nucleotides (Xhemalce, 2013).

The recent discovery that N6-methyladenosine (m6A), a modification present in mRNAs and long noncoding RNAs, can be removed by the activity of RNA demethylases, launched the field of epitranscriptomics; the study of how RNA function is regulated through the addition or removal of post-transcriptional modifications, similar to strategies used to regulate gene expression at the DNA and protein level. The abundance of RNA post-transcriptional modifications is determined by the activity of writer complexes (methylase) and eraser (RNA demethylase) proteins. Subsequently, the effects of RNA modifications materialize as changes in RNA structure and/or modulation of interactions between the modified RNA and RNA binding proteins or regulatory RNAs. Disruption of these pathways impairs gene expression and cellular function. RNA post-transcriptional modifications, through their impact on transcription, splicing, mRNA stability, and rate of translation, regulate essential features of a cell. It is clear that the balance between methylation and demethylation at specific RNA transcripts plays a critical role in human health and represents an attractive target for therapy (Batista, 2017).

3. POTENTIAL ANTICANCER DRUGS AGAINST RIBOSOME ASSEMBLY

Traditional anticancer chemotherapeutics targeting DNA replication and cell division have severe side effects, but they have been proved to be highly successful in treating some cancers. Drugs targeting signalling oncoproteins that have gained tumor-driving functions through mutations or overexpression were subsequently developed to increase specificity and thus reduce side effects, but have disadvantages such as the development of resistance. Now, a new wave of small-molecule anticancer agents is emerging, targeting complex multicomponent cellular machineries — including ribosome, chromatin modifiers, heat shock protein chaperones — which interfere with those support systems that are more essential for cancer cells than for normal cells.

In 2015 the Karbstein's group has confirmed that ribosome assembly process can be a potentially fertile new target for anti-cancer drugs by detailing the essential function of a key component in the assembly process (Ghalei et al., 2015).

Translation, along with DNA replication and transcription, is a highly conserved, fundamental cellular process essential for cell growth and survival (Bhat et al., 2015). In more recent years, a number of inhibitors of eukaryotic translation have been identified and shown to affect distinct components of the complicated eukaryotic translation machinery from initiation to elongation, including pateamine A (PatA), lactimidomycin, and mycalamide B, all of which have been investigated (Dang et al., 2011; Garreau de Loubresse et al., 2014; Low et al., 2005; Schneider-Poetsch et al., 2010). Due to their higher proliferation rate and consequently higher demand for newly synthesized proteins, cancer cells in general appear more sensitive to inhibitors of translation, creating a therapeutic window for these inhibitors as potential anticancer drugs (Bhat et al., 2015).

To date, homoharringtonine, a translation elongation inhibitor, has been approved by the U.S. Food and Drug Administration as a treatment of chronic myeloid leukemia (CML), validating inhibition of translation as a viable strategy to treat cancer (Gandhi et al., 2014).

Recently have been shown that small molecule translation inhibitors, which is considerable needed for progress in antibacterial as well could be used as anticancer therapy (Prokhorova et al., 2016). Those knowledge has an extremely impact in the development of anticancer drugs. This work is presented evidence for amicoumacin A activity toward the eukaryotic ribosome in both mammalian and yeast systems, and revealed crystal structural details of its interaction with the yeast 80S ribosome. This study from Yusupova G. laboratory could be used for rational drug design aiming to improve amicoumacin A therapeutic potential. Amicoumacin A is the universal translation inhibitor since its binding pocket in the E-site of the small ribosomal subunit is highly conserved (Figure 17). It interacts either with universally conserved rRNA residues or with a backbone of rRNA and mRNA in a sequence-independent manner. Comparison of the structures of amicoumacin A complexes with bacterial (Polikanov et al., 2014) and eukaryotic ribosomes paves the way to the development of derivatives that may have better selectivity. While the RNA elements of the amicoumacin A binding site are absolutely identical for bacterial and eukaryotic ribosomes, structures of ribosomal proteins surrounding amicoumacin A on the ribosome are different (Prokhorova et al., 2016).

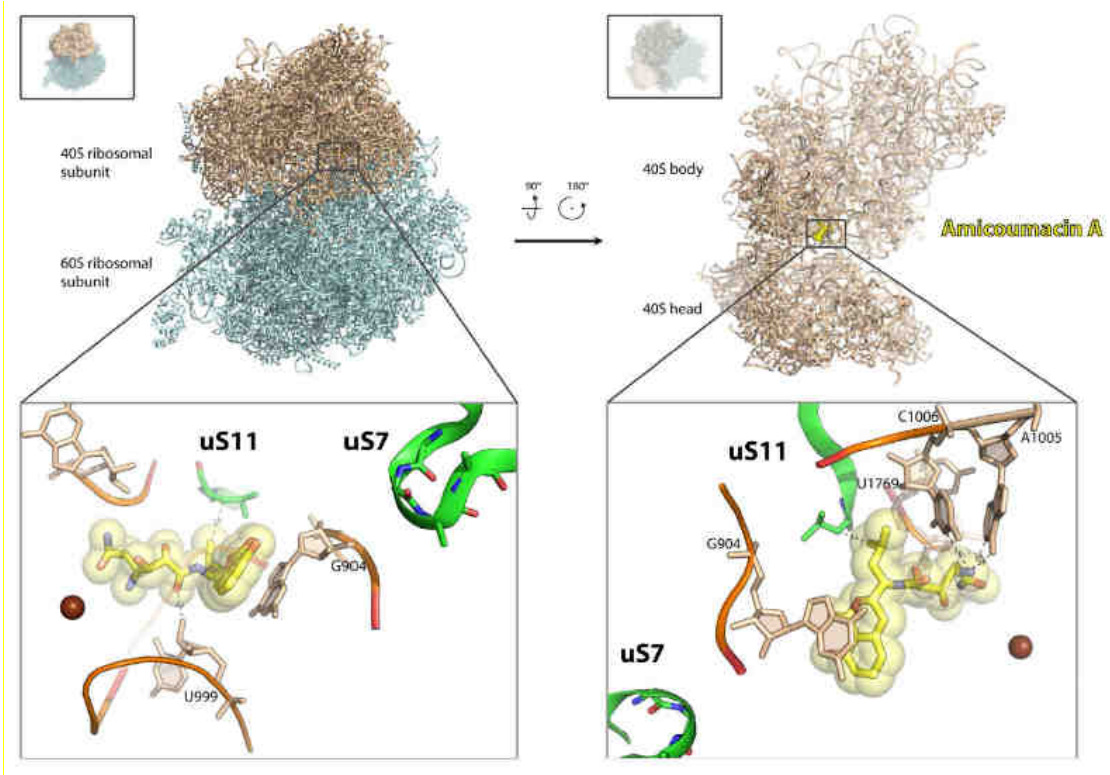

Figure 17: Structure of the amicoumacin A complex with yeast ribosome (Prokhorova et al., 2016). The binding pocket of amicoumacin A in small ribosomal subunit E-site. Two orientations of the 80S ribosome in complex with amicoumacin A are shown in the upper panel. The view from the side of the 40S head is shown on the left, and the view from the subunit interface is shown on the right.

A recently discovered, structurally unique alkaloid, (-)-agelastatin A (AglA), possesses potent antitumor activity, particularly against brain tumors due to its excellent penetration of the blood-brain barrier. AglA is a structurally unique brominated alkaloid isolated from the marine sponge *Agelas dendromorpha* by Pietra and coworkers in 1993 and belongs to the pyrrole-2-aminoimidazole alkaloid family along with the structurally related congeners Agelastatins B-F (AglB-AglF) (D'Ambrosio et al., 1993).

According to recent works, the Yusupov laboratory has contributed the X-ray crystal structure of the AglA in complex with the *Saccharomyces cerevisiae* 80S ribosome revealing further details of the interaction between AglA and the ribosome. AglA binds to the A-site of the peptidyl-transferase center (PTC) inducing multiple conformational changes upon its binding. The understanding of the molecular mechanism of binding of this drug to the ribosome will help to drive future design and synthesis of novel AglA analogs to increase potency and pharmacological properties.

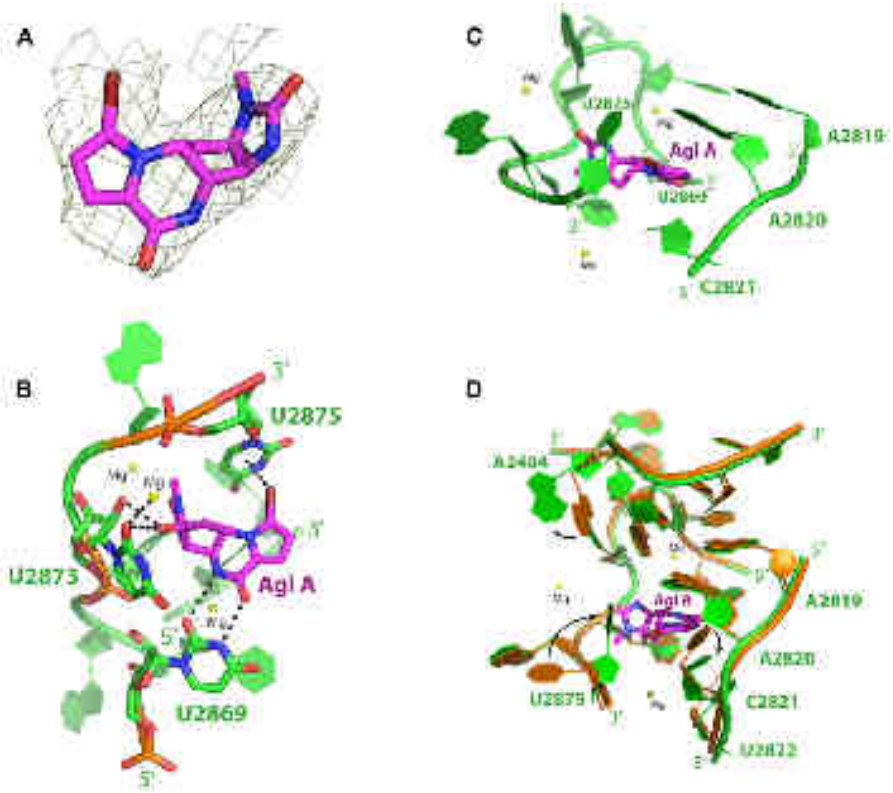

Figure 18: Crystal Structure of AglA-80S Ribosome (McClary et al., 2017). A) The 80S/AglA complex was solved a t a maximal resolution of 3.5 Å. They show the unbiased Fobs – Fcalc (Fo - Fc) map contoured at 3σ B) AglA forms hydrogen bonds with U2869 and U2873. The pyrimidine base of U2873 in the 25S rRNA tilts upon AglA binding to establish an additional bond with an ordered Mg^{2+} ion. In addition, the C13 bromine atom of AglA forms a halogen-π stacking interaction with U2875 (Reid et al., 2013), a quite unusual and unique feature for AglA binding to the A site of the PTC that further distinguishes it from all known elongation inhibitors. C). AglA binds the A-site cleft of the PTC in order to create stable contacts with the large subunit A site pocket, through the formation of π stacking interactions. D) Superimposition of the vacant ribosome structure (PDB: 4V88) and ribosome bound to AglA structure displaying major movements of nucleotides A2404, C2821, and U2875 induced upon binding of AglA to the A site pocket of the PTC, underscoring how natural products can fit into and modulate the conformation of the PTC of the eukaryotic ribosome.

Natural product inhibitors of eukaryotic protein synthesis have significant therapeutic potential to treat a wide range of human cancers. The structurally unusual labdane diterpenoids lissoclimides are powerful cytotoxins towards murine leukaemia and certain human carcinoma cell lines. Short semisynthesis and analogue-oriented synthesis approaches provide a series of lissoclimide natural products and analogues that expand the structure–activity relationships in this family. The semisynthesis approach yielded significant quantities of chlorolissoclimide (CL) to permit an evaluation against the National Cancer Institute's 60-cell line panel.

Recently, the Yusupov laboratory published a multidisciplinary study in which their unravel the mechanism of action of CL, a compound sharing chemical similarity to cycloheximide (CHX), but showing promising lower cytotoxicity (Könst et al., 2017). CL binds to the E-site of the 60S subunit and

creates novel interactions compared to CHX (Figure 19). In details, it creates an unusual halogen-π stacking interaction with residue G2794 through its chlorine atom.

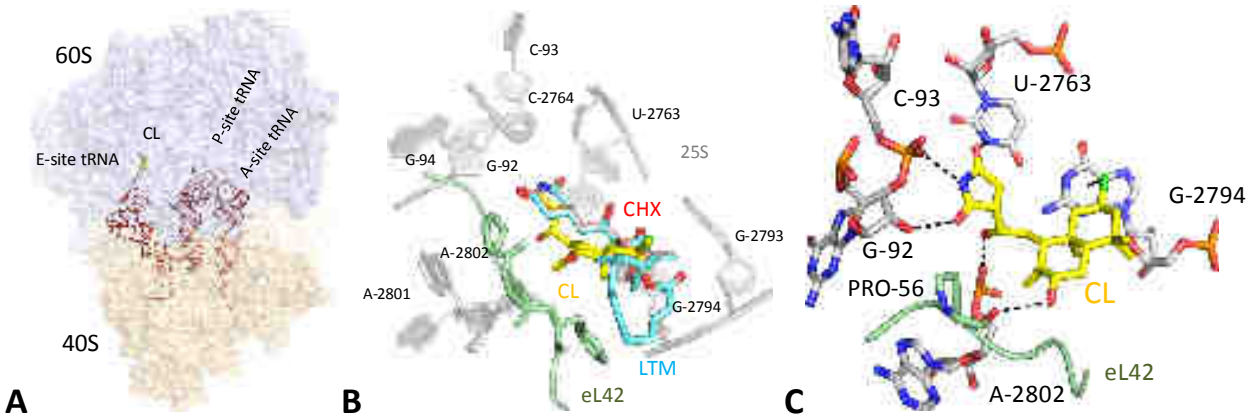

Figure 19: The X-ray co-crystal structure of CL with the eukaryotic 80S ribosome (adapted from Könst *et al*., 2017). A) CL clashes with the CCA-end of the E-site tRNA on the large ribosomal subunit (LSU). B) Comparison of the CL binding with that of CHX and lactidomycin (LTM) shows a similar network of interactions of the imide-containing moiety with a number of universally conserved nucleotides of the 25S rRNA, namely G92, C93 and U2763. C) Detail of the interaction that occur between the CL molecule and the neighboring residues. The 80S/CL complex has been determined to the resolution of 3.0 Å.

There are several unique features of CL binding to the eukaryotic ribosome:

1) C7-hydroxyl group present on the B ring forms a hydrogen bond with Pro56 on a stretched loop of the eukaryotic-specific ribosomal protein eL42;

2) Hydroxyl group on the linker between the decalin and the succinimide moieties interacts with the phosphate–oxygen backbone of nucleotide A2802 of the 25S rRNA;

3) Chlorine positioned on the decalin ring system interacts with G2794 of the 25S rRNA. The chlorine atom form a halogen–π interaction with the guanine residue with a face-on geometry.

Scientific interest also increases in the direction of already known small molecular inhibitors, which have been widely used in the treatment of cancerous tumors. The main tasks for researchers in this direction is to find new targets for binding drugs, to provide understanding in the design of more efficient drugs, to develop new therapeutic strategies and also to solve problems with different side effects. One of such known chemotherapeutic drug substances is a platinum-containing complex-cisplatin.

Platinum complexes are clinically used as adjuvant therapy of cancers aiming to induce tumor cell death. Depending on cell type and concentration, cisplatin induces cytotoxicity, for instance, by interference with transcription and/or DNA replication mechanisms. Additionally, cisplatin damages tumors via induction of apoptosis, mediated by the activation of various signal transduction pathways, including calcium signaling, death receptor signaling, and the activation of mitochondrial pathways. Unfortunately, neither cytotoxicity nor apoptosis are exclusively induced in cancer cells, thus, cisplatin

might also lead to diverse side-effects such as neuro- and/or renal-toxicity, bone marrow-suppression, allergic reactions, decrease immunity to infections, gastrointestinal disorders, hemorrhage, and hearing loss especially in younger patients. Moreover, the binding of cisplatin to proteins and enzymes may modulate their biochemical mechanism of action. While the chemotherapy with cisplatin is a cornerstone for the treatment of multiple cancers, but the challenge is that cancer cells could acquire resistance to cisplatin. Numerous mechanisms of cisplatin resistance were described before, including changes in cellular uptake, drug efflux, increased detoxification, inhibition of apoptosis and increased DNA repair.

Recent study demonstrated that cisplatin binds 20-fold more pervasively to RNA than to DNA, making RNA a potential new drug target for the platinum compound (Hostetter et al., 2012). Under the conditions of this study cisplatin toxicity was characterized by irreversible inhibition of cell division, but not apoptotic cell death of *S. cerevisiae*. This suggests that in comparison with mammalian systems, a mediator of cisplatin-induced apoptotic pathways, such as p53, is lacking in *S. cerevisiae*. These data showed significant accumulation of Pt adducts in eukaryotic RNA following treatment *in cellulo* with cisplatin, with significantly larger amounts of irreversible Pt-RNA adducts accumulating in ribosomal RNA as compared to mRNA, and a demonstrated specificity for particular binding sites in the eukaryotic ribosome. Later, according to the new information about cisplatin, structure biologists from Steitz laboratory solved the crystal structure of cisplatin in complex with the *Thermus thermophilus* 70S ribosome at 2.6 Å resolution. This structure provides the first high-resolution model of a cisplatin–RNA adduct. In this study, the authors identified nine cisplatin modification sites in the ribosome and described precise positions and interactions of cisplatin with ribosome components (Melnikov et al., 2016).Three of the observed moieties are coordinated by the N7-atoms of adenine bases: A790 of the 16S rRNA (Figure 20A and D), and A1848 and A2531 of the 23S rRNA (Figure 20B, E and F). Five moieties are coordinated by the N7-atoms of guanine bases at positions G1300 of the 16S rRNA and G27, G425, A1606, G2220, G2221 of the 23S rRNA (Figure 20). One cisplatin moiety is coordinated by the N-terminus of the ribosomal protein L9 (Figure 20I).

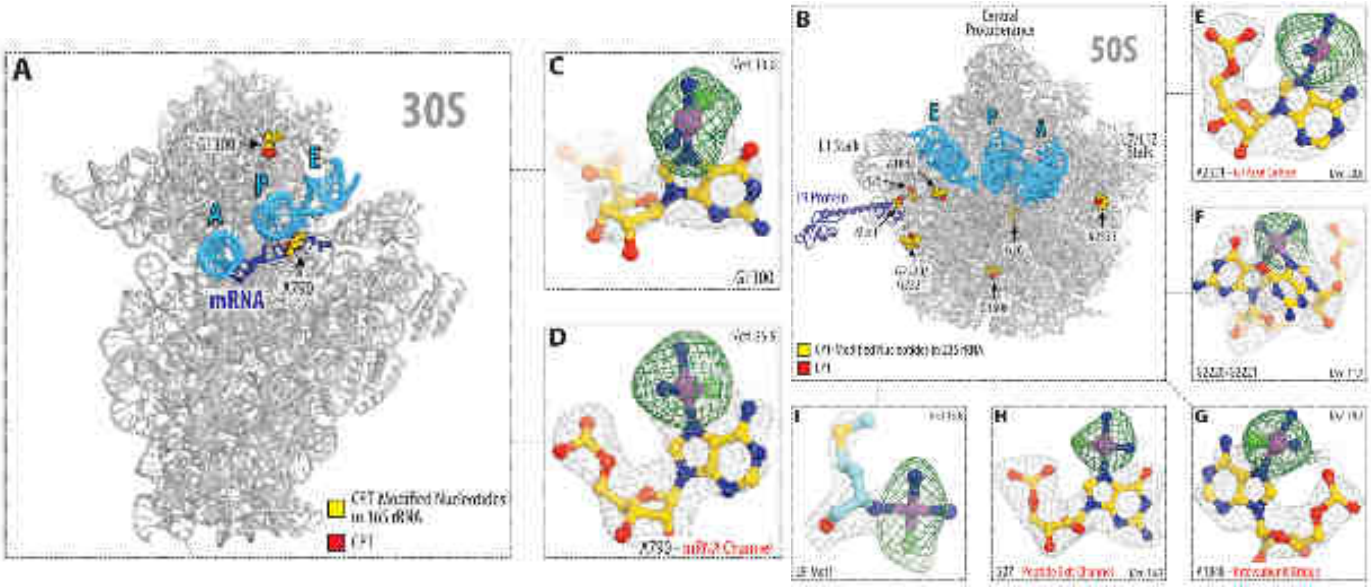

Figure 20: Cisplatin-binding sites on the ribosome (Melnikov et al., 2016).

In the small ribosomal subunit cisplatin targets the universally conserved nucleotide A790 of the 16S rRNA in the mRNA channel (Figure 21A). At this location, cisplatin forms an additional contact between the ribosome and the mRNA (Figure 21B), suggesting that cisplatin might stabilize mRNA binding to the ribosomal P site and thereby inhibit protein synthesis by preventing mRNA/tRNA translocation. Notably, the A790-modification site has a universally conserved structure, suggesting that the mRNA channel could be modified by cisplatin in the same way in the ribosomes from humans and other species (Figure 21C).

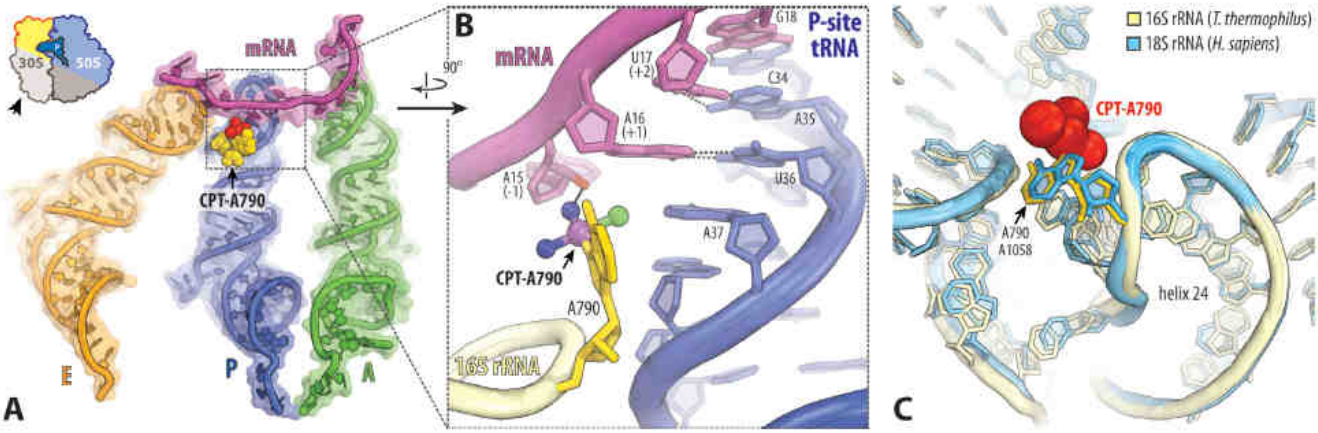

Figure 21: Cisplatin targets the mRNA channel in the ribosome (Melnikov et al., 2016). A) Overview and (B) close-up view of the cisplatin modification site in the mRNA channel, where cisplatin modifies the universally conserved base A790 and stabilizes contacts between the ribosome and the mRNA. C) Superposition of the 16S rRNA from *Thermus thermophilus* in the vicinity of the nucleotide A790 with the homologous region of the 18S rRNA from *Homo sapiens* (PDB ID: 4V6X (Anger et al., 2013)). Superposition is based on the alignment of nucleotides 787–795 from helix 24 of *T. thermophilus* 16S rRNA with nucleotides 1055–1063 of *H.sapiens* 18S rRNA.

In the large ribosomal subunit, cisplatin targets residue A2531 of the 23S rRNA, which contacts the GTPase activating center (A2662 in the sarcin-ricin loop) (Figure 22A). In this position, the cisplatin moiety lies at the binding interface of elongation factor G (EF-G) and clashes with the C-terminal portion of ribosomal protein L6, suggesting that cisplatin modification of A2531 could either alter EFG binding to the ribosome or affect GTP hydrolysis (Figure 22B). Notably, as is the case with the mRNA channel, the GTPase activating center is highly conserved across all species (Figure 22C), suggesting similar targeting of human ribosomes by cisplatin.

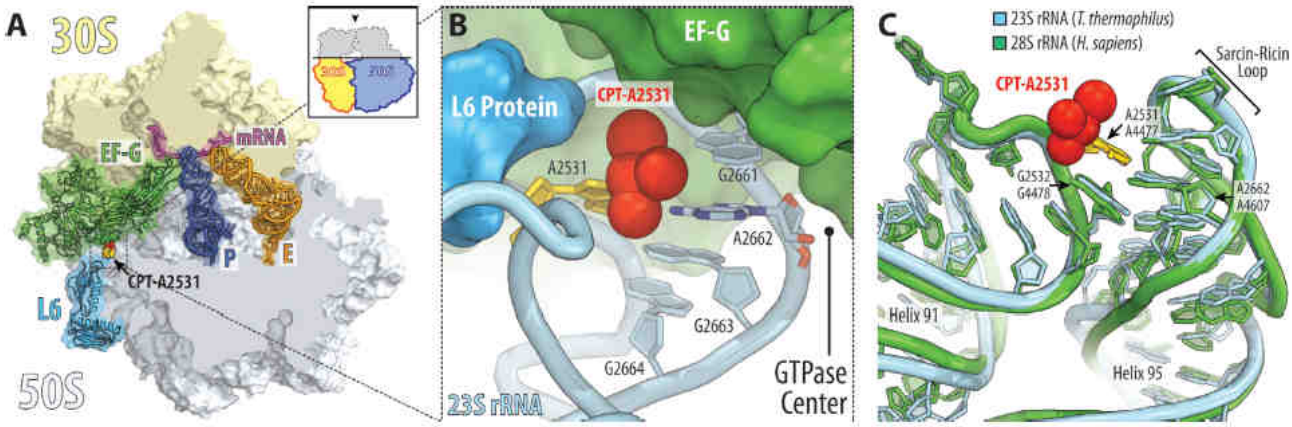

Figure 22: Cisplatin modification site near the GTPase activating center of the ribosome (Melnikov et al., 2016). A) Overview is from the top after removing the head of the 30S subunit and protuberances of the 50S subunit. B) Close-up view of the cisplatin position in the vicinity of the ribosome GTPase activating center. The structure of cisplatin-modified ribosome is superimposed with the structure of ribosome-bound EF-G (PDB ID: 4V5F (Gao et al., 2009)). Superposition is based on the alignment of the 23S rRNA. C) Superposition of the 23S rRNA from *Thermus thermophilus* in the vicinity of the GTPase activating center with the homologous region of the 28S rRNA from *Homo sapiens* (PDB ID: 4V6X (Anger et al., 2013)).

Until recently, it was thought that most of the ribosome-targeting drugs inhibit protein synthesis by altering the conformation of the ribosome or by preventing the proper binding of the ribosomal functional substrates. This paradigm, however, was challenged by recent structural studies of bacterial antibiotics blasticidin S (Svidritskiy et al., 2013), amicoumacin A (Polikanov et al., 2014), negamycin (Polikanov et al., 2014; Olivier et al., 2014) and hygromycin A (Polikanov et al., 2015; Kaminishi et al., 2015). These antibiotics were shown to tether the ligands (such as mRNA and tRNAs) to the ribosome or force their non-productive conformations. It appears from the structure of cisplatin modified ribosome that the inhibitory activity of cisplatin might rely on a similar mechanism, in which cisplatin stabilizes interactions between the ribosome and the messenger RNA (Melnikov et al., 2016).

Part I - Structural analysis and investigation of the *Staphylococcus aureus* ribosome

Results, Methods, Discussions and Perspectives

IV RIBOSOME PURIFICATION

In actively growing cells, ribosomes are relatively heterogeneous and have different conformational states, activity levels and are bound to a variety of ligands. Certainly, most ribosomes actively participate in the elongation step of translation, so they have minor conformational divergence and bind similar ligands involved in translation. However, there are other populations of non-translating ribosomes, which can be present as dissociated particles, stalled or inactive ribosomes.

When the cells are transferred to unfavourable conditions, all translating ribosomes continue the synthesis until they reach the stop codon and release newly synthesized protein. These ribosomes do not prepare for the next cycle and keep associated as 70S particles called run-off ribosomes. They are relatively homogeneous, although, some still have residual tRNAs, mRNA and translation factors bound.

Due to their mass, the total ribosome pool is rather easy to separate from other cellular components simply by several high-speed centrifugation steps. However, a sample for X-ray studies requires very high level of purity, homogeneity and stability. Therefore, purification of a unique population of ribosomes, capable of being crystallized, is a delicate procedure that requires a lot of effort, care and patience.

Two crucial parameters that have to be thoroughly controlled during purification are the concentrations of Mg2+ ions and monovalent salts. Magnesium stabilizes the ribosome and is particularly important for the association of small and large ribosomal subunits of bacterial ribosome. Monovalent salts at concentrations below 200 mM also contribute to the stability of bacterial ribosome, but at concentrations above 200 mM these salts can have an opposite effect and lead to destroying of ribosomal proteins (Spirin et al., 1971c; Stahli and Noll, 1977). Variations in the balance between magnesium and monovalent salts often help to ameliorate the selection of ribosomal populations.

Initially ribosome purification protocol from *S. aureus* was created and developed in laboratory Yusupov (Khusainov et al., 2016) based on the protocols used for bacteria *Thermus thermophilus* (Gogia et al., 1986; Yusupov et al., 2001) and yeast *Saccharomyces cerevisiae* (Ben-Shem et al., 2011). Unfortunately, sample which obtained after this protocol was not enough homogeneous, and crystals obtained from this sample gave poor diffractions (~18 Å), even after optimization of cryo-protection conditions.

Later, according cryo -EM analyzing of ribosomes, we obtained result in which approximately 10% ribosomes have tRNA contamination (A/P, P/p, P/E, E) and almost all of them bind with P-site of the ribosome. Thus, peptydil tRNA which probably has peptide on the surface of the ribosome could influence on diffraction. Also, cryo-EM analysis showed existing of tRNA in the E-site, however this contamination is not develop low diffraction, and even on the contrary improves it (Jenner et al., 2007). This suggestion found the proof in different works with *T. thermophilus* ribosome in the Yusupova G. laboratory, in which almost all ribosome contained deacylated tRNA in the E-site.

Thus, at this stage, my main task was to get rid of tRNA impurities. To achieve this goal, a number of experiments were performed to modify the ribosome purification protocol.

Ionic conditions, magnesium and polyethylene glycol (PEG) concentrations, sucrose gradients etc. were optimized during development of purification protocol.

Chemicals, plastic and kits were purchased from Sigma-Aldrich, Fluka, Merck Millipore, Hampton Research, Macherey Nagel, Qiagen. Ultrapure Milli Q water was used to prepare all buffers. All solutions were filtered using 0.22 µm filters or autoclaved.

1. DESCRIPTION OF INITIAL RIBOSOME PURIFICATION PROTOCOL FROM *S. AUREUS*, DEVELOPED IN THE YUSUPOV LABORATORY

1.1 *S. AUREUS* CELL GROWTH

Strain

Staphylococcus aureus strain *RN6390* the single most widely studied strain was used in the study, which is an 8325-4 strain generated by curing three prophage from NCTC 8325 clinical strain. RN6390 has an 11-bp deletion in *rsbU*, which encodes a positive regulator essential for the activity of the stress response sigma factor SigB. Thus the production of RNAIII is increased and the ability to form biofilms is decreased in this strain (Figure10). Avoiding biofilm formation is important for cells growth and harvesting.

Cells preparation

All manipulations with S. aureus cells were performed in special laboratory with safety level 2. Pre-culture inoculated according the ratio 1:2 (10ml of media in the 20ml of flasks). Single colony transferred in Brain Heart Infusion Broth (BHI) media in 180 rpm at 37°C for 17 h till OD^{600} ~ 5.0-5.5.

Two litres of S. aureus culture was grown at 37 °C / 180 rpm in Brain Heart Infusion broth (BHI) and harvested in early logarithmic phase (OD^{600} = 1.0), when the ribosomes are found in the highest concentration and are generally considered to be the most active (Gourse et al., 1996). Cells were washed two times with 10 mM Tris-HCl pH 7.5 and kept frozen at -80 °C. Freezing of the material was necessary due to time constraints and also it would be helpful for partly destroying cell wall.

Buffers

Numbers above the name indicate Mg^{2+}/salt concentrations, mM.

Buffer $A^{20/100}$	**Buffer $B^{25/500}$**	**Buffer $E^{10/100}$**	**Buffer $G^{10/60}$**
20 mM Hepes-KOH pH 7.5 100 mM NH_4Cl 21 mM $Mg(OAc)_2$ 1 mM DTT	10 mM Hepes-KOH pH 7.5 500 mM KCl 25 mM $Mg(OAc)_2$ 1.1 M Sucrose 0.5 mM EDTA 1 mM DTT	10 mM Hepes-KOH pH 7.5 100 mM KCl 10.5 mM $Mg(OAc)_2$ 0.5 mM EDTA 1 mM DTT	5 mM Hepes-KOH pH 7.5 50 mM KCl 10 mM NH_4Cl 10 mM $Mg(OAc)_2$ 1 mM DTT

1.2 LYSIS

Work with Staphylococcus cells have special safety requirements and should be done in a special laboratory with safety level 2. Usually these type laboratories are limited in space, and therefore they can accommodate only middle-sized incubators, shakers and centrifuges. This necessitated the adaption of purification procedure to use smaller amounts of cells initially, but nevertheless to obtain reasonable yields of ribosomes for crystallization. In the end, replacing mechanical lysis (French press, microfluidizer) with enzymatic lysis resulted in a very high efficiency of cell disruption. We used lysostaphin, a specific enzyme that cleaves cross-linking pentaglycin bridges in the cell wall of Staphylococci.

Frozen cells (5 g) were re-suspended in 30 ml of Buffer $A^{20/100}$ containing 1 mM EDTA, 30 µl DNAse I, 3.5 mg lysostaphin and protein inhibitors cocktail (Roche) according to recommendations of manufacturer. Then came step with incubation at 37 °C for 1 hours in which each 5 min was necessary to mix suspension, otherwise lysis give low yield. After incubation suspension was transferred on ice and all following steps were performed either at +4 °C or on ice. Cell debris was removed by centrifugation at 30000×g for 90 min.

1.3 PEG PRECIPITATION AND SUCROSE CUSHION

PEG precipitation step was adapted from purification of yeast ribosomes and used to fractionate the lysate quickly and gently in order to recover the fraction containing ribosomes. Pelleting through the sucrose cushion containing 0.5 – 1 M salt is classical procedure for purification of vacant bacterial ribosomes. High concentration of KCl is compensated with increased concentration of Mg2+ ions. It allows the washing out remaining ligands (tRNAs, mRNA, translation factors) and some other proteins bound to the ribosome but keep 70S particle stable. At the same time the treatment should not be too harsh, so that the ribosomal proteins will not dissociate.

The resulting supernatant (often called S30 for supernatant after centrifugation at 30000×g) was further subjected to a differential precipitation by PEG. PEG 20000 was added from a 30% w/v stock (Hampton Research) to a final concentration of 2.8% w/v for the first fractionation. The solution was centrifuged at 20000×g for 5 min. The ribosomes and light cellular components remained in soluble fraction, while components that are heavier than the ribosome such as residual polysomes, remaining cell debris, were precipitated. The supernatant was recovered and PEG 20,000 was increased to 4.2% for the second fractionation. Under these conditions the ribosomes become insoluble while the smaller components (small complexes, individual proteins) remain soluble. The solution was centrifuged at 20000×g for 10 min, the ribosome pellet re-suspended to 30 – 35 ml in buffer $A^{20/100}$ containing 1 mM EDTA, layered on 25 ml of Buffer $B^{25/500}$ and then centrifuged at 45000 rpm / 15 hours using Beckman Type 45 Ti rotor.

1.4 SUCROSE DENSITY GRADIENT CENTRIFUGATION

This step is typical for purification of ribosomes of any kind (full ribosomes or individual subunits), any origin (cytoplasmic, mitochondrial or chloroplast) and any organism (bacteria, archaea or eukaryotes). The idea is to separate full ribosomes from ribosomal subunits. Due to the different size, weight and density, 70S, 50S and 30S particles sediment with different speed through the gradient of viscous solution such as sucrose. It is important to select the right concentration of sucrose and maximum

amount of ribosomes for good resolutions of the particles along the gradient. It is also important to find the proper speed/time balance of centrifugation. Fractionation of gradients further allows selective collection of only the particles of interest.

Ribosome pellet after sucrose cushion was re-suspended in Buffer $E^{10/100}$ till 7 mg/ml and loaded on the sucrose density gradients. During development of the protocol, using sucrose gradients 10 – 30% (w/v) we found that our sample contains some particles, bigger than 70S, that were not detectable on 5 – 20% sucrose gradients usually used for purification of bacterial ribosome. Later we proved that these are ribosomal particles that sediment faster than monosomes. Later we proved that these particles are ribosomes that sediment faster than monosomes and called this fraction 100S. The presence of 100S and 50S fractions together with 70S ribosomes made sucrose gradient step difficult to set up. To purify only 70S ribosomes, the gradient was modified to 7 – 30% (w/v) and the amount of material loaded on one gradient was decreased to 3.5 mg. Sucrose gradients 7 – 30% were cast in 36 ml Beckman SW28 tubes using the Gradient Master machine (BioComp). Ribosomal sample (0.5 ml) was layered on each gradient and centrifuged at 17100 rpm / 15.5 hours in swinging rotor Beckman SW28.

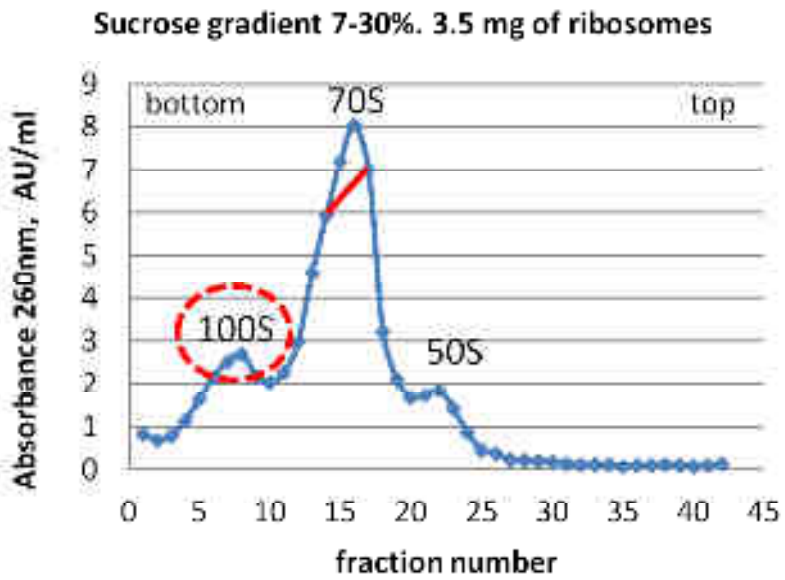

Figure 23: Sucrose gradient profile. Fractions (1 ml) were collected and absorbance was measured by Nanodrop 2000c (Thermo Scientific). The solid red line indicates pooled 70S fractions and red dashed circle indicates the peak of 100S ribosomes. One of the unique features of translational control in *S. aureus* is the presence of so-called 100S ribosomes in actively growing cultures (Ueta et al., 2010). Ribosomal dimers are referred to as 100S, and do not participate in translation. The phenomenon of ribosomal dimerization has been observed in many bacteria; however disomes were usually found during transition of cells to the stationary growth phase when the substrate is limited and the cells have to alter metabolism. The role of ribosomal dimers in actively growing cells of *S. aureus* remains unclear.

1.5 RIBOSOME CONCENTRATION AND STORAGE

The appropriate fractions were pooled and $Mg(OAc)_2$ concentration was adjusted to 25 mM. In order to precipitate ribosomes, PEG 20000 was added to a final concentration of 4.5% w/v. Ribosomes were

pelleted by centrifugation (20000×g / 12 min). The white pellet was gently dissolved in buffer G to a final concentration of 20 – 25 mg/ml; 30 µl aliquots were flash frozen in liquid nitrogen and stored at -80 °C. Typically 10 – 12 mg of pure ribosomes were obtained from 5 grams of cells.

2. MODIFICATIONS OF RIBOSOME PURIFICATION PROTOCOL

2.1 CELL PREPARATION

In this part we decided to change inoculation parameters for pre- culture single colony: 1:5 (10ml of medium in the 50ml of flasks) (standard ratio in microbiology for inoculation pre- culture) till OD600 ~ 4.5-5.0. According to this change accumulation of oxygen was enough for cells growing and getting more amount of cells for future culture growth process.

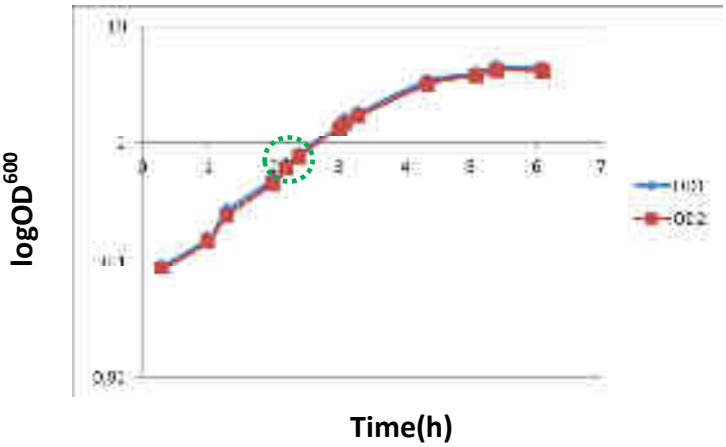

Figure 24: Growth curves of Staph RN6390 (OD1 and 2) strain in the BHI medium. According to measurements optical density, during cell growth, we calculated preferable time (2h) in early logarithmic phase (OD^{600} = 1.0) for harvesting cells.

In addition, in the cells washing process we changed 10 mM Tris-HCl pH 7.5 for Buffer A, which was much preferable due to procedure of lysis in the next step, and also in order not to create additional stress to cells with changes in the type of solutions, because Tris-HCl is not a component for further buffers of ribosome purification procedures.

2.2 LYSIS

Due to the lack of problems in the lysis procedure, and also because of the inability to use other types of lysis such as French press or microfluidizer, we left unchanged this step.

Modifications in sucrose cushion step were made according to Guo and Noller article (2012), in which was described, how they able to got rid of tRNA contamination in ribosome from *E.coli*. Two of the four experiments (I and II) were conducted on the basis of this article.

I Experiment: After main sucrose cushion with Buffer B $^{25/500}$ step was prepared second sucrose cushion step in four different salt conditions 100mM, 200mM, 300mM and 500mM of KCl. In order to

washing out different contaminations (mRNA, tRNA, non-ribosomal proteins) from ribosome we used different salt concentration to find optimal condition , which will not destroy the ribosomal proteins. After fist sucrose cushion step, pellet was re-suspended with Buffer $A^{20/100}$ containing 1mM EDTA till 60 ml and 15 ml of ribosome sample was layered on the top of each 10 ml of sucrose cushions. Then tubes centrifuged at 36200 rpm, 17 hours using Beckman Type 50.2 Ti rotor. All the rest steps followed the initial protocol.

II Experiment: After PEG precipitation step sample was divided for two parts and dissolved in two buffers separately (Buffer $C^{10/100}$ and Buffer $D^{10/500}$).

Buffer $C^{10/100}$	**Buffer $D^{10/500}$**
20 mM Hepes-KOH pH 7.5 100 mM NH_4Cl 10 mM $Mg(OAc)_2$ 1 mM DTT 0.5 mM EDTA	20 mM Hepes-KOH pH 7.5 500 mM NH_4Cl 10 mM $Mg(OAc)_2$ 1 mM DTT 0.5 mM EDTA

In this step was decreased Mg^{2+} concentration from 20 till 10 mM and increased NH_4Cl till 500mM. Also, according to H.Noller protocol, was decreased the Mg^{2+} concentration in Buffer B (in sucrose cushion step) from 25 till 10mM. Due to this modification we tried to wash out non-ribosomal protein and tRNA contamination, which we observed after initial protocol. Then further steps were followed the initial protocol.

III Experiment: Another modification procedure was introduced for same purpose, which call "light dissociation of ribosome". After normal sucrose cushion step with Buffer $B^{25/500}$ and re-suspension of pellet in Buffer $E^{10/100}$ we added step with incubation ribosome sample in dissociation conditions 2.5 mM $Mg(OAc)_2$ and 200mM KCl (this conditions were obtained by I.Khusainov during working under the initial protocol of ribosome purification). Ribosome sample were incubated in different time (0 min/15 min/30 min/45 min/1 hour) at $0C^{o}$. Then was prepared "sucrose cushion" (3.5% sucrose) with dissociation condition (Buffer $B1^{2.5/200}$) and layered 2ml of this cushion on the top of each sucrose gradients. After incubation, ribosome was loaded on the top of "sucrose cushion". According this low – sucrose cushion step we tried to wash- out tRNA contamination from dissociated ribosome. During sucrose gradient centrifugation step ribosomes subunits will be mixed with associated Buffer $E^{10/100}$ and subunits should associate again under these conditions.

IV Experiment: One more modification was introduced after sucrose cushion which is puromycin treatment. Puromycin is a structural analogue of the 3' end of aminoacyl-transfer RNA. First, puromycin binds to the A site of the peptidyl-transferase center of the ribosome in the pre-translocational state, where the P site is occupied by peptidyl-tRNA. Peptidyl-transferase then covalently links the antibiotic to the peptide residues of the peptidyl-tRNA in the P site. Because the ribosome cannot cleave the amide bond of puromycin and because peptidyl-puromycin, which lacks the whole tRNA body, has a lower affinity for the ribosome than peptidyl-tRNA, peptidyl-puromycin falls off the ribosome. Those help to cleave peptidyl-tRNA from ribosome and peptide as well.

After sucrose cushion step with Buffer $B^{25/500}$, we re-suspended pellet in the Buffer $E^{10/100}$. And then to respect the salt and buffer concentration we mixed puromycin with Buffer E5X and Buffer$E^{10/100}$ and added this mix to the sample with ribosome to have 1mM puromycin at the final concentration in the solution. Then ribosome sample with antibiotic was incubated during 1h at $0C^{o}$ and layered on sucrose density gradient. Then further steps were followed the initial protocol.

2.3 SUCROSE DENSITY GRADIENT CENTRIFUGATION

I Experiment: The profile after sucrose density gradient centrifugation has been no significant changes and shown same results as presented in the Figure 23. So, we could conclude that ribosome quite rigid and it withstand after high salt of second sucrose cushion step.

II Experiment: According to sucrose gradient profiles (Figure 25) we conclude, that decreasing of Mg^{2+} concentration in both cases give much more amount of 50S subunits compare with control. Thus could help us to separate ribosome from "weak" and "strong" ribosome and get only rigid ribosome without loose couples. However, peak in Figure 25A (green) is not preferable, because 70S partly mixed with 50S, which make separation of pure 70S ribosome more difficult.

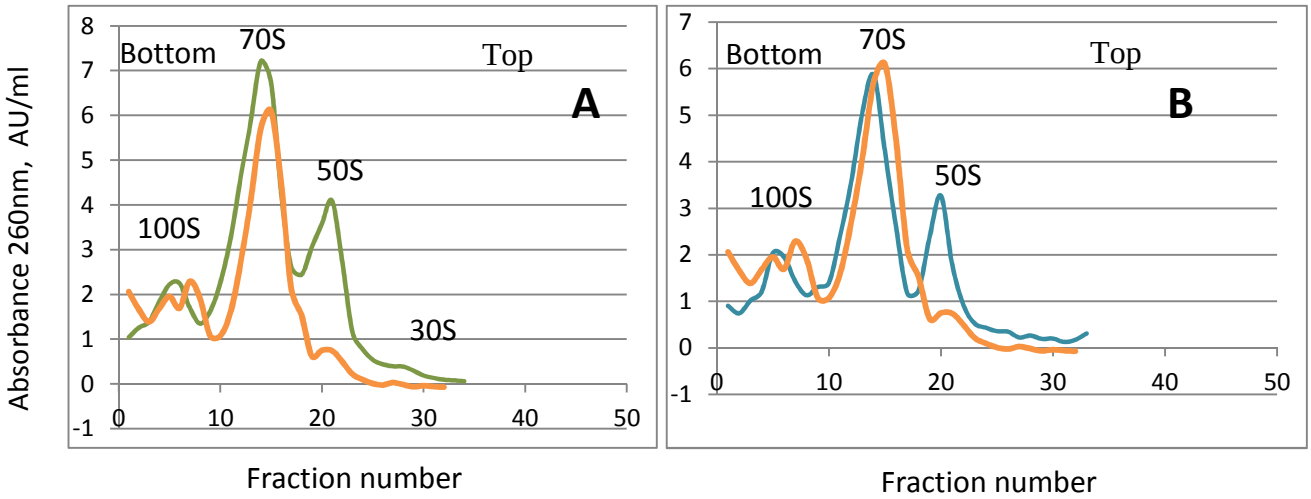

Figure 25: Sucrose gradient profiles after experiment II. After PEG precipitation step sample dissolved in buffer $D^{10/500}$ (high salt) (A) and in buffer $D^{10/100}$ (low salt) (B), control (orange).

III Experiment: With an increase in the incubation time of the ribosome under dissociation conditions, we can observe an increasing in the peaks of 50S and 30S and, conversely, a decreasing in the peak of 70S (Figure26).

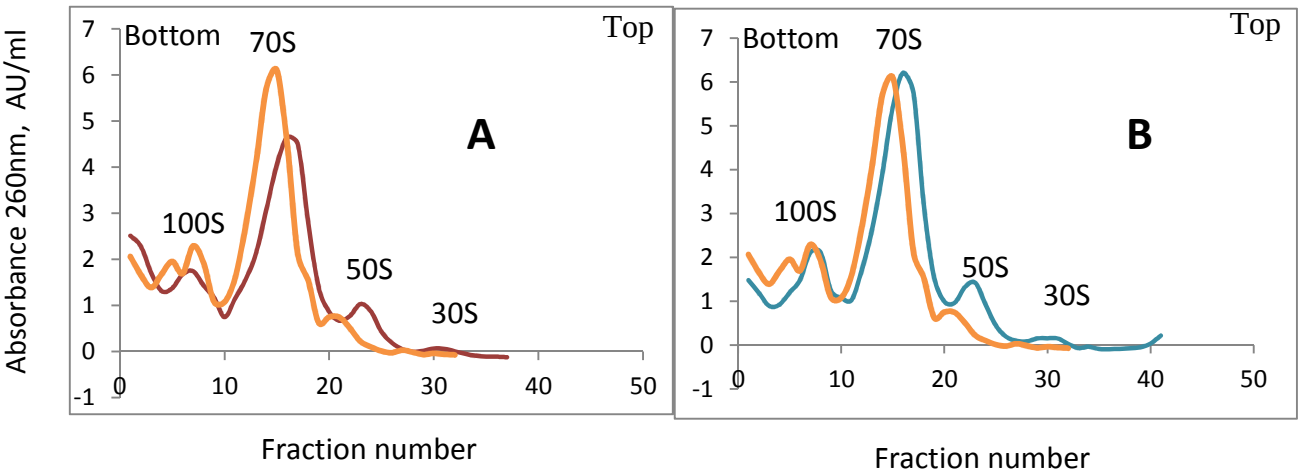

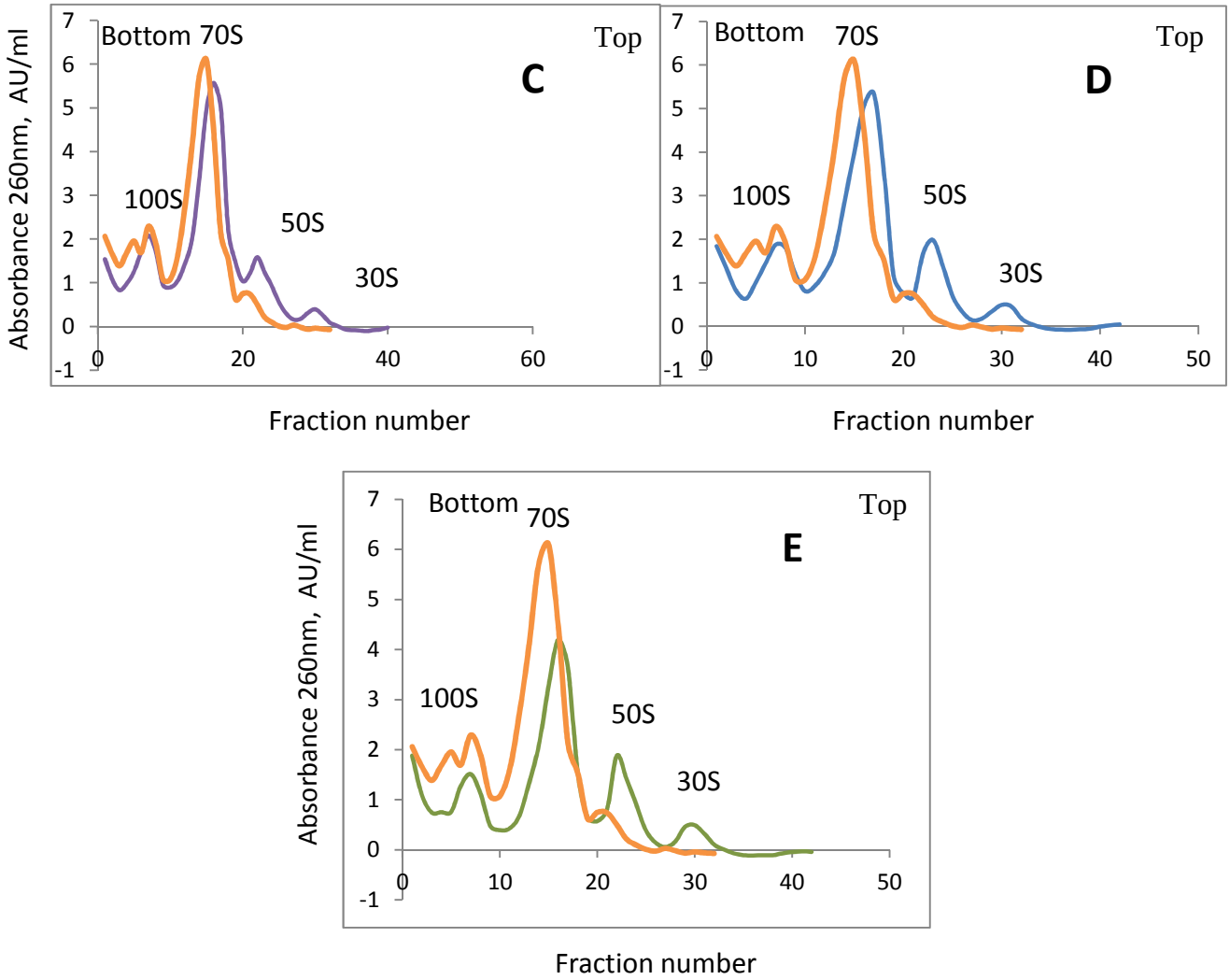

Figure 26: Sucrose gradient profiles after experiment III. A) Profile shows ribosome gradient without incubation time (0'). B) after incubation ribosomes during 15min, C) 30min, D) 45min, E) 1hour in dissociation condition (2,5mM $Mg(OAc)_2$ and 200mM KCl), control (orange).

Also we tried to check the ribosome behavior, and loaded ribosome after incubation in dissociation condition directly on the gradient, after 15' incubation, without "sucrose cushion" (3.5%), interestingly, that profile was almost the same with control. "Sucrose cushion" in dissociation condition influence on ribosome dissociation, especially if incubation time in dissociation condition was introduce before. Probably, ribosome subunits after incubation in dissociation condition and after low "sucrose cushion" step, dissociate completely and only after sucrose gradient step they associated partly. And if time for incubation is absent, ribosome could dissociate only partly which we can observe in the Figure 26A.

IV Experiment: After puromycin treatment sucrose gradient profile of ribosome shown stable peak of 70S without any specific changes (Figure 27).

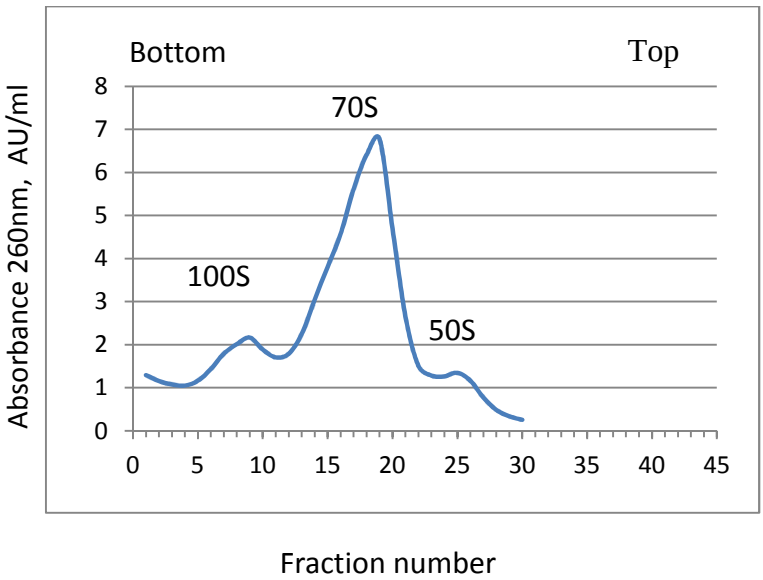

Figure 27: Sucrose gradient profiles after experiment IV.

2.4 RIBOSOME CONCENTRATION AND STORAGE

Typically 10 – 14 mg of pure ribosomes was obtained from 5 grams of cells (see initial protocol for ribosome concentration and storage).

V RIBOSOME SAMPLE CHARACTERIZATION

Sample preparation for SDS- PAGE

Sample preparation for analyses was performed according to method described by Hardy and co-workers (Hardy et al., 1969). Ribosomes were digested for 30 min / 0 °C with 66% acetic acid in presence of 33 mM $Mg(OAc)_2$. rRNA was precipitated by centrifugation at 11573 rpm/ 30 min. The soluble protein fraction was treated with by 80% acetone for at least 3 hours at -80 °C. Proteins were precipitated at 11573 rpm / 60 min, pellet was dried by speed-vac for 30 min and dissolved in buffer G. This preparation allowed the removal of PEG that caused diffusion of bands on 1D-PAGE and to eliminate rRNA that would occupy all positively charged ampholytes and block any movement of ribosomal proteins (RP) along the gel in the capillary.

One-dimensional SDS-PAGE

One-dimensional PAGE separates proteins in denaturing conditions according their molecular weight but not charge. There are no specifications for ribosomal proteins to run this type of gel. Therefore, the standard Laemmli method (Laemmli, 1970) with slight modifications was used. The gel was stained in Coomassie Brilliant Blue R-250 according to standard protocols.

Sample preparation for Denaturing PAGE of RNA

For extraction total RNA from ribosome was used phenol: chloroform: isoamylalcohol (PCI) and ethanol with LiCl precipitation method. For removal of proteins and most of the free nucleotides, PCI extraction and ethanol with LiCl precipitation of RNA transcripts is the preferred method.

At the first step was prepared mix with ribosome/1% SDS (denaturation agent) /5mM EDTA (for decreasing Mg^{2+} concentration in the ribosome) and adjusted this mix till 150µl volume with RNAs free water. After incubation at 37°C 10 min was added PCI (25:24:1 pH 8.0) to our mixture with ratio 1:1 and vortexed 1-2 min. Then was performed centrifugation at 13000rpm 10 min at RT and during this process phases separated (RNA comes in upper phase and PCI in the down). After centrifugation RNA was collected and transferred to the new tube for precipitation step with 3 volume of cold (-20°C) ethanol absolute and 1/10 volume of 8M LiCl. Then sample was leaved for at least 8 hours in the -20°C (for the proper RNA precipitation). LiCl precipitation offers major advantages over other RNA precipitation methods in that it does not efficiently precipitate DNA, protein or carbohydrate (Barlow et al., 1963). For harvesting total RNA we centrifuged sample at max speed 12000rpm from 20 min-1hour at +4°C. Pellet was dissolved in RNAs free water.

Denaturing PAGE of RNA with Urea

Denatures secondary DNA or RNA structures and is used for their separation in a polyacrylamide gel matrix based on the molecular weight. Fragments between 2 to 500 bases, with length differences as small as a single nucleotide, could be separated by protocol (Southern, 2002). The migration of the sample is dependent on the chosen acrylamide concentration. A higher percentage of polyacrylamide resolves lower molecular weight fragments. The combination of urea and temperatures of 45-55 °C during the gel run allows for the separation of unstructured DNA or RNA molecules. The experiment was based on the protocol E. Southern but with only slightly differences. In the preparation of RNA denaturing gel instead of Ficoll and Orange G in the loading buffer solution were used 8M urea and 0.025% xylene cyanol. Final polyacrylamide gel concentrations were 12% (to observe tRNA contamination) and 4% (to check the quality all bacterial rRNAs from 70S ribosome). For detecting RNAs was used ethidium bromide stain, according to the standard protocols.

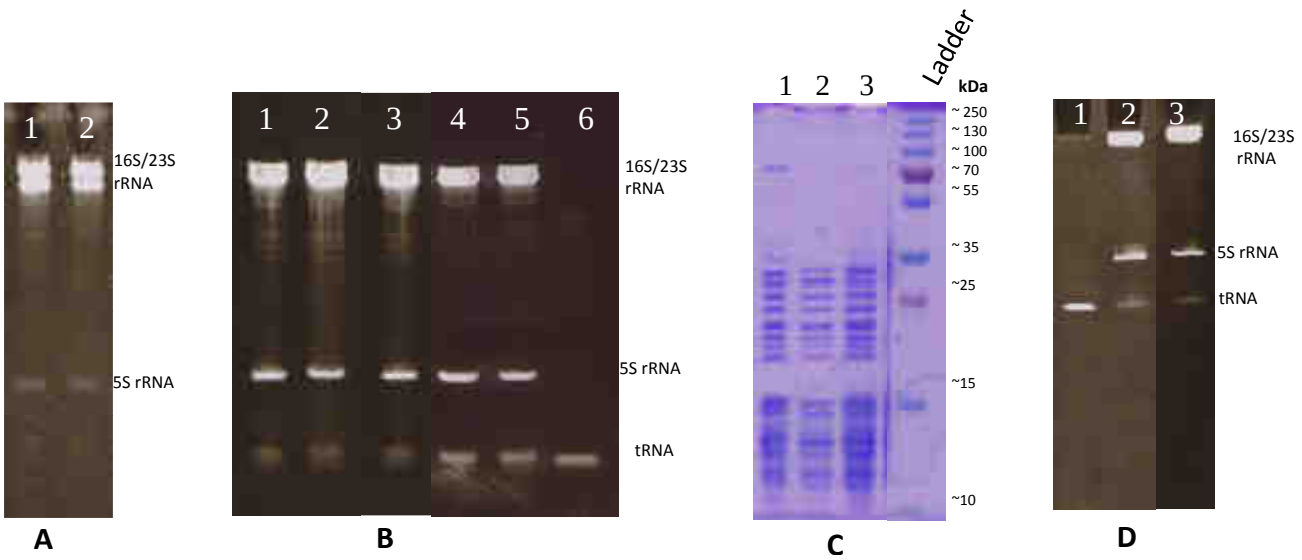

Figure 28: Polyacrylamide Gel Electrophoresis of *S. aureus* ribosome sample. A) RNA Denaturing PAGE 4%: 1 - ribosome sample after experiment IV (9µg), 2 - ribosome control (9µg). B) RNA Denaturing PAGE 12%: 1, 2, 3 - ribosome sample after experiment III (30min, 45min, 1h incubation in dissociation condition respectively) (9ug), 4 - sample after experiment IV (9 µg), 5 - ribosome control (9µg), 6 - $tRNA^{fMet}$ (2µg).C) One-dimensional SDS PAGE: 1,2,3 - ribosome sample after experiment III (30min, 45min, 1h incubation in dissociation condition respectively) (30 µg) D) RNA Denaturing PAGE 12%: 1 - $tRNA^{fMet}$ (1µg), 2 – sample after experiment II (with Buffer D $^{10/500}$) (9µg). 3 - sample after experiment II (with Buffer $C^{10/100}$) (9µg).

According to the Figure 28A we observed three bands corresponding to 23S, 16S rRNA and 5S RNA for control and for ribosome sample after puromycin treatment (experiment IV). However, due to PAGE 4% we cannot interpret results concerning to tRNA contamination, because the size of the gel pore was large for small size of tRNAs. For this purpose, was performed PAGE 12% and concluded that puromycin treatment didn't influence on removing tRNA contaminations (Figure 28B 2), because the band with tRNA identical with control (without treatment Figure 28B 3). The protocol with "light dissociation" (experiment III) decrease amount of tRNA contaminations in the ribosome sample, according to the results from Figure 28B 1, 3, 2 but didn't remove completely. In case of Figure 28C 1,ribosome sample was contaminated with non-ribosome proteins, but after 45 min and 1h incubation in dissociation conditions (experiment III) ribosome sample showed much less amount of non-ribosomal proteins. Interestingly, that in the Figure 28D 2, 3 (experiment II), we could observe reducing intensity in the bands of tRNA contaminations compare with control and experiment IV.

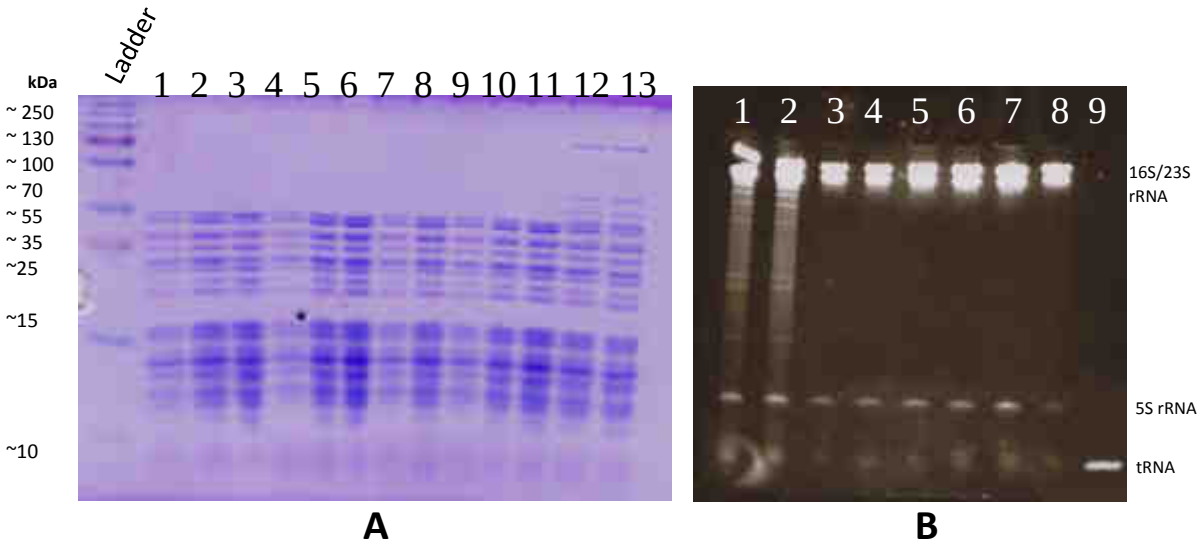

Figure 29: Electrophoresis of the *S. aureus* ribosome samples after two steps of sucrose cushion sedimentation purification protocol (experiment I). A) One-dimensional SDS PAGE: 1,2,3 – second step with 100mMKCl sucrose cushion sedimentation (15, 30, 60 µg respectively); 4,5,6 - 200mM KCl (15, 30, 60µg respectively); 7,8 - 300 mM KCl (15, 30 µg respectively); 9, 10, 11 – 500mM KCl (15, 30, 60µg respectively); 12, 13 – control (sample without modification of protocol (15, 30 µg respectively). B) RNA Denaturing PAGE 12%: 1, 2 - Before first sucrose cushion step (3 and 9 µg respectively); 3,4 - after first sucrose cushion sedimentation step (3µg and 9 µg); Ribosome sample after 2 step of sucrose cushion sedimentation purification protocol with (5) 100mMKCl (3µg), (6) 200mMKCl (3µg), (7) 300mM KCl (3µg), (8) 500mM KCl (3µg); 9 - $tRNA^{fMet}$ (2µg).

Ribosomal proteins are stable after two step of sucrose cushion sedimentation, even after 500 mM KCl of sucrose cushion conditions. Also, non- ribosomal protein completely washed-out after two steps of sucrose cushion sedimentation, compare with control (Figure 29A 12, 13). However, according RNA Denaturing 12% PAGE, we can observe presence of tRNA contaminations in the all samples (Figure 29B 5, 6, 7, 8). Thus, we could conclude that even high concentration salt in second sucrose cushion step can't remove tRNA contamination completely, but could remove non-ribosomal proteins.

Summarizing the various modifications of ribosome purification protocol from *S. aureus*, we settled on the protocol with decreasing magnesium concentration in the sample after PEG precipitation and in a sucrose cushion step (experiment II). In the case of increasing salt concentration NH_4Cl (500mM) in the sample and decreasing Mg^{2+} concentration we didn't observe of removing tRNA contaminations and also this step could most likely affect to the 70S ribosome as this is an additional stress factor for the ribosome, according to the profile after sucrose density gradient centrifugation (Figure 25A). Also we analyzed sample after experiment II for removing non-ribosomal proteins and the SDS gel demonstrated the purity of the ribosomal sample and did not reveal contamination by high molecular weight proteins such as components of the pyruvate dehydrogenase complex, which sometimes co-purify with bacterial ribosomes (Figure 30B).

Agarose gel electrophoresis

Agarose gel electrophoresis was performed according to the standard protocol (Sambrook et al., 1989). The gel was prepared in buffer TAE (40 mM Tris, 1 mM EDTA pH 8.0, 5.7% acetic acid) and

contained 1% agarose. Ribosome samples were loaded directly on the gel. The gel has demonstrated the intactness of the rRNA in this condition (Figure 30A), and the size of *S. aureus* rRNA is comparable to the size of rRNA of *T. thermophilus* and correspond to the 3000bp in case of 23S RNA and 1500bp for the 16S RNA. Ribosome subunits and 100S have been analyzed after sucrose density gradient centrifugation step in the experiment II.

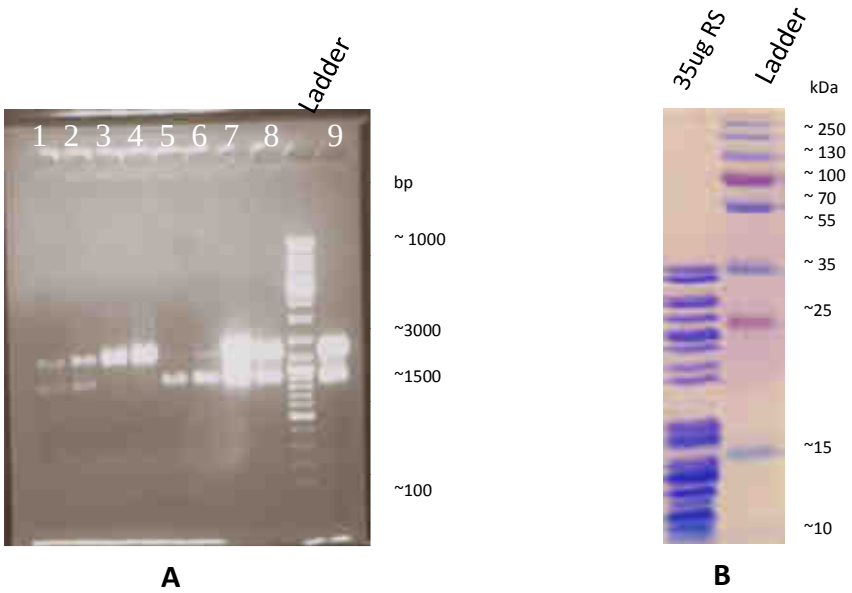

Figure 30: Electrophoresis of the *S. aureus* ribosome samples with decreasing magnesium concentration after PEG precipitation and in the sucrose cushion step (experiment II). A) Agarose gel 1%: 1 and 2 - *S. aureus* 100S (5µg), 3 and 4 - *S. aureus* 50S (15µg), 5 and 6 - *S. aureus* 30S (10µg), 7 and 8 - *S. aureus* 70S (18 and 15µg respectively), 9 - *T. thermophilus* 70S (15 µg).The upper and lower bands correspond to 23S and 16S rRNA respectively. B) One-dimensional SDS PAGE: sample after experiment II (with Buffer $C^{10/100}$)

VI COMPLEX FORMATION OF THE RIBOSOME FROM *S. AUREUS* WITH $tRNA^{fMet}$ AND mRNA

In order to stabilize the obtained ribosome sample has been performed complex formation with initiator tRNA and mRNA. This complex formation could help for improving crystals diffraction from *S.aureus* ribosome.

For the complex formation have been used two types of mRNA. First sequence of mRNA was constructed based on the data from Cell journal (Yusupova et al., 2001), but with slightly modification in the space between Shine Dalgarno - Anti-Shine Dalgarno (SD-anti-SD) and start codon. The idea about modification came from Vellanoweth and Rabinowitz (1992). They made several experiments to understand the differences between translation initiation in gram-negative and gram-positive bacteria. One important feature seems to be the length of the spacing between SD-anti-SD and start codon. Gram-positive bacteria translated messages with shorter spacing with much less efficiently than gram-negative, thus, instead of forming an interaction, translation initiation at the shorter-spaced messages could result from a slippage of the Shine Dalgarno (SD) interaction. According to this knowledge the length of spacing between SD-anti-SD and start codon has been increased for two nucleotides, these could help to get a strong SD interaction with 16S RNA (Sequence 1).

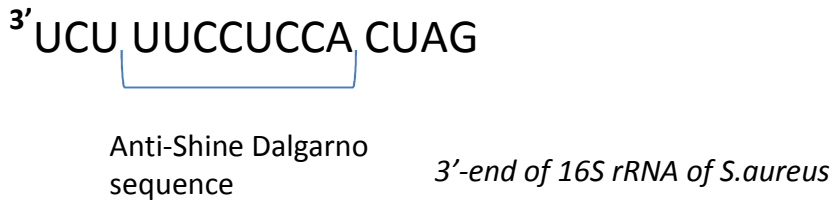

Sequence 1

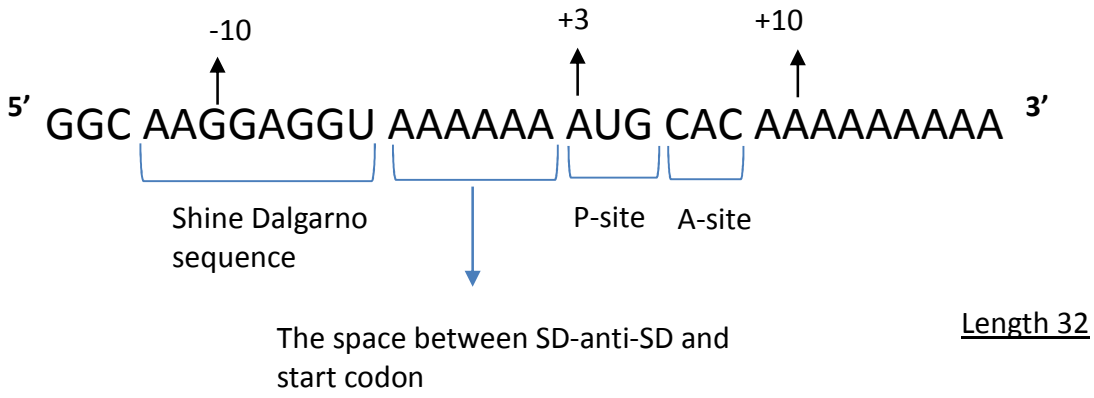

The second construct was unmodified mRNA sequence MK27 from Yusupova et al., 2001, that about 30 nucleotides (Sequence 2).

Sequence 2

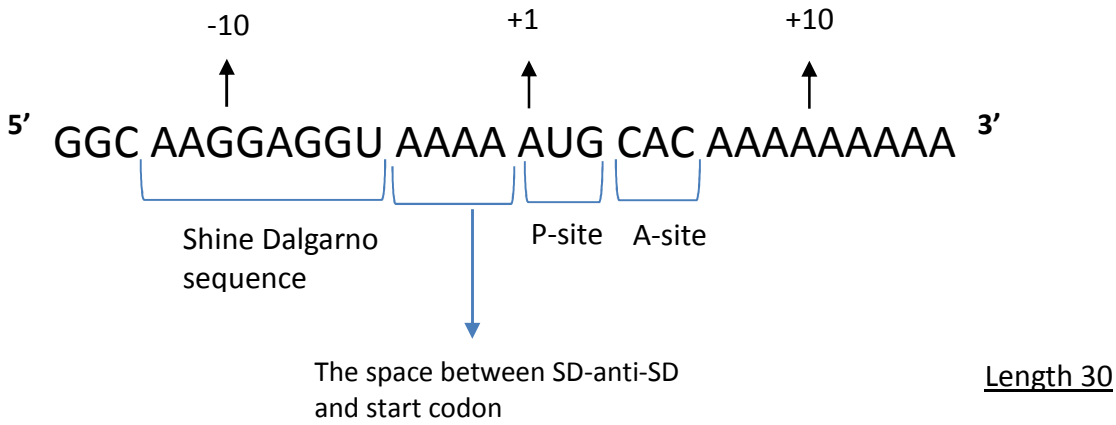

The Shine-Dalgarno helix is bound in a large cleft between the head and the back of the platform. At the interface, only about eight nucleotides (−1 to +7), centered on the junction between the A and P codons, are exposed, and bond almost exclusively to 16S rRNA. Binding of mRNA to the 30S subunit during translational initiation requires opening one or both of the tunnels (which are closed

noncovalently) depending on the length of the upstream leader, since it has been shown by Bretscher (1968) that the ribosome is able to initiate translation on a circular message. The contact point between the head and body has been described as a potential "latch," the closing of which was proposed to provide a geometry that guarantees processivity, provides directionality, and prevents dissociation (Schluenzen et al., 2000). The mRNA enters the ribosome around position +13 to +15, the location of downstream pseudoknots that stimulate −1 translational frame shifting (Yusupova et al., 2001).

Constructs of the mRNA sequences were ordered from Dharmacon Company and prepared according to the standard deprotection 2'-ACE protected RNA protocol (http://dharmacon.gelifesciences.com). Obtained water content RNA were aliquoted and frozen in liquid nitrogen, then stored at -20°C.

1. PURIFICATION OF THE INTACT tRNA^{fMET}

Initiation tRNA purification was based on the protocol of E. Schmitt et al., 1998 and adapted in the Yusupov laboratory.

Cells preparation

Maturated tRNA^{fMet} was produced in *E. coli* JM101 strain using the pBStRNAfMetY2 overproducing plasmid (Meinnel and Blanquet, 1995). Bacteria were grown in LuriaBertani (LB) medium with agar and ampicillin antibiotic at concentrations of 50 µg/ml at +37^{0}C overnight. Then single colony transferred to the pre-culture 2xTY medium and incubated at 37C during 7 hours (until OD^{600}=1-1.5).

2xTY	Buffer T1
0.16% Bacto-tryptone 0.1% Yeast extract 0.05% NaCl Ampicillin 50 µg/ml	1 mM Tris-HCl pH 7.5 10 mM $Mg(OAc)_2$

Culture were growth at 1L medium (2xTY) in two 5L flasks overnight (~ 13hours) at 37^{0}C 200rmp. When optical density reached 1-1.5, we centrifuged cells at 4000rmp 20 min and dissolved pellets in 50ml of Buffer T1 and cool down at 0°C. Then cells washed by two times centrifugations in 50ml of Buffer T1 at 4^{0}C during 10 min at 4000 rpm. After weighting pellets we dissolved 12.7g of cells with 12.54 ml of buffer T1 (according ratio 1g cells-1.2 ml of Buffer T1).

Before phenol extraction step we had to saturate buffer T1 with phenol in 1:1 ratio and vortexed for 3 min. Then we centrifuged 5 min this mix at 4000rpm at RT and after removing supernatant we repeated this procedure twice.

Phenol extraction

This method separates mixtures of molecules based on the differential solubilities of the individual molecules in two different immiscible liquids. According to this step we were able to separate cell proteins from nucleic acids.

After phenol saturation step we added 15 ml saturated phenol to the cells and vortexed intense for 3 min, then centrifuged in the rotor JLA 25.50 at 15000 rpm during 30min at RT. In the presence of phenol, the hydrophobic cores interact with phenol, causing precipitation of proteins and polymers (including carbohydrates) to collect at the interface between the two phases or for lipids to dissolve in the lower organic phase. During centrifugation step black phenol phase with proteins goes to the bottom and white layer of denatured proteins appears in the middle of tube. Purified phenol has a density of 1.07 g/cm3 and therefore forms the lower phase when mixed with water (1.00 g/cm3) (O'Neil, 2006). The overall solvation capacity of a solvent depends primarily on its polarity. Nucleic acids are polar because of their negatively charged phosphate backbone, and therefore nucleic acids are soluble in the upper aqueous phase instead of the lower organic phase (water is more polar than phenol) (McMurry, 2003). So, upper water phase included nucleic acids and we carefully took supernatant. Then we added NaCl 5M and ethanol absolute with ratio 1/10V and 2.2V respectively to the supernatant and centrifuged at 15000rpm, 30min at 4^0C.

High-salt precipitation of long RNAs

This step is accomplished by adding salt and ethanol to a solution containing RNA. In the presence of NaCl, ethanol efficiently precipitates nucleic acids.

Supernatant after centrifugation was discarded and white pellet ~1cm was obtained. Then pellet was re-suspended in 1M NaCl with max volume 10ml and briefly vortexed. Re-suspension was centrifuged at 15000 rpm during 30 min, 4°C. Supernatant was transferred to fresh tube and mixed with 2 volume of ethanol absolute and centrifuged at 15000rpm, 30 min, 4°C. Then pellet was frozen in liquid nitrogen and dried in the lyophilizer during ~30 min. According to this procedure, we were able to isolate RNA from sample containing large amount of polysaccharides.

tRNA deacylation

Pellet was re-suspended in 2 ml of 1.8 M Tris-HCl pH 8.0 and vortexed. After incubation during 1 hours, 30min, 37°C was added (1/10V) 5 M NaCl and (2.2V) cold 100% ethanol absolute. Mix stored at -20°C overnight, this supply tRNA precipitation.

Anion-exchange chromatography

For collecting tRNA was performed centrifugation by using rotor JA 25.50, at 15000rpm, 20min, 4°C. Then pellet was mixed and washed by 70% ethanol then centrifuged (JA 25.50) during 5min, 15000rpm, 4°C. Obtained pellet was dried at 0°C during ~30 min (to get rid of ethanol), then dissolved in 10ml of Buffer T2 and clarified at 15000rpm, 20min, 4°C.

Buffer T2	(Elution) Buffer T3
20 mM Tris-HCl pH 7.5 0.1 mM EDTA 8 mM $MgCl_2$ 0.2M NaCl	20 mM Tris-HCl pH 7.5 8 mM MgCl2 0.1 mM EDTA 1 M NaCl

Anion-exchange chromatography is a process that separates substances based on their charges using an ion-exchange resin containing positively charged groups, such as quaternary ammonium (Q) strong anion exchange groups. In solution, the resin is coated with positively charged counter-ions (cations). Anion exchange resins will bind to negatively charged molecules, displacing the counter-ion. So, nucleic acids are bound strongly to the column and elute at much higher salt concentrations.
After measuring optical density, 10ml of sample was loaded in the Q-Sepharose (25 ml). Then column washed with 1 column volume (CV) of Buffer T2 (100%). Column washing parameters: Pressure max=0.33MPa; Flow 2 ml/min. Then has been started gradient program with (20 – 30 %) 8CV of Buffer T3 during 100 min (50 fractions with 4ml were obtained).

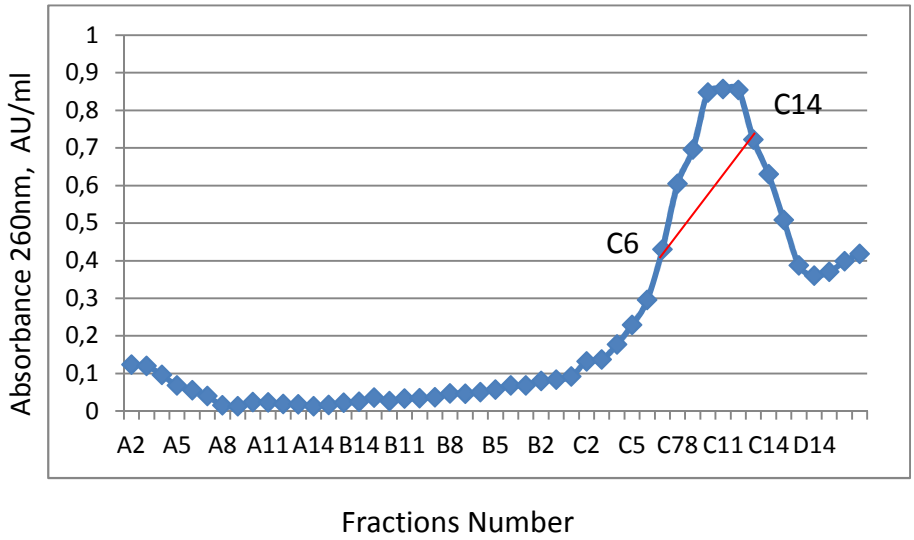

Figure 31: Anion-exchange chromatography (Q-Sepharose 25 ml). Peak appeared at 0.413M NaCl (26.6% Elution Buffer). Fractions pooled from C6-C14.

Obtained fractions were combine and mixed with 5M NaCl (in order to have 0.5M at final concentration of salt in the sample) and with 2.2 volume of ethanol absolute. Then tRNA was precipitated at -20°C, overnight. Sample was centrifuged after precipitation step (JLA 25.50) 15000rpm, 30 min at4°C. Then pellet was washed with 2ml of 70% EtOH and centrifuged during 5 min, 15000 rpm at 4°C. Pellet dried in lyophilizer ~ 20 min, dissolved in water and clarified through filter 3 min at 10000 rpm. Sample was aliquoted, frozen in liquid nitrogen and stored at-20°C. From 12.7 g of *E.coli* cell was obtained 1mg of $tRNA^{fMet}$.

2. $tRNA^{fMet}$ SAMPLE CHARACTERISZATION

Denaturing PAGE of RNA with Urea

tRNA samples for 12% PAGE denaturing was mixed with Loading buffer (see chapter with ribosome sample characterization).

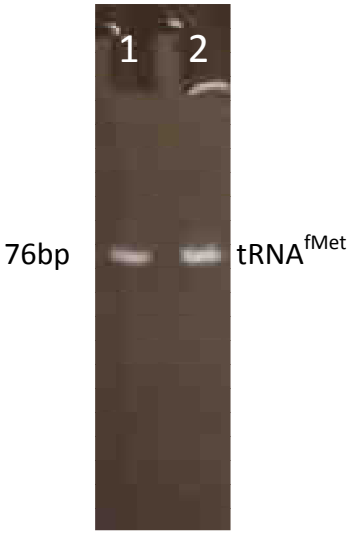

Figure 32: Denaturing 12% 8M urea PAGE of $tRNA^{fMet}$. 1 - Commercial phenylalanine-tRNA (0.5ug), 2 - Purified intact –$tRNA^{fMet}$ (0.5ug). According to Figure 32 we concluded that formylmethionine-tRNA is intact and we did not observe any impurities.

High-pressure liquid chromatography: C4-silica column

Purity analysis and impurities determination was performed by reverse phase fast protein liquid chromatography (FPLS) with High performance liquid chromatography (HPLC) column C4 silica gel (Butyl phase). HPLC is a technique used to separate the components in a mixture, to identify and to quantify each component. FPLS involves the separation of molecules on the basis of hydrophobicity. The separation depends on the hydrophobic binding of the solute molecule from the mobile phase to the immobilized hydrophobic ligands attached to the stationary phase, i.e., the sorbent. C4 is the most polar column that has a short butyl groups bonded to the polar polymeric surface. Butyl phase is using for reversed phase chromatography for separation hydrophobic substances. For the purpose of removing all liquid from sample and transferring it to Buffer A, tRNA sample (10ul) was dried in lyophilizer ~ 20 min. Then pellet was re-suspended in Buffer A (to respect the ratio 1 unit of sample for loading into column).

Buffer A	**Buffer B**
8mM MgCl2 20mM CH3COONH4 pH 5.0 1M NaCOOH	20mM CH3COONH4 pH 5.0 10% Methanol

Before sample injection column was equilibrated with Buffer A (3 column volume). After loading the sample, parameters have been set for chromatography (flow=0,4ml/min, pressure=5mPa (max) (for 10 min)) and in that time sample from loop was mixed with Buffer A and loaded to the column. Then the column was washed with Buffer A (3CV, 30min) from impurities in the sample. And was started making the gradient, with loading Buffer B 100% (flow_0,4ml/min, pressure=5mPa), 60min. During elution step was collected 1ml fractions in 96well Plate tube type and was obtained profile with peak of N-Formyl-Methionyl-tRNA (Figure 33A).

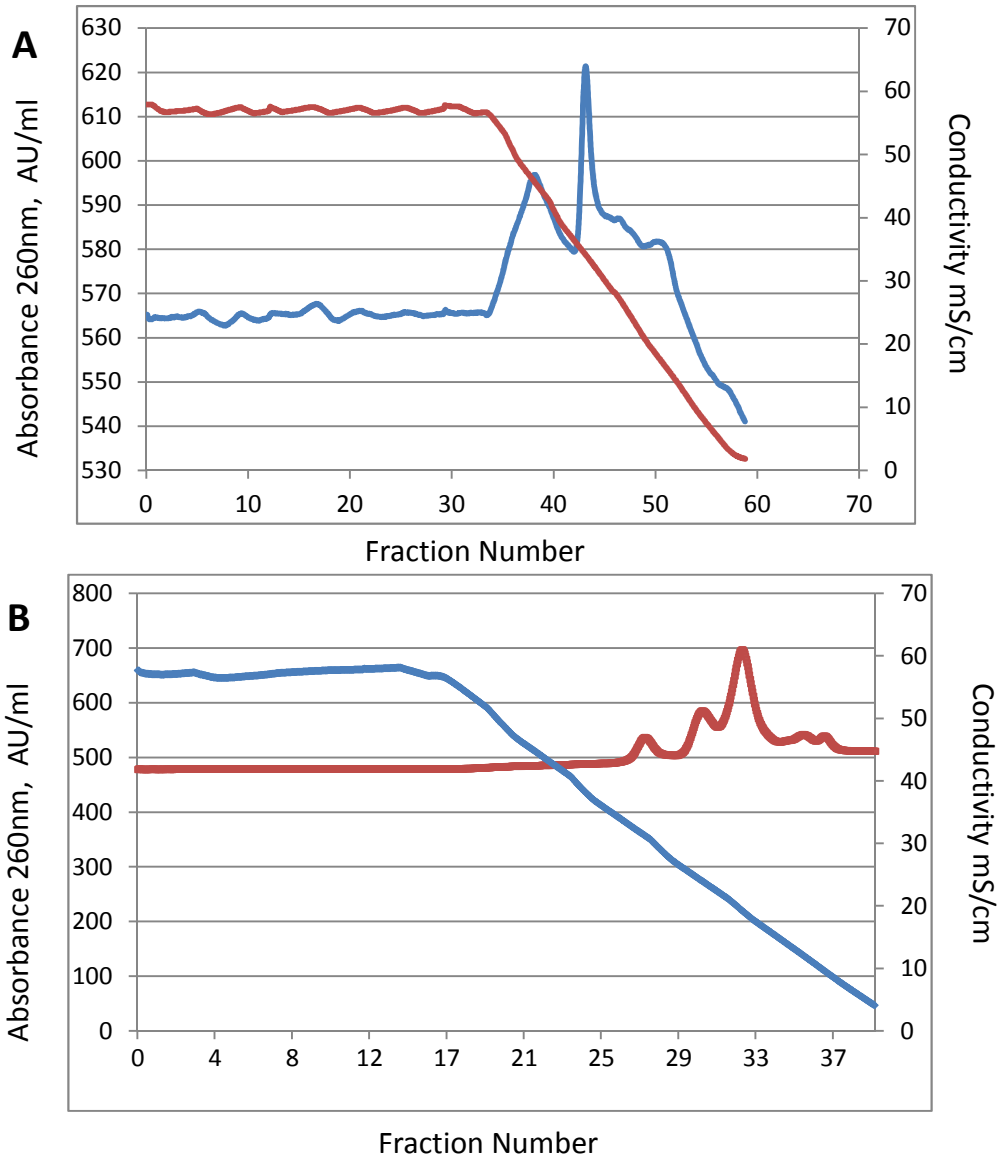

Figure 33: High-pressure liquid chromatography: C4-silica column. A) Purified formylmethionine-tRNA profile. B) Commercial phenylalanine-tRNA profile.

VII CRYSTALLOGRAPHIC STUDIES OF *S.AUREUS* RIBOSOME

Why we use x-rays and why we need to growth the crystals?

Information about three-dimensional atomic structures of biological molecules help us to understand the mechanism of their action and regulation, to visualize intermolecular interactions, and even to design new molecules with altered activity. Atomic structure can tell us almost everything what we want to know about the material: its bond length and angles, torsion angles, non-bonded distances.

There are several reasons why we cannot simply use powerful optical microscope and visible light but we need x-rays to determine the atomic structure of the molecules. First, atoms are too small to interact with visible light (390 – 700 nm wavelength) whereas the wavelength of x-rays is close to 1 A (0.1 nm). Second, in contrast to visible light that can give us information about the surface only, x-rays can penetrate the matter (inorganic or organic). This property of X-rays is extensively used in radiology, whereas structural scientists use another property – the ability of matter (more precisely the electrons of the atoms) to scatter X-rays. These scattered rays contain all information about the position of each atom of the molecule. However, if molecules are randomly spread in solution, they scatter randomly, in all possible directions. If we detect these randomly distributed signals, we will not be able to get any information from it. In order to make the information understandable, we need to force all x-rays to scatter in the same directions. That is why crystallographers cannot use sample in solution but rather have to crystallize it. Crystals are essentially a solid comprised of highly ordered identical units. When passing through such an ordered structure, photons are scattered in particular directions and registered on the detector forming a diffraction pattern. Diffraction pattern is representation of a structure in reciprocal space that contains the information about the directions of scattering and the intensity, but the information about the phase is missing. The phase information can be recovered using different methods such as anomalous scattering, isomorphous replacement, molecular replacement etc. Diffraction pattern with exact positions of diffraction spots, their intensities and phases then can be converted to the electron density (real space representation of protein structure) using Fourier transform method.

Thus, obtaining crystals of the object of interest is crucial in X-ray crystallography and is always challenging with biological molecules that are asymmetric and dynamic.

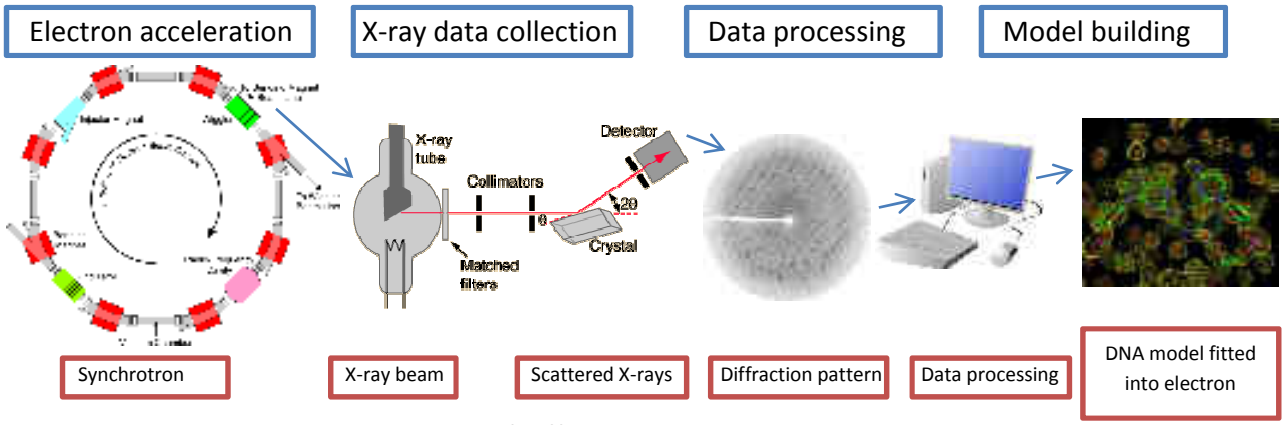

Figure 34: Schematic representation of diffraction experiment.

Electrons accelerated in the synchrotron ring can be partially transferred to experimental beamlines where the X-ray beam bombards the crystal that is mounted on goniometer. The most of the x-rays passing directly through the crystal and absorbed by the beam stop (these signals are not registered). Only scattered photons are captured on the detector forming a diffraction pattern (representation of crystal structure in reciprocal space). The data collected at the synchrotron are then processed at powerful computers and transformed into electron density (representation of crystal structure in real space) and 3D model of macromolecule is build according to the density thereafter.

1. MACROMOLECULAR CRYSTALLIZATION IN THEORY

The laws of physical chemistry and thermodynamics control the process of crystallization. Thermodynamically, crystallization of macromolecules (proteins, nucleic acids, macromolecular complexes, etc.) is not very different from the crystallization of salt. In both cases, we need to bring the solution into a supersaturated state after which the salt or the protein will start to crystallize. However, protein crystallization methods are very different and not as simple. Protein solubility depends on many factors: temperature, pressure, pH, concentration of protein, type and concentration of precipitant agent, type and concentration of salts, metal ions, co-factors and ligands interacting with the protein, etc.

The whole crystal growth process can be conveniently visualized in a two-dimensional phase diagram (Figure 35) representing the stable states (liquid, crystalline, precipitate) as a function of two crystallization variables. When the concentration of a protein solution is brought above its solubility limit, the solution becomes supersaturated. Depending on the level of supersaturation this zone of the diagram can be divided into three regions: very high supersaturation ("precipitation"), where molecules form amorphous aggregates, intermediate supersaturation ("labile"), where both growth and nucleation occur, and lower supersaturation ("metastable"), where only growth is supported.

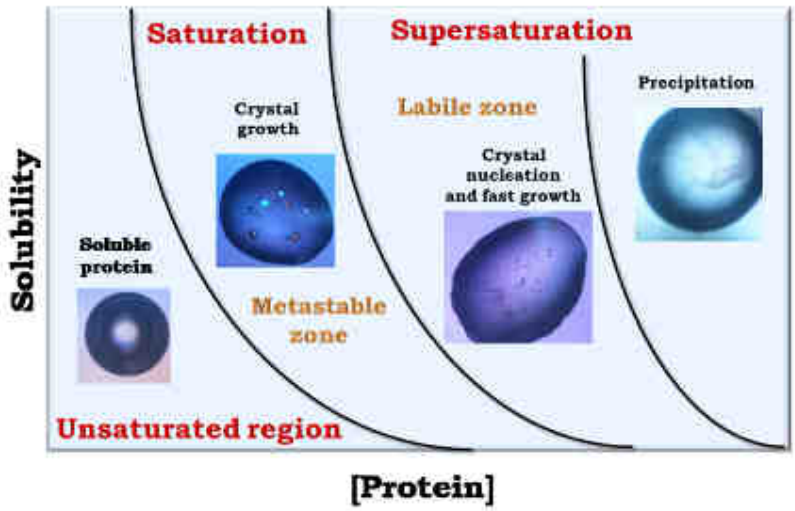

Figure 35: Schematic phase diagram of protein crystallization (Krauss et al, 2013)

The best strategy that should be employed is to induce nucleation at the lowest level of supersaturation just within the labile region. Following nuclei formation, the concentration of protein in the solution gradually decreases, driving the system into the metastable zone, where growth occurs slowly. However, it is very difficult to identify these ideal conditions and in order to obtain high-quality crystals it could be necessary to physically separate nucleation and growth steps. Chemical space in crystallization experiments is multidimensional, and several zones may correspond to nucleation and growth of different crystal forms. It is not yet possible to predict the conditions required to crystallize a protein from its chemico-physical properties. Changes in a single experimental parameter can simultaneously influence several aspects of a crystallization experiment.

Protein crystallization is generally a matter of searching, as systematically as possible, the ranges of the individual parameters that influence crystal formation, finding a set, or multiple sets of factors that yield some kind of crystals, and then optimizing the individual variables to obtain the best possible crystals. This is usually achieved by carrying out an extensive series of experiments, or establishing a vast matrix of crystallization trials, evaluating the results, and using the information obtained to improve conditions in successive rounds of trials. Because the number of variables is so large, and the ranges so broad, experience and insight into designing and evaluating the individual and collective trials becomes an important consideration (McPherson, 2004).

1.1 CRYSTALS GROWTH

In principle, crystals will form in any protein solution that is supersaturated i.e., when the protein concentration exceeds the solubility. In practice, considerable supersaturation is required to overcome the activation energy barrier which exists when forming the crystal. This barrier represents the free energy required to create the small microscopic cluster of proteins – known as a nucleus – from which the crystal will eventually grow (Kashchiev, 2000).

Since there is an energy barrier, nucleation (the process of forming a nucleus) takes time. If the supersaturation is too small, the nucleation rate will be so slow that no crystals form in a reasonable period of time. The corresponding area of the phase diagram is known as the "metastable zone" (Figure 35). In the "labile" or "crystallization" zone, the supersaturation is large enough that spontaneous nucleation is observable. If the supersaturation is too large, then disordered structures, such as aggregates or precipitates, may form. The "precipitation zone" is unfavorable for crystal formation, because the aggregates and precipitates form faster than the crystals. Because these zones are related to kinetic phenomena, the boundaries between the zones are not well defined (this in contrast to the solubility line which is an unambiguous delimitation of the equilibrium between solution and crystal). Even though the division in zones is qualitative, the different behaviors serve as guide when searching for the appropriate conditions to produce crystals (Mikol et al., 1990; Saridakis et al., 2003).

1.2 MACROMOLECULAR CRYSTALLIZATION IN PRACTICE

The kinetics of equilibration, through dehydration of the protein-containing experiment drop or through liquid diffusion, will determine the rate at which supersaturation is obtained as well as the trajectory through the phase diagram and can often be passively controlled (Luft and DeTitta, 1997). There are three main categories of crystallization methods: vapour-diffusion, batch and liquid-diffusion.

Vapour diffusion

Vapour diffusion crystallization techniques such as hanging drop, sitting drop and sandwich drop methods are the most commonly used techniques for crystallization. This technique utilizes evaporation and diffusion of water (and other volatile species) between a small droplet (0.5–10 µL), containing protein, buffer and precipitant, and a reservoir (well), containing a solution with similar buffer and precipitant, but at higher concentrations with respect to the droplet.

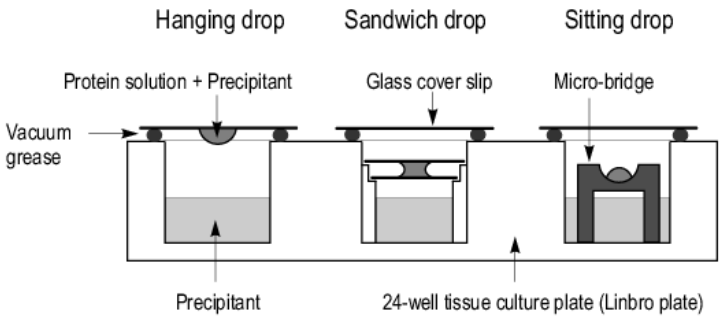

The wells are sealed by creating an interface of vacuum grease between the rim of each well and the cover slip, or by using, in specific cases, a sealing tape. The droplet is equilibrated over the well solution as either a hanging, a sitting or a sandwich drop to allow a slow increase of both the protein and precipitant concentration that could cause supersaturation and crystal growth. In the hanging method the drop is placed on the underside of a siliconized glass cover slide, while in the sitting method the drop is placed on a plastic or glass support above the surface of the reservoir. Finally in the sandwich drop the protein mixed with the precipitant is placed between two cover slips, one of which closes the well.

Microbatch

In the batch method the supersaturation is achieved directly rather than by diffusion. The sample is mixed with the precipitant and appropriate additives to create a homogeneous crystallization medium, then the mixture is left undisturbed.

Batch experiments, in particular microbatch under oil (Chayen et al., 1992) experiments, are conceptually simple: a protein solution is combined with a crystallization cocktail under oil; the oil is a barrier to dehydration of the experiment drop, but also acts as an interface that can affect crystallization.

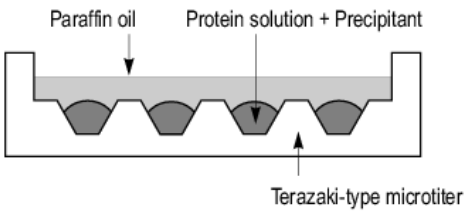

The dehydration rate can be controlled by making the oil barrier more or less water-permeable, for example by combining paraffin (less water-permeable) and silicone-based (more water-permeable) oils (D'Arcy et al., 1996). Microbatch experiments can be especially useful if the temperature is not stable, as they do not suffer from the condensation in the experiment well that can occur during vapour diffusion experiments.

Dialysis

This technique utilizes diffusion and equilibration of precipitant molecules through a semi-permeable membrane as a means of slowly approaching the concentration at which the macromolecule crystallizes. Provided that the precipitant is a small molecule like a salt or an alcohol, it can easily penetrate the dialysis membrane, and the protein is slowly brought into equilibrium with the precipitant solution. Dialysis tubes can be used by itself in the case of large amounts of protein being available.

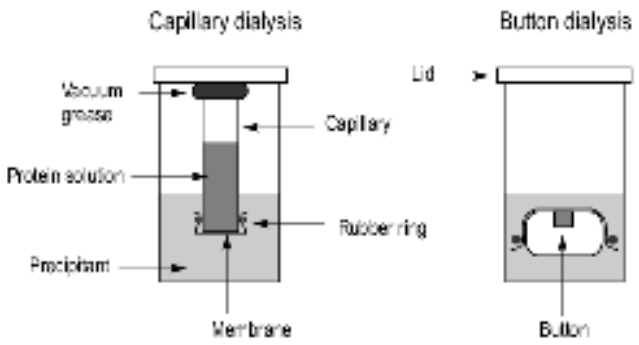

Microdialysis buttons, offer a convenient way to perform crystallization trials with a small amount of sample. In the last case, the protein sample is placed inside a small chamber on top of the button, which is able to accommodate volumes ranging from 5 to 100 µL; the sample is covered with a dialysis membrane of appropriate molecular weight cut-off and then is placed in a reservoir containing the precipitant solution. Dialysis has several advantages, including the possibility to change the reservoir composition accurately any number of times simply by moving the button from one condition to another. Furthermore, the rate of equilibration can be modulated by varying the differential between concentration inside and outside the membrane. On the other hand, this method does not work with concentrated PEG solutions, as they tend to draw all the water out of the button, thus resulting in protein precipitation, and does not allow to change protein concentration.

Free Interface Diffusion (FID)

This technique relies on carefully layering the precipitant solution on top of the concentrated protein solution in a capillary, whose ends are then sealed with wax (Salemme, 1972). The narrow diameter of the capillary minimizes mixing from natural convection in the system. Thus, the precipitant and the protein slowly inter-diffuse and the system reaches the equilibrium by a phenomenon called counter-diffusion.

This relatively new technique for crystallization *Counter-Diffusion in Gel*, that has been developed from essentially of the old free-interface diffusion method. In practice, a gel plug is used to separate protein and precipitant solutions, otherwise one of the two solutions can be gelled before it is introduced in a capillary (Otalora et al., 2009). A subsequent improvement of this procedure is the gel acupuncture method (Ruiz et al., 1993) that utilizes a small crystallization vessel containing a gelified medium (silica, agarose). A capillary tube is filled with the protein solution and one of its ends is sealed with wax or clay, while the other one is fixed in the gel at a penetration length of 6–7 mm. Then, the gelled matrix is over-layered with the precipitating solution. Finally, the growth box containing one or more capillary tubes is kept in a closed environment at constant temperature. After the progression of the precipitating agent into the capillary, a quick increment of high

supersaturation is observed and amorphous precipitation or microcrystals can be formed. Then, as the value of supersaturation decreases, fewer crystals of bigger size and quality are obtained.

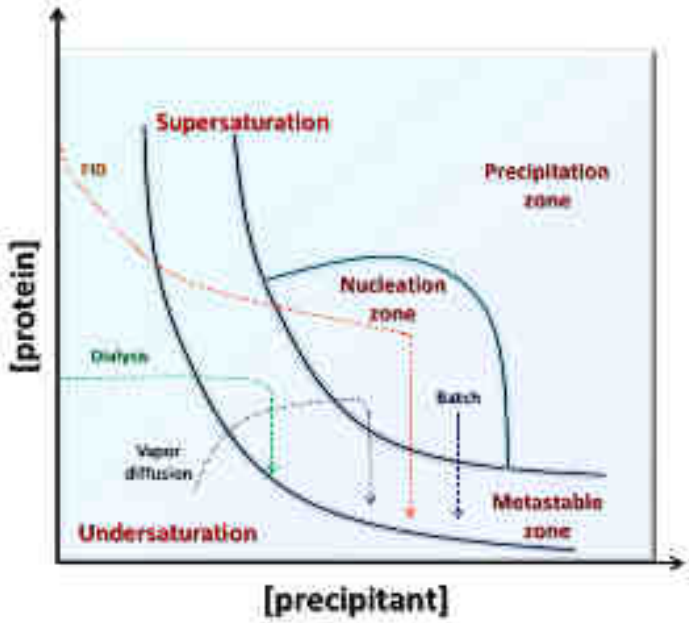

Figure 36: Idealized phase diagram of the trajectories of four different crystallization methods of reaching nucleation and metastable zones (adapted from Krauss et al, 2013).

In the vapour-diffusion method, the initial drop conditions are undersaturated (Figure 36). As the drop dehydrates, typically through a dynamic equilibrium with the reservoir solution, the relative concentration of the protein and precipitant will steadily increase until the drop reaches a metastable state that will kinetically and thermodynamically support spontaneous homogeneous nucleation. The drop will typically further dehydrate as it equilibrates with the reservoir solution and the crystal will pass through the metastable zone; here it will grow to a larger size, but the solution will not be sufficiently supersaturated to support nucleation events. The drop reaches a saturation point when the drop and reservoir have equilibrated with respect to the vapour pressure of water, and the protein in the drop is in a dynamic equilibrium between the liquid and solid. (crystalline) phase.

For batch method (Figure 35), a successful experiment involves setting up at labile supersaturation. A nucleation event takes place and protein in solution undergoes a phase change to the solid (crystalline) form. Equilibrium is reached when the protein in the surrounding solution reaches a state of saturation with the solid (crystal) phase.

In case of dialysis method (Figure 36) the protein solution is held at a fixed volume. As precipitant passes through the semi-permeable dialysis membrane, the concentration of the precipitant will continue to increase while the protein concentration remains constant. When the solution reaches a metastable state then the protein will form a solid phase (crystalline). At this point, the concentration of the protein in the solution will decrease as protein transitions from a liquid to a solid phase. Saturation is reached when the solid and liquid phases have reached a state of dynamic equilibrium. Finally in the FID method, when the solutions initially come into contact and diffusive mixing occurs, the region of the protein solution in the neighborhood of the interface becomes supersaturated and the ideal conditions for nuclei formation are created. As time proceeds, the two solutions inter-diffuse

along the axis of the capillary and dilute each other, thus promoting the dissolution of the smaller nuclei and the growth of the larger ones.

2. CRYSTALLIZATION OF *S.AUREUS* RIBOSOME

Difficulties in crystallization of the ribosome

The main challenge in crystallographic studies of any biological molecule is finding well-diffracting crystals. And it was obvious that macromolecular complex such as ribosome, with molecular weight 2 300 000 Da, is much more challenging to crystallize than single proteins. For today the ribosome is the largest asymmetric molecular assembly that has been solved crystallographically, and the complexity of ribosome crystallography continues to increase with the addition of translation factors and other accessory proteins. The challenge to crystallize the ribosome consist not only in its huge molecular weight, but also in the fact that the ribosome is an asymmetric complex, thus ordering and packing into the crystal can be very sophisticated. Moreover, ribosomes are very dynamic in the solution meaning that they can have high conformational heterogeneity within one crystallization drop. Heterogeneity may disturb some crystal contacts. Ribosome is composed of two different types of molecules, RNA and proteins, therefore it is rather tricky to find the conditions where ribosome would tend to crystallize rather than form an amorphous precipitate. The phase diagram for the ribosome is far more complex than for individual protein. Basically it is the result of convolution of phase diagrams of each individual molecule comprising the full ribosome and their intermolecular interactions. Hence, ribosomes from different organisms require unique new searches of correct crystallization conditions. Nowadays, there are several tens of commercially available crystallization screens developed to facilitate a comprehensive search of crystallization conditions for proteins. These screens are based on the knowledge of thousands of successful crystallization experiments, but unfortunately are suitable mostly for individual proteins rather than macromolecular complexes (because the better part of solved structures belongs to individual proteins). However, even if there are no commercial screens designed for the ribosomes, the compilation and analysis of crystallization conditions published for bacterial 70S ribosome revealed only a limited amount of variation summarized in Table 1.

Component	Concentration	Types			
Buffers, pH 6.5 – 7.5	0 – 100 mM	Tris	MES	Hepes	
Cations	0 – 380 mM	K^+	$NH4^+$	Arginine	
Anions	0 – 380 mM	Cl^-	SCN^-	$Acetate^-$	
Magnesium	0 – 35 mM	$MgCl_2$	$MgOAc_2$		
Precipitant	3.5 – 4.5%	PEG 400			
	3.5 – 4.5%	PEG 550 mme			
	2 – 4.5%	PEG 8000			
	2.5 – 4.5%	PEG 20000			
	11 – 26%	MPD			
Polyamines	0.5 – 5 mM	Spermine	Spermidine	Thermine	Putrescine
Additives	0.25 mM	ETDA			
	0.5 – 6 mM	2-mercaptoethanol			
Detergent	2.8 mM	Deoxy Big Chap			

Table 1: Published crystal conditions for 70S ribosomes (adapted from Pearson, 2011).Summary of the concentration and identity of salts, precipitants, and critical additives from multiple 70S ribosome crystallization conditions (Trakhanov et al., 1987; Yusupov et al., 1987; Yusupov et al.,2001; Korostelev et al., 2006; Korostelev et al., 2008; Petry et al., 2005; Selmer et al., 2006; Gao et al., 2009; Schuwirth et al., 2005; Vila-Sanjurjo et al., 2003; Zhang et al., 2009; Blaha et al., 2009).

2.1 CRYSTALLIZATION

First crystals of 70S *S. aureus* ribosome were obtained in the Yusupov laboratory from initial protocol of purification. Crystallization condition and crystal performed below. Typically, crystals appeared reproducibly within 7 – 10 days and reached their full size after two additional weeks (Table 2A). Unfortunately, almost all these crystals were attached to the plastic of crystallization plate, preventing any manipulations with them and diffracted at very low resolution. So, those results forced us for searching new crystallization condition for 70S ribosome.

After long screening of variety of crystallization conditions (listed in Table 1), crystals appeared and grown only with presence of **PEG 8000 and NH_4SCN** in the crystallization conditions (see below Table 2). And whenever we tried to replace PEG 8000 or NH_4SCN, crystals didn't appear.

First crystal obtained in new conditions has been shown in the Table 2B. We started with optimization crystallization condition for improving shape of the crystals. Several screening of different variations of concentration of Glycerol, NH_4SCN, $Mg(OAc)_2$ and PEG 8000 did not give positive results. Crystals were growth only with high concentration of NH_4SCN (not less than 400mM) and with high concentration of PEG 8000. Absence of Glycerol or $Mg(OAc)_2$ did not influenced to the crystal growth. Changing the temperature for 4°C stopped crystals growing.

Crystals	Crystallization conditions	Crystal growth conditions
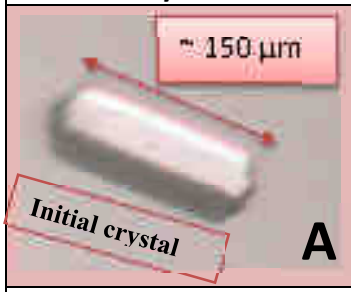	**CrysChem plate 2µl+2µl** 100 mM bis Tris propane pH 7.0 10 mM $Mg(OAc)_2$ 325 mM NH_4SCN 4.8 % PEG 8000 8 mg/ml Ribosomes	Crystals obtained at **24°C**
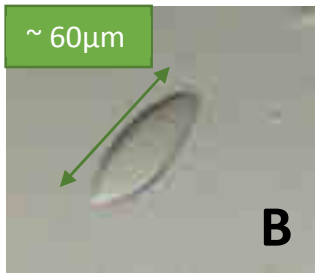	**MRC 2 drop plate 0.2µl+0.2µl** 100 mM Tris-Acetate pH 7.0 400 mM NH_4SCN 5.5 % PEG 8000 3% PEG550 mme 10% Glycerol 8 mg/ml Ribosomes	Crystals obtained at **24°C** and appeared after 4 days 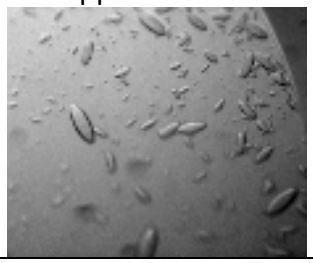
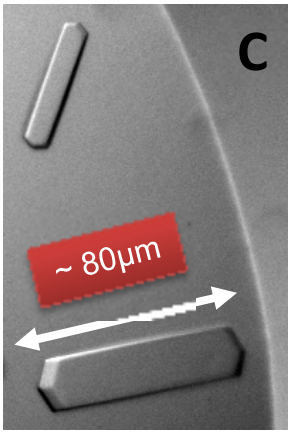	**MRC 2 drop plate 0.2µl+0.2µl** 100 mM Tris-Acetate pH 7.0 9 mM $Mg(OAc)_2$ 500 mM NH_4SCN 5 % PEG 8000 6% MPD 2% PEG400 10% Sucrose 8 mg/ml Ribosomes	Crystals obtained at **24°C** and appeared after 8 days 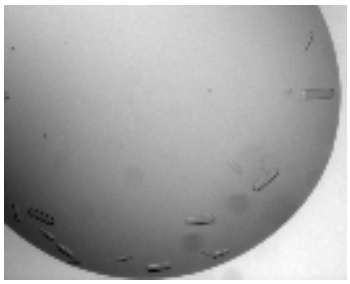
	MRC 2 drop plate 0.2µl+0.2µl 100 mM Tris-Acetate pH 7.0 9 mM $Mg(OAc)_2$ 500 mM NH_4SCN 5 % PEG 8000 6% MPD 2% PEG400 10% Sucrose 8 mg/ml Ribosomes	Crystals obtained at **4°C** and appeared after 30 days
	MRC 2 drop plate 0.2µl+0.2µl 100 mM Tris-Acetate pH 7.0 9 mM $Mg(OAc)_2$ 375 mM NH_4SCN 6.25 % PEG 8000 6% MPD 2% PEG400 10% Sucrose 8 mg/ml Ribosomes	Crystals obtained at **20°C** and appeared after 34 days

Table 2 Crystals of *S. aureus* 70S ribosome with presence PEG 8000 and NH_4SCN in the crystallization condition.

More perspective type of crystals was obtained in the conditions see Table 2C, D, F. According to this crystallization condition, crystals grown even at 4°C (Table 2D), which allowed to have a range of manipulation with two type of crystals. In additionally, the crystals obtained at 20°C (Table 2C), had already formed hexagonal prism shape, which was reduced amount of optimization with them. Also, the crystallization conditions included cryo- protectant compounds such as MPD, Sucrose and PEG400, which facilitates of further cryo-protection of these crystals. Different types of optimization crystallization was introduced with PEGs, Sucrose, MPD and salts in order to improve size and quality of crystals obtained at 4°C/20°C. Screening of Sucrose showed that increasing of Sucrose helps for getting bigger size crystals and in another hand decreasing of concentration gave small and tiny crystals. In case of PEG400, increasing of concentration gave melted crystals. Optimum for NH_4SCN is 475 mM, less concentration gave small size crystals and less nucleation in the drop. Initial concentration of $Mg(OAc)_2$and MPD showed best results.

We found optimum condition for crystals growing at 20°C, however in case of crystals at 4°C changes was minimum and the quality of crystal was low. These conditions are promising and need additional optimization in the future.

Finally, after long screening conditions, we were able to replace NH_4SCN (which most probably influenced to attaching crystals to the plastic of crystallization plate) for KSCN (which is quite often used for crystallization of ribosome). First crystals-like particles of the70S ribosome from *S. aureus with* KSCN in crystallization condition were obtained using robotic screening of variety of combination of conditions listed in Table1. Ribosome sample (0.2µl (8 mg/ml) containing 2.8 mM Deoxy Big Chap) was mixed with 0.2µl of reservoir solution (100 mM Tris-Acetate pH 7.0; 9mM $Mg(OAc)_2$, 400 mM KSCN; 5% PEG 8000;10% MPD) in MRC 2 drop plates by the Mosquito robot. Plates were stored at 24 °C, and crystalline particles appeared after 5 days.

Optimization of *S. aureus* ribosome crystallization was carried out at 24 °C and included several global steps:

1. Variation of salt and precipitant concentrations. As the first step, fine titration of KSCN and PEG 8000 and MPD concentrations improved shape of crystals.

2. Scale up. To grow bigger crystals we switched to larger scale crystallization, making drops 2 + 2 µl in 24 - well sitting drops in CrysChem plates (Hampton Research). This led to shift of PEG 8000 concentration a bit higher to 5.5%. KSCN remained 400 mM. As a result crystals grew to approximately 100 × 40 × 10 µm big on average (Figure 36).

3. Variation of Mg^{2+} and introduction of polyamines increased the size of the crystals to approximately 100 × 50 × 20 µm.

4. Ribosome concentration. In the next step of optimization we wanted to decrease of ribosome concentration in order to have less nucleation zones. We observed that even with 3mg/ml of ribosome, crystals appeared after 6 days and had same size with 8mg/ml.

5. Volume of reservoir. Changing volume of reservoir solution (400, 500, 600, 700 or 800 µl) didn't affect crystallization significantly. Thus, 500 µl was used in all further experiments.

6. Correlation of drop to reservoir. In the purpose to increasing the size of crystal we introduce different ratio of volume of drop to reservoir, but it didn't change the crystal size dramatically.

The following crystallization protocol was obtained after optimization. The ribosome sample was prepared as follows. The frozen sample of 70S ribosome was thawed at room temperature for 10 min, filtered through 0.22 µm filters (Merck, Millipore), diluted to 8 mg/ml ribosome solution in Buffer G containing 2.8 mM Deoxy Big Chap, incubated at 30 °C for 30 min and then left to cool down to room temperature before crystallization. Crystallization was performed at 24 °C using CrysChem sitting drop (Hampton Research) plates by mixing 2 µl of ribosome solution with 2 µl of 500 µl reservoir solution (100 mM Tris-Acetate pH 7.0; 400 mM KSCN; 5.5 % PEG 8000; 10% MPD). Typically, crystals appeared reproducibly within 5 – 7 days and reached their full size after two additional weeks.

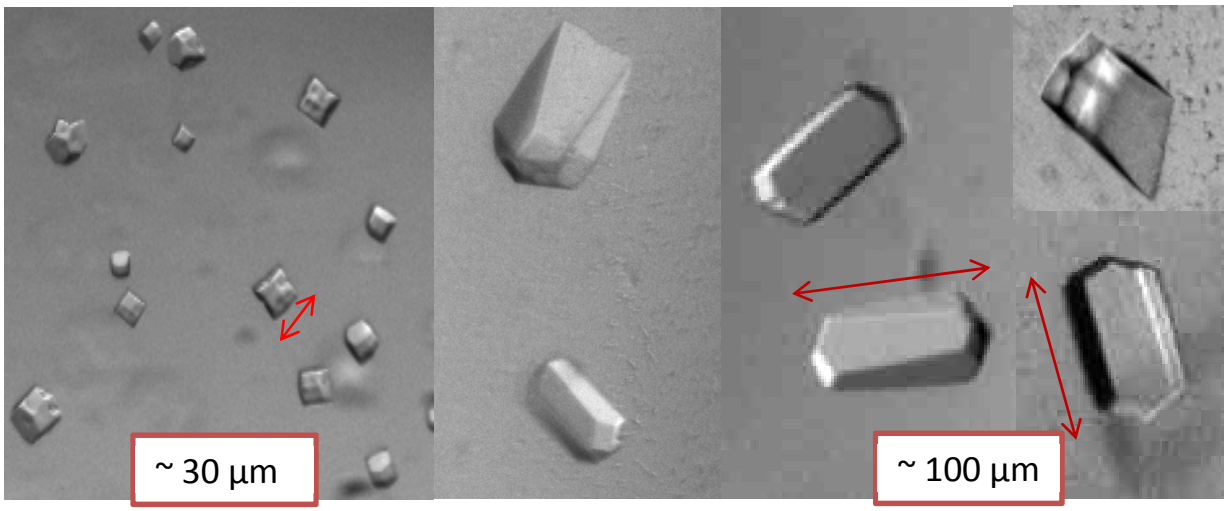

2 µl + 2 µl CrysChem plate
100 mM Tris-Acetate pH 7.0
375 mM KSCN
5.5 % PEG 8000
10% MPD
2.0 mM Spermedine
8 mg/ml Ribosomes

2 µl + 2 µl CrysChem plate
100 mM Tris-Acetate pH 7.0
400 mM KSCN
5.5 % PEG 8000
10% MPD
2.0 mM Spermedine
8 mg/ml Ribosomes

Figure 37: Crystals of *S. aureus* 70S ribosome in the CrysChem plate.

7. *Replacing cryo-protectant compound*. In the next step of optimization we wanted to replace MPD into the crystallization conditions to another cryo-protective compounds such as glycerol, EG (ethylene glycol), small PEGs (PEG 400, PEG 550 mme, PEG200), ethanol and 1.5 pentandiol. The hypothesis was that MPD could influence the diffraction of crystals. We obtained crystals only with conditions with ethanol, 1.5 pentandiol and EG the in the rest cryo-protective compounds conditions crystals didn't growth. However, the quality and shape of these crystals was the same with MPD.

8. *Replacing salts and precipitants.* To improve the crystal quality we have decided to replace SCN - anion in crystallization trials to another more commonly used salts. We tried to introduce KCl, K-acetate, NH_4Cl and NH_4-acetate in combination with KSCN or individually. We observed no changes in the kinetics of crystals growth, when we use combination of salt and in case of individual salts crystals didn't appear. Moreover, when we shifted away from using the KSCN • PEG 8000 pair the crystals stopped to growth.

9. Changing geometry and plastic. Another possible for increasing the size of crystal was to change geometry of the crystallization plates and the surface where crystallization drop was mixed. To do this, we used a hanging drop setup in VDX plates (Hampton Research). In this setup the drop is mixed on the glass cover slide and kept upside down during equilibration. Crystals were same size as crystals grow in the CrysChem plate, but melted.

10. *Changing the temperature.* Crystallization at 4 °C did not give expected results in crystals at the conditions used. Crystals appeared only if we transferred crystallization plate after 10-30 days from 4 °C to 24°C. In this case crystals appeared in 7 days, but they were less sharp and most of them were melted.

11. Changing detergent concentration. We tried to reduce concentration of Deoxy Big Chap in the crystallization drop in order to increase crystal size and have less nucleation zones in the drop. For this purpose we crystalized ribosome with 0.6/1/1,4/1.8/2.2mM of detergent. Crystals with 1.8 and 2.2 mM Deoxy Big Chap didn't show much differences with 2.8mM detergent. However, the concentrations from 1mM till 1.4 mM Deoxy Big Chap, have been performed big size crystals with size 250 x 100 x 50 µm. In cases of their form, they still needed optimization.

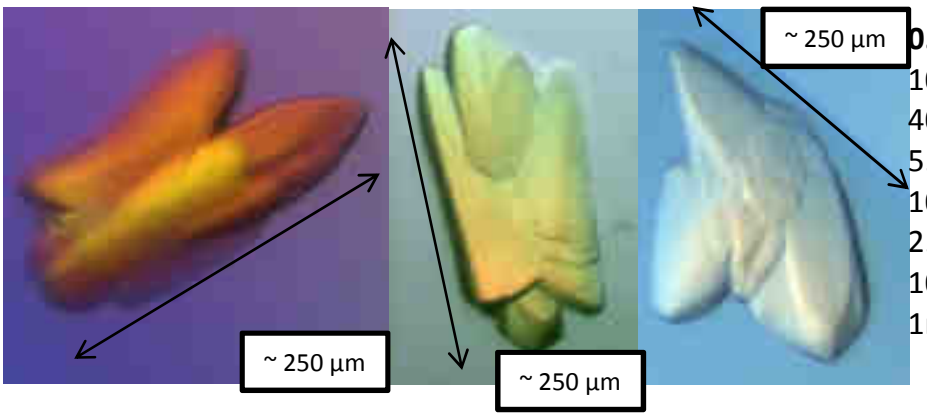

0.2µl+0.2µl MRC 2 drop plate
100 mM Tris-Acetate pH 7.0
400 mM KSCN
5.0 % PEG 8000
10% MPD
2.0 mM Spermedine
10 mg/ml Ribosomes
1mM Deoxy Big Chap

12. Seeding. Seeding was used as a last resort to change the kinetics of crystals growth. Seeding is a very powerful crystallization technique that can in some cases drastically improve the quality of crystals. We start the process of drop equilibration from metastable zone in the phase diagram (see Figure 35). Together with our ribosome in solution we put the seeds of crystals (usually smashed by mechanical force) of our crystallized ribosome sample. These seeds serve as nuclei for the formation of new crystals. Since we unaware of the exact phase diagram for S. aureus ribosome in particular crystallization conditions, we used different initial concentrations of every compound as initial point. Seeds were prepared by vortexing or using a seed-bead kit (Hampton Research) or by smashing the crystal with glass bead (all done in reservoir solution where crystal doesn't dissolve). Seeds were diluted up to 10000 times in reservoir solution. Crystallization drops were set up in CrysChem sitting drop at 24 °C: 1.8 µl of ribosomes were mixed with 2 µl of reservoir and 0.2 µl of seeds. Under these conditions, seeding did not improve crystallization. All crystals were exactly as before. Possibly, the treatment of the crystals was too harsh, and all the nuclei were destroyed during the preparation of the seeds.

13. Analysis of influence ribosome sample to the crystals quality/ Comparative analysis of crystals after modification of the purification protocol. Puromycin treatment of ribosome (experiment IV) didn't show any changes in crystallization conditions. However after two step of sucrose cushion sedimentation (experiment I) we observe less nucleation in the crystallization drop and best crystals shape showed purification with second sucrose cushion step (25mM $Mg(OAc)_2$and 500 mM KCl). Under this condition we observe new pyramidal form crystals and most of them were single and sharp (Table 3C).

After "light dissociation" step (experiment III) of ribosome purification, most of the crystals were small with a lot of nucleation in the drop. Only 30 minutes of incubation ribosome in dissociation conditions in the experiment III showed pyramidal form crystals, but with relatively small size. And crystals after 40 minutes of incubation were single, but most of them were deformed. Probably, 40 minutes and more were long time for incubation in dissociation conditions and the time and the procedure should be optimized.

Ribosome crystals after purification of 70S ribosome with decreasing Mg^{2+} till10 mM and increasing NH_4Cl till 500mM before sucrose cushion step (experiment II) (see modification of ribosome purification protocol) showed same results as with Mg 10 mM and NH_4Cl 100mM. Most of the crystals were single, sharp pyramidal form and with size 120 x 50 x 20µm. According to these results, we decided to keep 10mM of $Mg(OAc)_2$ before sucrose cushion step and to keep 100 mM NH_4Cl instead of 500 mM in ribosome purification, in order not to drive additional stress to the ribosome during purification process(as mentioned before in the ribosome sample characterization chapter).

Protocol with two steps of sucrose cushion sedimentation (Experiment I)	**Best shapes of the crystals**	**Crystallizations conditions**
A. Second step of sucrose cushion with **100** mM KCl and **25** mM $Mg(OAc)_2$	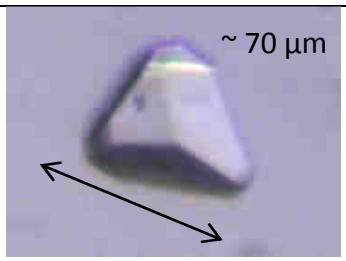 PEG8000 5.5%-5.6%	**2µl+2µl CrysChem plate** 100 mM Tris-Acetate pH 7.0 400 mM KSCN 4.9-6.0 % PEG 8000 10% MPD 10 mM $Mg(OAc)_2$ 8 mg/ml Ribosomes At 24°C Crystals appeared during 6-8 days
B. Second step of sucrose cushion with **300** mM KCl and **25** mM $Mg(OAc)_2$	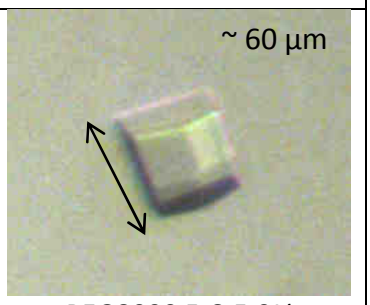 PEG8000 5.6-5.9%	
C. Second step of sucrose cushion with **500** mM KCl and **25** mM $Mg(OAc)_2$	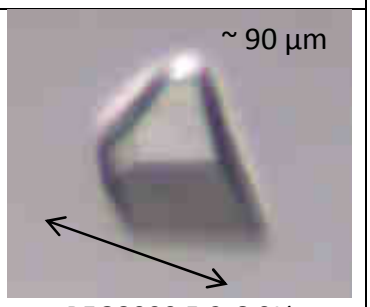 PEG8000 5.2-6.0%	
Protocol with "light dissociation" step (Experiment III)		

D. 15 minutes of incubation (see modification of ribosome purification protocol)	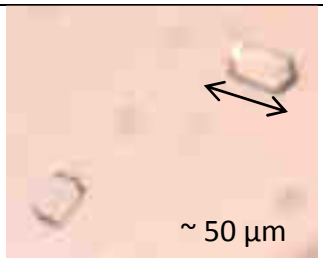 PEG8000 5.7-5.8.%	All crystallization condition same with previous protocol, except concentration of Ribosome 7.5mg/ml
E. 30 minutes of incubation (see modification of ribosome purification protocol)	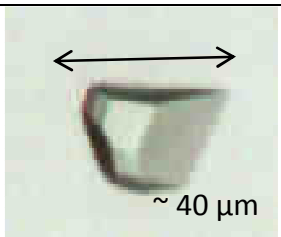 PEG8000 5.7-6.0.%	
F. 40 minutes of incubation (see modification of ribosome purification protocol)	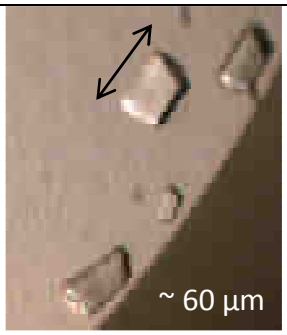 PEG8000 5.2%	

Table 3: Crystals of the *S. aureus* 70S ribosome after modification of purification protocol.

14. Complex formation with initiation tRNA^{fMet} , mRNA and 70S ribosome of S.aureus.

Initiation complex formation with *S.aureus* ribosome was based on the protocol of complex formation with 70S ribosome from *T. thermophilus* (Demeshkina et al., 2010).

The ribosome sample was prepared as follows. The frozen sample of 70S ribosome was thawed at 0°C during 10 min, and then transferred to 37°C for 30 min, filtered through 0.22 µm filters (Merck, Millipore). The tRNA^{fMet} sample was thawed at 0°C during 20 min, incubated at 55°C for 2min, then transferred to 20 °C for 20 min. The frozen mRNA transferred at 0°C for 20min. Then Buffer G was mixed with 5X of Buffer G in accordance with the concentrations of subsequent RNAs and ribosome. Then mRNA and tRNA^{fMet} were added to these buffers and mixed very carefully by pipetting. At the end ribosome was added according to final concentration 7 mg/ml, 10 mg/ml and mixed at room temperature 30 second, incubated 10 min at 37°C for complex formation. After incubation 2.8mM Deoxy Big Chap was added, mixed by pipetting and spin down 30 second, then left to cool down at room temperature before crystallization. Crystallization was performed in two temperatures 20 °C and 4°C. However, crystals appeared only at 20°C.

Complex formation was performed according to different ratios 70S ribosome: tRNA ^{fMet}: mRNA, however crystals appeared in the ratios:

1:1:1	1:1:0	1:0:1	1:0:2	1:0:3	1:0:4	1:0:5

Crystallization was performed at 20 °C using 96 MRC sitting drop plates (Hampton Research) by robot mosquito mixing 0.2µl of ribosome solution with 0.2µl of 50 µl reservoir solution (100 mM Tris acetate pH 7.0, 450/500/550/600 mM KSCN, 5 mM $Mg(OAc)_2$, 3.0 – 8.75% w/v PEG 8000, 10%-MPD, 2 mM spermidine).

Typically, crystals with 70S ribosome/ tRNA ^{fMet} appeared reproducibly after 30-34 days and reached their full size after two additional weeks (Figure 37A). In case of complex ribosome/tRNA^{fMet}/mRNA, crystals appeared after 10-14 days and reached their full size after two additional weeks (Figure 38B). Two of these complex formations showed different type of crystals which was grown only at high concentration of salt. Whenever we tried to decrease the concentration (less than 550 mM of KSCN) crystals became melted and deformed (Figure38B; 39A). Good crystals quality we obtained only with concentration of ribosome not less than 7 mg/ml.

Ribosome crystals with mRNA appeared after 6-8 days and did not show any differences in the crystals morphology.

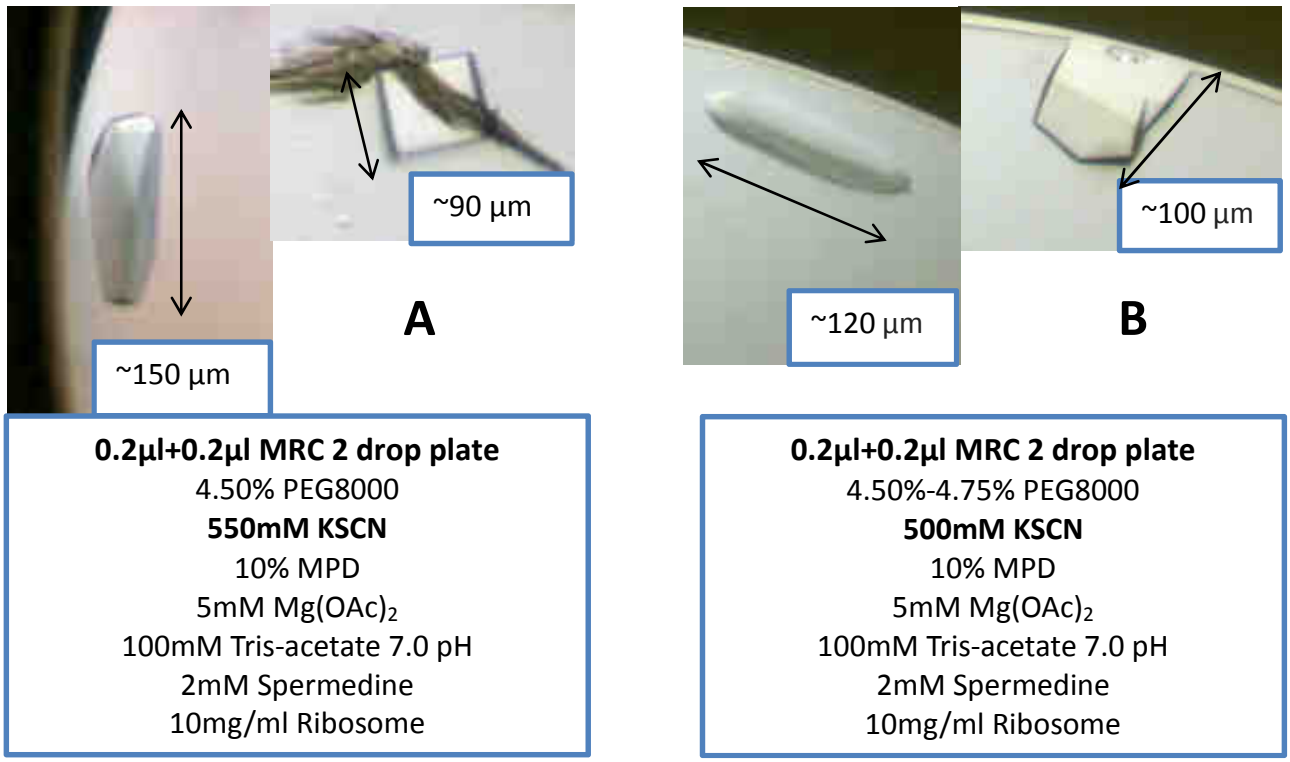

Figure 38: Crystals of 70S ribosome with tRNA ^{fMet} with ratio 1:1.

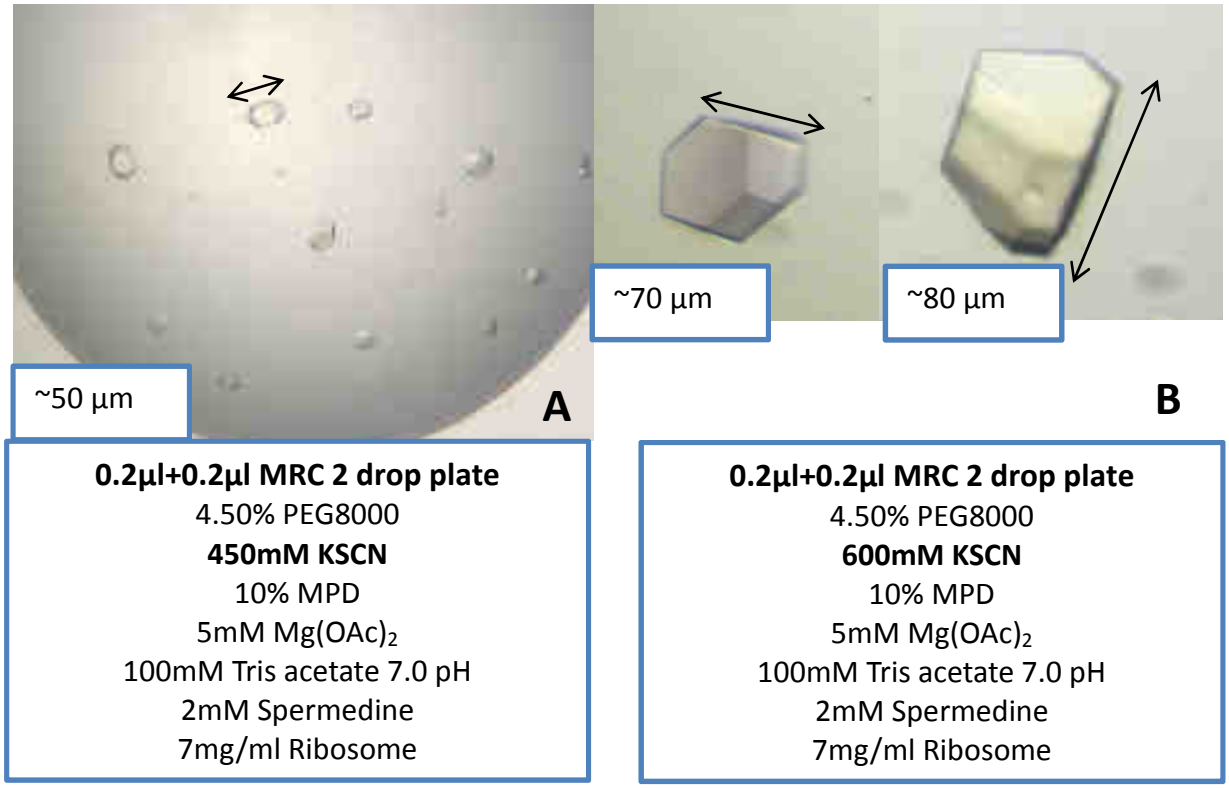

Figure 39: Crystals of 70S ribosome with tRNA ^{fMet} and mRNA with ratio 1:1:1.

15. Stabilization of 70S ribosome by co-crystallization with N-terminal domain hibernation promoting factor.

Hibernation promotion factor (HPF) is requiring for dimerization of active 70S ribosomes into 100S ribosomes under the stress condition. HPF bound in the mRNA channel between the head and the body of the 30S subunit. The nearly identical binding sites of HPF and YfiA from *E.coli*, which overlap with those of the mRNA, transfer RNA, and initiation factors, which prevents translation initiation in the *Thermus thermophilus* ribosome complex (Polikanov et al., 2012). Hence, recent studies reported that the interface is markedly different between 100S from *S. aureus* and E. coli. Cryo-electron microscopy structure of 100S *S. aureus* ribosomes reveal that the *S. aureus* HPF-N - terminal domain (SaHPF-NTD) binds to the 30S subunit as observed for shorter variants of HPF in other species and the C-terminal domain (CTD) protrudes out of each ribosome in order to mediate dimerization. SaHPF-NTD binds to the small subunit similarly to its homologs *E.coli* HPF, *E.coli* YfiA, and a plastid-specific YfiA (Khusainov et al., 2017). And according to the suggestion (Polikanov et al., 2012) that YfiA prevents head (30S) moving of ribosome and stabilizes whole macromolecule. We decided to co-crystalize SaHPF-NTD with ribosome in order to stabilize of our assembly and potentially improve our resolution of ribosomes from *S.aureus*.

N-terminal domain of SaHPF (SaHPF-NTD, residues 1-110) protein was expressed in *E. coli BL21*star(DE3) cells with a pGS21A plasmid with histidine tag fused protein at its C-terminus.

Purification of SaHPF-NTD was established in Yusupov laboratory and protein was kindly provided by researcher from the Kazan Federal University.

The ribosome sample for crystallization was prepared as described before. Fresh (not frozen) SaHPF-NTD filtered through 0.22 µm filters (Merck, Millipore) during 2 min, 13000rpm, at 4°C.Then protein mixed with Buffer G and spin down 2-3 seconds and stored at 0°C. After adding ribosome (10mg/ml) to the mixture, we incubated sample during 30 minutes at 37C for complex formation. At the last point was added detergent (2.8mM Deoxy Big Chap) and spin down 30 second and then was left to cool down at room temperature before crystallization. Crystallization was performed in two temperatures 20 °C and 4°C. However, crystals were grown only at 20°C.

Crystals appeared according different ratios of 70S ribosome: N-terminal domain of HPF:

1:1,05	**1:2**	**1:5**	**1:10**

Crystallization was performed as described before in previous part. Crystals appeared after 7-10 days and reached their full size after two additional weeks. Morphology and behavior of the crystals didn't change and was the same with vacant crystals. Optimum ratio for crystallization was 1:5 and the size of crystals were 100 x60 x 20µm. The crystals with ratios 1:2 and 1:1.05 were small 50 x 10x 10 µm. The ratio 1:10 showed same results as 1:5.

3. POST – CRYSTALLIZATION TREATMENT

Dehydration

Crystals of macromolecules and macromolecular complexes are usually composed of approximately 50% solvent on average, so that in many ways it represents an ordered gel with a very few intermolecular contacts. Since these contacts provide the lattice interactions essential for crystal maintenance, it is absolutely necessary to decrease the water content by dehydration procedure. Usually alcohols like EG, MPD, PEGs, Glycerol, DMSO are used as dehydration agents.

Several classic methods exist for protein crystal dehydration which includes: simple air drying, vapour diffusion using salts, and soaking with dehydrating compounds (Heras and Martin, 2005; Newman, 2006). The advantages of these methods are that the experiment can be performed with very small humidity steps over long periods of time, and that the number of crystals can be modified at the same time. Unfortunately, the outcome of the dehydration is unknown until the experiment is finished, and there is no direct way of assessing the progress of the experiment. Although, it is the most popular method, it is crystal and time-consuming and can be difficult to reproduce.

Cryo-protection

Special care has to be taken during post-crystallization treatment to avoid damaging the crystals (i.e., when transferring cryo-protection) and even for the freezing process itself we only use the most robust methods of freezing directly in the gaseous N2 stream at 100 K rather than plunging into liquid N2, ethane, or propane as is common practice in X-ray structural projects. A combination of severe radiation decay and generally weak diffracting power limits the amount of data that can be collected from each crystal making it necessary to merge data collected on different crystals to obtain complete

datasets which invariantly degrades the data quality. Several different methods for cooling macromolecular crystals have been developed. An excellent overview is given in the review by Garman and Schneider (1997). Currently the most common method is to fish the crystal with a polyethylene loop via surface tension and cool the crystal either by submerging it in a liquid cryogen or placing it directly into a cold gas stream (Teng, 1990). This usually vitrifies the bulk solvent, slowing diffusion of damaging free radicals produced by the ionizing radiation.

Another relatively recent development in cryo-cooling techniques is recovery of "lost" diffraction by cycling crystals between a low temperature and some higher temperature, which call annealing.

3.1 POST – CRYSTALLIZATION TREATMENT OF *S.AUREUS* RIBOSOME CRYSTALS

Several strategies were used to dehydrate crystals (Figure 40)

Plan of action 1

This involved soaking in a reservoir solution with increasing concentrations of dehydration agents (in future called dehydration solutions) for different periods of time. The dehydration solution was introduced into the drop stepwise by sequential transfer or directly into the crystallization drop. As dehydration agents we used different PEGs (PEG 400, PEG 500 mme, PEG 6000, PEG 8000, PEG 20000), MPD, EG, glycerol, or DMSO.

Scheme 1. Crystals were sequentially treated by reservoir solution containing increasing concentrations of MPD or another type of cryo-protectants. After different periods of time, crystals were fished using nylon cryo loops (Hampton Research) and immediately cryo-cooled in a stream of liquid nitrogen. This type of cry-protection also was used with increasing of $Mg(OAc)_2$till 10/20/25/30 mM and with incorporation of heavy atoms together with cryoprotectant agent.

Scheme 2. Crystals were sequentially treated by reservoir solution containing 5.3 – 10% of PEG 8000 and MPD or another cryo-protected compound with concentration 5-10%, up to 30%. After different periods of time, crystals were cryo-protected and were subsequently fished using nylon cryo loops and immediately cryo-cooled in a stream of liquid nitrogen. This type of cry-protection also was used with incorporation of heavy atom, for example osmium, at the last step.

Scheme 3. Crystals were sequentially treated by reservoir solution containing 5.3 – 30% of PEG 8000 or 10-30% MPD. After different periods of time, crystals were fished using nylon cryo loops and immediately cryo-cooled in a stream of liquid nitrogen.

Plan of action 2

This involved dehydration under vapour pressure of the reservoir (Scheme 4). The crystallization drop was diluted with 10 ul of reservoir solution. Then reservoir solution was replaced by 600 ul of dehydration agent: EG or MPD 50 – 80%; reservoir solution containing 120 mM $Mg(OAc)_2$ or 2 M KSCN or 30% PEG 8000. After a certain time (4 – 28 h) the drop was treated by reservoir solution containing 30% cryo-protectant. After different periods of time, crystals were fished using nylon cryo loops (Hampton Research) and immediately were cryo-cooled in a stream of liquid nitrogen.

The result of dehydration procedure is often an internal rearrangement of the molecules that form this crystal. Notably, if *S. aureus* ribosome crystals attached to the surface (plastic or glass), after

dehydration and cryo-protection, it could easily detached from the surface. It means that some changes in the internal organization of the crystals took place.

Also, we analyzed crystals before introductions of any treatment, because it is difficult to estimate whether these changes improved the diffraction limit or the contrary, by checking crystal quality directly from MRC 2drop plate in the Swiss Light Source (SLS). Sometimes the crystal packing changed so dramatically that it completely broke the order inside the crystal. If it happens, we could observe some cracks or other defects on the crystal. Usually, cracked or damaged crystals diffracted very poor.

1. Scheme of cryo-protection

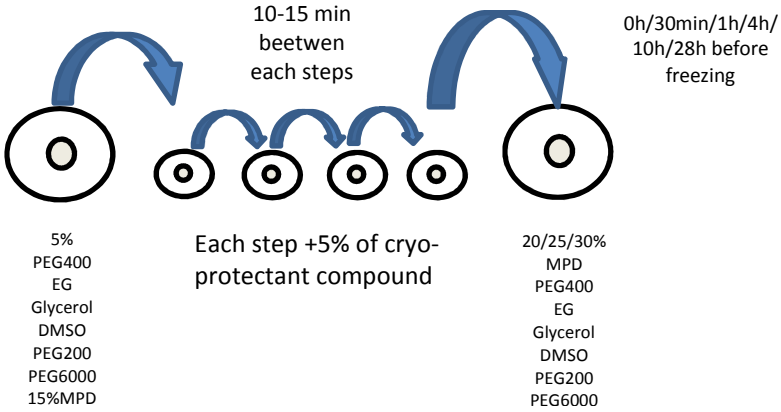

2. Scheme of dehydration and cryo-protection

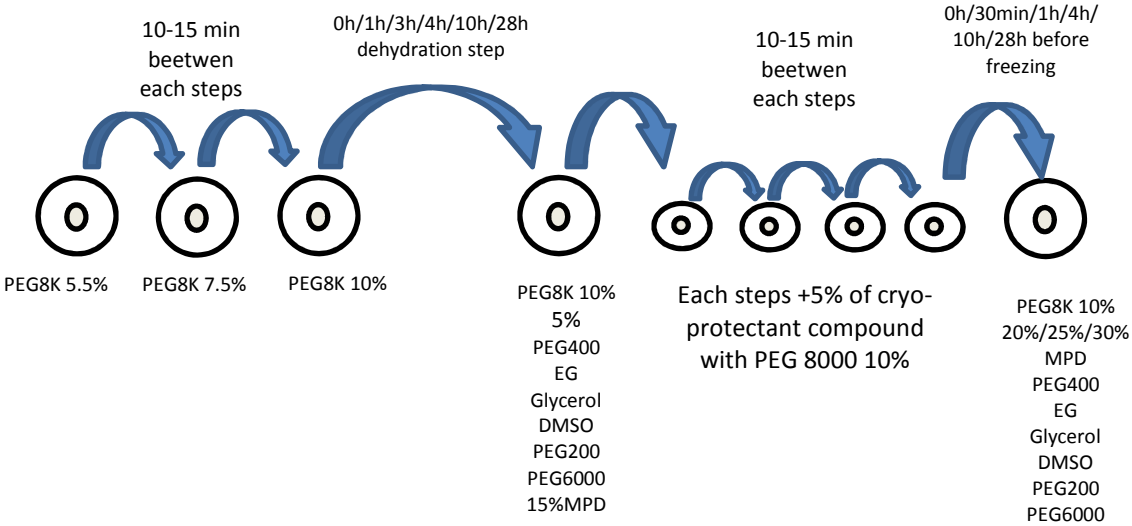

3. Scheme of dehydration and cryo-protection

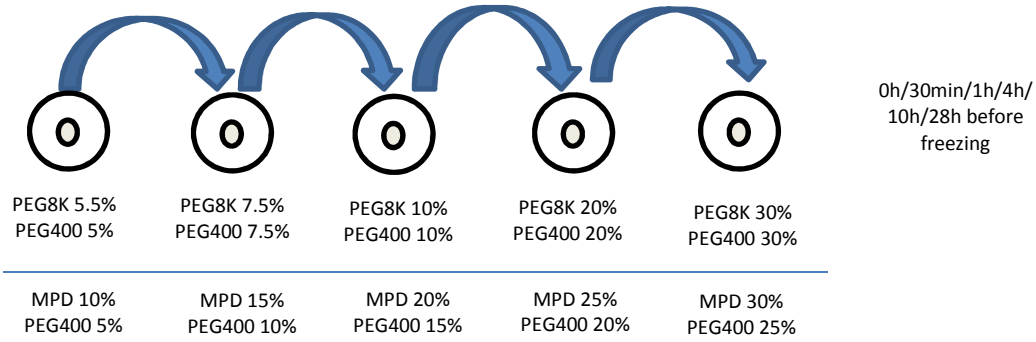

4. Scheme of dehydration and cryo-protection

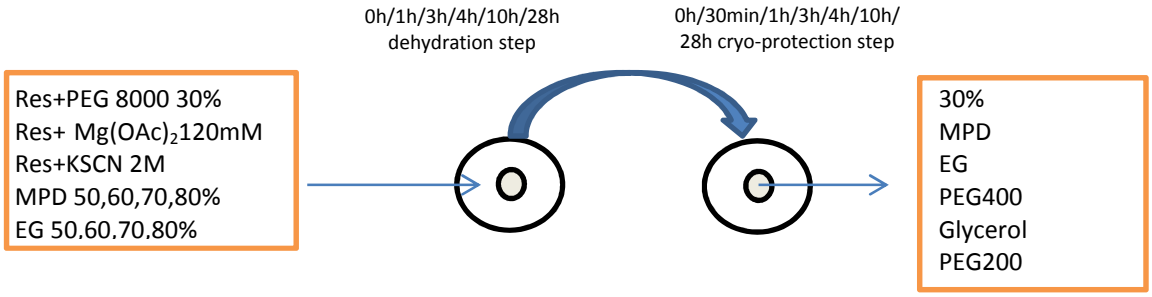

Figure 40: Scheme of post-crystallization treatment. Dehydration and cryo-protection of *S. aureus* ribosome crystals was performed according to the scheme. Treated crystals were further fished into crystallization loop and cryo-cooled at nitrogen stream at 100K and tested at the synchrotron.

4. X-RAY DATA COLLECTION

S. aureus 70S ribosome vacant crystals, initiator complex with tRNA/70S ribosome/ mRNA crystals and complex with N-terminal domain of HPF with ribosome crystals were tested at different synchrotrons and beamlines including Swiss Light Sourse (SLS), Villigen, Switzerland (PXI beamline); Soliel, Massy, France (Proxima1 and Proxima 2 beamlines).

Proper data collection from each individual crystal is one of the important parameter to obtain high quality data and get as much information from the crystal as possible. Different synchrotrons and beamlines require different conditions for data collection. Detector distance, beamstop distance, beam size and intensity, exposure time, oscillation angle and other parameters were optimized empirically according to the properties of crystals and specifications of the beamlines.

SLS

X-ray data collection at SLS synchrotron was performed at the the beamline PX1 - X06SA. All data was collected using single-photon-counting detector PILATUS 6M (Dectris). In average all crystals types without treating (directly from plate MRC 2) diffracted around 70-40Å resolution, reaching 30 Å. Crystals after treating process diffracted around 30Å resolution, reaching 19 Å. Depending on post-crystallization treatment crystals showed different resolution and mosaicity, although, such evaluation is quite subjective. Nevertheless, the "best" crystals were chosen to collect a full dataset. Dataset was collected at 100K and processed using XDS. The resolution limit was shown to be 18 - 19 Å. The space group was determined and belonged to the space group $P4_22_12$ and contained 1 ribosome per asymmetric unit with dimensions 450 × 450 × 280 Å (Figure 40 B).

Soleil

Data collection at Soleil synchrotron was performed at Proxima1 and Proxima2 beamlines. All data were collected at 100K under macro-focused X-ray beam using PILATUS 6M (Dectris Ltd.) detector in case of Proxima1 and micro-focused X-ray beam using ADSC Q315r detector (Area Detector System

Corporation) in case of Proxima2. All dehydrated, cryo-protected and cryo-cooled crystals were tested. Vacant ribosome crystals, which was treated according to the scheme 1 (Figure 39) with PEG 400 and EG 25-30% cryo-protectant compounds, showed good quality of spots without high mosaicity in all 4 angles (19-24 Å) and could reach up to 17.5 Å, compare with other cryo-protectant solutions .Only if they cryo-cooled before than 2h after cryo-protection. Dehydrated crystals according scheme 2 and 4 (Figure40) showed worse results according the diffraction pattern (40-50 Å).

In case of $tRNA^{fMet}$/ribosome crystals stepwise treating with DMSO till 25% in scheme 1 (Figure 40) showed best results (24-26 Å) with good quality of spots. Initiation complex with mRNA crystals diffracted in the range of 26-28 Å only with PEG400 25% stepwise treating according scheme 1 (Figure 40). Crystals of complex with N-terminal domain of HPF with ribosome diffracted at the range 25-30 Å. All the crystal belonged to the space group $P4_22_12$ and contained 1 ribosome per asymmetric unit with dimensions 450 × 450 × 280 Å. Maximum resolution reached was 19Å.

From the crystallographic studies of *S. aureus* ribosome, we can conclude that the purified sample was good enough to be crystallized and to give good quality of crystals. All of the compounds used for crystallization are very well known for ribosome crystallization. Crystals of vacant S. aureus ribosome can be grown reproducibly until they reach a reasonable size (150 × 50 × 20 µm in average) at 24 °C and 20°C. They appear in 7 - 10 days and grow till maximum size during next 2 weeks. The space group was determined as $P4_22_12$ and contained 1 ribosome per asymmetric unit with dimensions 450 × 450 × 280 Å. Crystals survived relatively well under radiation beam, but the resolution limit was always around 25 – 30 Å reaching 18 – 20 Å in rare cases. Complex formation with ribosome didn't change diffraction quality even if changed crystallization behavior and type of crystals.

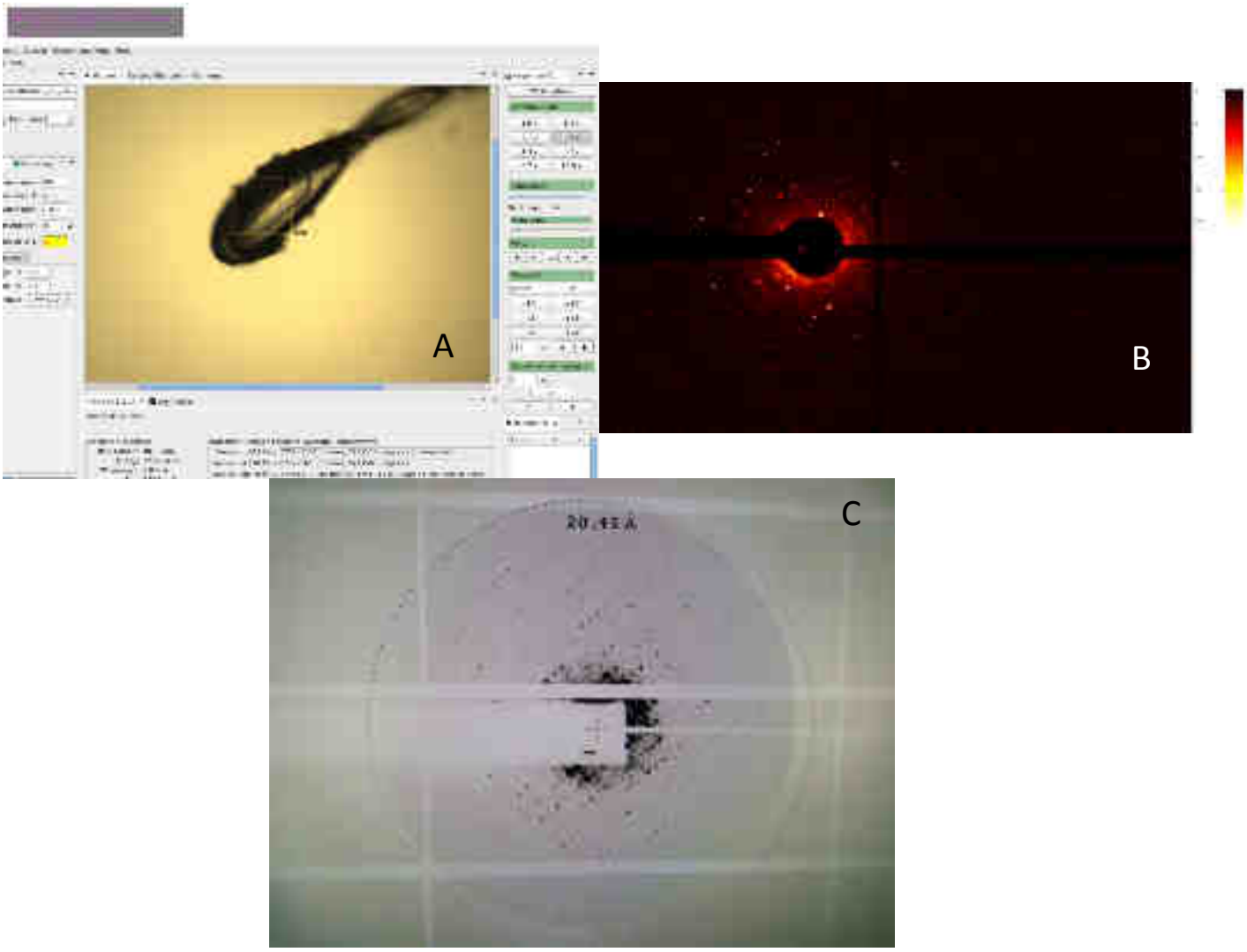

Figure 41: Diffraction patterns of different crystals. A) Cryo-cooled crystal in the loop. B) Diffraction pattern of the crystal reached 19 Å resolution limit (Pilatus 6M detector). C) Diffraction pattern of the crystal reached 21.7 Å resolution limit analysed at micro focused beam (ADSC Q315r detector).

PRESPECTIVES

Probably, there are several reasons which more or less influence on the diffraction of crystals. We managed to get rid of all the non-ribosomal proteins in the sample and minimalize the impurities of tRNA. However, there is still a small probability that the rest of impurities could give a nonsignificant deterioration in the diffraction. Ribosomes could have some conformational differences that did not influence crystal contacts. They could therefore be freely incorporated into the crystal without affecting crystal packing but may strongly diminish the diffraction. Probably for the decision of the given problem it is necessary to use the method of purification ribosome with "tight couples".

The 30S and 50S subunit associate together largely via RNA to RNA contacts mediated by magnesium ions. Reducing the concentration of magnesium ions therefore dissociates the 70S into subunits. By lowering the magnesium ion concentration to 5 mM, about half of the 70S, known as “loose couples”, dissociate into subunits, whereas the remaining “tight couple” 70S full dissociate at the lower concentration of 1 mM magnesium ion. In this way, the resulting 70S ribosomes can be dissociated at low magnesium concentrations (5 mM), which will lead us to obtain a multitude of free subunits “loose couples”. And the additional dissociation of the collected 70S under the condition of 1 mM magnesium ions will result in complete dissociation of 70S ribosome into 50S and 30S. Further with the obtained subunits, it will be possible to produce various process of washing, for example, using high salt concentrations in the conditions of the sucrose cushion. And most likely these stages will already produce more efficient purification of the ribosome. After the washing steps, the subunit must be associated with traditional concentration of magnesium ion and, as a result, we have to obtain pure “tight couple” 70S ribosomes.

During translation, the small subunit rotates against the large subunit in the 70S couple. This rotation (or “ratcheting”) is a fundamental mechanism of translation involved in the movement of transfer RNAs through the ribosome. In case of loose couple 70S probably it correspond to the ratcheted state and tight couple 70S is un-ratcheted ground state position. Thus, obtained "tight couples” most probably will be in one un-ratcheted ground state and this will influence to the crystal diffraction.

A second reason could be the post-crystallization treatment. Due to the fact, that most of the traditional cryo-protectants have been tested, there is small chance that “exotic” cryo-protectant agents and nontraditional methods of cryo-protection will improve diffraction quality. These crystals may require unique and specific dehydration and cryo-cooling procedures that were not identified yet. In addition, despite the fact, that we have tried different variants of the precipitants (PEG) for the crystallization of the ribosome, I believe that in order to further development of the project it is necessary to find a suitable PEG, which will allow us to improve the diffraction quality.

Part II - Structural analysis and investigation of potential anticancer drugs

Results, Methods, Discussions and Perspectives

VIII BACKGROUND AND AIM OF THE PROJECTS

1. CRYSTAL STRUCTURE OF POTENTIAL ANTICANCER DRUG C45 BOUND TO THE 80S RIBOSOME

Development of small molecule translation inhibitors is needed for progress in antibacterial as well as anticancer therapy. We already discussed in the cancer chapter that the ribosome is the most favored target for small-molecule inhibitors. Although the core functions of the ribosome are conserved throughout all kingdoms of life, very tiny differences at structural level make an inhibitor discriminating between bacteria and eukaryotes (Prokhorova et al., 2016). It has been also shown that natural product inhibitors of eukaryotic protein synthesis have significant therapeutic potential to treat a wide range of human cancers. Recently, interest in identifying additional inhibitors of translation has been renewed as a consequence of trying to repress this process to defeat particular diseases. Specifically, the translation initiation phase is usurped in many human cancers (Mamane et al., 2004). Hence, blocking signaling events that affect this process have significant therapeutic potential (Wendel et al., 2004). Particularly interesting, the lissoclimide family of compounds display cytotoxicity towards murine leukaemia and certain human carcinoma cell lines. Originally isolated from ascidians (sea squirts) by Malochet-Grivois et al., in the early 1990s, this small family of secondary metabolites was greatly expanded by the discovery of nearly 20 closely related compounds, called the haterumaimides, by the groups of Ueda and Schmitz (see reference with ***). Each of these compounds has been tested against the P388 murine leukaemia cell line, with some reaching subnanomolar potencies (half-maximum inhibitory concentration (IC50) values), but some were completely inactive (Konst et al., 2017).

Chlorolissoclimide (CL) and dichlorolissoclimide were shown by Pelletier and co-workers to be potent inhibitors of eukaryotic translation (Robert et al., 2006). They each interfere with the elongation step of protein synthesis and prevent tRNA from exiting the ribosome, which results in polysomal accumulation and eventual cell death. In this same study, these authors noted the structural homology between CL and the well-studied translation inhibitor cycloheximide (CHX). Clearly, the glutarimide moiety of CHX and the succinimide of the lissoclimides are structurally similar. CHX and the glutarimide lactimidomycin (Schneider-Poetsch et al., 2010; Sugawara et al., 1992; Ju et al., 2005; Micoine et al., 2013) have each been shown to stop the elongation phase of protein synthesis by inhibiting the entrance of the CCA-end of tRNA to the large ribosomal subunit (LSU) E-site, and the structural studies performed in the Yusupov's laboratory are consistent with this understanding (Garreau de Loubresse et al., 2014).

In a recent study (Konst et al., 2017), also based on the X-ray structure determination of CL with the 80S ribosome, we observe that the unusual labdane diterpenoids chlorolissoclimide (CL), which was obtained according to a newly defined semisynthesis and analogue-oriented synthesis approaches, binds to the E-site on the LSU of the 80S ribosome.

Moreover, different compounds obtained via sclareolide-based semisynthesis approache were tested against P388 murine leukaemia cell lines as well as against the aggressive melanoma (A2058), prostate cancer (DU145) cell lines and for eukaryotic translation inhibition

By comparison of IC50 on three different cancer cell lines and from the translation inhibition assay of twelve lissoclimide congeners, the newly derived compound C45 demonstrates to be a potent protein synthesis inhibitor and be able to kill cancer cells (Figure 42).

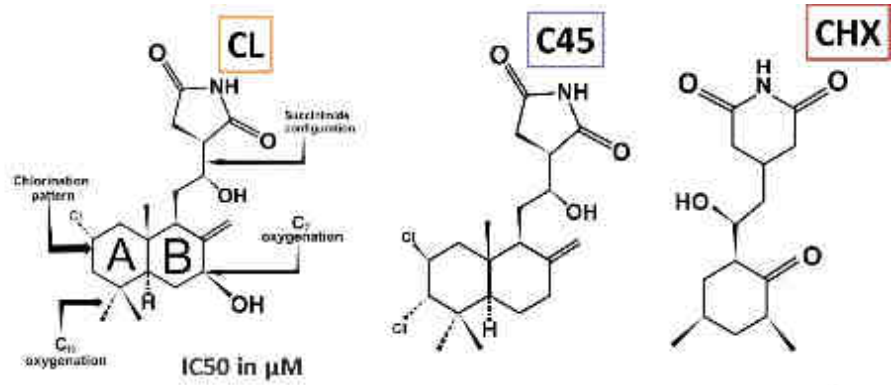

		CL	C45	CHX
cell line	leukemia P388	0.06	0.14	5.6
	melanoma A2058	0.25	0.97	>10
	prostate DU145	0.49	0.37	>10
translation assay		~0.5 µM	~1 µM	~0.5 µM

Figure 42: Cytotoxicity and translation-inhibitory activities of lissoclimide analogues and CHX (adapted from Konst et al., 2017).

According to these results, the CL analogue named C45, which bears C2/C3 diaxial chlorides, is the second most potent compound (Konst et al., 2017). And, since we observed a novel and quite unusual halogen–π interaction in CL within the 25S rRNA, the presence of a second chloride on the newly synthesized C45 was relevant to us in order to understand more the effect of this kind of interaction at the level of drug inhibition. In addition, docking studies predicted the B ring of C45 to adopt a twist-boat conformation, that bears the trans-decalin substructure, in which the pseudoequatorial chlorides are poised for two halogen–π interactions on the facing guanines (G2793/4) (Figure 43A).

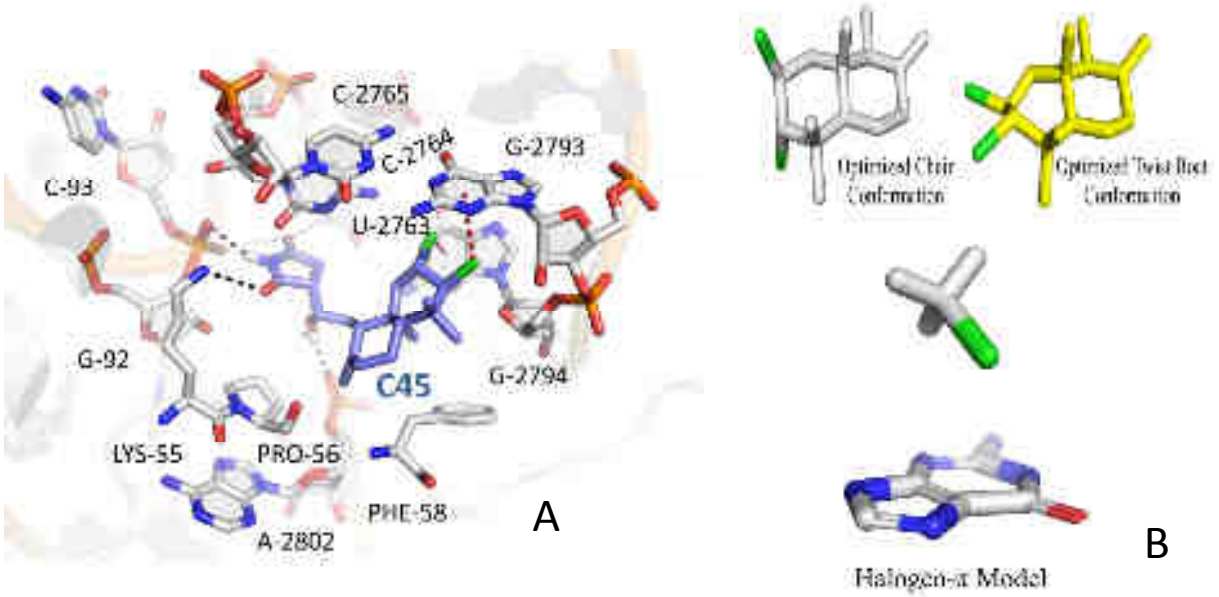

Figure 43: Computational modeling study of C45 compound. A) Docking-based structure of C45 bound to 80S ribosome; B) *Ab initio* calculations on the C2/C3 di-epi-dichloride that bears the trans-decalin substructure showed that energy difference between the chair (axial chlorides) and twist-boat conformation is less than 1.5 kcal mol^{-1}, presumably because of the alleviation of multiple 1,3-diaxial interactions (adapted from Konst et al., 2017). After *ab initio* calculations on the C2/C3 di-epi-dichloride energy showed that twist-boat conformation is much more favored than chair (axial) (Figure 43B).

Taking in account all these results we decided to obtain more detailed information about the principle of action on protein synthesis of the new potential anticancer drug C45. For this purpose, a number of studies and analysis have been carried out such as x-ray crystallography and fluorescence resonance energy transfer (FRET).

2. CRYSTAL STRUCTURE OF THE CHEMOTHERAPEUTIC DRUG CISPLATIN BOUND TO THE 80S RIBOSOME

During the last years, scientific interest has been constantly growing for resolving the problems of resistance and a large number of side effects of already known chemotherapeutic drugs. In this regard, the search is going in the directions of new mechanisms of action and new potential targets for binding known anti-cancer drugs. One of them is called cisplatin. In connection with the recent structural study (Melnikov et al., 2016) of cisplatin binding to the bacterial 70S ribosome, new details of the mechanism of binding of cisplatin with rRNA became available (see chapter potential anticancer drugs against ribosome assembly). However, despite this, there is still open question is whether cisplatin also have specific binding sites on the eukaryotic ribosomes. Knowing the exact location of such binding sites would be very informative in terms of both biology and medicine and, specifically, for anticancer therapy and mechanisms of resistance to cisplatin treatment. This caused us a great deal of interest in focusing our work in this direction.

Moreover, our collaborators from Brigham and Women's Hospital & Harvard Medical School have recently done a screening of FDA-approved chemotherapy drugs, analysing their ability to promote or suppress formation of Stress Granules (SGs), pro-survival RNA granules. They found that cisplatin (and

related platin-based drugs) causes formation of ribosomal aggregates in cisplatin-treated cancer cells. These ribosomal aggregates are distinct from SGs (that also contain 40S ribosomal subunits) in many respects, e.g. they do not contain mRNAs, selected translation initiation factors and they are not dynamic (meaning that they are not in equilibrium with translating polysomes, which are the source of 40S subunits for SG formation under stress). Importantly, these cisplatin-induced ribosomal aggregates contain many proteins that regulate SG formation, and pre-treatment of cancer cells with cisplatin actually blocks SG formation and thus suppresses their pro-survival functions. This could serve as a novel mechanism of cisplatin-induced cytotoxicity, which was traditionally attributed to the ability of cisplatin to promote DNA damage.

IX RESULTS AND METHODS

1. PURIFICATION OF 80S RIBOSOME

Purification and crystallization procedures follow the protocols previously developed (Ben-Shem et al., 2010). The *Saccharomyces cerevisiae* engineered strain JD1370 was provided by
Jonathan Dinman (University of Maryland, USA). It was engineered to avoid contaminations by the L-A virus particles in the ribosome preparation. The L-A virus is a double-stranded RNA virus that infects and replicates in the yeast *S. cerevisiae*; therefore the L-A virus was depleted from this strain. In addition, the JD1370 strain harbors deletions of key proteases and RNAses that are liberated upon cell lysis: PEP4 vacuolar protease and NUC1 mitochondrial nuclease.
Yeast pre-culture is performed in flasks under agitation in standard YPAD media overnight starting from a single fresh colony. Cells are harvested by centrifugation when OD600 reaches 1.0-1.5 and are subjected to glucose starvation treatment (Ashe et al., 2000). Glucose starvation is used to homogenize ribosome population *in vivo* by rapidly and reversibly inducing translation inhibition. After few minutes only, all translating ribosomes in polysomes are converted to inactive 80S monosomes by run-off (Ashe et al., 2000). Practically, the treatment requires to re-suspend the pellet in YPA media (i.e. without glucose) and to incubate the flasks at 30°C, 250rpm for 10 minutes and 30 seconds. The pellet is then recovered by centrifugation and all further steps are performed at 0-4°C. Cells are washed with buffer M (30mM Hepes-K pH 7.5, 50 mM KCl, 10 mM $MgCl_2$, 8.5% mannitol, 2mM DTT, 0.5 mM EDTA). Typically, 5-7 grams of cells are obtained from 4L culture.

After the washing steps, cells are prepared for lysis. The pellet is resuspended in 6.5 ml of buffer M and supplemented with additional 600 µL of protease inhibitor cocktail (PIC, Roche), 100 µL RNasin (Promega), 120 µL Pefablock at initial concentration of 100 mM and 56 µL of Na-heparin at initial concentration of 100 mg/ml. Heparin concentrations were found to have a key role in ribosome solubility, thus affecting the amount of polyethylene glycol (PEG) required at later steps to precipitate the ribosomes. Cells are disrupted with glass beads by vortexing the tube 5 times for 1 minute with 1 min breaks on ice between each run (adapted from Lang et al., 1977). This approach was originally used to isolate yeast mitochondria and introduced here to avoid contamination by mitochondrial ribosome.

All further steps require working in ice. Beads are removed by short centrifugation using the JA-25.50 rotor (13000 rpm - 2 min) and the lysate is further clarified by centrifugation (16000 rpm - 9 min) before being subjected to a differential precipitation by PEG. This step is used to fractionate quickly the lysate in order to recover the ribosome-containing fraction. Thus, PEG 20,000 is added from a 30% w/v stock (Hampton Research) to a final concentration of 4.5% w/v for the first fractionation. The solution is clarified by centrifugation (13000 rpm - 5 min), the supernatant is recovered and the KCl concentration is adjusted to 130 mM final concentration. PEG 20,000 concentration is increased to 8,5% for the second fractionation. Ribosomes are pelleted (12000 rpm - 10min) and the supernatant is discarded. Ribosome pellet is re-suspended (6.5-7 mg/ml) in buffer M2, which is composed of buffer M with KCl concentration adjusted to 150 mM and supplemented with protease inhibitors and heparin. At this stage, typically 30-35 mg of ribosomes are obtained from 4.5 grams of yeast cells. Ribosomes are further purified by a 10-30% sucrose gradient in buffer A (20 mM Hepes-K pH 7.5, 120 mM KCl, 8.3 mM $MgCl_2$, 2 mM DTT, 0.3 mM EDTA) using the SW28 rotor (18000 rpm - 15h).

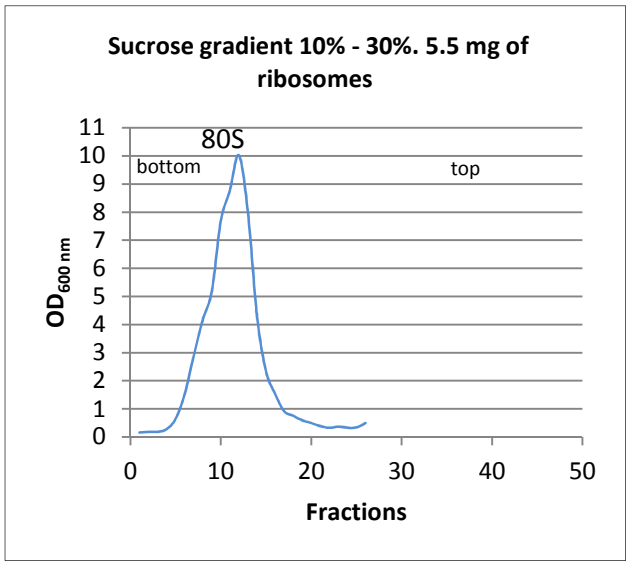

Figure 44: Sucrose gradient profile. Fractions (1 ml) were collected and absorbance was measured by Nanodrop 2000c (Thermo Scientific).

The appropriate fractions are pooled and both KCl and $MgCl_2$ concentrations are adjusted to 150 mM and 10 mM, respectively. In order to precipitate ribosomes, PEG 20,000 is added to a final concentration of 7% w/v. Ribosomes are pelleted by centrifugation (12000 rpm - 10 min). The resulting white pellet is gently suspended in buffer G (10 mM Hepes-K pH 7.5, 50 mM KOAc, 10 mM NH_4Cl, 2 mM. DTT, 5 mM $Mg(OAc)_2$) to a final concentration of 20 mg/mL. The suspension is further clarified by centrifugation at 12500 rpm for 5 minutes at 4°C Typically 14-19 mg of pure ribosomes are obtained from 5 grams of cells.

2. CO-CRYSTALLIZATION

C45 compound was synthesized by the group of Christopher D. Vanderwal (Department of Chemistry, University of California, Irvine, California, USA) and was dissolved in H_2O for initial stock concentration

at 200 µM. Cisplatin was ordered from Sigma and was dissolved in DMF to prepare initial stock solutions (500 µM).

The C45/80S complex was formed in 5.5 mM Tris-acetate at pH 7.0, 27 mM KOAc at pH 7.2, 5.5 mM $NH_4(OAc)$, 2 mM $Mg(OAc)_2$, 1.3 mM DTT by incubation of 80S ribosomes (1.5 µM) with 30 and 45-fold molar excess of C45 (45 and 67.5 µM respectively) for 15 min at 30 °C. Deoxy-Big Chap was subsequently added to a final concentration of 2.8 mM before incubation step. The final solution was cooled down at 4°C prior crystallization. The C45 /80 ribosome complex was crystallized using the hanging drop method at 4^oC by mixing 2-2.4 µL of ribosome solution with 1.6 µL of reservoir solution (100 mM Tris-Acetate pH 7.0, 100 mM KSCN, 3 mM $Mg(OAc)_2$, 20% glycerol, 3.0-5.4% w/v PEG 20,000, 5mM spermidine). Typically, crystals reproducibly appear within 7-10 days and reach their full size after two additional weeks. Mostly crystals were large and thick with size of about 200 x 150 x 70 µm.

The Cisplatin/80S ribosome complex formation was based on the described protocol, except several changes:

- Initially for cisplatin/80S complex formation we tried to use high fold excess of cisplatin as described by Melnikov and co-workers (Melnikov et al., 2016). However, increasing of the excess didn't give expected result, even 50- fold excess induced precipitation of the sample soon after equilibration started. Only at 25- fold excess (37. 5 µM) crystals were sharp and with average size 120 x 100 x 10 µm.

- Detergent. Deoxy-Big Chap was added to a final concentration of 2.8 mM before or after incubation of Cisplatin/80S ribosome complex. In presence of detergent in the incubation, crystal grew normally. Incubation without Deoxy-Big Chap showed thin, but sharp crystals with normal size. Crystals form also changed from usual rectangular parallelepiped (yeast WT crystal form) to hexagonal prism.

3. POST-CRYSTALLIZATION TREATMENT

Crystals of C45/80S complex located in the hanging-drop cover-slip were placed in a small Petri dish and the mother liquor was first replaced by a solution with slightly higher concentration of PEG 6000 (218 mM Tris-acetate pH 7.0, 191 mM KSCN, 109 mM KOAc, 20.5 mM $NH_4(OAc)$, 27.3 mM $Mg(OAc)_2$, 17.8 mM Spermidine, 20% v/v Glycerol, 13,6% PEG 20,000, 1.4 mM Deoxy Big Chap, 2mM DTT, 1% PEG 6000). This solution was then replaced step-wise by solutions with increasing concentrations of PEG 6000 to reach the final concentration of 20% (all the other components maintain the same concentration as described before except for the absence of detergent and DTT). This solution was then replaced with the same solution supplemented with 2 mM osmium hexamine and the drop was kept in the Petri dish sealed with parafilm for1 hour at 4^oC. Each steps of cryo-protection was with incorporation of C45 compound for 30 or 45-fold molar excess depending on the co-crystallization ratio. Treated crystals were further fished into crystallization loop and cryo-cooled on the nitrogen stream at 100K and tested at the synchrotron.

Crystals of cisplatin/80S complex were treated as described before, but with several changes from the initial standard protocol. In the first trial, cisplatin was not introduced into each step of treating. In the

second trial, cisplatin was added to each step of treating using 25-fold (over ribosome concentration) excess. Third way, osmium hexamine was not used for the treatment, although cisplatin was introduced into each step of treating. Also, for checking additional binding sites of cisplatin with the 80S ribosome, we applied several strategies implying soaking of empty 80S ribosome crystals with cisplatin. Cisplatin was introduced in concentration (100µM, 200µM, 250µM, 500µM), at the different steps of post-crystallization treatment (from the beginning, from the third step or at the last step) with osmium hexamine at the last step (2mM and 1mM) or without. All treated crystals were afterwards fished into crystallization loop and cryo-cooled at nitrogen stream at 100K and tested at the synchrotron.

4. X-RAY DATA COLLECTION AND STRUCTURE DETERMINATION

X-ray data collection for the two complexes was performed at Soleil synchrotron, X-ray beamline Proxima 1 equipped with a PILATUS 6M (Dectris Ltd.) detector, headed by Leonard Chavas. The crystal structure of the *S. cerevisiae* 80S ribosome in the complex with a synthetic sample of the inhibitor C45 has been solved at maximal resolution of 3.1 Å (Figure 45).

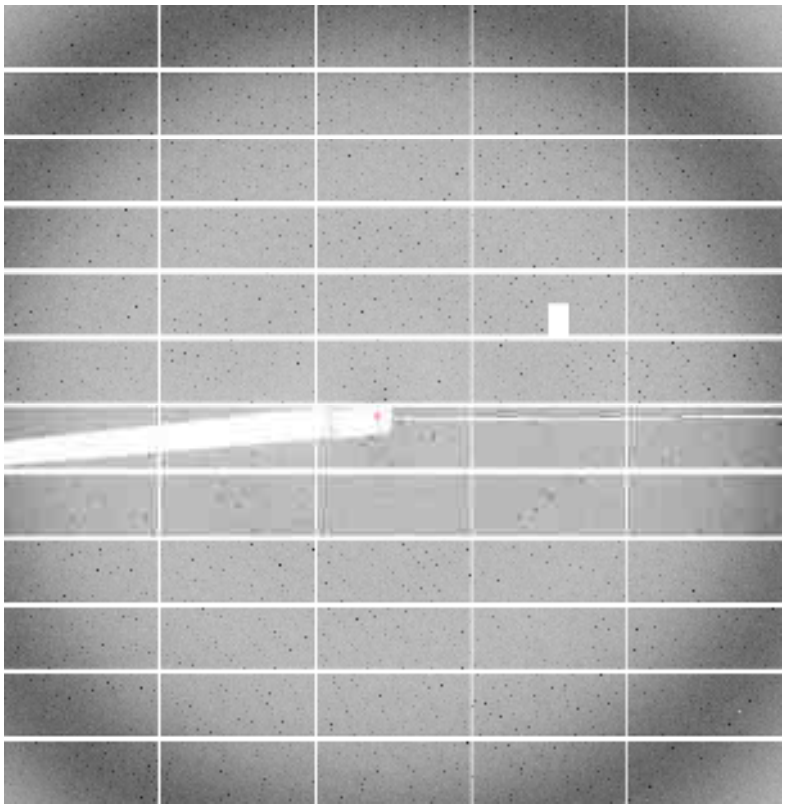

Figure 45: Diffraction patterns of C45/80S complex crystals.

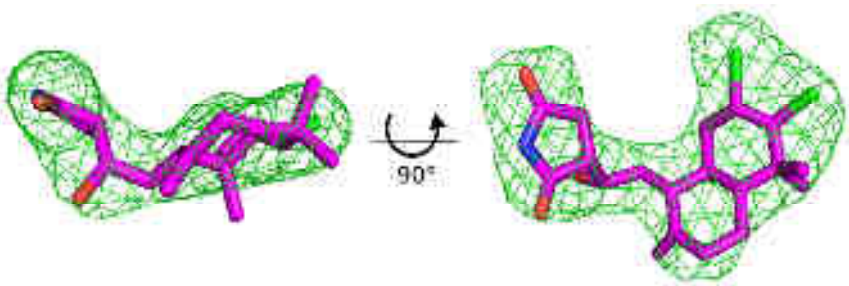

Figure 46: Unbiased difference density helped us to fit C45 unambiguously. $F_{obs} - F_{calc}$ density map obtained after the first run of rigid-body refinement, using the vacant yeast 80S ribosome structure (PDB ID: 4V88) (Ben-Shem et al., 2011) as reference model, is shown in green, contoured at 3σ and represented as two views, 90° apart.

Diffraction data were integrated and scaled using XDS software suite (Kabsch, 2010). Dataset collection statistics are presented in Table 4. The crystal structure was obtained by co-crystallization with a molar ratio C45/80S of 30 times: at this final concentration (45 µM) we did not observe any secondary binding site on the 80S ribosome.

	C45/80S complex
Data collection	
Space group	$P2_1$
Cell dimensions	
a, *b*, *c* (Å)	303.77, 287.95, 435.45
α, β, γ (°)	90.00, 98.96, 90.00
Resolution (Å)	100.00 – 3.10 (3.20 – 3.10) *
R_{meas} (%)	41.8 (277.6)
$I/\sigma I$	7.68 (1.20)
$CC_{1/2}$ (%)	99.2 (50.2)
Completeness (%)	100 (100)
Redundancy	16.43 (15.69)
Refinement	
Resolution (Å)	98.58 – 3.10
No. reflections	1332816
R_{work}/ R_{free} †	0.2193 / 0.2620
No. atoms	
Protein	178255
RNA	222470
Ions/ligands	8982
B-factors	
Protein	61.76
RNA	58.85
Ions/ligands	83.37
R.m.s deviations	
Bond lengths (Å)	0.008
Bond angles (º)	1.185

Number of crystals used: 11
[a] Values in parentheses are for highest-resolution shell.
† Rfree flags (2% of the total number of reflections) were taken from the CL/80S complex dataset (PDB ID: 5TBW)

Table 4: Data collection and refinement statistic of C45/80S complex.

Coordinates and restraints of the ligand were generated by submitting the 3D coordinates previously generated to the GradeWebServer (http://grade.globalphasing.org). Ligand fitting and remodelling of the large subunit E-site binding pocket was performed manually using Coot (Emsley and Cowtan, 2004). Further cycles of coordinates, TLS restraints and individual isotropic B-factor refinement were performed using phenix.refine. Structure validation was performed using Molprobity. Figures of the structure were prepared using PyMOL 1.4 (Schrödinger, http://pymol.org/).

In case of cisplatin/80S ribosome complex, we collected data at 3.3 Å from the crystals grown in presence of cisplatin at 25 - fold excess and incubation with detergent. However, cisplatin was not detected in the structure. We tried to locate the cisplatin moieties based on the superposition of the bacterial structure (*T. thermophilus* 70S) obtained in presence of cisplatin (Figure 21, 22), by soaking and also co-crystallization. In the case of incubation without detergent crystals did not grow as usual, meaning that cisplatin has some negative impact in crystallogenesis, confirmed also by poor diffraction quality patterns (around 6-7 Å). According, different soaking strategies enabled us to collect few data sets at around 4-4.5 Å. However, we encountered the problem that the yield of medium resolution crystals is very low (5% maximum).

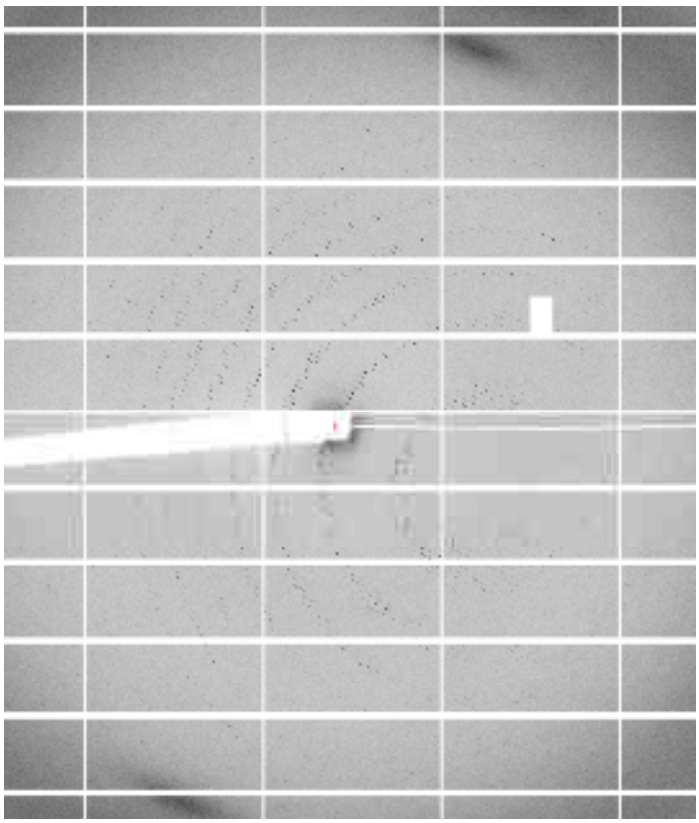

Figure 47: Diffraction patterns of ciplatin/80S complex crystals.

We also tried to collect anomalous data at the Pt edge but since in our condition we have osmium hexamine (which contributes a lot at the energy range tested), it is very difficult to extract the clean anomalous signal for Pt. We performed an X-ray fluorescence scan on the co-crystallized crystals with cisplatin and we didn't observe any Pt peak, probably because the concentration of cisplatin is too low. Soaked crystal with 500µM of cisplatin showed a peak of Pt in the crystal and in mother liquid, but this is not sufficient to tell us if the Pt is structured or not.

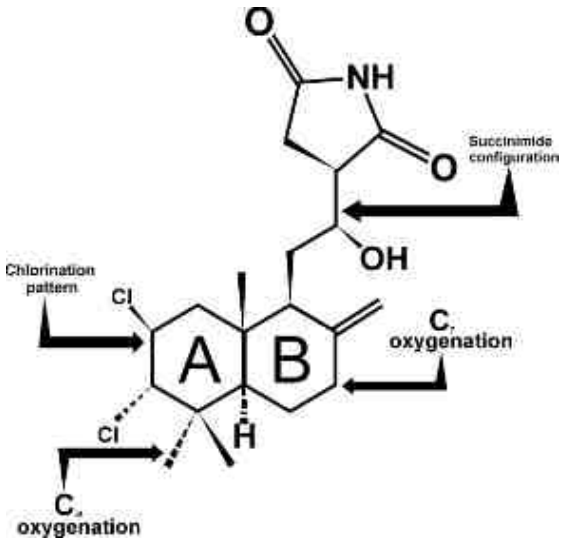

Figure 48: Chemical structure of C45 compound

C45 binding site is located at the E-site tRNA CCA-end on the LSU, as previously shown for the chlorolossoclimide (CL) and the glutarimide inhibitors cycloheximide (CHX) and lactimidomycin (LTM) (Figure 49).

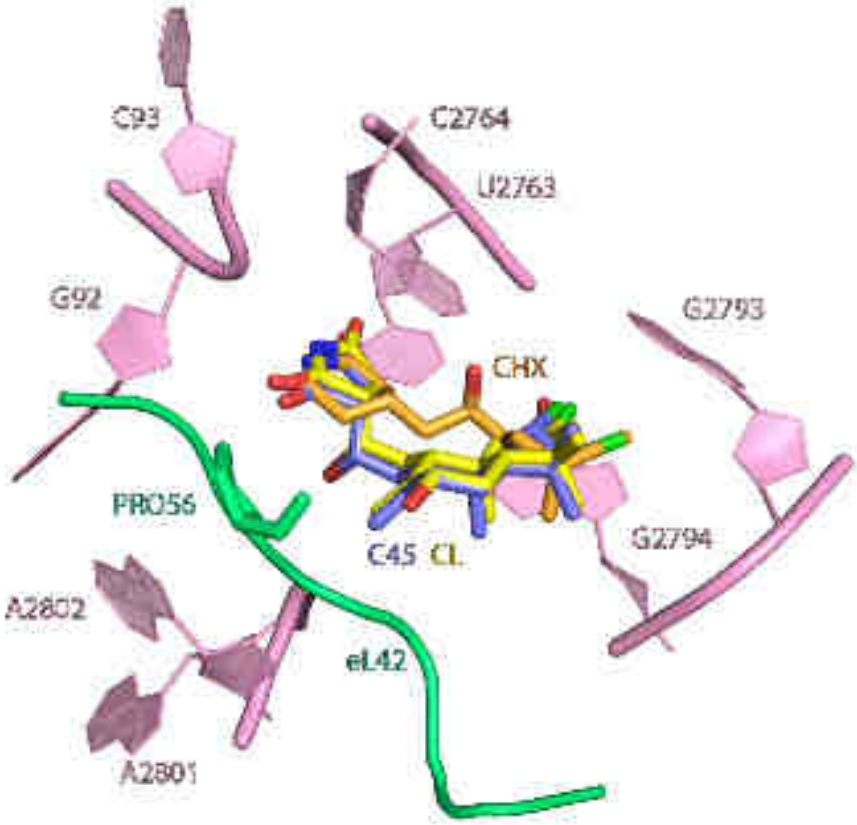

Figure 49: C45, chlorolissoclimide and cycloheximide share the same binding pocket in the 60S E-site.

Comparison of the C45 binding with that of CHX and CL shows a similar network of interactions of the imide-containing moiety with a number of universally conserved nucleotides of the 25S rRNA, namely G92, C93 and U2763 (Figure 49). Moreover, the hydroxyl group on the linker between the decalin and the succinimide moieties in the C45 and CL interacts with the phosphate–oxygen backbone of nucleotide A2802 of the 25S rRNA through another hydrogen bond, to complete a tetrad of hydrogen bonds that appears to 'anchor' CL and C45 into the binding site (Figure 50). Due to the absence of C7-hydroxyl group on the B ring in C45 we didn't observe a hydrogen bond with the peptide backbone of Pro56 on a stretched loop of the eukaryotic-specific ribosomal protein eL42, and thus distinguished from the CL. However, this behaviour is similar with most other known inhibitors, which exclusively bind rRNA (Garreau de Loubresse et al., 2014).

Interestingly, the two chlorine atoms positioned on the decalin ring of C45 interact with G2794 and G2793 of the 25S rRNA. In case of CL, the decalin ring system bears only one chloride, which binds to the G2794 of the 25S rRNA (Figure 50).

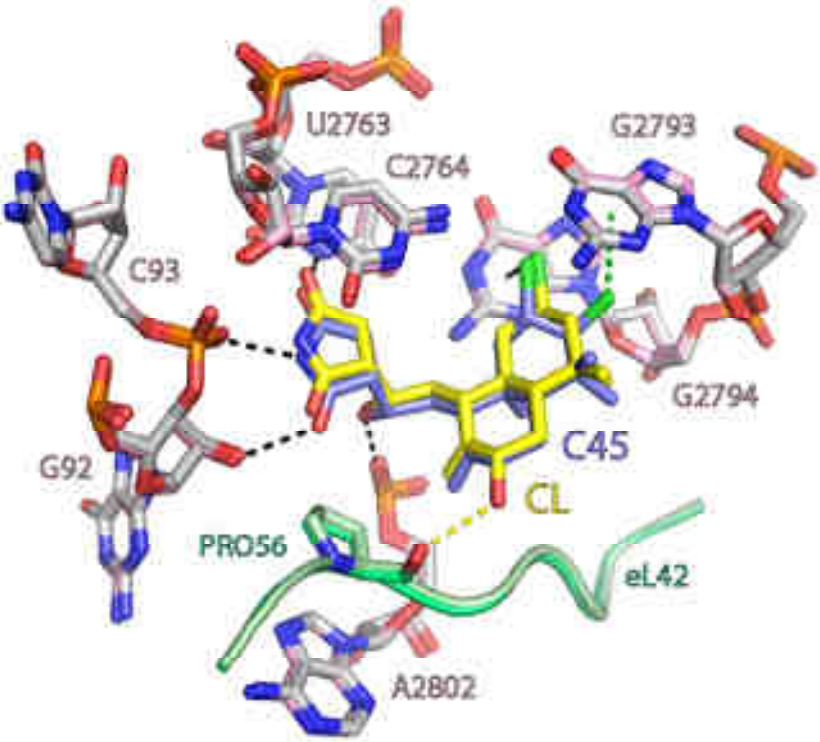

Figure 50: Comparison of binding sites between C45 and CL

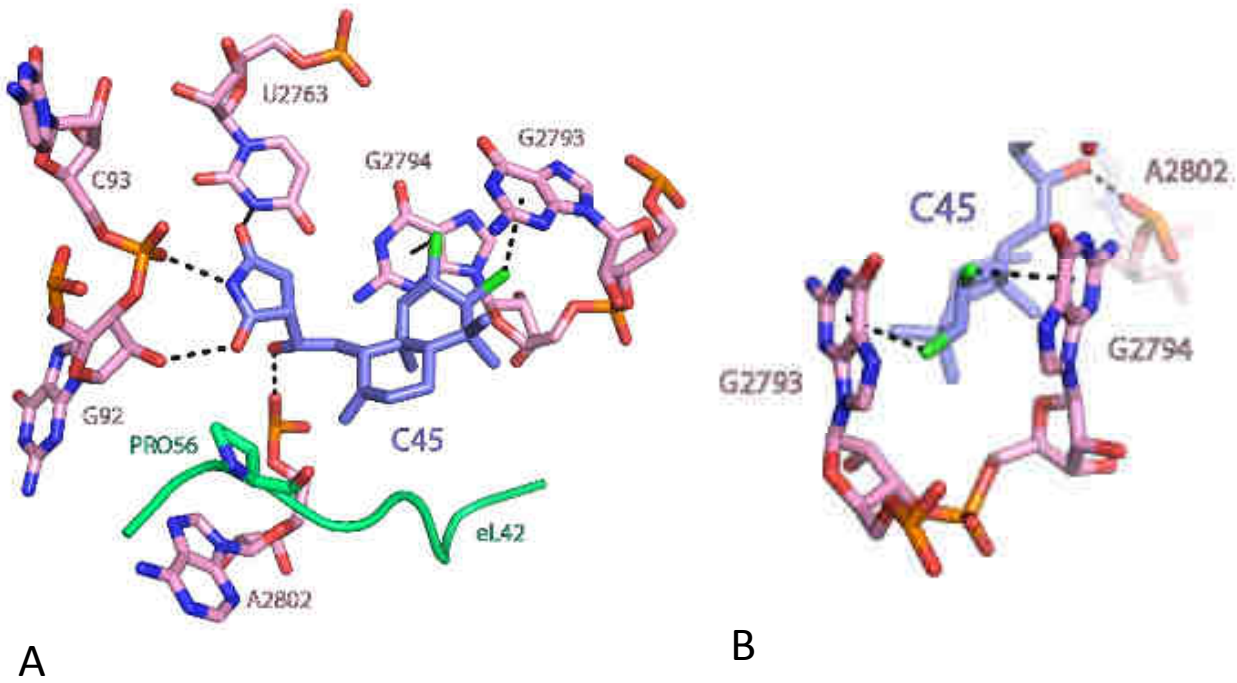

Figure 51: The X-ray crystal structure of C45 compound with the eukaryotic 80S ribosome reveals the molecular basis of translation inhibition. A) Details of the interactions that occur between the C45 molecule (blue, represented as sticks) and the neighbouring residues. Direct contacts take place with nucleotides G92, C93, U2763, A2802, G2794 and G2793 of the 25S rRNA. B) Zoom in of the binding pocket of C45, with the diaxial dichloride in the decalin ring system create twist-boat conformation in which pseudoequatorial chlorides are poised for two face-on geometry halogen–π interactions with guanines G2793 and G2794 of the 25S rRNA.

The chlorine atoms are positioned 3.2 Å away from the center of the six-membered ring of the purine heterocycle (Figure 51B), and they appear to form two halogen–π interactions with the guanine residues with a face-on geometry. Thus, the crystal structure we obtained confirms the prediction made by the previously conducted computational study with respect to the B-ring of C45 (Figure 43)

The examples of face-on halogen–π attractive forces have been documented in protein–ligand interactions with the aromatic side chains of Phe, Tyr, Trp and His29, to the best of our knowledge they have not been reported between halogens and nucleotide bases (according to a search of the Relibase database v3.2.1, Cambridge Crystallographic Data Centre) (Konst et al., 2017).

XI FLUORESCENCE RESONANCE ENERGY TRANSFER

This part of the project has been done by our collaborators: Mikael Holm and Scott Blanchard from Department of Physiology and Biophysics, Weill Cornell Medical College, USA.

Single molecule fluorescence imaging methods are used to quantify the nature and timing of structural processes in human ribosomes during single-turnover and processive translation reactions. These measurements reveal that functional complexes exhibit dynamic behaviors and thermodynamic stabilities distinct from those observed for bacterial systems. Structurally defined sub-states of pre-translocation complex have been shown to be sensitive to specific inhibitors of the eukaryotic ribosome, demonstrating the utility of this platform to probe drug mechanism. The application of three-color single-molecule fluorescence resonance energy transfer (smFRET) methods further reveal a long-distance allosteric coupling between distal tRNA binding sites within ribosomes bearing tRNAs, which contribute to the rate of processive translation (Ferguson et al., 2015).

The experiment that was carried out was to form a human ribosomal pre-translocation complex and observe its dynamics at equilibrium in the presence of varying concentration of the drugs C45, CHX and CL.

Subsequent to aa-tRNA accommodation at the A site, the PRE complex, imaged under steady-state conditions, exhibited predominantly non-classical (lower) FRET states, suggesting that the energy of aa-tRNA binding and/or peptide bond formation efficiently drives restructuring of the ribosome such that classical tRNA positions become disfavored (Marshall et al., 2008). Individual FRET traces revealed that the PRE complex spontaneously transits between low (~0.19), intermediate- (~0.37), and high- (0.69) FRET states. These observations suggested that tRNAs within the A and P sites of the human ribosome undergo largescale (ca. 15–25 Å) rearrangements in relative and absolute positions as a function of time. In the bacterial ribosome, such transitions reflect global remodeling events at the interface of the small and large subunits that are directly implicated in ribosome function. These movements also include a 6–9° subunit rotation that directs both coupled and independent movements of A and P-site tRNAs between classical (A/A and P/P) and hybrid (A/A and P/E; A/P and P/E) positions (Cornish et al., 2008; Dunkle et al., 2011; Feldman et al., 2010; Frank and Agrawal, 2000; Moazed and Noller, 1989; Munro et al., 2007, 2009; Wang et al., 2011).

Our main idea was to measure the effect of the drugs on translating human ribosome *in vitro*, to determine the Kd of binding of C45, CL and CHX at a single molecule level. For this purpose, the ribosomes carry **Cy3-tRNA^{Met}** in the P site and **Met-Phe-cy5-tRNA^{Phe}** in the A site.

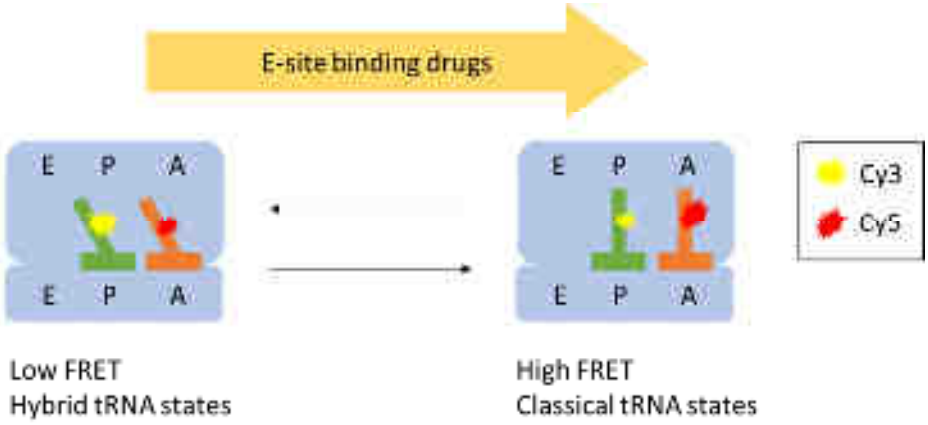

Figure 52: Schematic representation of pre-translocation complex.

We observe the fluorescence intensity of the two dyes when cy3 is excited at 532 nm, from the raw intensity values the FRET efficiency is calculated. When the two tRNAs occupy the classical binding sites FRET efficiency is high and when they occupy the hybrid binding sites FRET efficiency is low. One effect of the three drugs is that drug-bound ribosomes preferentially occupy the classical state while drug-free ribosomes preferentially occupy the hybrid state (Figure 52).

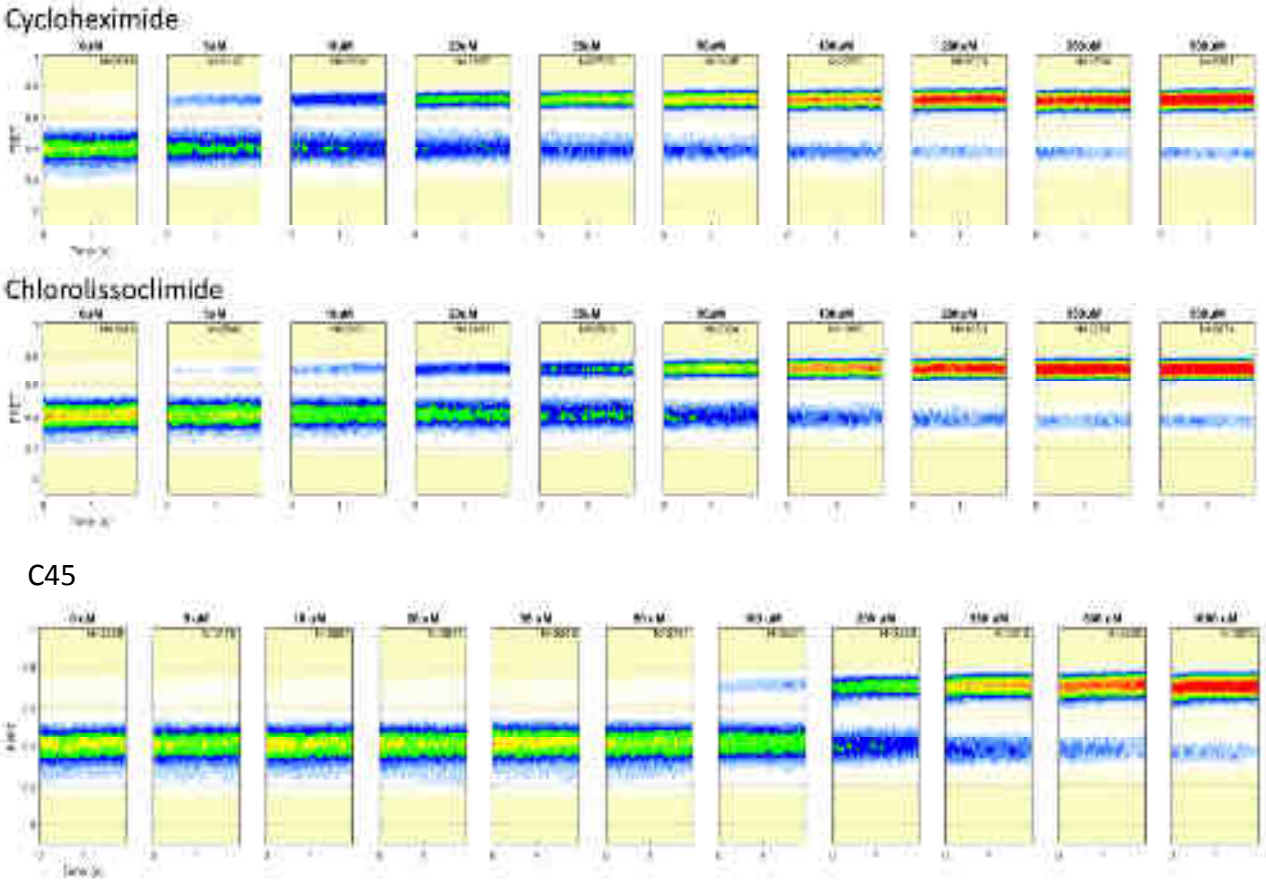

Figure 53: Ligand-Induced changes of the Human 80S Pre-translocation Complex visualized by FRET.

According to Figure 53, the histograms present the distribution of FRET efficiencies over the time after equilibration at the indicated drug concentration. Two distinct populations are observed, one 'high FRET', indicative of ribosomes where the two tRNA molecules occupy their classical binding state, and one 'low FRET', indicative of ribosomes where the two tRNA molecules occupy the hybrid binding state. It can be seen that for CL and CHXthe population of 'high FRET' ribosomes, corresponding to the classical tRNA state, increases with increasing drug. In case of C45 drug, the effect is not as pronounced since the high FRET state is equilibrating very slowly with the ribosome (on a timescale of tens of minutes at the lower concentrations).

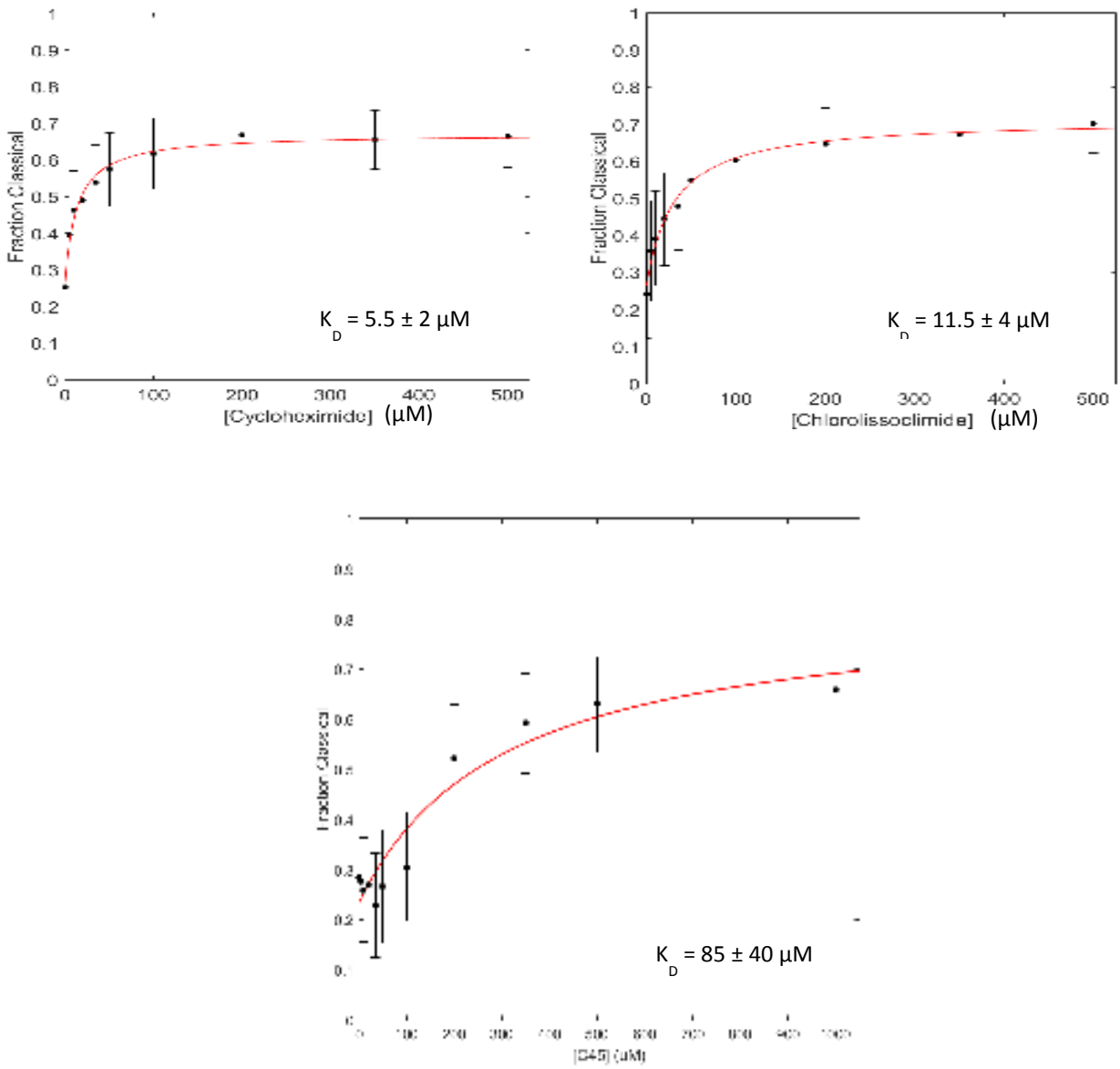

Figure 54: Quantification of the data for CHX, CL and C45. The error bars represent standard error of the mean (SEM).

Three graphics in Figure 54 show how the fraction of time that the tRNAs spend in the classical state changes with increasing drug concentration. In this way we can estimate apparent dissociation constants for CHX and CL and for C45. In the case of C45 measurements it is not certain that these values represent true equilibrium distributions, especially for the lower concentrations. We can see

from the graphic that the binding affinity for C45 appears to be lower than for CHX and CL. The poor fit of this curve compared to the others is likely due to an issue of very slow equilibration which causes the accuracy of the data to correlate with the concentration of the drug.

Moreover, we observed that ribosome is still dynamic even at saturating drug concentration in all cases. This is somewhat unexpected based on structural evidence and suggests that the P-site tRNA body can enter the E site even if the CCA-end of the tRNA is prevented from doing so by the presence of the drug.

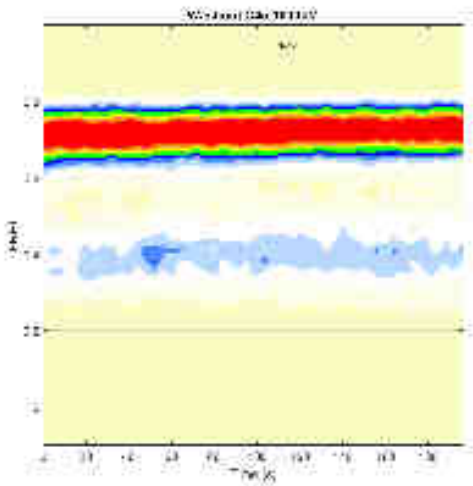

Figure 55: Population histogram of a washout experiment with C45.

After equilibration (1000µM) with the 80S ribosome, C45 has been washed away with imaging buffer (Figure 55). We observed that C45 had a long residence time on the ribosome and even after several minutes no dissociation is apparent, i.e. no ribosomes have returned to the FRET distribution observed in the absence of drug.

DISCUSSION AND PERSPECTIVES

Due to the lack of information on a new synthesized analog of lyssoclimide C45, any studies that have been or will be conducted in the CL direction could help us to formulate our knowledge about the principles of the action of a potential anti-cancer drug C45.

In summary, the high-resolution crystal structure of newly synthesized C45 compound reveals that this inhibitor binds the E-site of the large subunit using the same network of interactions as CL. C45 fully occupies and occludes the tRNA binding pocket. The fascinating binding mode includes two novel face-on chlorine–π interactions of the ligand with guanine residues (G2794 and G2793). To estimate the importance of this type of interaction, energy benefit was calculated for the interaction of the chlorine with both G2794 and G2793 and it is equal to 1.8 kcal mol^{-1} (Konst et al., 2017). This favorable dispersion-based interaction appears to afford stabilization to this arrangement of CL and C45 in the E-site of the ribosome, and related effects might be leveraged in the design of other nucleic acid ligands.

Another structural difference of C45 compound with CL is the absence of C7-hydroxyl group on the B ring which formed, in CL cause, a hydrogen bond with Pro56 on a stretched loop of the eukaryotic-specific ribosomal protein eL42. This difference relates C45 with most other known inhibitors which exclusively bind rRNA (Garreau de Loubresse et al., 2014).

According to FRET analysis, we observed that ribosome is still dynamic even at saturating drug concentration. On the basis of this, two mechanistic models can be proposed. First possibility is that CHX, C45 and CL blocks the tRNA in hybrid-like conformation, meaning that tRNA CCA-end is trapped in the vicinity of E-site on the LSU while the tRNA anticodon stem-loop stays in P-site on the small subunit. The second possibility is that CHX, C45 and CL alters tRNA dynamics on the ribosome and displaces the equilibrium in favor of classical states. This was done by measuring FRET signals between fluorescently-labeled tRNA, with which we can follow tRNA conformation on the ribosome.

Moreover, thanks to the FRET measurements we were able to determine Kd of binding for the newly synthesized inhibitor C45, CL and for CHX at a single molecule level. We can conclude that the dissociation constants for CHX and CL are similar, about two fold different (see before), thus showing similar binding affinities. C45 showed lower binding affinity compared with CL. Two possible reasons can explain this behavior: first, it could be due to the issue of very slow equilibration which causes the accuracy of the data to correlate with the concentration of the drug. The second is that C45 demonstrate lower eukaryotic translation inhibition activity, according to translation assay data as shown by Konst and coworkers in 2017, in comparison with CL.

Also we observed that C45 had a long residence time on the ribosome, after washing out the drug, where, even after several minutes, no dissociation was occuring. The ribosomes, once bound to C45, are unable to return to the FRET state observed in the absence of drug. According to this result, we can conclude that the potential anti-cancer drug C45 could show its effectiveness due to the long-term retention of the binding with the ribosome and its presence after washing out experiments is the confirmation of this hypothesis.

In accordance with comparison of cytotoxicity test of CL with homoharringtonine (the US Food and Drug Administration (FDA) approved the first translation inhibitor) and CHX, Konst and coworkers

concluded that CL is as cytotoxic as homoharringtonine in the three cell lines examined, and also the translation-inhibitory activity is comparable. However, CHX was significantly less cytotoxic than many observed synthetic lissoclimides, but its translation-inhibitory activity was equivalent to those of CL and homoharringtonine.

In the close future our laboratory plans to analyze other inhibitors, which could be congeners of CL or new molecules on which our collaborators are working on. These studies help us in order to understand how to improve potency of this scaffold molecule.

Concerning the cisplatin/80S complex project we found the optimal ratio of cisplatin (37.5 µM) for co-crystalization process with eukaryotic ribosome. These allowed us to obtain good shape and size of crystals to perform further diffraction experiments. In addition, we determined the influence of the detergent (Deoxy-Big Chap) on the cisplatin complex formation with the ribosome. Most probably in this case, incubation of complex together with detergent, before crystallization process, reduced binding affinity of cisplatin to 80S ribosome. Also we observed that cisplatin itself influenced on the crystal growth and changed crystal form from usual rectangular parallelepiped to hexagonal prism.

We were able to improve of the crystals diffraction till 4 Å. This data we obtained only in crystals which were soaked in presence of cisplatin (250 µM). However the yield of medium resolution was very low only 5% and this makes it difficult for us to build the structure. In case of co-crystallization ribosome with cisplatin we were got no more than 6-7 Å resolution.

So, the project would require a lot of optimization procedures and also, most probably, the avoidance of osmium hexamine in the crystals, to be able to use the anomalous signal coming from the few Pt atoms that should tightly bind to the ribosome. However, so far, the treatment of the *S.cerevisiae 80S* ribosome crystals without osmium hexamine gave only poor diffraction.

In spite of the fact that osmium hexamine and platinum have the same binding sites in the 80S ribosome of *S.cerevisiae* and belongs to the group of heavy metals, the replacement of osmium hexamine in cryo-protection procedure by platinum leads to a reducing of the crystals diffraction.

The attempt to exclude osmium from standard cryo-protection conditions was failed, and therefore one can conclude that it is necessary to change the concept of cryo-protection process of 80S ribosome crystals as a whole. In its turn, our laboratory is on the way of developing this in a more robust way.

INVISIBLE CONNECTION BETWEEN PROJECTS

Often, different directions in science for the target audience can be closely intertwined. On the example of my two completely different studies, one can trace a very close relationship for the end user, namely, cancer patients and patients with MRSA. Patients with cancer tumors are at unusually high risk for developing bloodstream infections, which are a major cause of in-hospital morbidity and mortality. According to statistics numbers 20% of them suffer from both illnesses simultaneously and this figure is growing steadily each year. In this case, the attending doctor has to make an uneasy choice in favor of treating one of the diseases, due to high toxicity and a wide range of side effects of both types (antibacterial and anticancer drugs) of medicinal substances.

In most cases, the attending physicians had to select treatment of infection (*S.aureus*) at first, due to the fact that the infection could lead to mortality in the immunocompromised patients much faster than the cancerous tumor itself. As well known, success in the cancer treatment very often depends on the timeliness of the treatment started and this delay associated with the inability to treat both diseases could lead to serious consequences and possible mortality of the patients. All this leads us to one of the main problems of modern medicines, to a large numbers of strong side effects of medicines. My research was aimed at helping to solve this problem.

In the science, a lot of researches have been done that proves the connection of a cancerous tumor with infectious diseases. For instance, more than 15% of malignancies worldwide are established to have an infectious cause (Pisani et al., 1997). The main mechanisms by which infections can cause cancer are (a) transformation of cells by insertion of oncogenes and/or inhibition of tumor suppressors (e.g., oncogenic HPV types, cervical cancer (Scheffner et al., 1992); (b) carcinogenesis induced by immunosuppression (e.g., in HIV-related cancers (Beral and Newton, 1998), and (c) infection induced chronic inflammation can produce nitric oxide and cytokines, which contribute to carcinogenesis (Ohshima and Bartsch, 1994; Aggarwal et al., 2006) (e.g., Helicobacter pylori (IARC Monographs, 1994) causes a chronic inflammation in the gastric mucosa, which is likely to be responsible for the development of cancer (Parsonnet, 1995).

Therefore in my opinion, it is not worth to separate the research aimed at the treatment of cancer and infectious diseases. All these once again show that different areas of scientific activity should closely cooperate among themselves to solve the global problems of mankind.

GENERAL CONCLUSION

Structure determination of *Staphylococcus aureus* 70S ribosome project showed certain amount of results. The growth of S. aureus cells and their harvesting were adapted for purification of ribosomes for structural studies. After variety of modifications of ribosome purification, the optimal protocol was obtained, which allowed us (1) to get rid of unwanted non- ribosome proteins, (2) to reduce the amount of contaminating tRNA, and (3) to improve the shape and the size of crystals. Also amount of obtained ribosomes was sufficient for broad search conditions of crystallization.

Different crystals in different conditions were obtained from the S. aureus 70S ribosomes, complexes with $tRNA^{fMet}$/70S ribosome/mRNA and 70S/N-terminal domain of HPF. Crystals were reproducible and reached appropriate size to perform diffraction experiments. The conditions of dehydration and cryo-cooling were optimized for obtained crystals. The diffraction data of *S. aureus* 70S ribosome and its complexes crystals were collected. However, the resolution obtained was too low (~17-19 Å) for high-resolution structure determination.

In case of small-molecular inhibitor project, thanks to knowledge which came from combination of semisynthesis and analogue-oriented synthesis, supported by docking studies we had opportunity to expand our understanding of structural-activity relationship in the lissoclimide family of translation inhibition cytostatic agents. We uncovered the structural basis for inhibition of protein syntesis with co-crystallographic study of synthetic C45 bound to the ribosome. The interesting binding mode includes a two novel face-on chlorine-π interaction of the ligand with two guanine residues. This favorable dispersion-based interaction appears to afford a stabilization of C45 compound in the E-site of the ribosome, and thus related effects might be leveraged in the design of other nucleic acid ligands. Also, according FRET analysis in the human ribosome pre-translocation complex we observe that C45 equilibrates very slowly with the ribosome on a timescale of tens of minutes, however, it has a very long residence time once bound. In addition we calculated dissociation constant for C45 and it is in average 50 – 150 µM. In comparison, CHX and CL approximately 5.5 µM and 11.5 µM respectively, therefore showing similar binding affinities. The C45 is a weaker binder than CL, which is well correlated with the published data (Konst et al., 2017).

Crystallographic studies of cisplatin drug with 80S ribosome showed a certain degree of success. We found optimal ratio of cisplatin for co-crystalization process with eukaryotic ribosome. Also we determined the influence of the detergent (Deoxy-Big Chap) on the cisplatin complex formation with the ribosome and on the crystals growth. And we improved crystal diffraction till 4 Å.
However we encountered several problems with it. First is the yield of medium resolution is very low (5% maximum), thus we have a difficulties to get a structure of this complex. Second, are overlapping platinum binding sites with an osmium hexamine binding sites in the 80S ribosome. This forced us not to use osmium hexamine for the usual cryo-protection of the crystals with Pt. But, so far *S.cerevisiae* 80S ribosome crystals treatment without osmium hexamine gave only poor diffraction.

LIST OF PUBLICATIONS AND COMMUNICATIONS

List of publications

Article in preparation: "Analysis of halogen-π interactions in inhibitors binding to the eukaryotic ribosome" Daniya Kashinskaya[1], Simone Pellegrino[1], Melanie Meyer[1], Zef A. Könst[2], Sharon E. Michalak[2], Mikael Holm[3], Scott Blanchard[3], Vamsee K. Voora[4] , Gulnara Yusupova[1], Marat Yusupov[1] et Christopher D. Vanderwal[2]. (1)Institut de Génétique et de Biologie Moléculaire et Cellulaire (IGBMC), INSERM U964, CNRS UMR7104, Université de Strasbourg, 67404 Illkirch, France. (2)Department of Chemistry, University of California, 1102 Natural Sciences II,Irvine, California 92697-2025, USA. (3) Department of Physiology and Biophysics, Weill Cornell Medical College, New York 10065, USA. (4) Irvine Department of Chemistry, University of California, 1102 Natural Sciences II Irvine, CA 92697-2025, USA.

List of communications: talk - poster

Poster: "Structure analysis of potential anticancer drugs" Daniya Kashinskaya[1], Simone Pellegrino[1], Melanie Meyer[1], Zef A. Könst[2], Sharon E. Michalak[2], Mikael Holm[3], Scott Blanchard[3], Vamsee K. Voora[4] , Gulnara Yusupova[1], Marat Yusupov[1] et Christopher D. Vanderwal[2]. (1)Institut de Génétique et de Biologie Moléculaire et Cellulaire (IGBMC), INSERM U964, CNRS UMR7104, Université de Strasbourg, 67404 Illkirch, France. (2) Department of Chemistry, University of California, 1102 Natural Sciences II,Irvine, California 92697-2025, USA. (3) Department of Physiology and Biophysics, Weill Cornell Medical College, New York 10065, USA. (4) Irvine Department of Chemistry, University of California, 1102 Natural Sciences II Irvine, CA 92697-2025, USA.

EMBO Conference: "Protein Synthesis and Translational Control".

6-7 September 2017/EMBL Advanced Training Centre/ Heidelberg/Germany.

REFERENCES

Aas T, Borresen AL, Geisler S, Smith-Sorensen B, Johnsen H, Varhaug JE, et al. Specific P53 mutations are associated with de novo resistance to doxorubicin in breast cancer patients. Nature medicine. 1996;2(7):811-4. PubMed PMID: 8673929.

Abraham EP, Adler E. The specificity of diaphorase (coenzyme factor). The Biochemical journal. 1940;34(1):119-27. PubMed PMID: 16747129; PubMed Central PMCID: PMC1265256.

Abraham EP, Chain E. An enzyme from bacteria able to destroy penicillin. Nature. 1940; 146:837.

Adrian M, Dubochet J, Lepault J, McDowall AW. Cryo-electron microscopy of viruses. Nature. 1984;308(5954):32-6. PubMed PMID: 6322001.

Aggarwal BB, Shishodia S, Sandur SK, Pandey MK, Sethi G. Inflammation and cancer: how hot is the link? Biochemical pharmacology. 2006;72(11):1605-21. doi: 10.1016/j.bcp.2006.06.029. PubMed PMID: 16889756.

Aggarwal BB, Shishodia S, Sandur SK, Pandey MK, Sethi G. Inflammation and cancer: how hot is the link? Biochemical pharmacology. 2006;72(11):1605-21. doi: 10.1016/j.bcp.2006.06.029. PubMed PMID: 16889756.

**Agirrezabala, X., Lei, J., Brunelle, J.L., Ortiz-Meoz, R.F., Green, R., and Frank, J. (2008). Visualization of the Hybrid State of tRNA Binding Promoted by Spontaneous Ratcheting of the Ribosome. Mol. Cell 32, 190–197.

**Agirrezabala, X., Liao, H.Y., Schreiner, E., Fu, J., Ortiz-Meoz, R.F., Schulten, K., Green, R., and Frank, J. (2012). Structural characterization of mRNA-tRNA translocation intermediates. Proc. Natl. Acad. Sci. 109, 6094–6099.

Agrawal RK, Sharma MR. Structural aspects of mitochondrial translational apparatus. Current opinion in structural biology. 2012;22(6):797-803. doi: 10.1016/j.sbi.2012.08.003. PubMed PMID: 22959417; PubMed Central PMCID: PMC3513651.

Aitken CE, Lorsch JR. A mechanistic overview of translation initiation in eukaryotes. Nature structural & molecular biology. 2012;19(6):568-76. doi: 10.1038/nsmb.2303. PubMed PMID: 22664984.

Alkalaeva EZ, Pisarev AV, Frolova LY, Kisselev LL, Pestova TV. In vitro reconstitution of eukaryotic translation reveals cooperativity between release factors eRF1 and eRF3. Cell. 2006;125(6):1125-36. doi: 10.1016/j.cell.2006.04.035. PubMed PMID: 16777602.

**Amunts A, Brown A, Bai XC, Llacer JL, Hussain T, Emsley P, et al. Structure of the yeast mitochondrial large ribosomal subunit. Science. 2014;343(6178):1485-9. doi: 10.1126/science.1249410. PubMed PMID: 24675956; PubMed Central PMCID: PMC4046073.

**Amunts A, Brown A, Toots J, Scheres SHW, Ramakrishnan V. Ribosome. The structure of the human mitochondrial ribosome. Science. 2015;348(6230):95-8. doi: 10.1126/science.aaa1193. PubMed PMID: 25838379; PubMed Central PMCID: PMC4501431.

Anger AM, Armache JP, Berninghausen O, Habeck M, Subklewe M, Wilson DN, et al. Structures of the human and Drosophila 80S ribosome. Nature. 2013;497(7447):80-5. doi: 10.1038/nature12104. PubMed PMID: 23636399.

Apperley JF. Part I: mechanisms of resistance to imatinib in chronic myeloid leukaemia. The Lancet Oncology. 2007;8(11):1018-29. doi: 10.1016/S1470-2045(07)70342-X. PubMed PMID: 17976612.

Arber N, Doki Y, Han EK, Sgambato A, Zhou P, Kim NH, et al. Antisense to cyclin D1 inhibits the growth and tumorigenicity of human colon cancer cells. Cancer research. 1997;57(8):1569-74. PubMed PMID: 9108461.

Arias CA, Panesso D, McGrath DM, Qin X, Mojica MF, Miller C, et al. Genetic basis for in vivo daptomycin resistance in enterococci. The New England journal of medicine. 2011;365(10):892-900. doi: 10.1056/NEJMoa1011138. PubMed PMID: 21899450; PubMed Central PMCID: PMC3205971.

Ashe MP, De Long SK, Sachs AB. Glucose depletion rapidly inhibits translation initiation in yeast. Molecular biology of the cell. 2000;11(3):833-48. PubMed PMID: 10712503; PubMed Central PMCID: PMC14814.

Balak MN, Gong Y, Riely GJ, Somwar R, Li AR, Zakowski MF, et al. Novel D761Y and common secondary T790M mutations in epidermal growth factor receptor-mutant lung adenocarcinomas with acquired resistance to kinase inhibitors. Clinical cancer research : an official journal of the American Association for Cancer Research. 2006;12(21):6494-501. doi: 10.1158/1078-0432.CCR-06-1570. PubMed PMID: 17085664.

Ban N, Nissen P, Hansen J, Moore PB, Steitz TA. The complete atomic structure of the large ribosomal subunit at 2.4 A resolution. Science. 2000;289(5481):905-20. PubMed PMID: 10937989.

Bardenheuer W, Lehmberg K, Rattmann I, Brueckner A, Schneider A, Sorg UR, et al. Resistance to cytarabine and gemcitabine and in vitro selection of transduced cells after retroviral expression of cytidine deaminase in human hematopoietic progenitor cells. Leukemia. 2005;19(12):2281-8. doi: 10.1038/sj.leu.2403977. PubMed PMID: 16304576.

Barlow JJ, Mathias AP, Williamson R, Gammack DB. A Simple Method for the Quantitative Isolation of Undegraded High Molecular Weight Ribonucleic Acid. Biochemical and biophysical research communications. 1963;13:61-6. PubMed PMID: 14069514.

Bartesaghi A, Merk A, Banerjee S, Matthies D, Wu X, Milne JL, et al. 2.2 A resolution cryo-EM structure of beta-galactosidase in complex with a cell-permeant inhibitor. Science. 2015;348(6239):1147-51. doi: 10.1126/science.aab1576. PubMed PMID: 25953817.

Batista PJ. The RNA Modification N6-methyladenosine and Its Implications in Human Disease. Genomics, proteomics & bioinformatics. 2017;15(3):154-63. doi: 10.1016/j.gpb.2017.03.002. PubMed PMID: 28533023; PubMed Central PMCID: PMC5487527.

Bayer AS, Schneider T, Sahl HG. Mechanisms of daptomycin resistance in Staphylococcus aureus: role of the cell membrane and cell wall. Annals of the New York Academy of Sciences. 2013;1277:139-58. doi: 10.1111/j.1749-6632.2012.06819.x. PubMed PMID: 23215859; PubMed Central PMCID: PMC3556211.

Bean J, Riely GJ, Balak M, Marks JL, Ladanyi M, Miller VA, et al. Acquired resistance to epidermal growth factor receptor kinase inhibitors associated with a novel T854A mutation in a patient with EGFR-mutant lung adenocarcinoma. Clinical cancer research : an official journal of the American Association for Cancer Research. 2008;14(22):7519-25. doi: 10.1158/1078-0432.CCR-08-0151. PubMed PMID: 19010870; PubMed Central PMCID: PMC2596620.

Becker T, Armache JP, Jarasch A, Anger AM, Villa E, Sieber H, et al. Structure of the no-go mRNA decay complex Dom34-Hbs1 bound to a stalled 80S ribosome. Nature structural & molecular biology. 2011;18(6):715-20. doi: 10.1038/nsmb.2057. PubMed PMID: 21623367.

Becker T, Bhushan S, Jarasch A, Armache JP, Funes S, Jossinet F, et al. Structure of monomeric yeast and mammalian Sec61 complexes interacting with the translating ribosome. Science. 2009;326(5958):1369-73. doi: 10.1126/science.1178535. PubMed PMID: 19933108; PubMed Central PMCID: PMC2920595.

Becker T, Franckenberg S, Wickles S, Shoemaker CJ, Anger AM, Armache JP, et al. Structural basis of highly conserved ribosome recycling in eukaryotes and archaea. Nature. 2012;482(7386):501-6. doi: 10.1038/nature10829. PubMed PMID: 22358840.

**Behrmann, E., Loerke, J., Budkevich, T.V., Yamamoto, K., Schmidt, A., Penczek, P.A., Vos, M.R., Bürger, J., Mielke, T., Scheerer, P., et al. (2015). structural snapshots of actively translating human ribosomes. Cell 161, 845–857.

***Belle A, Tanay A, Bitincka L, Shamir R, O'Shea EK. Quantification of protein half-lives in the budding yeast proteome. Proceedings of the National Academy of Sciences of the United States of America. 2006;103(35):13004-9. doi: 10.1073/pnas.0605420103. PubMed PMID: 16916930; PubMed Central PMCID: PMC1550773.

Belousoff MJ, Eyal Z, Radjainia M, Ahmed T, Bamert RS, Matzov D, et al. Structural Basis for Linezolid Binding Site Rearrangement in the Staphylococcus aureus Ribosome. mBio. 2017;8(3). doi: 10.1128/mBio.00395-17. PubMed PMID: 28487427; PubMed Central PMCID: PMC5424203.

Belova L, Tenson T, Xiong L, McNicholas PM, Mankin AS. A novel site of antibiotic action in the ribosome: interaction of evernimicin with the large ribosomal subunit. Proceedings of the National Academy of Sciences of the United States of America. 2001;98(7):3726-31. doi: 10.1073/pnas.071527498. PubMed PMID: 11259679; PubMed Central PMCID: PMC31120.

***Ben-Shem A, Garreau de Loubresse N, Melnikov S, Jenner L, Yusupova G, Yusupov M. The structure of the eukaryotic ribosome at 3.0 A resolution. Science. 2011;334(6062):1524-9. doi: 10.1126/science.1212642. PubMed PMID: 22096102.

Ben-Shem A, Jenner L, Yusupova G, Yusupov M. Crystal structure of the eukaryotic ribosome. Science. 2010;330(6008):1203-9. doi: 10.1126/science.1194294. PubMed PMID: 21109664.

Beral V, Newton R. Overview of the epidemiology of immunodeficiency-associated cancers. Journal of the National Cancer Institute Monographs. 1998(23):1-6. PubMed PMID: 9709294.

Bhat M, Robichaud N, Hulea L, Sonenberg N, Pelletier J, Topisirovic I. Targeting the translation machinery in cancer. Nature reviews Drug discovery. 2015;14(4):261-78. doi: 10.1038/nrd4505. PubMed PMID: 25743081.

Bien J, Sokolova O, Bozko P. Characterization of Virulence Factors of Staphylococcus aureus: Novel Function of Known Virulence Factors That Are Implicated in Activation of Airway Epithelial Proinflammatory Response. Journal of pathogens. 2011;2011:601905. doi: 10.4061/2011/601905. PubMed PMID: 22567334; PubMed Central PMCID: PMC3335658.

Bischoff M, Dunman P, Kormanec J, Macapagal D, Murphy E, Mounts W, et al. Microarray-based analysis of the Staphylococcus aureus sigmaB regulon. Journal of bacteriology. 2004;186(13):4085-99. doi: 10.1128/JB.186.13.4085-4099.2004. PubMed PMID: 15205410; PubMed Central PMCID: PMC421609.

Bischoff M, Entenza JM, Giachino P. Influence of a functional sigB operon on the global regulators sar and agr in Staphylococcus aureus. Journal of bacteriology. 2001;183(17):5171-9. PubMed PMID: 11489871; PubMed Central PMCID: PMC95394.

*Blaha G, Stanley RE, Steitz TA. Formation of the first peptide bond: the structure of EF-P bound to the 70S ribosome. Science. 2009;325(5943):966-70. doi: 10.1126/science.1175800. PubMed PMID: 19696344; PubMed Central PMCID: PMC3296453.

Blencke S, Ullrich A, Daub H. Mutation of threonine 766 in the epidermal growth factor receptor reveals a hotspot for resistance formation against selective tyrosine kinase inhibitors. The Journal of biological chemistry. 2003;278(17):15435-40. doi: 10.1074/jbc.M211158200. PubMed PMID: 12594213.

Blundell TL, Cutfield JF, Cutfield SM, Dodson EJ, Dodson GG, Hodgkin DC, et al. Atomic positions in rhombohedral 2-zinc insulin crystals. Nature. 1971;231(5304):506-11. PubMed PMID: 4932997.

Bonanno L, Favaretto A, Rosell R. Platinum drugs and DNA repair mechanisms in lung cancer. Anticancer research. 2014;34(1):493-501. PubMed PMID: 24403507.

Bretscher MS. Direct translation of a circular messenger DNA. Nature. 1968;220(5172):1088-91. PubMed PMID: 5723604.

**Brilot, A.F., Korostelev, A.A., Ermolenko, D.N., and Grigorieff, N. (2013). Structure of the ribosome with elongation factor G trapped in the pretranslocation state. Proc. Natl. Acad. Sci. U. S. A. 110, 20994–20999.

Brodersen DE, Clemons WM, Jr., Carter AP, Morgan-Warren RJ, Wimberly BT, Ramakrishnan V. The structural basis for the action of the antibiotics tetracycline, pactamycin, and hygromycin B on the 30S ribosomal subunit. Cell. 2000;103(7):1143-54. PubMed PMID: 11163189.

**Brown A, Amunts A, Bai XC, Sugimoto Y, Edwards PC, Murshudov G, et al. Structure of the large ribosomal subunit from human mitochondria. Science. 2014;346(6210):718-22. doi: 10.1126/science.1258026. PubMed PMID: 25278503; PubMed Central PMCID: PMC4246062.

**Budkevich, T. V., Giesebrecht, J., Behrmann, E., Loerke, J., Ramrath, D.J.F., Mielke, T., Ismer, J., Hildebrand, P.W., Tung, C.S., Nierhaus, K.H., et al. (2014). Regulation of the mammalian elongation cycle by subunit rolling: A eukaryotic-specific ribosome rearrangement. Cell 158, 121–131.

**Budkevich, T., Giesebrecht, J., Altman, R.B., Munro, J.B., Mielke, T., Nierhaus, K.H., Blanchard, S.C., and Spahn, C.M.T. (2011). Structure and dynamics of the mammalian ribosomal pretranslocation complex. Mol. Cell 44, 214–224.

Bush K. Proliferation and significance of clinically relevant beta-lactamases. Annals of the New York Academy of Sciences. 2013;1277:84-90. doi: 10.1111/nyas.12023. PubMed PMID: 23346859.

Campanile F, Bongiorno D, Borbone S, Stefani S. Hospital-associated methicillin-resistant Staphylococcus aureus (HA-MRSA) in Italy. Annals of clinical microbiology and antimicrobials. 2009;8:22. doi: 10.1186/1476-0711-8-22. PubMed PMID: 19552801; PubMed Central PMCID: PMC2708121.

Carter AP, Clemons WM, Brodersen DE, Morgan-Warren RJ, Wimberly BT, Ramakrishnan V. Functional insights from the structure of the 30S ribosomal subunit and its interactions with antibiotics. Nature. 2000;407(6802):340-8. doi: 10.1038/35030019. PubMed PMID: 11014183.

Cate JH, Yusupov MM, Yusupova GZ, Earnest TN, Noller HF. X-ray crystal structures of 70S ribosome functional complexes. Science. 1999;285(5436):2095-104. PubMed PMID: 10497122.

CDC National Nosocomial Infections Surveillance (NNIS) System Report, data summary from January 1990–May 1999, issued June 1999. Am J Infect Control 1999; 27:520–32.

Chambers HF, Deleo FR. Waves of resistance: Staphylococcus aureus in the antibiotic era. Nature reviews Microbiology. 2009;7(9):629-41. doi: 10.1038/nrmicro2200. PubMed PMID: 19680247; PubMed Central PMCID: PMC2871281.

Chan PF, Foster SJ. Role of SarA in virulence determinant production and environmental signal transduction in Staphylococcus aureus. Journal of bacteriology. 1998;180(23):6232-41. PubMed PMID: 9829932; PubMed Central PMCID: PMC107708.

Chayen SD, Gross D, Makhoul O, Glaser B. TSH producing pituitary tumor: biochemical diagnosis and long-term medical management with octreotide. Hormone and metabolic research = Hormon- und Stoffwechselforschung = Hormones et metabolisme. 1992;24(1):34-8. doi: 10.1055/s-2007-1003247. PubMed PMID: 1612557.

Chen C, Tang J, Dong W, Wang C, Feng Y, Wang J, et al. A glimpse of streptococcal toxic shock syndrome from comparative genomics of S. suis 2 Chinese isolates. PloS one. 2007;2(3):e315. doi: 10.1371/journal.pone.0000315. PubMed PMID: 17375201; PubMed Central PMCID: PMC1820848.

Cheung AL, Bayer AS, Zhang G, Gresham H, Xiong YQ. Regulation of virulence determinants in vitro and in vivo in Staphylococcus aureus. FEMS immunology and medical microbiology. 2004;40(1):1-9. PubMed PMID: 14734180.

Cheung AL, Koomey JM, Butler CA, Projan SJ, Fischetti VA. Regulation of exoprotein expression in Staphylococcus aureus by a locus (sar) distinct from agr. Proceedings of the National Academy of Sciences of the United States of America. 1992;89(14):6462-6. PubMed PMID: 1321441; PubMed Central PMCID: PMC49521.

Cheung AL, Projan SJ, Gresham H. The Genomic Aspect of Virulence, Sepsis, and Resistance to Killing Mechanisms in Staphylococcus aureus. Current infectious disease reports. 2002;4(5):400-10. PubMed PMID: 12228026.

Cheung AL, Projan SJ. Cloning and sequencing of sarA of Staphylococcus aureus, a gene required for the expression of agr. Journal of bacteriology. 1994;176(13):4168-72. PubMed PMID: 8021198; PubMed Central PMCID: PMC205618.

Cheung AL, Schmidt K, Bateman B, Manna AC. SarS, a SarA homolog repressible by agr, is an activator of protein A synthesis in Staphylococcus aureus. Infection and immunity. 2001;69(4):2448-55. doi: 10.1128/IAI.69.4.2448-2455.2001. PubMed PMID: 11254606; PubMed Central PMCID: PMC98178.

Chevalier, C. (2009). Function and mechanism of action of RNAIII and new ncRNAs in Staphylococcus aureus (Doctoral thesis, University of Strasbourg, Strasbourg, France). Retrieved from: http://scd-theses.u-strasbg.fr/1714/

Chien Y, Manna AC, Projan SJ, Cheung AL. SarA, a global regulator of virulence determinants in Staphylococcus aureus, binds to a conserved motif essential for sar-dependent gene regulation. The Journal of biological chemistry. 1999;274(52):37169-76. PubMed PMID: 10601279.

Cimolai N. MRSA and the environment: implications for comprehensive control measures. European journal of clinical microbiology & infectious diseases : official publication of the European Society of Clinical Microbiology. 2008;27(7):481-93. doi: 10.1007/s10096-008-0471-0. PubMed PMID: 18273652.

Clatworthy AE, Pierson E, Hung DT. Targeting virulence: a new paradigm for antimicrobial therapy. Nature chemical biology. 2007;3(9):541-8. doi: 10.1038/nchembio.2007.24. PubMed PMID: 17710100.

Cole AM, Tahk S, Oren A, Yoshioka D, Kim YH, Park A, et al. Determinants of Staphylococcus aureus nasal carriage. Clinical and diagnostic laboratory immunology. 2001;8(6):1064-9. doi: 10.1128/CDLI.8.6.1064-1069.2001. PubMed PMID: 11687441; PubMed Central PMCID: PMC96227.

*Colussi, T.M., Costantino, D.A., Zhu, J., Donohue, J.P., Korostelev, A.A., Jaafar, Z.A., Plank, T.-D.M., Noller, H.F., and Kieft, J.S. (2015). Initiation of translation in bacteria by a structured eukaryotic IRES RNA. Nature 519, 110–113.

Connell SR, Tracz DM, Nierhaus KH, Taylor DE. Ribosomal protection proteins and their mechanism of tetracycline resistance. Antimicrobial agents and chemotherapy. 2003;47(12):3675-81. PubMed PMID: 14638464; PubMed Central PMCID: PMC296194.

Cornish PV, Ermolenko DN, Noller HF, Ha T. Spontaneous intersubunit rotation in single ribosomes. Molecular cell. 2008;30(5):578-88. doi: 10.1016/j.molcel.2008.05.004. PubMed PMID: 18538656; PubMed Central PMCID: PMC2491453.

Costa DB, Halmos B, Kumar A, Schumer ST, Huberman MS, Boggon TJ, et al. BIM mediates EGFR tyrosine kinase inhibitor-induced apoptosis in lung cancers with oncogenic EGFR mutations. PLoS medicine. 2007;4(10):1669-79; discussion 80. doi: 10.1371/journal.pmed.0040315. PubMed PMID: 17973572; PubMed Central PMCID: PMC2043012.

Crowfoot, D., Bunn, C.W., Rogers-Low, B.W., and Turner-Jones, A. (1949). The chemistry of penicillin. Princet. Univ. Press, New Jersey.

D'Ambrosio, M., Guerriero, A., Debitus, C.c., Ribes, O., Pusset, J., Leroy, S.,and Pietra, F. (1993). Agelastatin a, a new skeleton cytotoxic alkaloid of the oroidin family. Isolation from the axinellid sponge Agelas dendromorpha of the coral sea. J. Chem. Soc. Chem. Comm, 1305.

Dang Y, Schneider-Poetsch T, Eyler DE, Jewett JC, Bhat S, Rawal VH, et al. Inhibition of eukaryotic translation elongation by the antitumor natural product Mycalamide B. Rna. 2011;17(8):1578-88. doi: 10.1261/rna.2624511. PubMed PMID: 21693620; PubMed Central PMCID: PMC3153980.

D'Arcy TJ, Hughes SW, Chiu WS, Clark T, Milner AD, Saunders J, et al. Estimation of fetal lung volume using enhanced 3-dimensional ultrasound: a new method and first result. British journal of obstetrics and gynaecology. 1996;103(10):1015-20. PubMed PMID: 8863701.

D'Costa VM, King CE, Kalan L, Morar M, Sung WW, Schwarz C, et al. Antibiotic resistance is ancient. Nature. 2011;477(7365):457-61. doi: 10.1038/nature10388. PubMed PMID: 21881561.

Demeshkina N, Jenner L, Yusupova G, Yusupov M. Interactions of the ribosome with mRNA and tRNA. Current opinion in structural biology. 2010;20(3):325-32. doi: 10.1016/j.sbi.2010.03.002. PubMed PMID: 20392630.

*Demeshkina, N., Jenner, L., Westhof, E., Yusupov, M., and Yusupova, G. (2012). A new understanding of the decoding principle on the ribosome. Nature 484, 256–259.

Deora R, Misra TK. Characterization of the primary sigma factor of Staphylococcus aureus. The Journal of biological chemistry. 1996;271(36):21828-34. PubMed PMID: 8702982.

Deora R, Tseng T, Misra TK. Alternative transcription factor sigmaSB of Staphylococcus aureus: characterization and role in transcription of the global regulatory locus sar. Journal of bacteriology. 1997;179(20):6355-9. PubMed PMID: 9335283; PubMed Central PMCID: PMC179550.

**des Georges, A., Hashem, Y., Unbehaun, A., Grassucci, R.A., Taylor, D., Hellen, C.U.T., Pestova, T. V., and Frank, J. (2014). Structure of the mammalian ribosomal pre-termination complex associated with eRF1•eRF3•GDPNP. Nucleic Acids Res. 42, 3409–3418.

Dunkle JA, Wang L, Feldman MB, Pulk A, Chen VB, Kapral GJ, et al. Structures of the bacterial ribosome in classical and hybrid states of tRNA binding. Science. 2011;332(6032):981-4. doi: 10.1126/science.1202692. PubMed PMID: 21596992; PubMed Central PMCID: PMC3176341.

Emsley P, Cowtan K. Coot: model-building tools for molecular graphics. Acta crystallographica Section D, Biological crystallography. 2004;60(Pt 12 Pt 1):2126-32. doi: 10.1107/S0907444904019158. PubMed PMID: 15572765.

Engelman JA, Zejnullahu K, Mitsudomi T, Song Y, Hyland C, Park JO, et al. MET amplification leads to gefitinib resistance in lung cancer by activating ERBB3 signaling. Science. 2007;316(5827):1039-43. doi: 10.1126/science.1141478. PubMed PMID: 17463250.

Entenza JM, Moreillon P, Senn MM, Kormanec J, Dunman PM, Berger-Bachi B, et al. Role of sigmaB in the expression of Staphylococcus aureus cell wall adhesins ClfA and FnbA and contribution to infectivity in a rat model of experimental endocarditis. Infection and immunity. 2005;73(2):990-8. doi: 10.1128/IAI.73.2.990-998.2005. PubMed PMID: 15664942; PubMed Central PMCID: PMC547034.

Eyal Z, Matzov D, Krupkin M, Paukner S, Riedl R, Rozenberg H, et al. A novel pleuromutilin antibacterial compound, its binding mode and selectivity mechanism. Scientific reports. 2016;6:39004. doi: 10.1038/srep39004. PubMed PMID: 27958389; PubMed Central PMCID: PMC5154188 Austria and King of Prussia, PA, United States). Dr. Paukner and Dr. Riedl are employees of Nabriva Therapeutics and own Nabriva stocks.

Eyal Z, Matzov D, Krupkin M, Wekselman I, Paukner S, Zimmerman E, et al. Structural insights into species-specific features of the ribosome from the pathogen Staphylococcus aureus. Proceedings of the National Academy of Sciences of the United States of America. 2015;112(43):E5805-14. doi: 10.1073/pnas.1517952112. PubMed PMID: 26464510; PubMed Central PMCID: PMC4629319.

Fattom A, Fuller S, Propst M, Winston S, Muenz L, He D, et al. Safety and immunogenicity of a booster dose of Staphylococcus aureus types 5 and 8 capsular polysaccharide conjugate vaccine (StaphVAX) in hemodialysis patients. Vaccine. 2004;23(5):656-63. doi: 10.1016/j.vaccine.2004.06.043. PubMed PMID: 15542186.

Feil EJ, Cooper JE, Grundmann H, Robinson DA, Enright MC, Berendt T, et al. How clonal is Staphylococcus aureus? Journal of bacteriology. 2003;185(11):3307-16. PubMed PMID: 12754228; PubMed Central PMCID: PMC155367.

Feldman MB, Terry DS, Altman RB, Blanchard SC. Aminoglycoside activity observed on single pre-translocation ribosome complexes. Nature chemical biology. 2010;6(1):54-62. doi: 10.1038/nchembio.274. PubMed PMID: 19946275; PubMed Central PMCID: PMC2914512.

Ferguson A, Wang L, Altman RB, Terry DS, Juette MF, Burnett BJ, et al. Functional Dynamics within the Human Ribosome Regulate the Rate of Active Protein Synthesis. Molecular cell. 2015;60(3):475-86. doi: 10.1016/j.molcel.2015.09.013. PubMed PMID: 26593721; PubMed Central PMCID: PMC4660248.

**Fernández, I.S., Bai, X.-C., Hussain, T., Kelley, A.C., Lorsch, J.R., Ramakrishnan, V., and Scheres, S.H.W. (2013). Molecular architecture of a eukaryotic translational initiation complex. Science 342, 1240585.

**Fernández, I.S., Bai, X.C., Murshudov, G., Scheres, S.H.W., and Ramakrishnan, V. (2014). Initiation of translation by cricket paralysis virus IRES requires its translocation in the ribosome. Cell 157, 823–831.

Fischer N, Neumann P, Konevega AL, Bock LV, Ficner R, Rodnina MV, et al. Structure of the E. coli ribosome-EF-Tu complex at <3 A resolution by Cs-corrected cryo-EM. Nature. 2015;520(7548):567-70. doi: 10.1038/nature14275. PubMed PMID: 25707802.

Franckenberg S, Becker T, Beckmann R. Structural view on recycling of archaeal and eukaryotic ribosomes after canonical termination and ribosome rescue. Current opinion in structural biology. 2012;22(6):786-96. doi: 10.1016/j.sbi.2012.08.002. PubMed PMID: 23031510.

Frank J, Agrawal RK. A ratchet-like inter-subunit reorganization of the ribosome during translocation. Nature. 2000;406(6793):318-22. doi: 10.1038/35018597. PubMed PMID: 10917535.

Freistroffer DV, Pavlov MY, MacDougall J, Buckingham RH, Ehrenberg M. Release factor RF3 in E.coli accelerates the dissociation of release factors RF1 and RF2 from the ribosome in a GTP-dependent manner. The EMBO journal. 1997;16(13):4126-33. doi: 10.1093/emboj/16.13.4126. PubMed PMID: 9233821; PubMed Central PMCID: PMC1170035.

Fridkin SK, Hageman JC, Morrison M, Sanza LT, Como-Sabetti K, Jernigan JA, et al. Methicillin-resistant Staphylococcus aureus disease in three communities. The New England journal of medicine. 2005;352(14):1436-44. doi: 10.1056/NEJMoa043252. PubMed PMID: 15814879.

Gabashvili IS, Agrawal RK, Spahn CM, Grassucci RA, Svergun DI, Frank J, et al. Solution structure of the E. coli 70S ribosome at 11.5 A resolution. Cell. 2000;100(5):537-49. PubMed PMID: 10721991.

*Gagnon, M.G., Lin, J., Bulkley, D., and Steitz, T. a. (2014). Crystal structure of elongation factor 4 bound to a clockwise ratcheted ribosome. Science (80-.). 345, 684–687.

*Gagnon, M.G., Seetharaman, S. V., Bulkley, D., and Steitz, T.A. (2012). structural basis for the rescue of stalled ribosomes: structure of YaeJ bound to the ribosome. Science (80-.). 335, 1370–1372.

***Gandhi V, Plunkett W, Cortes JE. Omacetaxine: a protein translation inhibitor for treatment of chronic myelogenous leukemia. Clinical cancer research : an official journal of the American Association for Cancer Research. 2014;20(7):1735-40. doi: 10.1158/1078-0432.CCR-13-1283. PubMed PMID: 24501394; PubMed Central PMCID: PMC4048124.

Gao YG, Selmer M, Dunham CM, Weixlbaumer A, Kelley AC, Ramakrishnan V. The structure of the ribosome with elongation factor G trapped in the posttranslocational state. Science. 2009;326(5953):694-9. doi: 10.1126/science.1179709. PubMed PMID: 19833919; PubMed Central PMCID: PMC3763468.

Garcia Ruiz, J.M.; Moreno, A.; Viedma, C.; Coll, M. Crystal quality of lysozyme single crystals grown by the gel acupuncture method. Mater. Res. Bull. 1993, 28, 541–546.

Garman, E.F., and Schneider, T.R. (1997). Macromolecular Cryocrystallography. J. Appl. Crystallogr. 30, 211–237.

***Garreau de Loubresse N, Prokhorova I, Holtkamp W, Rodnina MV, Yusupova G, Yusupov M. Structural basis for the inhibition of the eukaryotic ribosome. Nature. 2014;513(7519):517-22. doi: 10.1038/nature13737. PubMed PMID: 25209664.

Geoffrey M Cooper. The Cell, 2nd edition Sunderland (MA): Sinauer Associates; 2000.ISBN-10: 0-87893-106-6

Ghalei H, Schaub FX, Doherty JR, Noguchi Y, Roush WR, Cleveland JL, et al. Hrr25/CK1delta-directed release of Ltv1 from pre-40S ribosomes is necessary for ribosome assembly and cell growth. The Journal of cell biology. 2015;208(6):745-59. doi: 10.1083/jcb.201409056. PubMed PMID: 25778921; PubMed Central PMCID: PMC4362465.

Gioeli, D.(2011). TargetedTherapies MechanismsofResistance. NewYork: HumanaPress

Giraudo AT, Cheung AL, Nagel R. The sae locus of Staphylococcus aureus controls exoprotein synthesis at the transcriptional level. Archives of microbiology. 1997;168(1):53-8. PubMed PMID: 9211714.

Giraudo AT, Raspanti CG, Calzolari A, Nagel R. Characterization of a Tn551-mutant of Staphylococcus aureus defective in the production of several exoproteins. Canadian journal of microbiology. 1994;40(8):677-81. PubMed PMID: 7922890.

Goerke C, Fluckiger U, Steinhuber A, Bisanzio V, Ulrich M, Bischoff M, et al. Role of Staphylococcus aureus global regulators sae and sigmaB in virulence gene expression during device-related infection. Infection and immunity. 2005;73(6):3415-21. doi: 10.1128/IAI.73.6.3415-3421.2005. PubMed PMID: 15908369; PubMed Central PMCID: PMC1111833.

Gogia PP, Braatz JH. Validity and reliability of leg length measurements. The Journal of orthopaedic and sports physical therapy. 1986;8(4):185-8. PubMed PMID: 18802226.

Gogia, Z. V, Yusupov, M.M., and Spirina, T.N. (1986). Structure of Thermus thermophilus ribosomes. I. Method of isolation and purification of ribosomes. MOL. BIOL.(MOSCOW). 20, 519–526.

Gorre ME, Mohammed M, Ellwood K, Hsu N, Paquette R, Rao PN, et al. Clinical resistance to STI-571 cancer therapy caused by BCR-ABL gene mutation or amplification. Science. 2001;293(5531):876-80. doi: 10.1126/science.1062538. PubMed PMID: 11423618.

Gottesman MM, Fojo T, Bates SE. Multidrug resistance in cancer: role of ATP-dependent transporters. Nature reviews Cancer. 2002;2(1):48-58. doi: 10.1038/nrc706. PubMed PMID: 11902585.

Gottesman MM. Mechanisms of cancer drug resistance. Annual review of medicine. 2002;53:615-27. doi: 10.1146/annurev.med.53.082901.103929. PubMed PMID: 11818492.

Gourse RL, Gaal T, Bartlett MS, Appleman JA, Ross W. rRNA transcription and growth rate-dependent regulation of ribosome synthesis in Escherichia coli. Annual review of microbiology. 1996;50:645-77. doi: 10.1146/annurev.micro.50.1.645. PubMed PMID: 8905094.

Graham PL, 3rd, Lin SX, Larson EL. A U.S. population-based survey of Staphylococcus aureus colonization. Annals of internal medicine. 2006;144(5):318-25. PubMed PMID: 16520472.

Greber BJ, Bieri P, Leibundgut M, Leitner A, Aebersold R, Boehringer D, et al. Ribosome. The complete structure of the 55S mammalian mitochondrial ribosome. Science. 2015;348(6232):303-8. doi: 10.1126/science.aaa3872. PubMed PMID: 25837512.

Greber BJ, Boehringer D, Leibundgut M, Bieri P, Leitner A, Schmitz N, et al. The complete structure of the large subunit of the mammalian mitochondrial ribosome. Nature. 2014;515(7526):283-6. doi: 10.1038/nature13895. PubMed PMID: 25271403.

Grundmann H, Aires-de-Sousa M, Boyce J, Tiemersma E. Emergence and resurgence of meticillin-resistant Staphylococcus aureus as a public-health threat. Lancet. 2006;368(9538):874-85. doi: 10.1016/S0140-6736(06)68853-3. PubMed PMID: 16950365.

Grundmann H, Hori S, Winter B, Tami A, Austin DJ. Risk factors for the transmission of methicillin-resistant Staphylococcus aureus in an adult intensive care unit: fitting a model to the data. The Journal of infectious diseases. 2002;185(4):481-8. doi: 10.1086/338568. PubMed PMID: 11865400.

*Guo Z, Noller HF. Rotation of the head of the 30S ribosomal subunit during mRNA translocation. Proceedings of the National Academy of Sciences of the United States of America. 2012;109(50):20391-4. doi: 10.1073/pnas.1218999109. PubMed PMID: 23188795; PubMed Central PMCID: PMC3528506.

Halic M, Blau M, Becker T, Mielke T, Pool MR, Wild K, et al. Following the signal sequence from ribosomal tunnel exit to signal recognition particle. Nature. 2006;444(7118):507-11. doi: 10.1038/nature05326. PubMed PMID: 17086193.

Halic M, Gartmann M, Schlenker O, Mielke T, Pool MR, Sinning I, et al. Signal recognition particle receptor exposes the ribosomal translocon binding site. Science. 2006;312(5774):745-7. doi: 10.1126/science.1124864. PubMed PMID: 16675701.

Hall AE, Domanski PJ, Patel PR, Vernachio JH, Syribeys PJ, Gorovits EL, et al. Characterization of a protective monoclonal antibody recognizing Staphylococcus aureus MSCRAMM protein clumping factor A. Infection and immunity. 2003;71(12):6864-70. PubMed PMID: 14638774; PubMed Central PMCID: PMC308922.

Hardy SJ, Kurland CG, Voynow P, Mora G. The ribosomal proteins of Escherichia coli. I. Purification of the 30S ribosomal proteins. Biochemistry. 1969;8(7):2897-905. PubMed PMID: 4897206.

Hartman JLt, Garvik B, Hartwell L. Principles for the buffering of genetic variation. Science. 2001;291(5506):1001-4. PubMed PMID: 11232561.

**Hashem, Y., Des Georges, A., Dhote, V., Langlois, R., Liao, H.Y., Grassucci, R.A., Hellen, C.U.T., Pestova, T. V., and Frank, J. (2013a). XStructure of the mammalian ribosomal 43S preinitiation complex bound to the scanning factor DHX29. Cell 153.

**Hashem, Y., des Georges, A., Dhote, V., Langlois, R., Liao, H.Y., Grassucci, R. a, Pestova, T. V, Hellen, C.U.T., and Frank, J. (2013b). Hepatitis-C-virus-like internal ribosome entry sites displace eIF3 to gain access to the 40S subunit. Nature 503, 539–543.

**Hashem, Y., des Georges, A., Fu, J., Buss, S.N., Jossinet, F., Jobe, A., Zhang, Q., Liao, H.Y., Grassucci, R. a, Bajaj, C., et al. (2013c). High-resolution cryo-electron microscopy structure of the Trypanosoma brucei ribosome. Nature 494, 385–389.

He C. Grand challenge commentary: RNA epigenetics? Nature chemical biology. 2010;6(12):863-5. doi: 10.1038/nchembio.482. PubMed PMID: 21079590.

Hentschel J, Burnside C, Mignot I, Leibundgut M, Boehringer D, Ban N. The Complete Structure of the Mycobacterium smegmatis 70S Ribosome. Cell reports. 2017;20(1):149-60. doi: 10.1016/j.celrep.2017.06.029. PubMed PMID: 28683309.

Heras B, Martin JL. Post-crystallization treatments for improving diffraction quality of protein crystals. Acta crystallographica Section D, Biological crystallography. 2005;61(Pt 9):1173-80. doi: 10.1107/S0907444905019451. PubMed PMID: 16131749.

Hidron AI, Edwards JR, Patel J, Horan TC, Sievert DM, Pollock DA, et al. NHSN annual update: antimicrobial-resistant pathogens associated with healthcare-associated infections: annual summary of data reported to the National Healthcare Safety Network at the Centers for Disease Control and Prevention, 2006-2007. Infection control and hospital epidemiology. 2008;29(11):996-1011. doi: 10.1086/591861. PubMed PMID: 18947320.

Hinnebusch AG. Molecular mechanism of scanning and start codon selection in eukaryotes. Microbiology and molecular biology reviews : MMBR. 2011;75(3):434-67, first page of table of contents. doi: 10.1128/MMBR.00008-11. PubMed PMID: 21885680; PubMed Central PMCID: PMC3165540.

Hirashima A, Kaji A. Role of elongation factor G and a protein factor on the release of ribosomes from messenger ribonucleic acid. The Journal of biological chemistry. 1973;248(21):7580-7. PubMed PMID: 4583357.

Hirokawa G, Nijman RM, Raj VS, Kaji H, Igarashi K, Kaji A. The role of ribosome recycling factor in dissociation of 70S ribosomes into subunits. Rna. 2005;11(8):1317-28. doi: 10.1261/rna.2520405. PubMed PMID: 16043510; PubMed Central PMCID: PMC1370814.

Hirokawa G, Nijman RM, Raj VS, Kaji H, Igarashi K, Kaji A. The role of ribosome recycling factor in dissociation of 70S ribosomes into subunits. Rna. 2005;11(8):1317-28. doi: 10.1261/rna.2520405. PubMed PMID: 16043510; PubMed Central PMCID: PMC1370814.

Hodgkin DC, Kamper J, Mackay M, Pickworth J, Trueblood KN, White JG. Structure of vitamin B12. Nature. 1956;178(4524):64-6. PubMed PMID: 13348621.

Hofmann WK, Komor M, Wassmann B, Jones LC, Gschaidmeier H, Hoelzer D, et al. Presence of the BCR-ABL mutation Glu255Lys prior to STI571 (imatinib) treatment in patients with Ph+ acute lymphoblastic leukemia. Blood. 2003;102(2):659-61. doi: 10.1182/blood-2002-06-1756. PubMed PMID: 12663457.

Hollenbeck BL, Rice LB. Intrinsic and acquired resistance mechanisms in enterococcus. Virulence. 2012;3(5):421-33. doi: 10.4161/viru.21282. PubMed PMID: 23076243; PubMed Central PMCID: PMC3485979.

Horsburgh MJ, Aish JL, White IJ, Shaw L, Lithgow JK, Foster SJ. sigmaB modulates virulence determinant expression and stress resistance: characterization of a functional rsbU strain derived from Staphylococcus aureus 8325-4. Journal of bacteriology. 2002;184(19):5457-67. PubMed PMID: 12218034; PubMed Central PMCID: PMC135357.

Hostetter AA, Osborn MF, DeRose VJ. RNA-Pt adducts following cisplatin treatment of Saccharomyces cerevisiae. ACS chemical biology. 2012;7(1):218-25. doi: 10.1021/cb200279p. PubMed PMID: 22004017; PubMed Central PMCID: PMC3262962.

Housman G, Byler S, Heerboth S, Lapinska K, Longacre M, Snyder N, et al. Drug resistance in cancer: an overview. Cancers. 2014;6(3):1769-92. doi: 10.3390/cancers6031769. PubMed PMID: 25198391; PubMed Central PMCID: PMC4190567.

Hughes TP, Kaeda J, Branford S, Rudzki Z, Hochhaus A, Hensley ML, et al. Frequency of major molecular responses to imatinib or interferon alfa plus cytarabine in newly diagnosed chronic myeloid leukemia. The New England journal of medicine. 2003;349(15):1423-32. doi: 10.1056/NEJMoa030513. PubMed PMID: 14534335.

**Hussain, T., Llácer, J.L., Fernández, I.S., Munoz, A., Martin-Marcos, P., Savva, C.G., Lorsch, J.R., Hinnebusch, A.G., and Ramakrishnan, V. (2015). Structural changes enable start codon recognition by the eukaryotic translation initiation complex. Cell 159, 597–607.

Ingavale S, van Wamel W, Luong TT, Lee CY, Cheung AL. Rat/MgrA, a regulator of autolysis, is a regulator of virulence genes in Staphylococcus aureus. Infection and immunity. 2005;73(3):1423-31. doi: 10.1128/IAI.73.3.1423-1431.2005. PubMed PMID: 15731040; PubMed Central PMCID: PMC1064946.

***Ingolia NT, Lareau LF, Weissman JS. Ribosome profiling of mouse embryonic stem cells reveals the complexity and dynamics of mammalian proteomes. Cell. 2011;147(4):789-802. doi: 10.1016/j.cell.2011.10.002. PubMed PMID: 22056041; PubMed Central PMCID: PMC3225288.

Inukai M, Toyooka S, Ito S, Asano H, Ichihara S, Soh J, et al. Presence of epidermal growth factor receptor gene T790M mutation as a minor clone in non-small cell lung cancer. Cancer research. 2006;66(16):7854-8. doi: 10.1158/0008-5472.CAN-06-1951. PubMed PMID: 16912157.

Ishikawa T, Ali-Osman F. Glutathione-associated cis-diamminedichloroplatinum(II) metabolism and ATP-dependent efflux from leukemia cells. Molecular characterization of glutathione-platinum complex and its biological significance. The Journal of biological chemistry. 1993;268(27):20116-25. PubMed PMID: 8376370.

Jabbour E, Kantarjian H, Jones D, Breeden M, Garcia-Manero G, O'Brien S, et al. Characteristics and outcomes of patients with chronic myeloid leukemia and T315I mutation following failure of imatinib mesylate therapy. Blood. 2008;112(1):53-5. doi: 10.1182/blood-2007-11-123950. PubMed PMID: 18403620; PubMed Central PMCID: PMC4081375.

Jabbour E, Kantarjian H, Jones D, Talpaz M, Bekele N, O'Brien S, et al. Frequency and clinical significance of BCR-ABL mutations in patients with chronic myeloid leukemia treated with imatinib mesylate. Leukemia. 2006;20(10):1767-73. doi: 10.1038/sj.leu.2404318. PubMed PMID: 16855631.

Jackson RJ, Hellen CU, Pestova TV. The mechanism of eukaryotic translation initiation and principles of its regulation. Nature reviews Molecular cell biology. 2010;11(2):113-27. doi: 10.1038/nrm2838. PubMed PMID: 20094052; PubMed Central PMCID: PMC4461372.

Janosi L, Hara H, Zhang S, Kaji A. Ribosome recycling by ribosome recycling factor (RRF)--an important but overlooked step of protein biosynthesis. Advances in biophysics. 1996;32:121-201. PubMed PMID: 8781287.

Janzon L, Bergqvist D, Boberg J, Boberg M, Eriksson I, Lindgarde F, et al. Prevention of myocardial infarction and stroke in patients with intermittent claudication; effects of ticlopidine. Results from STIMS, the Swedish Ticlopidine Multicentre Study. Journal of internal medicine. 1990;227(5):301-8. PubMed PMID: 2187948.

Jenner L, Rees B, Yusupov M, Yusupova G. Messenger RNA conformations in the ribosomal E site revealed by X-ray crystallography. EMBO reports. 2007;8(9):846-50. doi: 10.1038/sj.embor.7401044. PubMed PMID: 17721443; PubMed Central PMCID: PMC1973951.

*Jenner, L., Demeshkina, N., Yusupova, G., and Yusupov, M. (2010a). Structural aspects of messenger RNA reading frame maintenance by the ribosome. Nat. Struct. Mol. Biol. 17, 555–560.

*Jenner, L., Demeshkina, N., Yusupova, G., and Yusupov, M. (2010b). Structural rearrangements of the ribosome at the tRNA proofreading step. Nat. Struct. Mol. Biol. 17, 1072–1078.

Ji G, Beavis RC, Novick RP. Cell density control of staphylococcal virulence mediated by an octapeptide pheromone. Proceedings of the National Academy of Sciences of the United States of America. 1995;92(26):12055-9. PubMed PMID: 8618843; PubMed Central PMCID: PMC40295.

Ju J, Lim SK, Jiang H, Seo JW, Shen B. Iso-migrastatin congeners from Streptomyces platensis and generation of a glutarimide polyketide library featuring the dorrigocin, lactimidomycin, migrastatin, and NK30424 scaffolds. Journal of the American Chemical Society. 2005;127(34):11930-1. doi: 10.1021/ja053118u. PubMed PMID: 16117518.

Kabsch W. Integration, scaling, space-group assignment and post-refinement. Acta crystallographica Section D, Biological crystallography. 2010;66(Pt 2):133-44. doi: 10.1107/S0907444909047374. PubMed PMID: 20124693; PubMed Central PMCID: PMC2815666.

Kaminishi T, Schedlbauer A, Fabbretti A, Brandi L, Ochoa-Lizarralde B, He CG, et al. Crystallographic characterization of the ribosomal binding site and molecular mechanism of action of Hygromycin A. Nucleic acids research. 2015;43(20):10015-25. doi: 10.1093/nar/gkv975. PubMed PMID: 26464437; PubMed Central PMCID: PMC4787777.

Karimi R, Pavlov MY, Buckingham RH, Ehrenberg M. Novel roles for classical factors at the interface between translation termination and initiation. Molecular cell. 1999;3(5):601-9. PubMed PMID: 10360176.

Kasahara K, Fujiwara Y, Nishio K, Ohmori T, Sugimoto Y, Komiya K, et al. Metallothionein content correlates with the sensitivity of human small cell lung cancer cell lines to cisplatin. Cancer research. 1991;51(12):3237-42. PubMed PMID: 1645616.

Kashchiev, D. (2000). Nucleation (Butterworth-Heinemann).

Kastner B, Stoffler-Meilicke M, Stoffler G. Arrangement of the subunits in the ribosome of Escherichia coli: demonstration by immunoelectron microscopy. Proceedings of the National Academy of Sciences

of the United States of America. 1981;78(11):6652-6. PubMed PMID: 7031657; PubMed Central PMCID: PMC349107.

Kaushal PS, Sharma MR, Booth TM, Haque EM, Tung CS, Sanbonmatsu KY, et al. Cryo-EM structure of the small subunit of the mammalian mitochondrial ribosome. Proceedings of the National Academy of Sciences of the United States of America. 2014;111(20):7284-9. doi: 10.1073/pnas.1401657111. PubMed PMID: 24799711; PubMed Central PMCID: PMC4034187.

Kelley SL, Basu A, Teicher BA, Hacker MP, Hamer DH, Lazo JS. Overexpression of metallothionein confers resistance to anticancer drugs. Science. 1988;241(4874):1813-5. PubMed PMID: 3175622.

Khatter H, Myasnikov AG, Natchiar SK, Klaholz BP. Structure of the human 80S ribosome. Nature. 2015;520(7549):640-5. doi: 10.1038/nature14427. PubMed PMID: 25901680.

Khoshnevis S, Gross T, Rotte C, Baierlein C, Ficner R, Krebber H. The iron-sulphur protein RNase L inhibitor functions in translation termination. EMBO reports. 2010;11(3):214-9. doi: 10.1038/embor.2009.272. PubMed PMID: 20062004; PubMed Central PMCID: PMC2838684.

Khusainov I, Vicens Q, Ayupov R, Usachev K, Myasnikov A, Simonetti A, et al. Structures and dynamics of hibernating ribosomes from Staphylococcus aureus mediated by intermolecular interactions of HPF. The EMBO journal. 2017;36(14):2073-87. doi: 10.15252/embj.201696105. PubMed PMID: 28645916; PubMed Central PMCID: PMC5510003.

Khusainov I, Vicens Q, Bochler A, Grosse F, Myasnikov A, Menetret JF, et al. Structure of the 70S ribosome from human pathogen Staphylococcus aureus. Nucleic acids research. 2016;44(21):10491-504. doi: 10.1093/nar/gkw933. PubMed PMID: 27906650; PubMed Central PMCID: PMC5137454.

Klevens RM, Morrison MA, Nadle J, Petit S, Gershman K, Ray S, et al. Invasive methicillin-resistant Staphylococcus aureus infections in the United States. Jama. 2007;298(15):1763-71. doi: 10.1001/jama.298.15.1763. PubMed PMID: 17940231.

Klinge S, Voigts-Hoffmann F, Leibundgut M, Arpagaus S, Ban N. Crystal structure of the eukaryotic 60S ribosomal subunit in complex with initiation factor 6. Science. 2011;334(6058):941-8. doi: 10.1126/science.1211204. PubMed PMID: 22052974.

Kluytmans J, van Belkum A, Verbrugh H. Nasal carriage of Staphylococcus aureus: epidemiology, underlying mechanisms, and associated risks. Clinical microbiology reviews. 1997;10(3):505-20. PubMed PMID: 9227864; PubMed Central PMCID: PMC172932.

Knox KW, Wicken AJ. Immunological properties of teichoic acids. Bacteriological reviews. 1973;37(2):215-57. PubMed PMID: 4578758; PubMed Central PMCID: PMC413812.

Kobayashi S, Boggon TJ, Dayaram T, Janne PA, Kocher O, Meyerson M, et al. EGFR mutation and resistance of non-small-cell lung cancer to gefitinib. The New England journal of medicine. 2005;352(8):786-92. doi: 10.1056/NEJMoa044238. PubMed PMID: 15728811.

Konst ZA, Szklarski AR, Pellegrino S, Michalak SE, Meyer M, Zanette C, et al. Synthesis facilitates an understanding of the structural basis for translation inhibition by the lissoclimides. Nature chemistry. 2017;9(11):1140-9. doi: 10.1038/nchem.2800. PubMed PMID: 29064494.

Kornblum, J., B. Kreiswirth, S. J. Projan, H. Ross, and R. P. Novick. 1990. agr: a polycistronic locus regulating exoprotein synthesis in Staphylococcus aureus, p. 373–402. In R. P. Novick (ed.), Molecular biology of the staphylococci. VCH Publishers, New York, N.Y.

Korostelev A, Asahara H, Lancaster L, Laurberg M, Hirschi A, Zhu J, et al. Crystal structure of a translation termination complex formed with release factor RF2. Proceedings of the National Academy of Sciences of the United States of America. 2008;105(50):19684-9. doi: 10.1073/pnas.0810953105. PubMed PMID: 19064930; PubMed Central PMCID: PMC2604991.

Korostelev A, Trakhanov S, Laurberg M, Noller HF. Crystal structure of a 70S ribosome-tRNA complex reveals functional interactions and rearrangements. Cell. 2006;126(6):1065-77. doi: 10.1016/j.cell.2006.08.032. PubMed PMID: 16962654.

*Korostelev, A.A. (2011). Structural aspects of translation termination on the ribosome. RNA 17, 1409–1421.

Krauss IR, Merlino A, Vergara A and Sica F. An Overview of Biological Macromolecule Crystallization. Int. J. Mol. Sci. 2013, 14, 11643-11691; doi:10.3390/ijms140611643

Kufe DW, Spriggs DR. Biochemical and cellular pharmacology of cytosine arabinoside. Seminars in oncology. 1985;12(2 Suppl 3):34-48. PubMed PMID: 3925560.

Laemmli UK. Cleavage of structural proteins during the assembly of the head of bacteriophage T4. Nature. 1970;227(5259):680-5. PubMed PMID: 5432063.

Lake JA. Ribosome structure determined by electron microscopy of Escherichia coli small subunits, large subunits and monomeric ribosomes. Journal of molecular biology. 1976;105(1):131-9. PubMed PMID: 792456.

*Laurberg, M., Asahara, H., Korostelev, A., Zhu, J., Trakhanov, S., and Noller, H.F. (2008). Structural basis for translation termination on the 70S ribosome. Nature 454, 852–857.

le Coutre,P.,Tassi,E.,Varella-Garcia, M., Barni,R.,Mologni,L.,Cabrita, G., etal.(2000).Inductionofresis-tancetotheAbelsoninhibitorSTI571 in humanleukemiccellsthrough gene amplification. Blood 95, 1758–1766.

Le Loir, Y., Baron, F., and Gautier, M. (2003). Staphylococcus aureus and food poisoning. Genet. Mol. Res. 2, 63–76.

Leclercq R. Mechanisms of resistance to macrolides and lincosamides: nature of the resistance elements and their clinical implications. Clinical infectious diseases : an official publication of the Infectious Diseases Society of America. 2002;34(4):482-92. doi: 10.1086/324626. PubMed PMID: 11797175.

Levine AJ. p53, the cellular gatekeeper for growth and division. Cell. 1997;88(3):323-31. PubMed PMID: 9039259.

Li X, Mooney P, Zheng S, Booth CR, Braunfeld MB, Gubbens S, et al. Electron counting and beam-induced motion correction enable near-atomic-resolution single-particle cryo-EM. Nature methods.

2013;10(6):584-90. doi: 10.1038/nmeth.2472. PubMed PMID: 23644547; PubMed Central PMCID: PMC3684049.

Liang X, Yu C, Sun J, Liu H, Landwehr C, Holmes D, et al. Inactivation of a two-component signal transduction system, SaeRS, eliminates adherence and attenuates virulence of Staphylococcus aureus. Infection and immunity. 2006;74(8):4655-65. doi: 10.1128/IAI.00322-06. PubMed PMID: 16861653; PubMed Central PMCID: PMC1539584.

*Lin, J., Gagnon, M.G., Bulkley, D., and Steitz, T.A. (2015). Conformational changes of elongation factor G on the ribosome during tRNA translocation. Cell 160, 219–227.

Locke JB, Zurenko GE, Shaw KJ, Bartizal K. Tedizolid for the management of human infections: in vitro characteristics. Clinical infectious diseases : an official publication of the Infectious Diseases Society of America. 2014;58 Suppl 1:S35-42. doi: 10.1093/cid/cit616. PubMed PMID: 24343830.

Loughman JA, Fritz SA, Storch GA, Hunstad DA. Virulence gene expression in human community-acquired Staphylococcus aureus infection. The Journal of infectious diseases. 2009;199(3):294-301. doi: 10.1086/595982. PubMed PMID: 19115951; PubMed Central PMCID: PMC2843142.

Low WK, Dang Y, Schneider-Poetsch T, Shi Z, Choi NS, Merrick WC, et al. Inhibition of eukaryotic translation initiation by the marine natural product pateamine A. Molecular cell. 2005;20(5):709-22. doi: 10.1016/j.molcel.2005.10.008. PubMed PMID: 16337595.

Lowy FD. Staphylococcus aureus infections. The New England journal of medicine. 1998;339(8):520-32. doi: 10.1056/NEJM199808203390806. PubMed PMID: 9709046.

Luft JR, Detitta GT. [7] Kinetic aspects of macromolecular crystallization. Methods in enzymology. 1997;276:110-31. doi: 10.1016/S0076-6879(97)76053-1. PubMed PMID: 27799087.

Luo J, Solimini NL, Elledge SJ. Principles of cancer therapy: oncogene and non-oncogene addiction. Cell. 2009;136(5):823-37. doi: 10.1016/j.cell.2009.02.024. PubMed PMID: 19269363; PubMed Central PMCID: PMC2894612.

Lynch TJ, Bell DW, Sordella R, Gurubhagavatula S, Okimoto RA, Brannigan BW, et al. Activating mutations in the epidermal growth factor receptor underlying responsiveness of non-small-cell lung cancer to gefitinib. The New England journal of medicine. 2004;350(21):2129-39. doi: 10.1056/NEJMoa040938. PubMed PMID: 15118073.

Ma X, Yu H. Global burden of cancer. The Yale journal of biology and medicine. 2006;79(3-4):85-94. PubMed PMID: 17940618; PubMed Central PMCID: PMC1994799.

***Malochet-Grivois, C.-F. et al. Dichlorolissoclimide, a new cytotoxic labdane derivative from Lissoclinum voeltzkowi Michaelson (Urochordata). TetrahedronLett. 32, 6701–6702 (1991).

Mamane Y, Petroulakis E, Rong L, Yoshida K, Ler LW, Sonenberg N. eIF4E--from translation to transformation. Oncogene. 2004;23(18):3172-9. doi: 10.1038/sj.onc.1207549. PubMed PMID: 15094766.

Manuell AL, Quispe J, Mayfield SP. Structure of the chloroplast ribosome: novel domains for translation regulation. PLoS biology. 2007;5(8):e209. doi: 10.1371/journal.pbio.0050209. PubMed PMID: 17683199; PubMed Central PMCID: PMC1939882.

Marshall RA, Dorywalska M, Puglisi JD. Irreversible chemical steps control intersubunit dynamics during translation. Proceedings of the National Academy of Sciences of the United States of America. 2008;105(40):15364-9. doi: 10.1073/pnas.0805299105. PubMed PMID: 18824686; PubMed Central PMCID: PMC2563075.

Matzov D, Aibara S, Basu A, Zimmerman E, Bashan A, Yap MF, et al. The cryo-EM structure of hibernating 100S ribosome dimer from pathogenic Staphylococcus aureus. Nature communications. 2017;8(1):723. doi: 10.1038/s41467-017-00753-8. PubMed PMID: 28959035; PubMed Central PMCID: PMC5620080.

McClary B, Zinshteyn B, Meyer M, Jouanneau M, Pellegrino S, Yusupova G, et al. Inhibition of Eukaryotic Translation by the Antitumor Natural Product Agelastatin A. Cell chemical biology. 2017;24(5):605-13 e5. doi: 10.1016/j.chembiol.2017.04.006. PubMed PMID: 28457705; PubMed Central PMCID: PMC5562292.

McMurry J. Organic Chemistry. 6th edition. Brooks Cole; 2003.

McMurry L, Petrucci RE, Jr., Levy SB. Active efflux of tetracycline encoded by four genetically different tetracycline resistance determinants in Escherichia coli. Proceedings of the National Academy of Sciences of the United States of America. 1980;77(7):3974-7. PubMed PMID: 7001450; PubMed Central PMCID: PMC349750.

McNamara PJ, Milligan-Monroe KC, Khalili S, Proctor RA. Identification, cloning, and initial characterization of rot, a locus encoding a regulator of virulence factor expression in Staphylococcus aureus. Journal of bacteriology. 2000;182(11):3197-203. PubMed PMID: 10809700; PubMed Central PMCID: PMC94507.

McPherson A. Protein crystallization in the structural genomics era. Journal of structural and functional genomics. 2004;5(1-2):3-12. doi: 10.1023/B:JSFG.0000029199.43875.92. PubMed PMID: 15263838.

Meijer C, Mulder NH, Timmer-Bosscha H, Sluiter WJ, Meersma GJ, de Vries EG. Relationship of cellular glutathione to the cytotoxicity and resistance of seven platinum compounds. Cancer research. 1992;52(24):6885-9. PubMed PMID: 1458477.

Meinnel T, Blanquet S. Maturation of pre-tRNA(fMet) by Escherichia coli RNase P is specified by a guanosine of the 5'-flanking sequence. The Journal of biological chemistry. 1995;270(26):15908-14. PubMed PMID: 7797595.

Melles DC, Gorkink RF, Boelens HA, Snijders SV, Peeters JK, Moorhouse MJ, et al. Natural population dynamics and expansion of pathogenic clones of Staphylococcus aureus. The Journal of clinical investigation. 2004;114(12):1732-40. doi: 10.1172/JCI23083. PubMed PMID: 15599398; PubMed Central PMCID: PMC535072.

Melnikov S, Ben-Shem A, Garreau de Loubresse N, Jenner L, Yusupova G, Yusupov M. One core, two shells: bacterial and eukaryotic ribosomes. Nature structural & molecular biology. 2012;19(6):560-7. doi: 10.1038/nsmb.2313. PubMed PMID: 22664983.

Melnikov SV, Soll D, Steitz TA, Polikanov YS. Insights into RNA binding by the anticancer drug cisplatin from the crystal structure of cisplatin-modified ribosome. Nucleic acids research. 2016;44(10):4978-87. doi: 10.1093/nar/gkw246. PubMed PMID: 27079977; PubMed Central PMCID: PMC4889946.

Mendes RE, Deshpande LM, Jones RN. Linezolid update: stable in vitro activity following more than a decade of clinical use and summary of associated resistance mechanisms. Drug resistance updates : reviews and commentaries in antimicrobial and anticancer chemotherapy. 2014;17(1-2):1-12. doi: 10.1016/j.drup.2014.04.002. PubMed PMID: 24880801.

Micoine K, Persich P, Llaveria J, Lam MH, Maderna A, Loganzo F, et al. Total syntheses and biological reassessment of lactimidomycin, isomigrastatin and congener glutarimide antibiotics. Chemistry. 2013;19(23):7370-83. doi: 10.1002/chem.201300393. PubMed PMID: 23595541.

Mikol V, Hirsch E, Giege R. Diagnostic of precipitant for biomacromolecule crystallization by quasi-elastic light-scattering. Journal of molecular biology. 1990;213(1):187-95. doi: 10.1016/S0022-2836(05)80130-5. PubMed PMID: 2338713.

Mikolajka A, Liu H, Chen Y, Starosta AL, Marquez V, Ivanova M, et al. Differential effects of thiopeptide and orthosomycin antibiotics on translational GTPases. Chemistry & biology. 2011;18(5):589-600. doi: 10.1016/j.chembiol.2011.03.010. PubMed PMID: 21609840; PubMed Central PMCID: PMC3102230.

Moazed D, Noller HF. Intermediate states in the movement of transfer RNA in the ribosome. Nature. 1989;342(6246):142-8. doi: 10.1038/342142a0. PubMed PMID: 2682263.

Moran Jr, C.P. (1993). RNA polymerase and transcription factors. Bacillus Subtilis Other Gram-Positive Bact. Biochem. Physiol. Mol. Genet. Am. Soc. Microbiol. Washington, DC 653–667.

Morfeldt E, Taylor D, von Gabain A, Arvidson S. Activation of alpha-toxin translation in Staphylococcus aureus by the trans-encoded antisense RNA, RNAIII. The EMBO journal. 1995;14(18):4569-77. PubMed PMID: 7556100; PubMed Central PMCID: PMC394549.

**Muhs, M., Hilal, T., Mielke, T., Skabkin, M.A., Sanbonmatsu, K.Y., Pestova, T. V, and Spahn, C.M.T. (2015). Cryo-EM of ribosomal 80S complexes with termination factors reveals the translocated cricket paralysis virus IRES. Mol. Cell 57, 422–432.

Munita JM, Arias CA. Mechanisms of Antibiotic Resistance. Microbiology spectrum. 2016;4(2). doi: 10.1128/microbiolspec.VMBF-0016-2015. PubMed PMID: 27227291; PubMed Central PMCID: PMC4888801.

Munro JB, Altman RB, O'Connor N, Blanchard SC. Identification of two distinct hybrid state intermediates on the ribosome. Molecular cell. 2007;25(4):505-17. doi: 10.1016/j.molcel.2007.01.022. PubMed PMID: 17317624; PubMed Central PMCID: PMC2244649.

Munro JB, Sanbonmatsu KY, Spahn CM, Blanchard SC. Navigating the ribosome's metastable energy landscape. Trends in biochemical sciences. 2009;34(8):390-400. doi: 10.1016/j.tibs.2009.04.004. PubMed PMID: 19647434; PubMed Central PMCID: PMC2914510.

Newman J. A review of techniques for maximizing diffraction from a protein crystal in stilla. Acta crystallographica Section D, Biological crystallography. 2006;62(Pt 1):27-31. doi: 10.1107/S0907444905032130. PubMed PMID: 16369091.

Nicolini FE, Corm S, Le QH, Sorel N, Hayette S, Bories D, et al. Mutation status and clinical outcome of 89 imatinib mesylate-resistant chronic myelogenous leukemia patients: a retrospective analysis from the French intergroup of CML (Fi(phi)-LMC GROUP). Leukemia. 2006;20(6):1061-6. doi: 10.1038/sj.leu.2404236. PubMed PMID: 16642048.

Nijman SM. Synthetic lethality: general principles, utility and detection using genetic screens in human cells. FEBS letters. 2011;585(1):1-6. doi: 10.1016/j.febslet.2010.11.024. PubMed PMID: 21094158; PubMed Central PMCID: PMC3018572.

Novick RP, Geisinger E. Quorum sensing in staphylococci. Annual review of genetics. 2008;42:541-64. doi: 10.1146/annurev.genet.42.110807.091640. PubMed PMID: 18713030.

Novick RP, Jiang D. The staphylococcal saeRS system coordinates environmental signals with agr quorum sensing. Microbiology. 2003;149(Pt 10):2709-17. doi: 10.1099/mic.0.26575-0. PubMed PMID: 14523104.

Novick RP, Projan SJ, Kornblum J, Ross HF, Ji G, Kreiswirth B, et al. The agr P2 operon: an autocatalytic sensory transduction system in Staphylococcus aureus. Molecular & general genetics : MGG. 1995;248(4):446-58. PubMed PMID: 7565609.

Novick RP, Ross HF, Projan SJ, Kornblum J, Kreiswirth B, Moghazeh S. Synthesis of staphylococcal virulence factors is controlled by a regulatory RNA molecule. The EMBO journal. 1993;12(10):3967-75. PubMed PMID: 7691599; PubMed Central PMCID: PMC413679.

Ohshima H, Bartsch H. Chronic infections and inflammatory processes as cancer risk factors: possible role of nitric oxide in carcinogenesis. Mutation research. 1994;305(2):253-64. PubMed PMID: 7510036.

Olaussen KA, Dunant A, Fouret P, Brambilla E, Andre F, Haddad V, et al. DNA repair by ERCC1 in non-small-cell lung cancer and cisplatin-based adjuvant chemotherapy. The New England journal of medicine. 2006;355(10):983-91. doi: 10.1056/NEJMoa060570. PubMed PMID: 16957145.

Olivier NB, Altman RB, Noeske J, Basarab GS, Code E, Ferguson AD, et al. Negamycin induces translational stalling and miscoding by binding to the small subunit head domain of the Escherichia coli ribosome. Proceedings of the National Academy of Sciences of the United States of America. 2014;111(46):16274-9. doi: 10.1073/pnas.1414401111. PubMed PMID: 25368144; PubMed Central PMCID: PMC4246262.

O'Neil M. The Merck Index. 14th edition. New Jersey: Merck & Co.; 2006.

Oscarsson J, Tegmark-Wisell K, Arvidson S. Coordinated and differential control of aureolysin (aur) and serine protease (sspA) transcription in Staphylococcus aureus by sarA, rot and agr (RNAIII).

International journal of medical microbiology : IJMM. 2006;296(6):365-80. doi: 10.1016/j.ijmm.2006.02.019. PubMed PMID: 16782403.

Otalora F, Gavira JA, Ng JD, Garcia-Ruiz JM. Counterdiffusion methods applied to protein crystallization. Progress in biophysics and molecular biology. 2009;101(1-3):26-37. doi: 10.1016/j.pbiomolbio.2009.12.004. PubMed PMID: 20018206.

Pages JM, James CE, Winterhalter M. The porin and the permeating antibiotic: a selective diffusion barrier in Gram-negative bacteria. Nature reviews Microbiology. 2008;6(12):893-903. doi: 10.1038/nrmicro1994. PubMed PMID: 18997824.

**Pallesen, J., Hashem, Y., Korkmaz, G., Koripella, R.K., Huang, C., Ehrenberg, M., Sanyal, S., and Frank, J. (2013). Cryo-EM visualization of the ribosome in termination complex with apo-RF3 and RF1. Elife 2013.

Pao W, Miller VA, Politi KA, Riely GJ, Somwar R, Zakowski MF, et al. Acquired resistance of lung adenocarcinomas to gefitinib or erlotinib is associated with a second mutation in the EGFR kinase domain. PLoS medicine. 2005;2(3):e73. doi: 10.1371/journal.pmed.0020073. PubMed PMID: 15737014; PubMed Central PMCID: PMC549606.

Parsonnet J. Bacterial infection as a cause of cancer. Environmental health perspectives. 1995;103 Suppl 8:263-8. PubMed PMID: 8741796; PubMed Central PMCID: PMC1518971.

Pearson, M. (2011) Crystal structures of naturally inhibited ribosomes (Doctoral thesis, University of California, Santa Cruz). Retrieved from: http://gradworks.umi.com /34/52/3452518.html

Peng HL, Novick RP, Kreiswirth B, Kornblum J, Schlievert P. Cloning, characterization, and sequencing of an accessory gene regulator (agr) in Staphylococcus aureus. Journal of bacteriology. 1988;170(9):4365-72. PubMed PMID: 2457579; PubMed Central PMCID: PMC211451.

Perutz MF, Rossmann MG, Cullis AF, Muirhead H, Will G, North AC. Structure of haemoglobin: a three-dimensional Fourier synthesis at 5.5-A. resolution, obtained by X-ray analysis. Nature. 1960;185(4711):416-22. PubMed PMID: 18990801.

Peske F, Rodnina MV, Wintermeyer W. Sequence of steps in ribosome recycling as defined by kinetic analysis. Molecular cell. 2005;18(4):403-12. doi: 10.1016/j.molcel.2005.04.009. PubMed PMID: 15893724.

*Petry S, Brodersen DE, Murphy FVt, Dunham CM, Selmer M, Tarry MJ, et al. Crystal structures of the ribosome in complex with release factors RF1 and RF2 bound to a cognate stop codon. Cell. 2005;123(7):1255-66. doi: 10.1016/j.cell.2005.09.039. PubMed PMID: 16377566.

Piccart-Gebhart MJ, Procter M, Leyland-Jones B, Goldhirsch A, Untch M, Smith I, et al. Trastuzumab after adjuvant chemotherapy in HER2-positive breast cancer. The New England journal of medicine. 2005;353(16):1659-72. doi: 10.1056/NEJMoa052306. PubMed PMID: 16236737.

Piddock LJ. Clinically relevant chromosomally encoded multidrug resistance efflux pumps in bacteria. Clinical microbiology reviews. 2006;19(2):382-402. doi: 10.1128/CMR.19.2.382-402.2006. PubMed PMID: 16614254; PubMed Central PMCID: PMC1471989.

Pisani P, Parkin DM, Munoz N, Ferlay J. Cancer and infection: estimates of the attributable fraction in 1990. Cancer epidemiology, biomarkers & prevention : a publication of the American Association for Cancer Research, cosponsored by the American Society of Preventive Oncology. 1997;6(6):387-400. PubMed PMID: 9184771.

Pisarev AV, Hellen CU, Pestova TV. Recycling of eukaryotic posttermination ribosomal complexes. Cell. 2007;131(2):286-99. doi: 10.1016/j.cell.2007.08.041. PubMed PMID: 17956730; PubMed Central PMCID: PMC2651563.

Pisarev MA. Interrelationships between the pancreas and the thyroid. Current opinion in endocrinology, diabetes, and obesity. 2010;17(5):437-9. doi: 10.1097/MED.0b013e32833e0750. PubMed PMID: 20717019.

*Polikanov YS, Blaha GM, Steitz TA. How hibernation factors RMF, HPF, and YfiA turn off protein synthesis. Science. 2012;336(6083):915-8. doi: 10.1126/science.1218538. PubMed PMID: 22605777; PubMed Central PMCID: PMC3377384.

Polikanov YS, Osterman IA, Szal T, Tashlitsky VN, Serebryakova MV, Kusochek P, et al. Amicoumacin a inhibits translation by stabilizing mRNA interaction with the ribosome. Molecular cell. 2014;56(4):531-40. doi: 10.1016/j.molcel.2014.09.020. PubMed PMID: 25306919; PubMed Central PMCID: PMC4253140.

Polikanov YS, Starosta AL, Juette MF, Altman RB, Terry DS, Lu W, et al. Distinct tRNA Accommodation Intermediates Observed on the Ribosome with the Antibiotics Hygromycin A and A201A. Molecular cell. 2015;58(5):832-44. doi: 10.1016/j.molcel.2015.04.014. PubMed PMID: 26028538; PubMed Central PMCID: PMC4458074.

Polikanov YS, Szal T, Jiang F, Gupta P, Matsuda R, Shiozuka M, et al. Negamycin interferes with decoding and translocation by simultaneous interaction with rRNA and tRNA. Molecular cell. 2014;56(4):541-50. doi: 10.1016/j.molcel.2014.09.021. PubMed PMID: 25306922; PubMed Central PMCID: PMC4334386.

Poole K. Efflux-mediated antimicrobial resistance. The Journal of antimicrobial chemotherapy. 2005;56(1):20-51. doi: 10.1093/jac/dki171. PubMed PMID: 15914491.

Prokhorova IV, Akulich KA, Makeeva DS, Osterman IA, Skvortsov DA, Sergiev PV, et al. Amicoumacin A induces cancer cell death by targeting the eukaryotic ribosome. Scientific reports. 2016;6:27720. doi: 10.1038/srep27720. PubMed PMID: 27296282; PubMed Central PMCID: PMC4906347.

*Pulk, A., and Cate, J.H.D. (2013). Control of ribosomal subunit rotation by elongation factor G. Science 340, 1235970.

*Qu, X., Wen, J.-D., Lancaster, L., Noller, H.F., Bustamante, C., and Tinoco, I. (2011). The ribosome uses two active mechanisms to unwind messenger RNA during translation. Nature 475, 118–121.

Rabl J, Leibundgut M, Ataide SF, Haag A, Ban N. Crystal structure of the eukaryotic 40S ribosomal subunit in complex with initiation factor 1. Science. 2011;331(6018):730-6. doi: 10.1126/science.1198308. PubMed PMID: 21205638.

**Ramrath, D.J.F., Lancaster, L., Sprink, T., Mielke, T., Loerke, J., Noller, H.F., and Spahn, C.M.T. (2013). Visualization of two transfer RNAs trapped in transit during elongation factor G-mediated translocation. Proc. Natl. Acad. Sci. U. S. A. 110, 20964–20969.

Reid SA, Nyambo S, Muzangwa L, Uhler B. pi-Stacking, C-H/pi, and halogen bonding interactions in bromobenzene and mixed bromobenzene-benzene clusters. The journal of physical chemistry A. 2013;117(50):13556-63. doi: 10.1021/jp407544c. PubMed PMID: 23978255.

Reynolds PE. Structure, biochemistry and mechanism of action of glycopeptide antibiotics. European journal of clinical microbiology & infectious diseases : official publication of the European Society of Clinical Microbiology. 1989;8(11):943-50. PubMed PMID: 2532132.

Robert F, Gao HQ, Donia M, Merrick WC, Hamann MT, Pelletier J. Chlorolissoclimides: new inhibitors of eukaryotic protein synthesis. Rna. 2006;12(5):717-25. doi: 10.1261/rna.2346806. PubMed PMID: 16540697; PubMed Central PMCID: PMC1440909.

Roche FM, Meehan M, Foster TJ. The Staphylococcus aureus surface protein SasG and its homologues promote bacterial adherence to human desquamated nasal epithelial cells. Microbiology. 2003;149(Pt 10):2759-67. doi: 10.1099/mic.0.26412-0. PubMed PMID: 14523109.

Rodnina MV, Wintermeyer W. Recent mechanistic insights into eukaryotic ribosomes. Current opinion in cell biology. 2009;21(3):435-43. doi: 10.1016/j.ceb.2009.01.023. PubMed PMID: 19243929.

Rossi F, Diaz L, Wollam A, Panesso D, Zhou Y, Rincon S, et al. Transferable vancomycin resistance in a community-associated MRSA lineage. The New England journal of medicine. 2014;370(16):1524-31. doi: 10.1056/NEJMoa1303359. PubMed PMID: 24738669; PubMed Central PMCID: PMC4112484.

*Rozov, A., Demeshkina, N., Westhof, E., Yusupov, M., and Yusupova, G. (2015). Structural insights into the translational infidelity mechanism. Nat Commun 6.

Said-Salim B, Dunman PM, McAleese FM, Macapagal D, Murphy E, McNamara PJ, et al. Global regulation of Staphylococcus aureus genes by Rot. Journal of bacteriology. 2003;185(2):610-9. PubMed PMID: 12511508; PubMed Central PMCID: PMC145333.

Said-Salim B, Mathema B, Kreiswirth BN. Community-acquired methicillin-resistant Staphylococcus aureus: an emerging pathogen. Infection control and hospital epidemiology. 2003;24(6):451-5. doi: 10.1086/502231. PubMed PMID: 12828324.

Salemme FR. A free interface diffusion technique for the crystallization of proteins for x-ray crystallography. Archives of biochemistry and biophysics. 1972;151(2):533-9. PubMed PMID: 4625692.

Sambrook, J; Frisch, E.F.M.T. (1989). Molecular Cloning: A laboratory manual. In Cold Spring Harbour

Sampath D, Cortes J, Estrov Z, Du M, Shi Z, Andreeff M, et al. Pharmacodynamics of cytarabine alone and in combination with 7-hydroxystaurosporine (UCN-01) in AML blasts in vitro and during a clinical trial. Blood. 2006;107(6):2517-24. doi: 10.1182/blood-2005-08-3351. PubMed PMID: 16293603; PubMed Central PMCID: PMC1895741.

Savelsbergh A, Rodnina MV, Wintermeyer W. Distinct functions of elongation factor G in ribosome recycling and translocation. Rna. 2009;15(5):772-80. doi: 10.1261/rna.1592509. PubMed PMID: 19324963; PubMed Central PMCID: PMC2673078.

Scheffner M, Takahashi T, Huibregtse JM, Minna JD, Howley PM. Interaction of the human papillomavirus type 16 E6 oncoprotein with wild-type and mutant human p53 proteins. Journal of virology. 1992;66(8):5100-5. PubMed PMID: 1321290; PubMed Central PMCID: PMC241378.

Schistosomes, liver flukes and Helicobacter pylori. IARC Working Group on the Evaluation of Carcinogenic Risks to Humans. Lyon, 7-14 June 1994. IARC monographs on the evaluation of carcinogenic risks to humans. 1994;61:1-241. PubMed PMID: 7715068.

Schluenzen F, Tocilj A, Zarivach R, Harms J, Gluehmann M, Janell D, et al. Structure of functionally activated small ribosomal subunit at 3.3 angstroms resolution. Cell. 2000;102(5):615-23. PubMed PMID: 11007480.

Schmidt KA, Manna AC, Cheung AL. SarT influences sarS expression in Staphylococcus aureus. Infection and immunity. 2003;71(9):5139-48. PubMed PMID: 12933857; PubMed Central PMCID: PMC187355.

Schneider-Poetsch T, Ju J, Eyler DE, Dang Y, Bhat S, Merrick WC, et al. Inhibition of eukaryotic translation elongation by cycloheximide and lactimidomycin. Nature chemical biology. 2010;6(3):209-17. doi: 10.1038/nchembio.304. PubMed PMID: 20118940; PubMed Central PMCID: PMC2831214.

Schneider-Poetsch T, Ju J, Eyler DE, Dang Y, Bhat S, Merrick WC, et al. Inhibition of eukaryotic translation elongation by cycloheximide and lactimidomycin. Nature chemical biology. 2010;6(3):209-17. doi: 10.1038/nchembio.304. PubMed PMID: 20118940; PubMed Central PMCID: PMC2831214.

Schuwirth BS, Borovinskaya MA, Hau CW, Zhang W, Vila-Sanjurjo A, Holton JM, et al. Structures of the bacterial ribosome at 3.5 A resolution. Science. 2005;310(5749):827-34. doi: 10.1126/science.1117230. PubMed PMID: 16272117.

Schwarz S, Kehrenberg C, Doublet B, Cloeckaert A. Molecular basis of bacterial resistance to chloramphenicol and florfenicol. FEMS microbiology reviews. 2004;28(5):519-42. doi: 10.1016/j.femsre.2004.04.001. PubMed PMID: 15539072.

Selmer M, Dunham CM, Murphy FVt, Weixlbaumer A, Petry S, Kelley AC, et al. Structure of the 70S ribosome complexed with mRNA and tRNA. Science. 2006;313(5795):1935-42. doi: 10.1126/science.1131127. PubMed PMID: 16959973.

Selvakumaran M, Pisarcik DA, Bao R, Yeung AT, Hamilton TC. Enhanced cisplatin cytotoxicity by disturbing the nucleotide excision repair pathway in ovarian cancer cell lines. Cancer research. 2003;63(6):1311-6. PubMed PMID: 12649192.

Sharma SV, Settleman J. Oncogene addiction: setting the stage for molecularly targeted cancer therapy. Genes & development. 2007;21(24):3214-31. doi: 10.1101/gad.1609907. PubMed PMID: 18079171.

Shepherd FA, Rodrigues Pereira J, Ciuleanu T, Tan EH, Hirsh V, Thongprasert S, et al. Erlotinib in previously treated non-small-cell lung cancer. The New England journal of medicine. 2005;353(2):123-32. doi: 10.1056/NEJMoa050753. PubMed PMID: 16014882.

Shockman GD, Barrett JF. Structure, function, and assembly of cell walls of gram-positive bacteria. Annual review of microbiology. 1983;37:501-27. doi: 10.1146/annurev.mi.37.100183.002441. PubMed PMID: 6139058.

Shoemaker CJ, Green R. Kinetic analysis reveals the ordered coupling of translation termination and ribosome recycling in yeast. Proceedings of the National Academy of Sciences of the United States of America. 2011;108(51):E1392-8. doi: 10.1073/pnas.1113956108. PubMed PMID: 22143755; PubMed Central PMCID: PMC3251084.

Shoham M, Dijk J, Reinhardt R, Wittmann-Liebold B. Purification and characterization of ribosomal proteins from the 30 S subunit of the extreme halophile Halobacterium marismortui. FEBS letters. 1986;204(2):323-30. PubMed PMID: 22937542.

Sievert DM, Rudrik JT, Patel JB, McDonald LC, Wilkins MJ, Hageman JC. Vancomycin-resistant Staphylococcus aureus in the United States, 2002-2006. Clinical infectious diseases : an official publication of the Infectious Diseases Society of America. 2008;46(5):668-74. doi: 10.1086/527392. PubMed PMID: 18257700.

Slamon DJ, Leyland-Jones B, Shak S, Fuchs H, Paton V, Bajamonde A, et al. Use of chemotherapy plus a monoclonal antibody against HER2 for metastatic breast cancer that overexpresses HER2. The New England journal of medicine. 2001;344(11):783-92. doi: 10.1056/NEJM200103153441101. PubMed PMID: 11248153.

Sohmen D, Chiba S, Shimokawa-Chiba N, Innis CA, Berninghausen O, Beckmann R, et al. Structure of the Bacillus subtilis 70S ribosome reveals the basis for species-specific stalling. Nature communications. 2015;6:6941. doi: 10.1038/ncomms7941. PubMed PMID: 25903689; PubMed Central PMCID: PMC4423224.

Southern EM, Denaturing Gel Electrophoresis of RNA and DNA Using Urea–Polyacrylamide Gels. Citable reviewes in the life sciences, Wiley online library, 2002, doi: 10.1038/npg.els.0003778

Soverini S, Martinelli G, Rosti G, Bassi S, Amabile M, Poerio A, et al. ABL mutations in late chronic phase chronic myeloid leukemia patients with up-front cytogenetic resistance to imatinib are associated with a greater likelihood of progression to blast crisis and shorter survival: a study by the GIMEMA Working Party on Chronic Myeloid Leukemia. Journal of clinical oncology : official journal of the American Society of Clinical Oncology. 2005;23(18):4100-9. doi: 10.1200/JCO.2005.05.531. PubMed PMID: 15867198.

**Spahn, C.M.T., Gomez-Lorenzo, M.G., Grassucci, R.A., Jørgensen, R., Andersen, G.R., Beckmann, R., Penczek, P.A., Ballesta, J.P.G., and Frank, J. (2004a). Domain movements of elongation factor eEF2 and the eukaryotic 80S ribosome facilitate tRNA translocation. EMBO J. 23, 1008–1019.

**Spahn, C.M.T., Jan, E., Mulder, A., Grassucci, R.A., Sarnow, P., and Frank, J. (2004b). Cryo-EM visualization of a viral internal ribosome entry site bound to human ribosomes: The IRES functions as an RNA-based translation factor. Cell 118, 465–475.

Spirin AS, Sabo B, Kovalenko VA. Dependence of dissociation-association of uncharged ribosomes of Escherichia coli on the Mg(2+) concentration, ionic strength, pH and temperature. FEBS letters. 1971;15(3):197-200. PubMed PMID: 11945844.

Stahli C, Noll H. Structural dynamics of bacterial ribosomes. VI. Denaturation of active ribosomes by Mg2+ dependent conformational transitions. Molecular & general genetics : MGG. 1977;153(2):159-68. PubMed PMID: 329113.

Stansfield I, Jones KM, Tuite MF. The end in sight: terminating translation in eukaryotes. Trends in biochemical sciences. 1995;20(12):489-91. PubMed PMID: 8571447.

Stark H, Mueller F, Orlova EV, Schatz M, Dube P, Erdemir T, et al. The 70S Escherichia coli ribosome at 23 A resolution: fitting the ribosomal RNA. Structure. 1995;3(8):815-21. PubMed PMID: 7582898.

Stefani S, Goglio A. Methicillin-resistant Staphylococcus aureus: related infections and antibiotic resistance. International journal of infectious diseases : IJID : official publication of the International Society for Infectious Diseases. 2010;14 Suppl 4:S19-22. doi: 10.1016/j.ijid.2010.05.009. PubMed PMID: 20843722.

Stefani S, Monaco M, Campanile F, Cafiso V, Sanchini A, Marone P, et al. Characterization of Panton–Valentine leukocidin positive methicillin-resistant Staphylococcus aureus in Italy. European Congress of Clinical Microbiology and Infectious Diseases, Helsinki, 2009; P1573.

***Stern-Ginossar N, Weisburd B, Michalski A, Le VT, Hein MY, Huang SX, et al. Decoding human cytomegalovirus. Science. 2012;338(6110):1088-93. doi: 10.1126/science.1227919. PubMed PMID: 23180859; PubMed Central PMCID: PMC3817102.

Sugawara K, Nishiyama Y, Toda S, Komiyama N, Hatori M, Moriyama T, et al. Lactimidomycin, a new glutarimide group antibiotic. Production, isolation, structure and biological activity. The Journal of antibiotics. 1992;45(9):1433-41. PubMed PMID: 1429229.

Svidritskiy E, Ling C, Ermolenko DN, Korostelev AA. Blasticidin S inhibits translation by trapping deformed tRNA on the ribosome. Proceedings of the National Academy of Sciences of the United States of America. 2013;110(30):12283-8. doi: 10.1073/pnas.1304922110. PubMed PMID: 23824292; PubMed Central PMCID: PMC3725078.

**Svidritskiy, E., Brilot, A.F., Koh, C.S., Grigorieff, N., and Korostelev, A.A. (2014). Structures of yeast 80S ribosome-tRNA complexes in the rotated and nonrotated conformations. Structure 22, 1210–1218.

Taron M, Ichinose Y, Rosell R, Mok T, Massuti B, Zamora L, et al. Activating mutations in the tyrosine kinase domain of the epidermal growth factor receptor are associated with improved survival in gefitinib-treated chemorefractory lung adenocarcinomas. Clinical cancer research : an official journal of the American Association for Cancer Research. 2005;11(16):5878-85. doi: 10.1158/1078-0432.CCR-04-2618. PubMed PMID: 16115929.

**Taylor, D., Unbehaun, A., Li, W., Das, S., Lei, J., Liao, H.Y., Grassucci, R.A., Pestova, T. V., and Frank, J. (2012). Cryo-EM structure of the mammalian eukaryotic release factor eRF1-eRF3-associated termination complex. Proc. Natl. Acad. Sci.

Tegmark K, Karlsson A, Arvidson S. Identification and characterization of SarH1, a new global regulator of virulence gene expression in Staphylococcus aureus. Molecular microbiology. 2000;37(2):398-409. PubMed PMID: 10931334.

Teicher,B.A.(2006). Cancer Drug Resistance. Totowa:HumanaPress.

Teng, T.Y. (1990). Mounting of crystals for macromolecular crystallography in a free-standing thin film. J. Appl. Crystallogr. 23, 387–391.

Toh SM, Xiong L, Arias CA, Villegas MV, Lolans K, Quinn J, et al. Acquisition of a natural resistance gene renders a clinical strain of methicillin-resistant Staphylococcus aureus resistant to the synthetic antibiotic linezolid. Molecular microbiology. 2007;64(6):1506-14. doi: 10.1111/j.1365-2958.2007.05744.x. PubMed PMID: 17555436; PubMed Central PMCID: PMC2711439.

Torres VJ, Attia AS, Mason WJ, Hood MI, Corbin BD, Beasley FC, et al. Staphylococcus aureus fur regulates the expression of virulence factors that contribute to the pathogenesis of pneumonia. Infection and immunity. 2010;78(4):1618-28. doi: 10.1128/IAI.01423-09. PubMed PMID: 20100857; PubMed Central PMCID: PMC2849423.

***Toupet, L., Biard, J.-F. & Verbist, J.-F. Dichlorolissoclimide from Lissoclinum voeltzkowi Michaelson (Urochordata): crystal structure and absolutestereochemistry. J. Nat. Prod. 59, 1203–1204 (1996).

*Tourigny, D.S., Fernández, I.S., Kelley, A.C., and Ramakrishnan, V. (2013). Elongation factor G bound to the ribosome in an intermediate state of translocation. Science 340, 1235490.

Toyooka S, Kiura K, Mitsudomi T. EGFR mutation and response of lung cancer to gefitinib. The New England journal of medicine. 2005;352(20):2136; author reply doi: 10.1056/NEJM200505193522019. PubMed PMID: 15901872.

Trakhanov, S.D., Yusupov, M.M., Agalarov, S.C., Garber, M.B., Ryazantsev, S.N., Tischenko, S.V., and Shirokov, V.A. (1987). Crystallization of 70 S ribosomes and 30 S ribosomal subunits from Thermus thermophilus. FEBS Lett. 220, 319–322.

Tran TT, Panesso D, Mishra NN, Mileykovskaya E, Guan Z, Munita JM, et al. Daptomycin-resistant Enterococcus faecalis diverts the antibiotic molecule from the division septum and remodels cell membrane phospholipids. mBio. 2013;4(4). doi: 10.1128/mBio.00281-13. PubMed PMID: 23882013; PubMed Central PMCID: PMC3735187.

Tucker CL, Fields S. Lethal combinations. Nature genetics. 2003;35(3):204-5. doi: 10.1038/ng1103-204. PubMed PMID: 14593402.

Ueta M, Wada C, Wada A. Formation of 100S ribosomes in Staphylococcus aureus by the hibernation promoting factor homolog SaHPF. Genes to cells : devoted to molecular & cellular mechanisms. 2010;15(1):43-58. doi: 10.1111/j.1365-2443.2009.01364.x. PubMed PMID: 20015224.

Vasiliev VD, Selivanova OM, Baranov VI, Spirin AS. Structural study of translating 70 S ribosomes from Escherichia coli. I. Electron microscopy. FEBS letters. 1983;155(1):167-72. PubMed PMID: 6341084.

Vasiliev VD. Morphology of the ribosomal 30S subparticle according to electron microscopic data. Acta biologica et medica Germanica. 1974;33(5-6):779-93. PubMed PMID: 4143298.

Vellanoweth RL, Rabinowitz JC. The influence of ribosome-binding-site elements on translational efficiency in Bacillus subtilis and Escherichia coli in vivo. Molecular microbiology. 1992;6(9):1105-14. PubMed PMID: 1375309.

Vernachio J, Bayer AS, Le T, Chai YL, Prater B, Schneider A, et al. Anti-clumping factor A immunoglobulin reduces the duration of methicillin-resistant Staphylococcus aureus bacteremia in an experimental model of infective endocarditis. Antimicrobial agents and chemotherapy. 2003;47(11):3400-6. PubMed PMID: 14576094; PubMed Central PMCID: PMC253806.

Vila-Sanjurjo, A., Ridgeway, W.K., Seymaner, V., Zhang, W., Santoso, S., Yu, K., and Cate, J.H.D. (2003). X-ray crystal structures of the WT and a hyper-accurate ribosome from Escherichia coli. Proc. Natl. Acad. Sci. U. S. A. 100, 8682–8687.

von der Haar T, McCarthy JE. Intracellular translation initiation factor levels in Saccharomyces cerevisiae and their role in cap-complex function. Molecular microbiology. 2002;46(2):531-44. PubMed PMID: 12406227.

Voorhees RM, Fernandez IS, Scheres SH, Hegde RS. Structure of the mammalian ribosome-Sec61 complex to 3.4 A resolution. Cell. 2014;157(7):1632-43. doi: 10.1016/j.cell.2014.05.024. PubMed PMID: 24930395; PubMed Central PMCID: PMC4081569.

Wagenknecht T, Carazo JM, Radermacher M, Frank J. Three-dimensional reconstruction of the ribosome from Escherichia coli. Biophysical journal. 1989;55(3):455-64. doi: 10.1016/S0006-3495(89)82839-5. PubMed PMID: 2649163; PubMed Central PMCID: PMC1330499.

Waldvogel A. [Karl Kraus and psychoanalysis. A historical documentary study]. Psyche. 1990;44(5):412-44. PubMed PMID: 2193317.

Walsh C. Where will new antibiotics come from? Nature reviews Microbiology. 2003;1(1):65-70. doi: 10.1038/nrmicro727. PubMed PMID: 15040181.

Wang L, Altman RB, Blanchard SC. Insights into the molecular determinants of EF-G catalyzed translocation. Rna. 2011;17(12):2189-200. doi: 10.1261/rna.029033.111. PubMed PMID: 22033333; PubMed Central PMCID: PMC3222131.

Warner JR. The economics of ribosome biosynthesis in yeast. Trends in biochemical sciences. 1999;24(11):437-40. PubMed PMID: 10542411.

Watson JD, Crick FH. Molecular structure of nucleic acids; a structure for deoxyribose nucleic acid. Nature. 1953;171(4356):737-8. PubMed PMID: 13054692.

Weidenmaier C, Kokai-Kun JF, Kristian SA, Chanturiya T, Kalbacher H, Gross M, et al. Role of teichoic acids in Staphylococcus aureus nasal colonization, a major risk factor in nosocomial infections. Nature medicine. 2004;10(3):243-5. doi: 10.1038/nm991. PubMed PMID: 14758355.

Weinstein IB, Joe AK. Mechanisms of disease: Oncogene addiction--a rationale for molecular targeting in cancer therapy. Nature clinical practice Oncology. 2006;3(8):448-57. doi: 10.1038/ncponc0558. PubMed PMID: 16894390.

Weinstein IB. Cancer. Addiction to oncogenes--the Achilles heal of cancer. Science. 2002;297(5578):63-4. doi: 10.1126/science.1073096. PubMed PMID: 12098689.

Weisblum B. Erythromycin resistance by ribosome modification. Antimicrobial agents and chemotherapy. 1995;39(3):577-85. PubMed PMID: 7793855; PubMed Central PMCID: PMC162587.

*Weixlbaumer, A., Jin, H., Neubauer, C., Voorhees, R.M., Petry, S., Kelley, A.C., and Ramakrishnan, V. (2008). Insights into translational termination from the structure of RF2 bound to the ribosome. Science 322, 953–956.

Wendel HG, De Stanchina E, Fridman JS, Malina A, Ray S, Kogan S, et al. Survival signalling by Akt and eIF4E in oncogenesis and cancer therapy. Nature. 2004;428(6980):332-7. doi: 10.1038/nature02369. PubMed PMID: 15029198.

Wilkinson, B.J. (1997). The staphylococci in human disease. Biology (Basel)

Williamson MP, Havel TF, Wuthrich K. Solution conformation of proteinase inhibitor IIA from bull seminal plasma by 1H nuclear magnetic resonance and distance geometry. Journal of molecular biology. 1985;182(2):295-315. PubMed PMID: 3839023.

Wilson DN. On the specificity of antibiotics targeting the large ribosomal subunit. Annals of the New York Academy of Sciences. 2011;1241:1-16. doi: 10.1111/j.1749-6632.2011.06192.x. PubMed PMID: 22191523.

Wilson DN. Ribosome-targeting antibiotics and mechanisms of bacterial resistance. Nature reviews Microbiology. 2014;12(1):35-48. doi: 10.1038/nrmicro3155. PubMed PMID: 24336183.

Wilson DN. The A-Z of bacterial translation inhibitors. Critical reviews in biochemistry and molecular biology. 2009;44(6):393-433. doi: 10.3109/10409230903307311. PubMed PMID: 19929179.

Wilson TR, Longley DB, Johnston PG. Chemoresistance in solid tumours. Annals of oncology : official journal of the European Society for Medical Oncology. 2006;17 Suppl 10:x315-24. doi: 10.1093/annonc/mdl280. PubMed PMID: 17018746.

Wimberly BT, Brodersen DE, Clemons WM, Jr., Morgan-Warren RJ, Carter AP, Vonrhein C, et al. Structure of the 30S ribosomal subunit. Nature. 2000;407(6802):327-39. doi: 10.1038/35030006. PubMed PMID: 11014182.

Wolz, C., C. Goerke, R. Landmann, W. Zimmerli, and U. Fluckiger. 2000.Transcription of clumping factor A in attached and unattached Staphylococcusaureus in vitro and during device-related infection. Infect. Immun. 70:2758–2762.

Wong AL, Lee SC. Mechanisms of Resistance to Trastuzumab and Novel Therapeutic Strategies in HER2-Positive Breast Cancer. International journal of breast cancer. 2012;2012:415170. doi: 10.1155/2012/415170. PubMed PMID: 22649737; PubMed Central PMCID: PMC3357513.

**Wong W, Bai XC, Brown A, Fernandez IS, Hanssen E, Condron M, et al. Cryo-EM structure of the Plasmodium falciparum 80S ribosome bound to the anti-protozoan drug emetine. eLife. 2014;3. doi: 10.7554/eLife.03080. PubMed PMID: 24913268; PubMed Central PMCID: PMC4086275.

Wu S, de Lencastre H, Tomasz A. Sigma-B, a putative operon encoding alternate sigma factor of Staphylococcus aureus RNA polymerase: molecular cloning and DNA sequencing. Journal of bacteriology. 1996;178(20):6036-42. PubMed PMID: 8830703; PubMed Central PMCID: PMC178463.

Xhemalce B. From histones to RNA: role of methylation in cancer. Briefings in functional genomics. 2013;12(3):244-53. doi: 10.1093/bfgp/els064. PubMed PMID: 23313959.

Xu Y, Villalona-Calero MA. Irinotecan: mechanisms of tumor resistance and novel strategies for modulating its activity. Annals of oncology : official journal of the European Society for Medical Oncology. 2002;13(12):1841-51. PubMed PMID: 12453851.

Yonath A, Bartunik HD, Bartels KS, Wittmann HG. Some x-ray diffraction patterns from single crystals of the large ribosomal subunit from Bacillus stearothermophilus. Journal of molecular biology. 1984;177(1):201-6. PubMed PMID: 6748083.

Yonath A, Saper MA, Makowski I, Mussig J, Piefke J, Bartunik HD, et al. Characterization of single crystals of the large ribosomal particles from Bacillus stearothermophilus. Journal of molecular biology. 1986;187(4):633-6. PubMed PMID: 3712439.

Yusupov MM, Yusupova GZ, Baucom A, Lieberman K, Earnest TN, Cate JH, et al. Crystal structure of the ribosome at 5.5 A resolution. Science. 2001;292(5518):883-96. doi: 10.1126/science.1060089. PubMed PMID: 11283358.

Yusupov, M.M., Trakhanov, S.D., Barynin, V. V, Boroviagin, V.L., and Garber, M.B. (1987). Crystallization of 30S subparticles from Thermus thermophilus ribosomes(Kristallizatsiia 30 S subchastits ribosom Thermus thermophilus). In Doklady Akad Nauk (USSR), pp. 1271–1274.

Yusupova GZ, Yusupov MM, Cate JH, Noller HF. The path of messenger RNA through the ribosome. Cell. 2001;106(2):233-41. PubMed PMID: 11511350.

Zavialov AV, Hauryliuk VV, Ehrenberg M. Splitting of the posttermination ribosome into subunits by the concerted action of RRF and EF-G. Molecular cell. 2005;18(6):675-86. doi: 10.1016/j.molcel.2005.05.016. PubMed PMID: 15949442.

Zhang W, Dunkle JA, Cate JH. Structures of the ribosome in intermediate states of ratcheting. Science. 2009;325(5943):1014-7. doi: 10.1126/science.1175275. PubMed PMID: 19696352; PubMed Central PMCID: PMC2919209.

*Zhou, J., Korostelev, A., Lancaster, L., and Noller, H.F. (2012). Crystal structures of 70S ribosomes bound to release factors RF1, RF2 and RF3. Curr. Opin. Struct. Biol. 22, 733–742.

*Zhou, J., Lancaster, L., Donohue, J.P., and Noller, H.F. (2013). Crystal structures of EF-G-ribosome complexes trapped in intermediate states of translocation. Science 340, 1236086.

*Zhou, J., Lancaster, L., Donohue, J.P., and Noller, H.F. (2014). How the ribosome hands the A-site tRNA to the P site during EF-G–catalyzed translocation. Sci. 345 , 1188–1191.

Zhouravleva G, Frolova L, Le Goff X, Le Guellec R, Inge-Vechtomov S, Kisselev L, et al. Termination of translation in eukaryotes is governed by two interacting polypeptide chain release factors, eRF1 and eRF3. The EMBO journal. 1995;14(16):4065-72. PubMed PMID: 7664746; PubMed Central PMCID: PMC394485.

Ziebandt AK, Becher D, Ohlsen K, Hacker J, Hecker M, Engelmann S. The influence of agr and sigmaB in growth phase dependent regulation of virulence factors in Staphylococcus aureus. Proteomics. 2004;4(10):3034-47. doi: 10.1002/pmic.200400937. PubMed PMID: 15378746.

Structural analysis and investigation of the *Staphylococcus aureus* ribosome and potential anticancer drugs

The ribosome – protein synthesis machinery, is essential to all living cells, and it is one of the major targets for clinical treatment of bacterial infections. Many antibiotics act by selectively inhibiting the protein synthesis in bacteria, without perturbing the host ribosomes and, therefore, their cells. Staphylococcus aureus is one of the major human pathogens, which causes numerous community-associated and hospital-acquired infections. The crystal structures of complexes of antibiotics with ribosomes from Gram-negative non-pathogenic non-resistant bacteria have provided unparalleled insight into mechanisms of antibiotics action and promoted the development of new semi-synthetic and synthetic antibiotics. However, the crystal structure of the full ribosome from Gram-positive pathogenic and highly resistant bacteria such as *S.* aureus was still unidentified. In this study we performed optimizations of the purification protocol of *S. aureus* ribosome and showed different crystallization conditions for *S. aureus* ribosome. In addition, we performed complex formation of *S. aureus* ribosome with tRNA ^{fMet}/mRNA and N-terminal domain of HPF. All obtained results in this work will help to further researchers systematize their studies in the direction of *S.aureus* ribosome crystal structure determination. And also concentrate their efforts in those aspects that are disclosed in this project and exclude the possibility of further investigation in unpromising directions.

Ribosomes are ribo-nucleoprotein complexes that read mRNA to synthesize proteins. It is well known that the amount of ribosomes correlates with the rate of protein synthesis and with cell growth and proliferation. This is important to consider in the case of cancer cells, which show a global increase in protein synthesis to support their hyper-proliferative behaviour. The ribosome has therefore become an important druggable target. Inhibitors of eukaryotic protein synthesis have been shown to have significant therapeutic potential to treat a wide range of human cancers. Recently was published a multidisciplinary study in which was unravel the mechanism of action of chlorolissoclimide (CL), a compound sharing chemical similarity to cycloheximide (CHX), but showing promising lower cytotoxicity. CL binds to the E-site of the 60S subunit and creates novel interactions compared to CHX. In details, it creates an unusual halogen-π stacking interaction with residue G2794 through its chlorine atom. We were interested in this new type of interaction with the ribosome and therefore we solved a new crystal structure of the *S.cerevisiae* 80S in complex with another lissoclimide compound, bearing an additional chlorine atom, at 3.1 Å resolution. The coupling of high-resolution structures with computationally-driven drug design and FRET analysis will further guide the design of more selective and less cytotoxic inhibitors.

Daniya KASHINSKAYA

Analyse structurale et étude du ribosome de *Staphylococcus aureus* et des médicaments antitumoraux potentiels

Résumé

Les ribosomes sont des complexes ribo-nucléoprotéiques qui lisent l'ARNm pour synthétiser les protéines. Il a été démontré que les inhibiteurs de la synthèse des protéines eucaryotes ont un potentiel thérapeutique important pour traiter un large éventail de cancers humains. Récemment, nous avons publié une étude multidisciplinaire dans laquelle nous démêlons le mécanisme d'action du chlorolissoclimide (CL), un composé qui partage la similarité chimique avec le cycloheximide (CHX), mais qui présente une cytotoxicité inférieure prometteuse. Nous nous sommes intéressés aux nouveaux types d'interactions de CL avec le ribosome et nous avons donc résolu une nouvelle structure cristalline du complexe *S.cerevisiae* 80S en complexe avec un autre composé de lissoclimide à une résolution de 3.1 Å. Le couplage de structures à haute résolution avec la conception de médicaments axée sur le calcul et l'analyse FRET guidera davantage la conception d'inhibiteurs plus sélectifs et moins cytotoxiques.

Mots-clés: Ribosome, inhibiteurs, cancer, lissoclimide, structure cristalline, haute résolution.

Résumé en anglais

Ribosomes are ribo-nucleoprotein complexes that read mRNA to synthesize proteins. This is important to consider in the case of cancer cells, which show a global increase in protein synthesis to support their hyper-proliferative behaviour. Inhibitors of eukaryotic protein synthesis have been shown to have significant therapeutic potential to treat a wide range of human cancers. Recently we published a multidisciplinary study in which we unravel the mechanism of action of chlorolissoclimide (CL), a compound sharing chemical similarity to cycloheximide (CHX), but showing promising lower cytotoxicity. We were interested in the new types of interactions of CL with the ribosome and therefore we solved a new crystal structure of the *S.cerevisiae* 80S in complex with another lissoclimide compound at 3.1 Å resolution. The coupling of high-resolution structures with computationally-driven drug design and FRET analysis will further guide the design of more selective and less cytotoxic inhibitors.

Keywords: Ribosome, inhibitors, cancer, lissoclimide, crystal structure, high-resolution.